NASA Technical Memorandum 80145

Transonic Aerodynamic Characteristics of a Supersonic Cruise Aircraft Research Model With the Engines Suspended Above the Wing

Charles E. Mercer and George T. Carson, Jr.

DECEMBER 1979

NASA

NASA Technical Memorandum 80145

Transonic Aerodynamic Characteristics of a Supersonic Cruise Aircraft Research Model With the Engines Suspended Above the Wing

Charles E. Mercer and George T. Carson, Jr.
Langley Research Center
Hampton, Virginia

National Aeronautics
and Space Administration

**Scientific and Technical
Information Branch**

1979

SUMMARY

An investigation was conducted in the Langley 16-foot transonic tunnel to determine the influence of upper-surface nacelle exhaust flow on the aerodynamic characteristics of a supersonic cruise aircraft research configuration at Mach numbers from 0.60 to 1.20. The configuration included a wing-body combination with detached engines suspended over the wing to produce upper-surface exhaust flow effects. The configuration was tested at angles of attack from -4° to 6° and jet total-pressure ratios from 1 (jet off) to approximately 13. Wing-tip leading-edge flap deflections of -10° to 10° were tested with the wing-body configuration only (no nacelles). Various nacelle locations (chordwise, spanwise, and vertical) were tested over the ranges of Mach numbers, angles of attack, and jet total-pressure ratios. The results show that deflecting the wing-tip leading-edge flap from 0° to -10° increased the maximum lift-drag ratio by 1.0 at subsonic speeds. Jet exhaust interference effects were negligible.

INTRODUCTION

Extensive research programs have been conducted to define and meet the design requirements of a commercially acceptable supersonic cruise aircraft. The highly swept arrow-wing supersonic configuration with engine nacelles mounted under the wing has been shown to be aerodynamically efficient at transonic and supersonic speeds (refs. 1 and 2). However, this type of configuration exhibits poor take-off and landing aerodynamic performance (refs. 3 and 4). Tests conducted in low-speed wind tunnels have shown that blowing the jet exhaust over the upper surface of the wing provides an effective means for providing the high lift required for improved take-off and landing performance (ref. 5). An additional benefit from over-the-wing nacelles is the attenuation of the exhaust flow noise during take-off and landing (ref. 6).

The purpose of the present investigation was to determine the influence of upper-surface nacelle exhaust flow on the longitudinal aerodynamic characteristics of a supersonic cruise aircraft research (SCAR) configuration at transonic speeds. The tests were conducted in the Langley 16-foot transonic tunnel at Mach numbers from 0.60 to 1.20 and angles of attack from -4° to 6°. Jet total-pressure ratio was varied from 1 (jet off) to approximately 13. Several chordwise, spanwise, and vertical height locations of the nacelles were investigated. The theoretical program used for this investigation is described in the appendix; a comparison of theoretical results with experimental results is also given.

SYMBOLS

The symbols used in the computer printouts are listed in the second column.

A/B		engine nozzle afterburning-power setting
b	B	wing span, 84.66 cm
C_D		drag coefficient, $\frac{\text{Drag}}{q_\infty S}$
C_L		lift coefficient, $\frac{\text{Lift force}}{q_\infty S}$
C_m		pitching-moment coefficient, $\frac{\text{Pitching moment}}{q_\infty S \bar{c}}$
C_p	CP	pressure coefficient, $\frac{p - p_\infty}{q_\infty}$
c	C	local wing chord at any spanwise location, cm
$\bar{c}$		mean geometric chord of reference wing, 68.92 cm
d_N		maximum nacelle diameter, 4.99 cm
l	L	fuselage length, 141.61 cm
L/D		lift-drag ratio
M		Mach number
p		local static pressure, kPa
$p_{t,j}$		jet total pressure, kPa
p_∞		free-stream static pressure, kPa
$p_{t,j}/p_\infty$		jet total-pressure ratio
q_∞		free-stream dynamic pressure, kPa
S		reference area, 4189.5 cm^2
x	X	longitudinal distance from either fuselage nose or wing leading edge, positive downstream, cm

x_e axial distance from wing leading edge to nacelle exit at any spanwise station, positive downstream, cm

y Y lateral distance from model center plane to nacelle center plane, perpendicular to body center plane, cm

z vertical distance from model reference line, positive up, cm

z_w vertical height of jet exhaust center line (relative to wing upper surface for positive x_e; relative to wing leading edge for negative x_e), positive up, cm

α angle of attack of model, deg

δ_f wing-tip flap deflection angle, relative to model reference line, positive leading edge up, deg

Δz distance from mean camber line, positive up, cm

Subscript:

max maximum

APPARATUS AND METHODS

Wind Tunnel

The Langley 16-foot transonic tunnel is a single-return, continuous-flow, exchange-air-cooled, atmospheric wind tunnel with an octagonal slotted-throat test section. The tunnel has a continuously variable speed range from Mach 0.20 to 1.30. A description of the Langley 16-foot transonic tunnel is given in reference 7. The average Reynolds number per meter varies from 9.4×10^6 at $M = 0.60$ to 12.0×10^6 at $M = 1.20$.

Model Description

A three-view computer-generated drawing of the SCAR configuration, including fundamental model dimensions and jet-nacelle reference planes, is presented in figure 1. The moment center location is for an aircraft with its afterbody and tail. The method used to generate these drawings and the generic development leading to this model are discussed briefly in the appendix. The model consisted of an arrow-wing/body combination having a fuselage length of 141.61 cm and a wing span of 84.66 cm. The wing was highly swept back, twisted, and cambered with reflexed trailing edge. The main wing section had a leading-edge sweep of 74° and the wing tips were swept 60°. A geometric description of the model is given in table I. The wing tips were detachable from the main wing (fig. 1(b)) and were available with both positive and negative leading-edge flap deflections (-10° to 10°). Twin vertical fins were located at the juncture of the main wing and the wing tip. Two engine nacelles were suspended over the wing by pylons as shown in figure 2. However, on the model the engine nacelles

were not mounted on the wing-body configuration and no wing-nacelle pylon was provided to simulate this attachment. A photograph of the model installed in the tunnel test section is shown in figure 3. The sting support system, which also provided the means for supplying high-pressure air, is shown in figures 2 and 3. The high-pressure air was maintained at a controlled temperature near 300 K. The nacelle support was designed to independently support the two nacelles above the wing-body configuration while providing the capability to vary the location of both nacelles relative to the configuration. (See table in fig. 1(a).) The nacelle geometry consisted of an ogive forebody and nozzles configured to simulate a turbofan jet engine operating in both nonafterburning- and afterburning-power modes. (See fig. 4.)

Instrumentation and Tests

Aerodynamic forces and moments on the wing-body configuration were measured with a six-component internal strain-gage balance. Cavity base-pressure measurements were used to adjust the force and moment data to correspond to free-stream static pressure over the model base area. Forces and moments on the nacelles were not measured for these tests. The upper surface of the left wing and lower surface of the right wing were instrumented with static pressure orifices. Pressures were measured on all configurations; however, pressure data are presented for only the basic wing-body and wing-body-nacelle configurations.

Tests were conducted in the Langley 16-foot transonic tunnel over a range of Mach numbers from 0.60 to 1.20. Angle of attack was varied from -4° to 6° and jet total-pressure ratio was varied from 1 (jet off) to approximately 13 depending on Mach number. Summarized in table II are the various test configurations. To insure a turbulent boundary layer, transition trips were applied to the wing-body configuration and nacelles in accordance with the results presented in references 8 and 9.

PRESENTATION OF RESULTS

The results of the investigation are presented in the following figures:

RESULTS AND DISCUSSION

Effects of Wing-Tip Leading-Edge Flap Deflections

The longitudinal aerodynamic characteristics of several wing-tip leading-edge flap deflections are presented in figure 5. These effects are for the wing-body configuration only without the influence of the nacelles. Maximum

lift-drag ratio occurs near a lift coefficient of 0.15 at all Mach numbers. The unstable pitching-moment coefficient (about the center of gravity chosen) results from the model not having the horizontal tail, which is required to balance the longitudinal loads of the aircraft.

Figure 6 shows the variation of maximum lift-drag ratio and pitching-moment coefficient as a function of flap angle. Leading-edge flap deployment from 0° to -10° (leading edge down) increased $(L/D)_{max}$ by 1.0 at most subsonic Mach numbers and by 0.5 at $M = 1.20$. Pitching-moment coefficient also showed a positive trend (destabilizing effect) which indicated that a slight change in tail position would be required to trim the aircraft. As the result of having produced the highest level of L/D, the wing-body configuration with the -10° flap deflection was selected as the baseline configuration to be used in combination with the nacelle variations for all subsequent testing presented in this paper.

Effects of Nacelle-Pylon-Strut Interference

Force and moment measurements.- Aerodynamic force and moment characteristics of the wing-body configuration with and without interference effects due to the jet nacelle-strut assembly (jet-off exhaust flow) are presented in figures 7 to 9. Longitudinal displacement of the nacelle-strut assembly near or ahead of the wing leading edge ($x_e/c = -0.17$ and 0.10) produced higher wing-body pitching moments at all Mach numbers than those for the wing-body with no nacelles. Locating the nacelles near the wing trailing edge ($x_e/c = 0.82$) produced lower pitching moments than those for the no-nacelle configuration. Longitudinal nacelle displacement generally decreased the wing-body minimum drag for the forward wing positions and increased the drag for the aft position (data referenced to wing-body-alone configuration). Lateral displacement of the nacelle-strut assembly from the quarter-semispan station ($y/(b/2) = 0.25$) to the half-semispan station ($y/(b/2) = 0.58$) decreased the wing-body pitching moment for all Mach numbers; this indicated that the nacelle assembly interference effect was diminishing. It should be noted that the level of wing-body pitching moment is greater for the wing-body-nacelle configuration than for the wing-body alone. Lateral movement of the nacelles generally resulted in lower wing-body minimum drag at subsonic speeds than that for the no-nacelle configuration. Vertical nacelle movement (fig. 9) generally had little to no effect on the forces and moments compared with the basic wing-body-nacelle configuration ($x_e/c = -0.17$, $y/(b/2) = 0.46$).

The installation of the nacelle assembly appears to destabilize the flow field over the wing when the nacelle is positioned near the wing leading edge, but the nacelle tends to stabilize the flow field (acts as a tail) when positioned near the wing trailing edge. Whether these effects were the result of just the presence of the jet nacelle or of the combination of the jet nacelle-strut assembly was not determined. Therefore, no correction was applied to the forces and moments due to the nacelle installation effects.

Wing pressure measurements.- The fuselage and wing pressure distributions are presented in figure 10 for the configuration without the jet nacelle-strut assembly and in figure 11 for the configuration with the assembly. Wing pressures in the proximity of the jet nacelles (jet off) appear to be more positive

over both the upper and lower surfaces of the wing at subsonic speeds. Although the nacelle-strut installation influenced the pressure measurements on the upper- and lower-wing surfaces at subsonic speeds, little effect due to the nacelle-strut installation was observed on the wing lower surface at $M = 1.20$.

Effects of Jet Exhaust Flow

The effect of jet operation on the longitudinal aerodynamic characteristics is presented in figures 13 to 20. Jet exhaust flow was varied from jet-off conditions up to a jet total-pressure ratio of approximately 13. Jet interference effects on the wing appeared to have negligible influence on the wing-body forces and moments at all Mach numbers and nacelle locations investigated. This result indicates that the jet plume did not wash the wing upper surface and that there was no overall variation of the wing flow field due to jet operation. Pressure distributions, shown in figure 12 at a jet total-pressure ratio of 6 to indicate maximum influence of the jet exhaust flow, show pronounced local effect from jet operation. (See $y/(b/2) = 0.450$ and 0.555 in fig. 12.) These pressure perturbations appeared to be self-compensating, however, such that little effect of jet operation occurred in the total wing-body forces and moments, as noted earlier. Comparison of figures 13 and 20 shows that nozzle exit size (A/B or non-A/B) had no apparent effect on the aerodynamic forces and moments. (Table III lists the symbols used in these figures to represent the various angles of attack.)

SUMMARY OF RESULTS

An investigation was conducted in the Langley 16-foot transonic tunnel to determine the influence of upper-surface nacelles on a supersonic cruise aircraft at Mach numbers from 0.60 to 1.20. The following results are indicated from this study:

1. Wing-tip leading-edge flap deployment of -10° increased maximum lift-drag ratio by 1.0 at most subsonic speeds.

2. Jet exhaust interference effects were negligible at all test conditions.

Langley Research Center
National Aeronautics and Space Administration
Hampton, VA 23665
September 27, 1979

APPENDIX

THEORETICAL PREDICTIONS OF PRESSURE DISTRIBUTIONS AND LIFT COEFFICIENTS

The computer program described in reference 10 was used to generate drawings of the four-engine aircraft of references 1 to 4 and the two-engine aircraft of reference 5. These drawings are shown in figures 21(a) and 21(b), respectively. Drawings of any aircraft configuration at any viewing angle can be generated by this program. Figure 21(c) shows a computer-generated drawing of the model of this investigation modified as required for the theoretical prediction program described in references 11 and 12.

The three-dimensional aerodynamics computer program (refs. 11 and 12) was used to predict static pressure distributions and forces and moments on the SCAR configuration with upper-surface nacelles. The method of computations is summarized as follows: The configuration surface is divided into numerous quadrilateral panel sections, each containing an aerodynamic singularity. A constant source distribution is used on the body panels, and a vortex distribution having a linear variation in the streamwise direction is used on the wing and tail panels. The normal components of velocity induced at specified control points by each singularity distribution are calculated and make up the coefficients of a system of linear equations relating the strengths of the singularities to the magnitudes of the normal velocities. Singularity strengths which satisfy the boundary condition of the tangential flow of the control points for a given Mach number and angle of attack are determined by solving this system of equations with an iterative procedure. Once the singularity strengths are known, the pressure, force, and moment coefficients acting on the configuration can be determined. This program accepts the jet nacelles as input but does not take into account the influence of the nacelles in the aerodynamic calculations. Therefore, the nacelles were input as bodies parallel to the main body in order to determine their effect on pressure distribution and lift. The jet plumes were numerically described as solid bodies having a diameter equal to the real jet exhaust and extending downstream from the nozzle exit to the end of the model sting support.

Although all configurations listed in table I were processed over a wide range of Mach numbers and angles of attack, only a few representative samples are presented in this paper, since only minor variations in the computed values are observed. Predicted lift coefficients at various angles of attack for Mach numbers of 0.90 and 1.20 are shown in figure 22. The computer program of references 11 and 12 considers the lift-curve slope to be linear. Therefore, only two cases per Mach number were considered. The lift-curve slopes for the subsonic Mach numbers are the same; therefore, data are presented only for $M = 0.90$. The predicted lift curve is similar to the measured values but at a slightly higher level, as indicated by the dashed line shown in figure 23.

Using reference 10 as a base, a computer program was developed to visualize the model fuselage center line profile and wing airfoil profiles at 11 spanwise locations. These profiles obtained from the numerical model also describe the

physical model and are used in the computation of predicted pressure coefficients. Predicted longitudinal pressure coefficients are presented in figure 24 for Mach numbers of 0.90 and 1.20, angle of attack of 4^{o}, and with and without jet nacelles and exhaust plumes. A comparison between experimental pressure coefficients and the theory of reference 11 is shown in figure 25. The comparison appears to be poor, mainly because the theory did not account for vortex flow, which apparently forms on the wing leading edge.

REFERENCES

1. Morris, Odell A.; and Fournier, Roger H.: Aerodynamic Characteristics at Mach Numbers 2.30, 2.60, and 2.96 of a Supersonic Transport Model Having a Fixed, Warped Wing. NASA TM X-1115, 1965.

2. Harris, Roy V., Jr.; and Corlett, William A.: Transonic Aerodynamic Characteristics of a Supersonic Transport Model With Variable-Sweep Auxiliary Wing Panels, Outboard Tail Surfaces, and a Design Mach Number of 2.6. NASA TM X-1075, 1965.

3. Henderson, William P.: Low-Speed Aerodynamic Characteristics of a Supersonic Transport Model With a Highly Swept, Twisted and Cambered, Fixed Wing. NASA TM X-1249, 1966.

4. Henderson, William P.: A Low-Speed Longitudinal Stability Improvement Study on a Highly Swept Supersonic Transport Configuration. NASA TM X-1071, 1965.

5. Shivers, James P.; McLemore, H. Clyde; and Coe, Paul L., Jr.: Low-Speed Wind-Tunnel Investigation of a Large-Scale Advanced Arrow-Wing Supersonic Transport Configuration With Engines Mounted Above Wing for Upper-Surface Blowing. NASA TN D-8350, 1976.

6. Campbell, John P.: Overview of Powered-Lift Technology. Powered-Lift Aerodynamics and Acoustics, NASA SP-406, 1976, pp. 1-27.

7. Corson, Blake W., Jr.; Runckel, Jack F.; and Igoe, William B.: Calibration of the Langley 16-Foot Transonic Tunnel With Test Section Air Removal. NASA TR R-423, 1974.

8. Braslow, Albert L.; Hicks, Raymond M.; and Harris, Roy V., Jr.: Use of Grit-Type Boundary-Layer-Transition Trips on Wind-Tunnel Models. NASA TN D-3579, 1966.

9. Braslow, Albert L.; and Knox, Eugene C.: Simplified Method for Determination of Critical Height of Distributed Roughness Particles for Boundary-Layer Transition at Mach Numbers From 0 to 5. NACA TN 4363, 1958.

10. Craidon, Charlotte B.: Description of a Digital Computer Program for Airplane Configuration Plots. NASA TM X-2074, 1970.

11. Woodward, F. A.: An Improved Method for the Aerodynamic Analysis of Wing-Body-Tail Configurations in Subsonic and Supersonic Flow. Part I - Theory and Application. NASA CR-2228, Pt. I, 1973.

12. Woodward, F. A.: An Improved Method for the Aerodynamic Analysis of Wing-Body-Tail Configurations in Subsonic and Supersonic Flow. Part II - Computer Program Description. NASA CR-2228, Pt. II, 1973.

TABLE I.- GEOMETRIC DESCRIPTION OF MODEL

(a) Wing

Spanwise airfoil section coordinates				
Airfoil section	x/l	y/l	z/l	c/l
1	0.269	0.024	-0.018	0.710
2	.286	.029	-.022	.692
3	.328	.041	-.029	.650
4	.389	.059	-.036	.589
5	.491	.088	-.043	.486
6	.532	.100	-.046	.444
7	.593	.117	-.050	.389
8	.678	.142	-.053	.311
9	.743	.164	-.055	.252
10	.776	.176	-.057	.229
11	.895	.217	-.061	.148
12	.895	.217	-.061	.148
13	1.036	.298	-.061	.081

TABLE I.- Continued

(a) Continued

Chord location, x/c, percent	Mean camber line, Δz/l, for -												
	Airfoil section												
	1	2	3	4	5	6	7	8	9	10	11	12	13
0	0.000	0.000	0.000	0.000	0.000	0.000	0.000	0.000	0.000	0.000	0.000	0.000	0.000
.125	.000	.000	.000	.000	.000	.000	.000	.000	.000	.000	.000	.000	.000
.25	.000	.000	.000	.000	.000	.000	.000	.000	.000	.000	.000	.000	.000
.5	.000	.000	.000	.000	.000	.000	.000	.000	.000	.000	.000	.000	.000
.75	.000	.000	.000	.000	.000	.000	.000	.000	.000	.000	.000	.000	.000
1.0	.000	.000	.000	.000	.000	.000	.000	.000	.000	.000	.000	.000	.000
1.5	-.000	.000	.000	.000	.000	.000	.000	.000	.000	.000	.000	.000	.000
2.5	-.000	-.000	.000	.000	.000	.001	.000	.000	.000	.000	.000	.000	.000
5.0	-.001	-.000	.000	.001	.001	.001	.001	.001	.000	.000	.000	.000	.000
10.0	-.002	-.001	-.000	.000	.001	.002	.001	.001	.001	.000	.000	.000	.000
15.0	-.005	-.004	-.002	-.001	.001	.001	.001	.001	.001	.001	.000	.000	.000
20.0	-.008	-.006	-.004	-.002	.000	.001	.001	.001	.001	.001	.000	.000	.000
30.0	-.015	-.012	-.009	-.005	-.002	-.000	.001	.001	.001	.001	.000	.000	.000
40.0	-.023	-.019	-.014	-.009	-.004	-.002	-.001	-.000	.000	.000	.000	.000	.000
50.0	-.030	-.026	-.019	-.013	-.006	-.004	-.002	-.001	-.000	-.000	-.000	-.000	.000
60.0	-.037	-.032	-.025	-.017	-.009	-.006	-.004	-.002	-.001	-.001	-.000	-.000	.000
65.0	-.040	-.035	-.027	-.019	-.010	-.008	-.005	-.002	-.001	-.001	-.001	-.001	.000
70.0	-.043	-.038	-.029	-.021	-.012	-.009	-.006	-.003	-.001	-.001	-.001	-.001	.000
75.0	-.045	-.040	-.032	-.023	-.013	-.010	-.006	-.003	-.002	-.001	-.001	-.001	.000
80.0	-.048	-.043	-.034	-.025	-.015	-.011	-.007	-.004	-.002	-.002	-.001	-.001	.000
85.0	-.050	-.045	-.036	-.027	-.016	-.012	-.008	-.005	-.002	-.002	-.001	-.001	.000
90.0	-.052	-.047	-.038	-.029	-.017	-.013	-.009	-.005	-.003	-.002	-.001	-.001	.000
95.0	-.054	-.049	-.040	-.030	-.019	-.015	-.010	-.006	-.003	-.003	-.002	-.002	.000
100.0	-.056	-.050	-.041	-.032	-.020	-.016	-.011	-.006	-.004	-.003	-.002	-.002	.000

TABLE I.- Continued

(a) Concluded

Chord location, x/c, percent	Half thickness, z/c, for - Airfoil section												
	1	2	3	4	5	6	7	8	9	10	11	12	13
0	0.000	0.000	0.000	0.000	0.000	0.000	0.000	0.000	0.000	0.000	0.000	0.000	0.000
.125	.182	.182	.182	.182	.182	.182	.182	.182	.198	.198	.198	.007	.007
.25	.253	.253	.253	.253	.253	.253	.253	.253	.275	.275	.275	.014	.014
.5	.345	.345	.345	.345	.345	.345	.345	.345	.371	.371	.371	.028	.028
.75	.405	.405	.405	.405	.405	.405	.405	.405	.431	.431	.431	.042	.042
1.0	.452	.452	.452	.452	.452	.452	.452	.452	.470	.470	.470	.056	.056
1.5	.526	.526	.526	.526	.526	.526	.526	.526	.521	.521	.521	.083	.084
2.5	.653	.653	.653	.653	.653	.653	.653	.653	.594	.594	.594	.137	.139
5.0	.839	.835	.828	.826	.823	.826	.823	.823	.716	.716	.723	.267	.271
10.0	1.022	1.010	.992	.975	.965	.975	.965	.965	.879	.879	.903	.505	.512
15.0	1.131	1.110	1.083	1.055	1.039	1.055	1.039	1.039	.982	.982	1.032	.716	.726
20.0	1.217	1.190	1.151	1.120	1.096	1.120	1.096	1.096	1.065	1.065	1.128	.898	.911
30.0	1.348	1.317	1.256	1.207	1.175	1.207	1.175	1.175	1.192	1.192	1.268	1.179	1.196
40.0	1.430	1.392	1.317	1.270	1.233	1.252	1.234	1.232	1.292	1.274	1.364	1.347	1.367
50.0	1.485	1.432	1.357	1.297	1.259	1.264	1.269	1.254	1.329	1.307	1.403	1.403	1.424
60.0	1.514	1.455	1.363	1.284	1.224	1.220	1.218	1.203	1.276	1.254	1.347	1.347	1.367
65.0	1.490	1.425	1.321	1.233	1.165	1.159	1.155	1.141	1.209	1.189	1.277	1.277	1.295
70.0	1.419	1.351	1.242	1.150	1.079	1.071	1.066	1.053	1.116	1.098	1.179	1.179	1.196
75.0	1.301	1.233	1.127	1.038	.967	.959	.952	.940	.997	.980	1.052	1.052	1.068
80.0	1.136	1.071	.973	.892	.827	.818	.812	.802	.851	.836	.898	.898	.911
85.0	.922	.869	.785	.716	.661	.653	.647	.639	.678	.666	.719	.716	.726
90.0	.662	.621	.559	.507	.468	.460	.457	.451	.478	.470	.507	.505	.512
95.0	.354	.332	.298	.270	.247	.244	.241	.238	.253	.248	.268	.267	.271
100.0	.000	.000	.000	.000	.000	.000	.000	.000	.000	.000	.000	.000	.000

TABLE I.- Continued

(b) Fuselage half section coordinates

Fuselage station, x/l													
1, x/l = 0.0		2, x/l = 0.043		3, x/l = 0.087		4, x/l = 0.130		5, x/l = 0.174		6, x/l = 0.260		7, x/l = 0.347	
y/l	z/l	y/l	z/l	y/l	z/l	y/l	z/l	y/l	z/l	y/l	z/l	y/l	z/l
0.000	0.000	0.000	-0.007	0.000	-0.013	0.000	-0.017	0.000	-0.021	0.000	-0.026	0.000	-0.032
		.002	-.007	.003	-.012	.005	-.016	.006	-.020	.007	-.025	.008	-.031
		.004	-.006	.006	-.011	.009	-.014	.011	-.018	.013	-.023	.016	-.026
		.006	-.004	.010	-.008	.014	-.010	.017	-.012	.019	-.013	.024	-.013
		.008	.000	.013	.000	.018	.001	.022	.001	.026	-.000	.025	-.007
		.008	.002	.013	.004	.017	.005	.021	.007	.025	.007	.024	-.001
		.007	.005	.011	.009	.014	.012	.018	.014	.021	.016	.020	.008
		.000	.009	.000	.015	.000	.019	.000	.023	.000	.026	.000	.018

8, x/l = 0.434		9, x/l = 0.521		10, x/l = 0.608		11, x/l = 0.695		12, x/l = 0.738		13, x/l = 0.781		14, x/l = 0.825	
y/l	z/l	y/l	z/l	y/l	z/l	y/l	z/l	y/l	z/l	y/l	z/l	y/l	z/l
0.000	-0.040	0.000	-0.050	0.000	-0.060	0.000	-0.069	0.000	-0.072	0.000	-0.074	0.000	-0.075
.006	-.040	.007	-.049	.011	-.059	.012	-.068	.012	-.071	.011	-.073	.011	-.075
.012	-.037	.014	-.048	.019	-.058	.020	-.066	.020	-.070	.020	-.072	.020	-.074
.024	-.019	.024	-.027	.024	-.036	.024	-.044	.024	-.048	.024	-.052	.024	-.056
.024	-.016	.024	-.024	.024	-.036	.024	-.043	.024	-.046	.024	-.050	.024	-.054
.024	-.010	.024	-.018	.024	-.026	.024	-.032	.024	-.034	.024	-.037	.024	-.041
.019	-.001	.019	-.010	.020	-.017	.020	-.024	.019	-.026	.019	-.029	.020	-.032
.000	.008	.000	-.000	.000	-.007	.000	-.014	.000	-.017	.000	-.020	.000	-.022

15, x/l = 0.868		16, x/l = 0.912		17, x/l = 1.000	
y/l	z/l	y/l	z/l	y/l	z/l
0.000	-0.076	0.000	-0.077	0.000	-0.079
.010	-.076	.009	-.076	.009	-.077
.019	-.075	.018	-.075	.018	-.076
.024	-.061	.024	-.066	.024	-.076
.023	-.057	.022	-.061	.021	-.065
.024	-.043	.023	-.046	.022	-.050
.019	-.035	.019	-.038	.019	-.043
.000	-.025	.000	-.028	.000	-.034

TABLE I.- Concluded

(c) Vertical stabilizers

Airfoil coordinates		
	Upper	Lower
x/l	0.905	1.061
y/l	.215	.215
z/l	-.059	-.012
c/l	.166	.023

Chord location x/c, percent	Half thickness, z/c
0.0	0.0
10.0	.466
20.0	.846
30.0	1.138
40.0	1.345
50.0	1.465
70.0	1.498
80.0	1.390
90.0	.641
100.0	0

TABLE II.- TEST CONFIGURATIONS

[Nacelle locations are fuselage oriented]

δ_f, deg	x_e/c	$y/(b/2)$	z_w/d_N	Engine power
Force tests				
0				No jets
10				No jets
-5				No jets
-10				No jets
-10	-0.170	0.462	1.497	A/B, basic configuration
-10	.102	.462	1.467	A/B
-10	.820	.462	1.626	A/B
-10	.308	.249	1.166	A/B
-10	-.686	.580	1.602	A/B
-10	-.170	.462	1.748	A/B
-10	-.170	.462	1.247	A/B
-10	-.170	.462	1.497	Non-A/B
Pressure tests				
-10				No jets
-10	-0.170	0.462	1.497	A/B, basic configuration
-10	.102	.462	1.467	A/B
-10	.820	.462	1.626	A/B
-10	.308	.249	1.166	A/B
-10	-.686	.580	1.602	A/B
-10	-.170	.462	1.748	A/B
-10	-.170	.462	1.247	A/B
-10	-.170	.462	1.497	Non-A/B

TABLE III.- SYMBOLS USED FOR THE ANGLES OF ATTACK IN AERODYNAMIC DATA FIGURES 13 AND 20

Mach number	α, deg	Figure 13 (A/B)	Figure 20 (non-A/B)
0.60	-4.0	○	None
	-1.8	□	○
	.4	◇	□
	1.5	△	None
	2.6	◺	◇
	3.7	◹	None
	4.8	⌓	△
	7.1	◇	◺
0.80	-4.0	○	None
	-1.7	□	○
	.6	◇	□
	1.7	△	None
	2.9	◺	◇
	4.1	◹	None
	5.3	⌓	△
	7.8	◇	◺
0.90	-4.0	○	None
	-1.7	□	○
	.6	None	□
	.7	◇	None
	1.9	△	None
	3.0	None	◇
	3.1	◺	None
	4.3	◹	None
	5.5	⌓	△
	7.9	None	◺
	8.0	◇	None
0.95	-4.0	None	○
	-3.9	○	None
	-1.6	□	□
	.7	None	◇
	.8	◇	None
	2.0	△	None
	3.1	None	△
	3.2	◺	None
	4.4	◹	None
	5.6	None	◺
	5.7	⌓	None
	8.1	◇	None
1.20	-3.7	○	○
	-1.4	□	□
	.9	◇	◇
	2.2	△	None
	3.3	None	△
	3.4	◺	None
	4.6	◹	None
	5.7	None	◺
	5.8	⌓	None

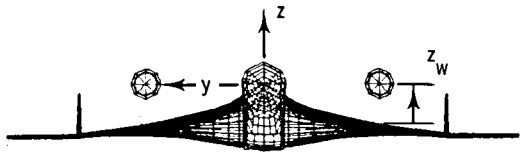

Front view

Wing oriented jet nacelle locations

x_e/c	$y/(b/2)$	z_w/d_N
0.170	0.462	1.50
.102	.462	1.47
.820	.462	1.63
.308	.249	1.17
-0.686	.580	1.60
-0.170	.462	1.75
-0.170	.462	1.25

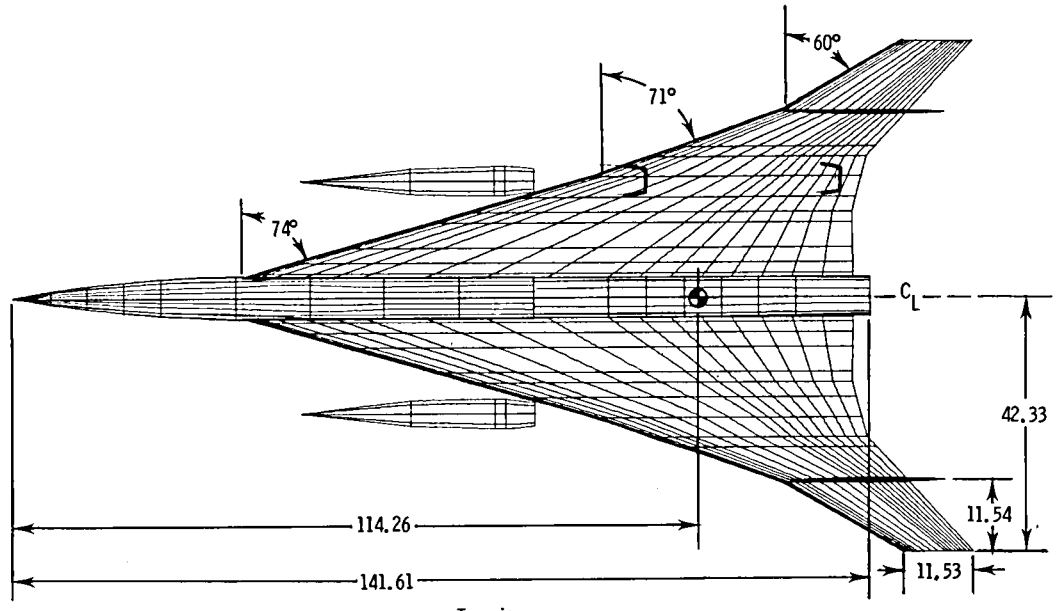

Top view

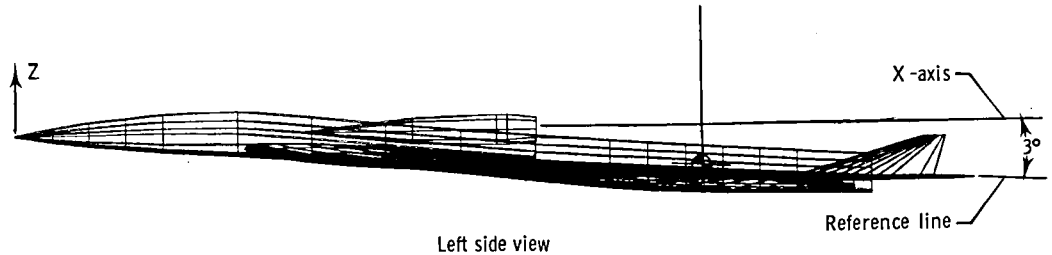

Left side view

(a) Three-view computer drawing.

Figure 1.- Assembly, dimensions, and orientation of model and jet nacelles. Dimensions are in centimeters.

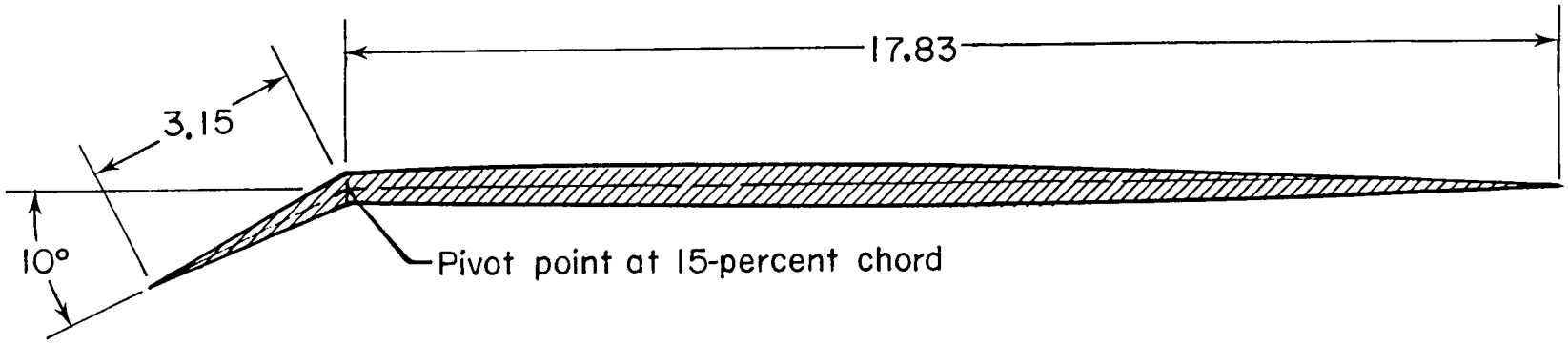

(b) Root section of outboard wing with leading-edge flap deflection of -10°.

Figure 1.- Concluded.

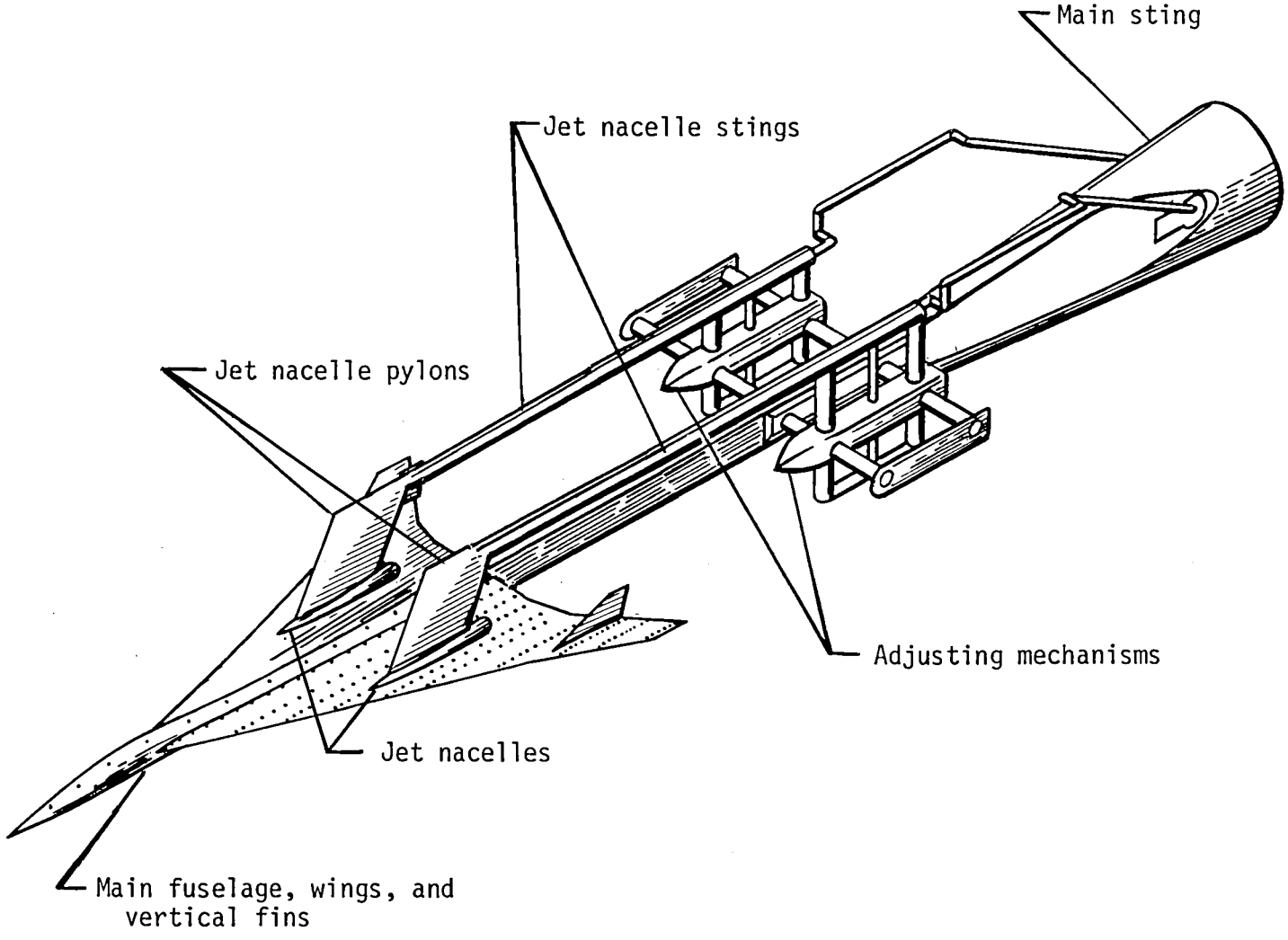

Figure 2.- Sketch of model and air-powered sting system.

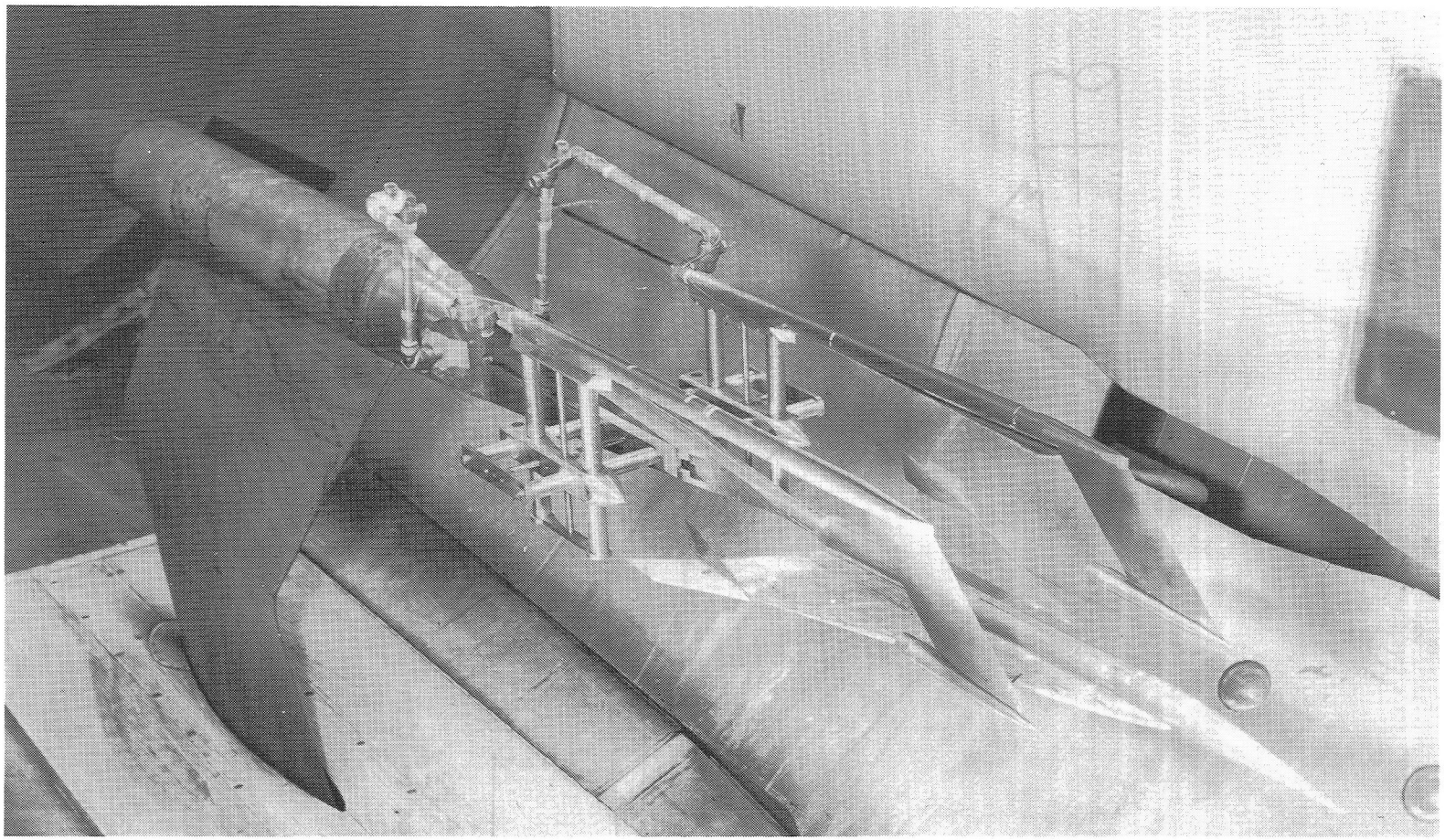

L-75-9120

Figure 3.- Model in Langley 16-foot transonic tunnel test section.

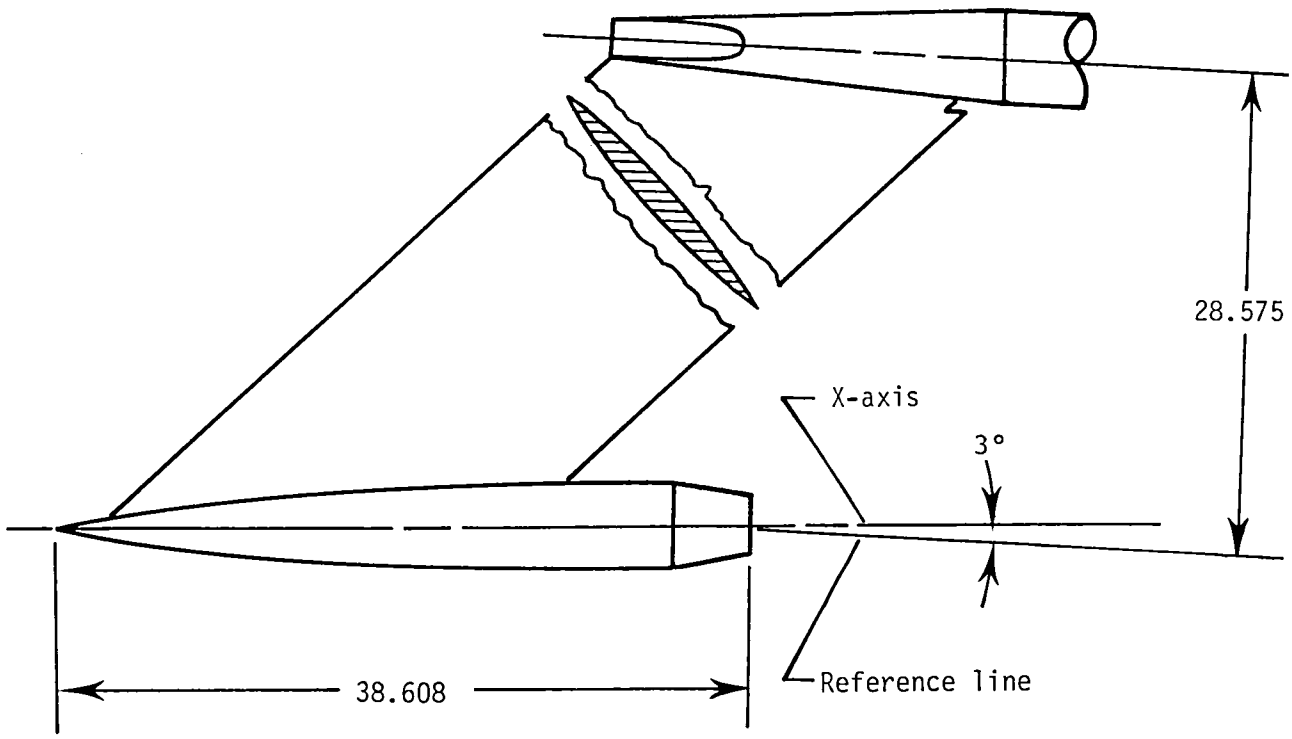

(a) Jet nacelle with A/B nozzle and forward suspension strut assembly.

Figure 4.- Propulsion simulation system. Dimensions are in centimeters.

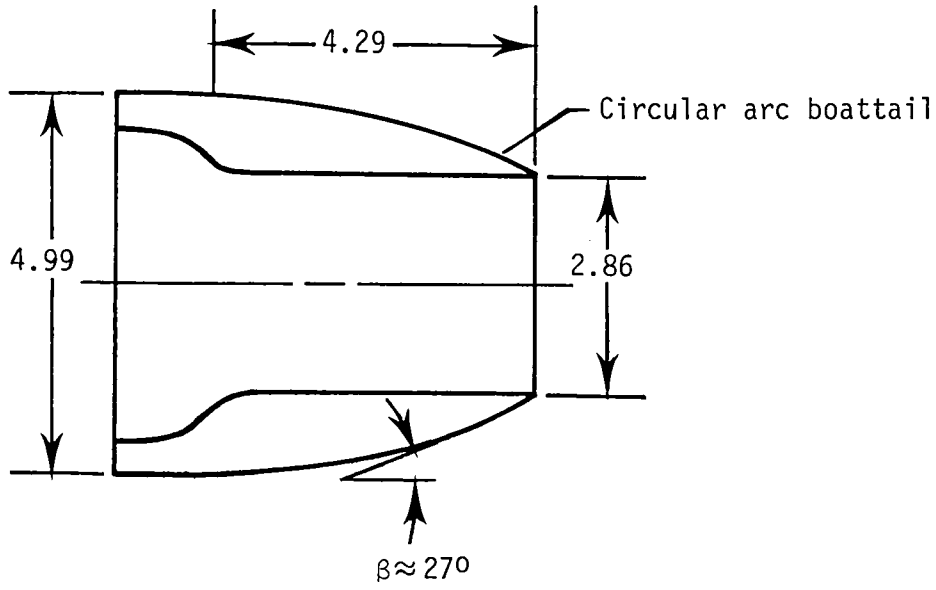

Non A/B

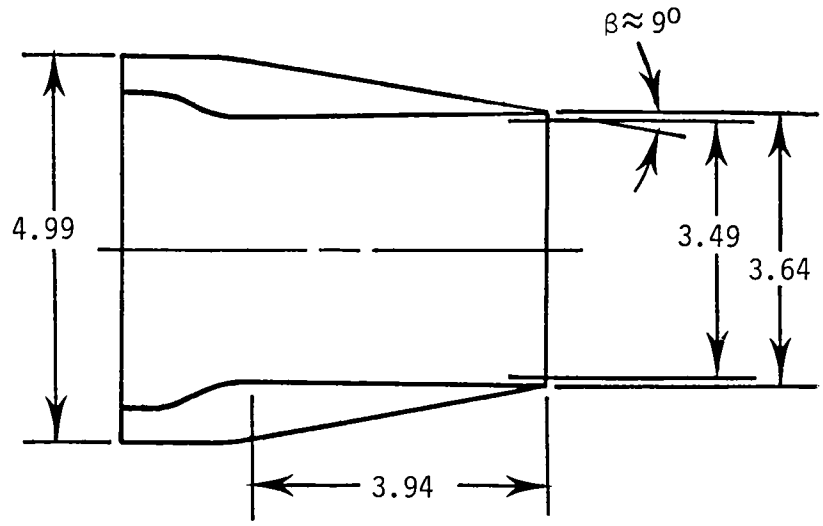

A/B

(b) Detail of nozzles.

Figure 4.- Concluded.

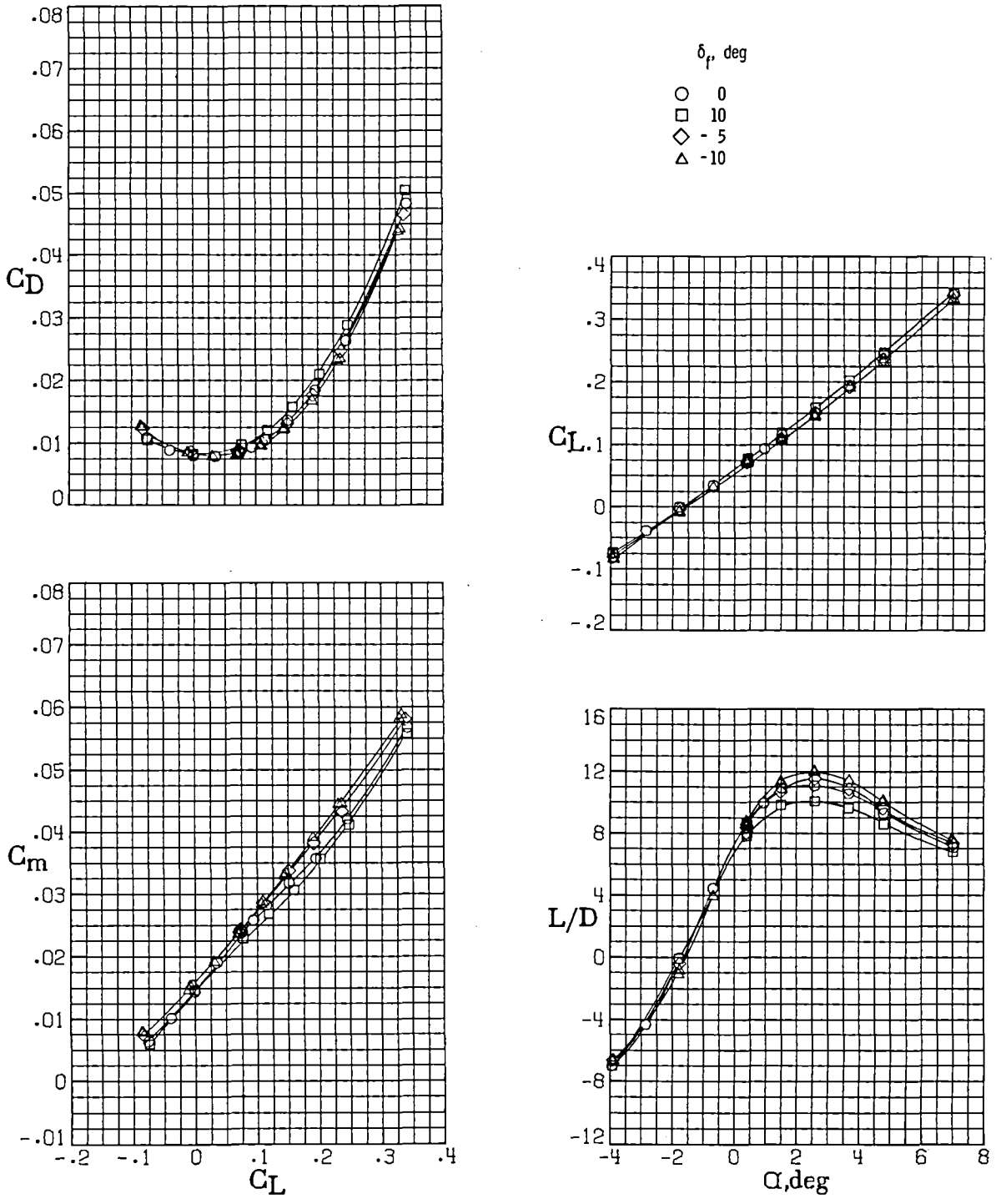

(a) M = 0.60.

Figure 5.- Effect of several wing-tip leading-edge flap deflections on longitudinal aerodynamic characteristics of wing-body configuration.

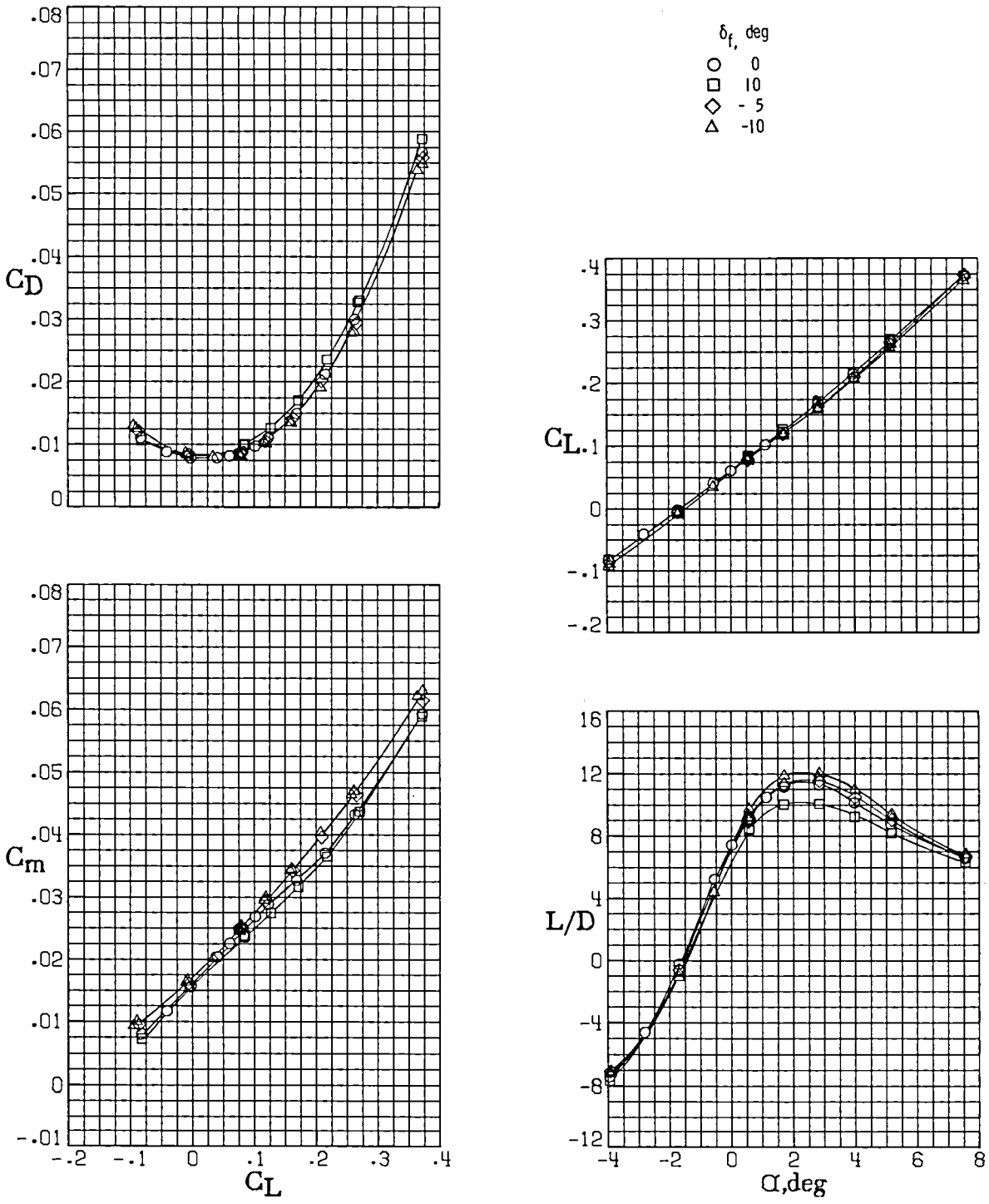

(b) M = 0.80.

Figure 5.- Continued.

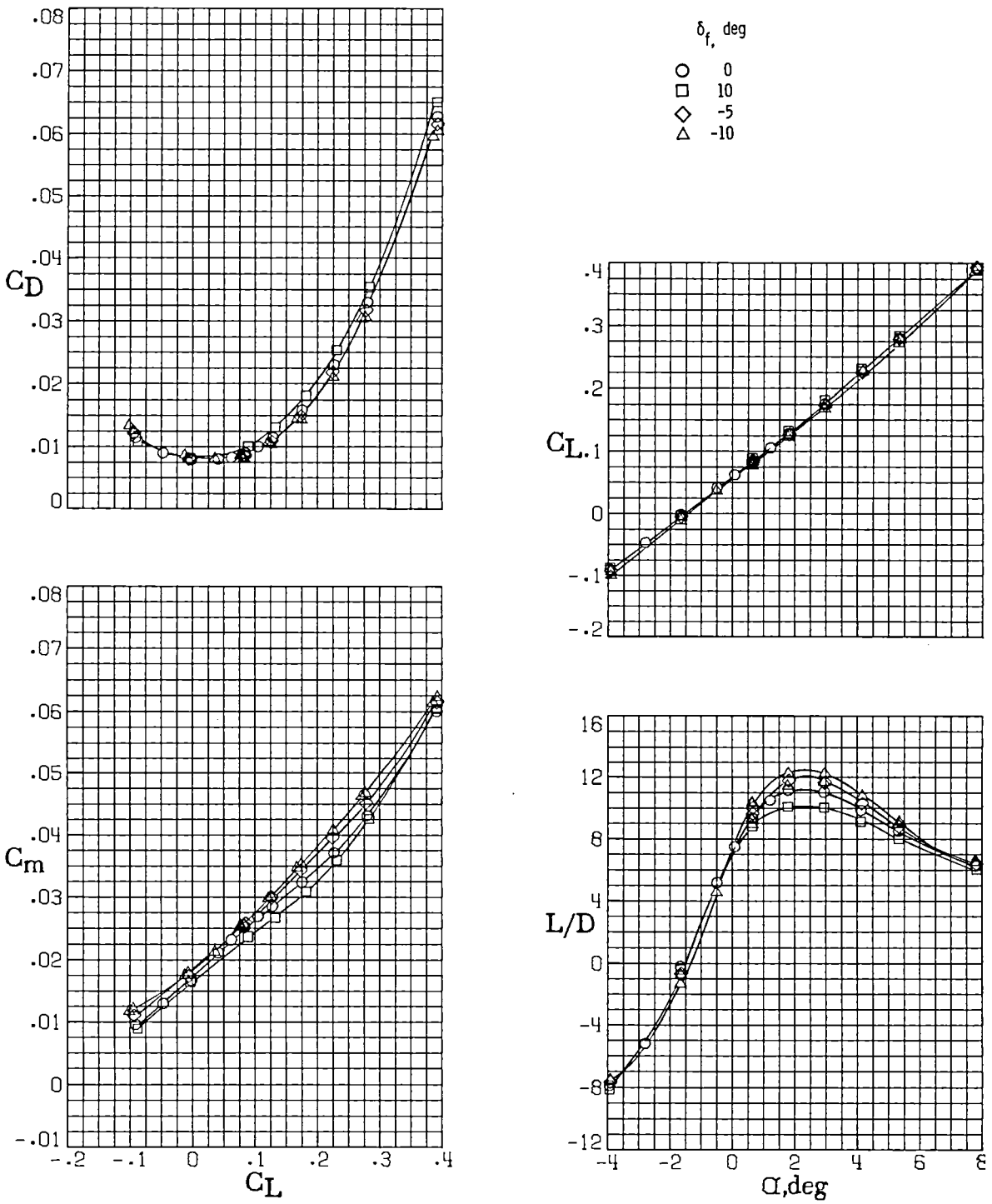

(c) M = 0.90.

Figure 5.- Continued.

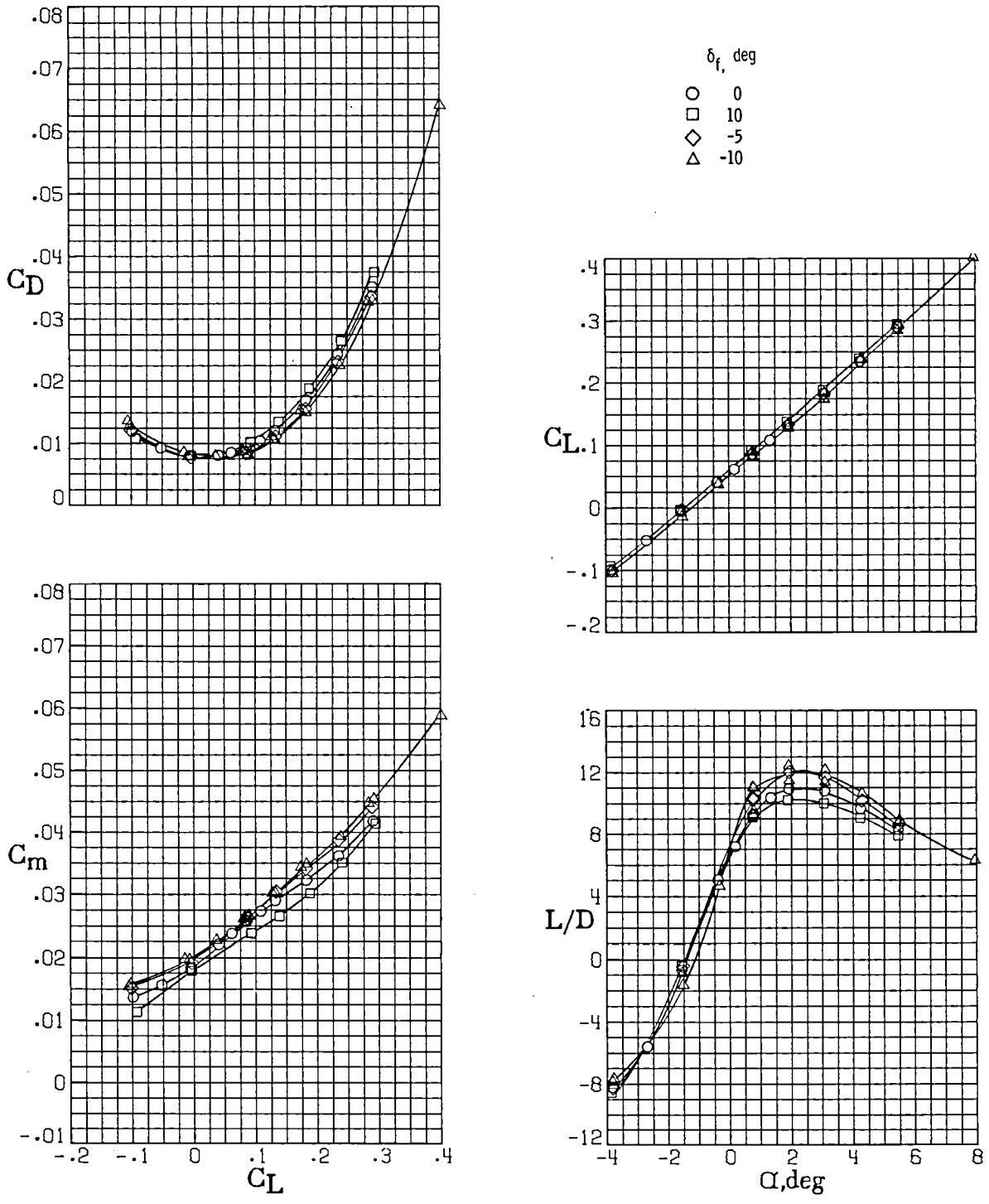

(d) M = 0.95.

Figure 5.- Continued.

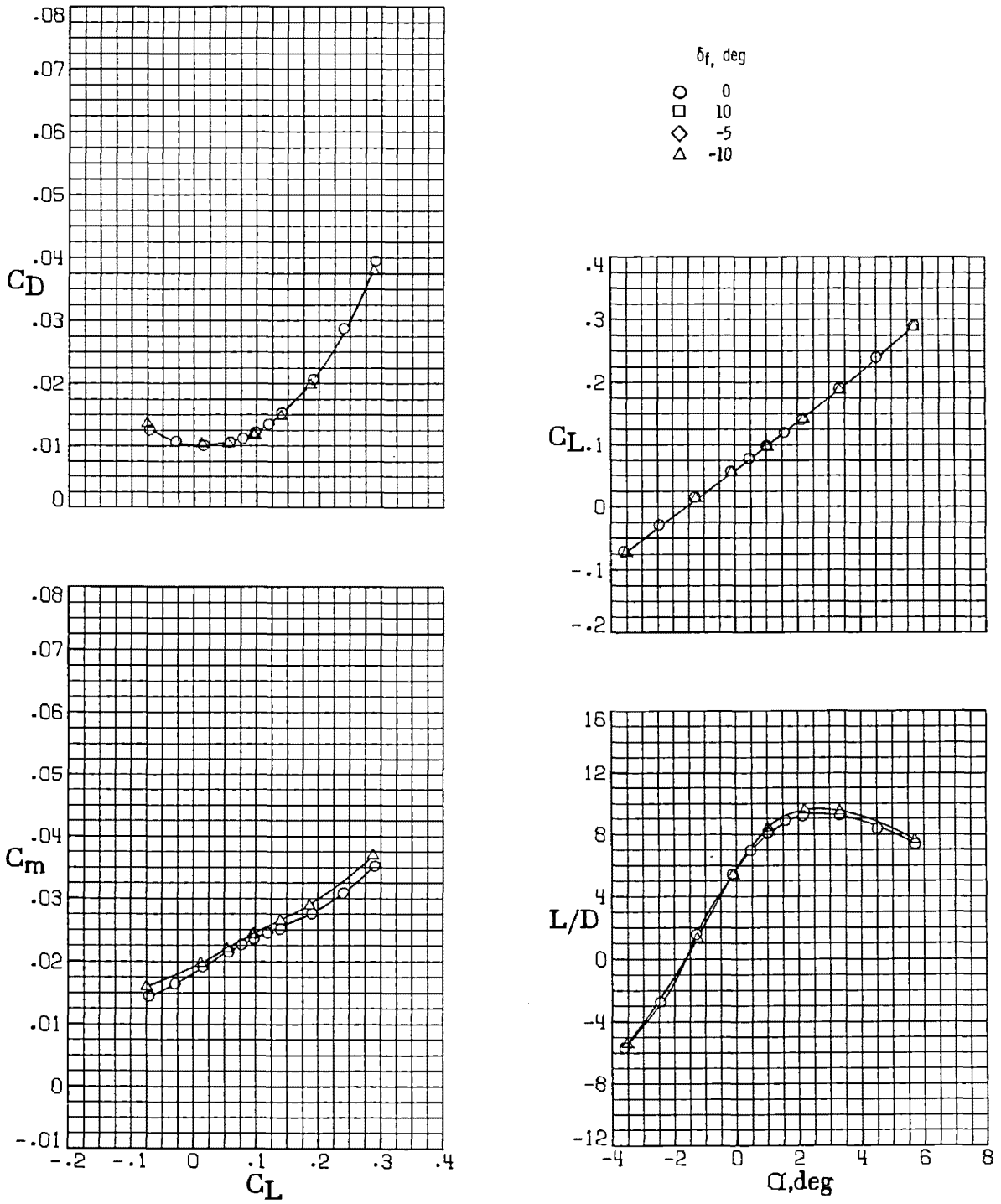

(e) M = 1.20.

Figure 5.- Concluded.

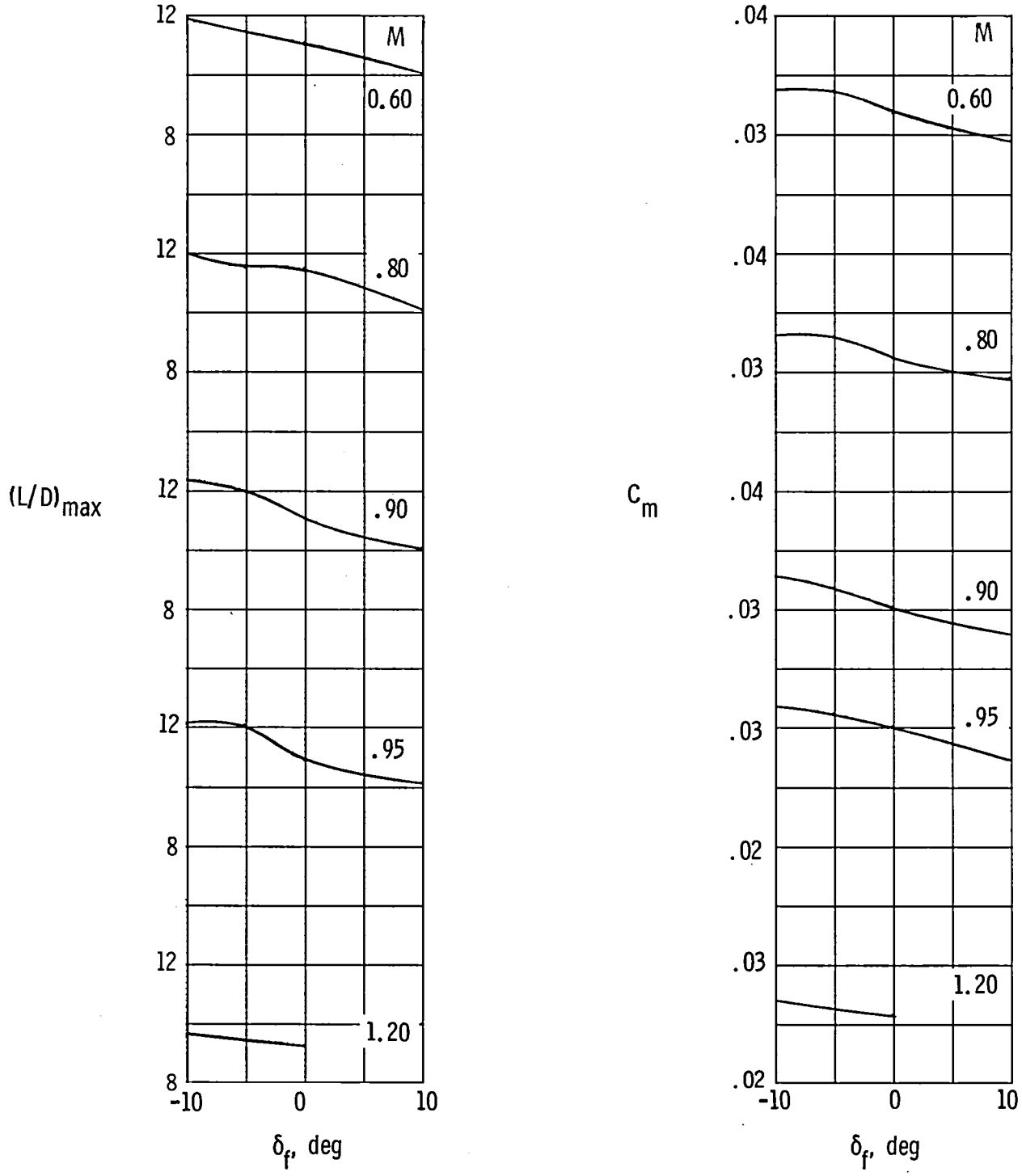

Figure 6.- Effect of wing-tip leading-edge flap deflections on maximum lift-drag ratio and pitching-moment coefficient at $C_L = 0.15$.

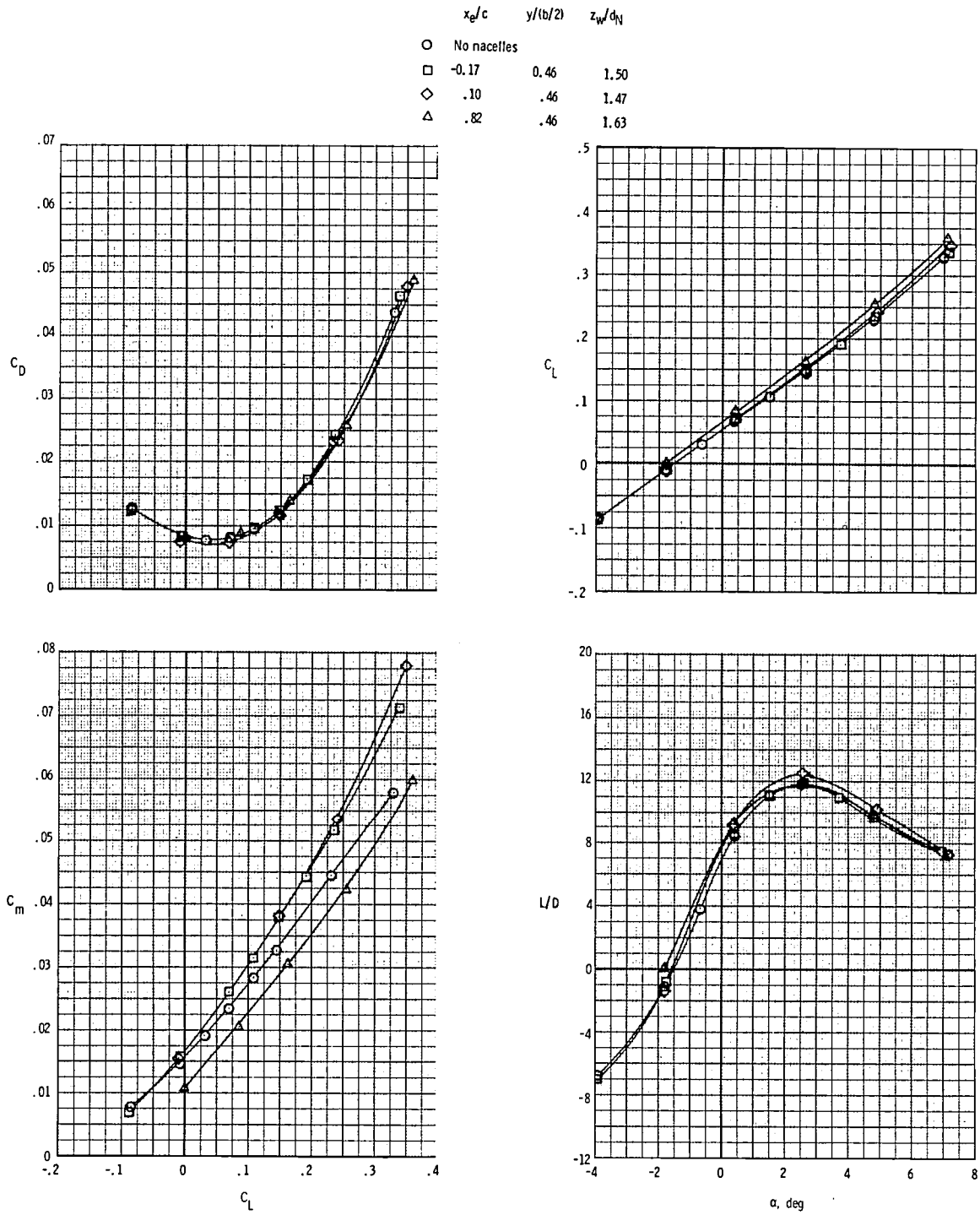

(a) M = 0.60.

Figure 7.- Effects of longitudinal displacement of nacelle-strut assembly on longitudinal aerodynamic force and moment characteristics with jet off and δ_f at -10°.

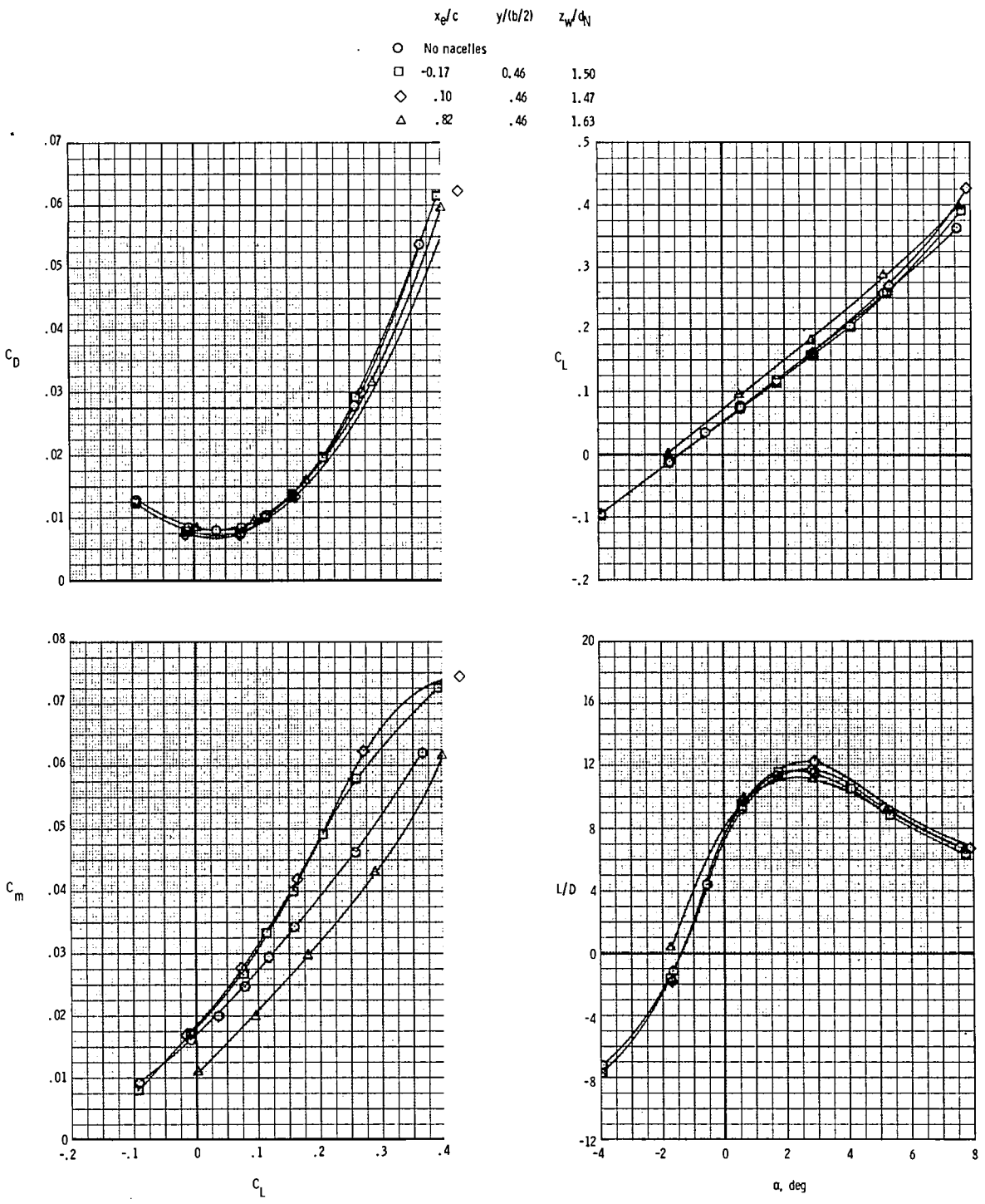

(b) M = 0.80.

Figure 7.- Continued.

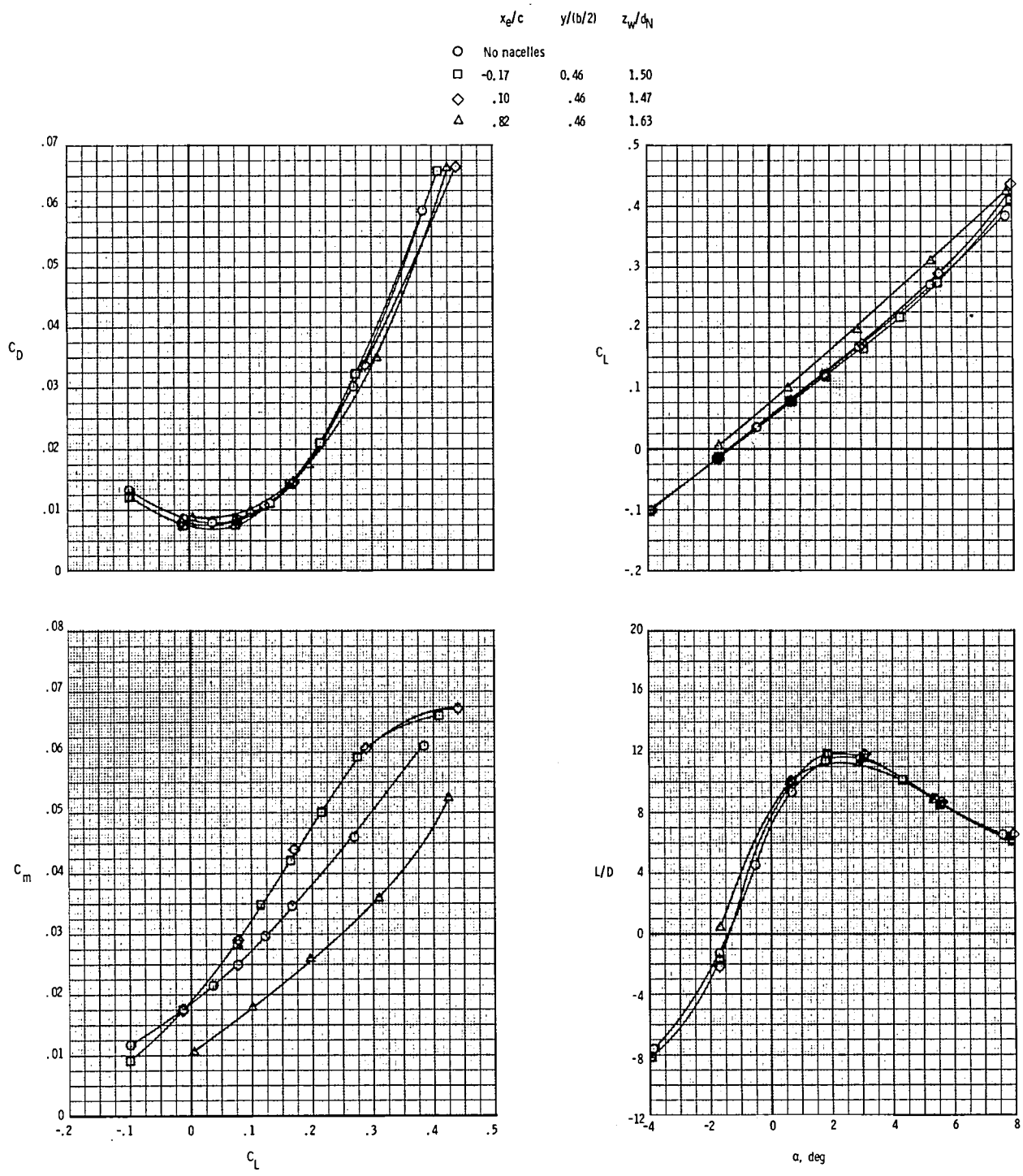

(c) M = 0.90.

Figure 7.- Continued.

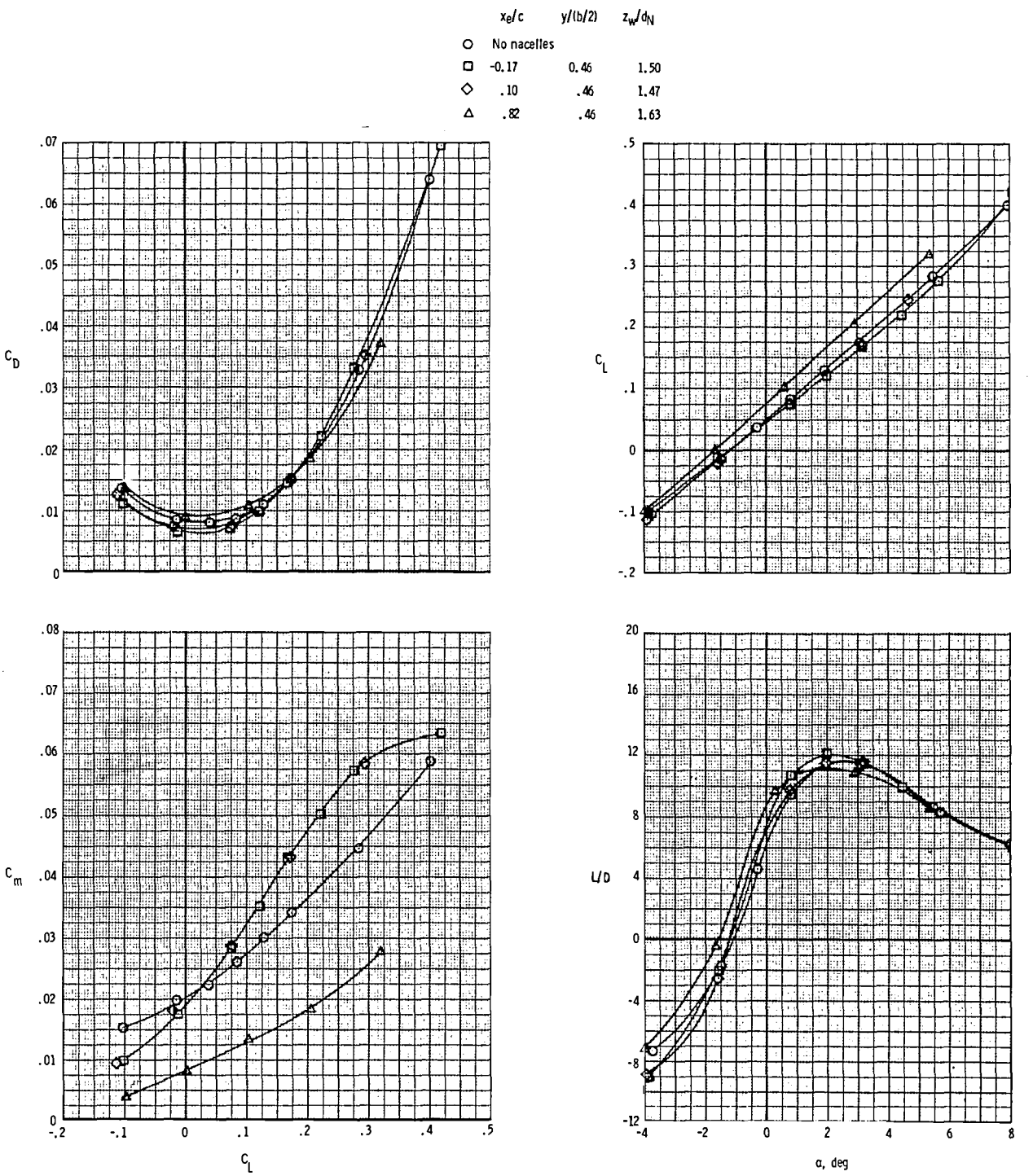

(d) M = 0.95.

Figure 7.- Continued.

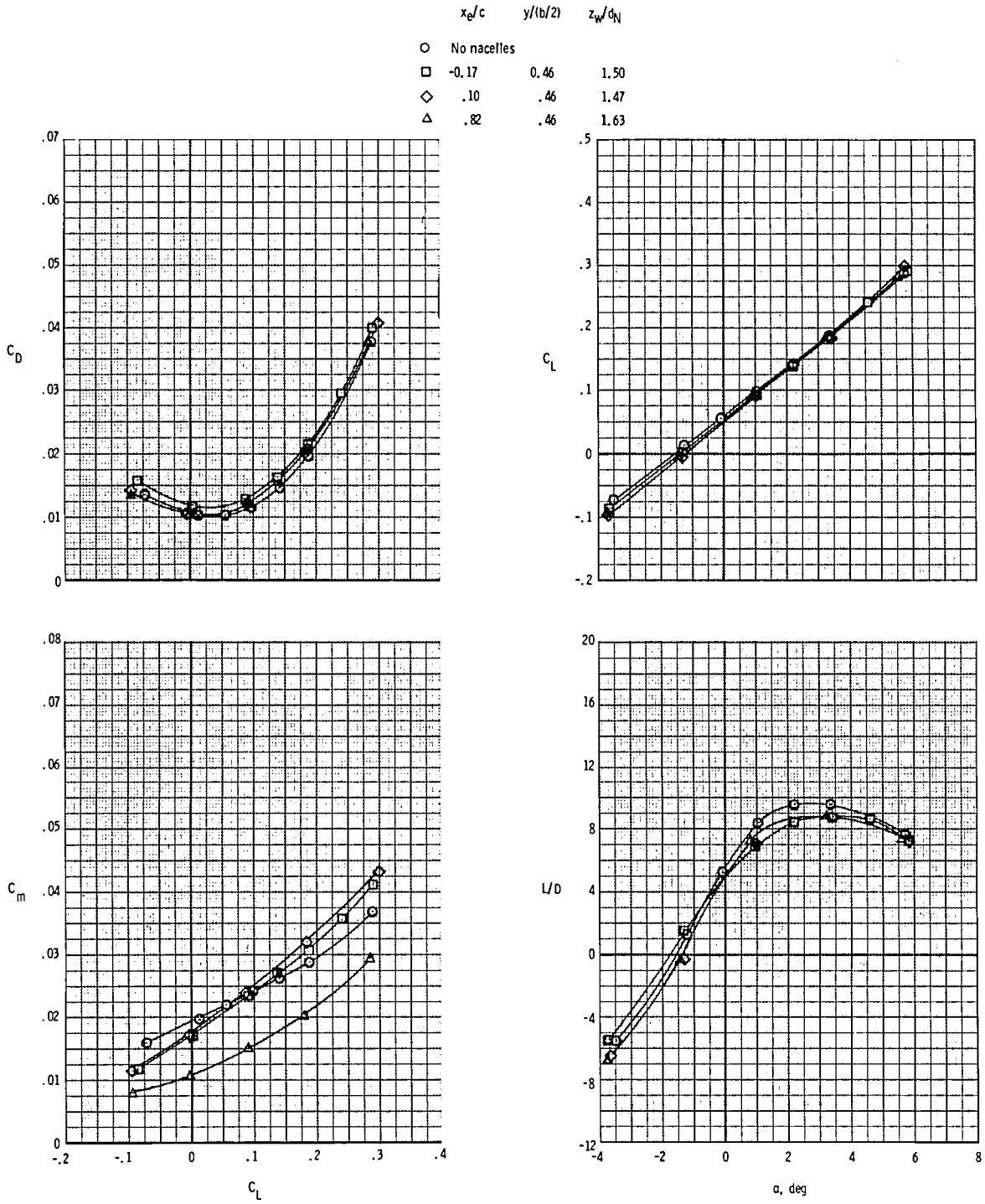

(e) M = 1.20.

Figure 7.- Concluded.

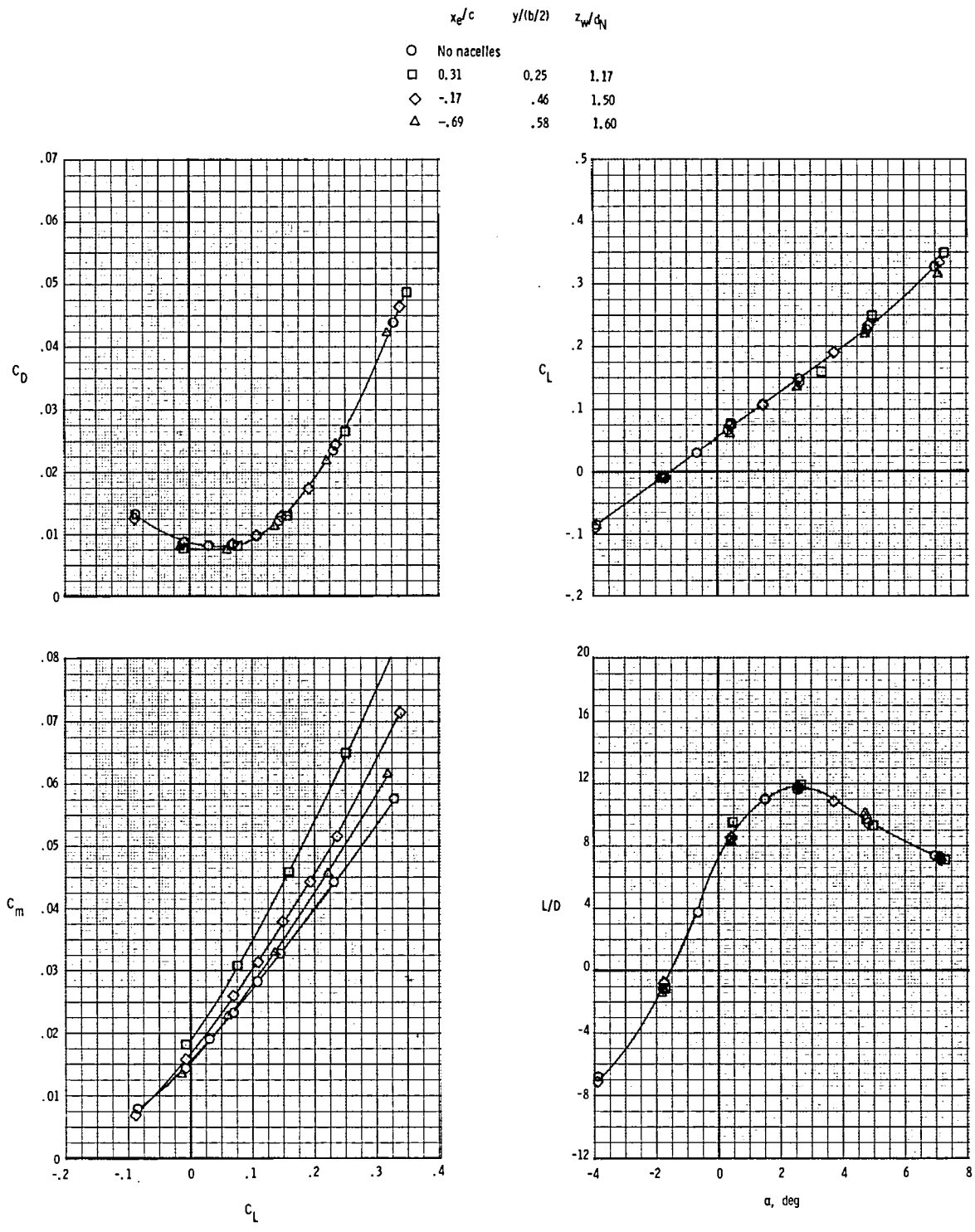

(a) M = 0.60.

Figure 8.- Effects of lateral displacement of nacelle-strut assembly on longitudinal aerodynamic force and moment characteristics with jet off and δ_f at -10°.

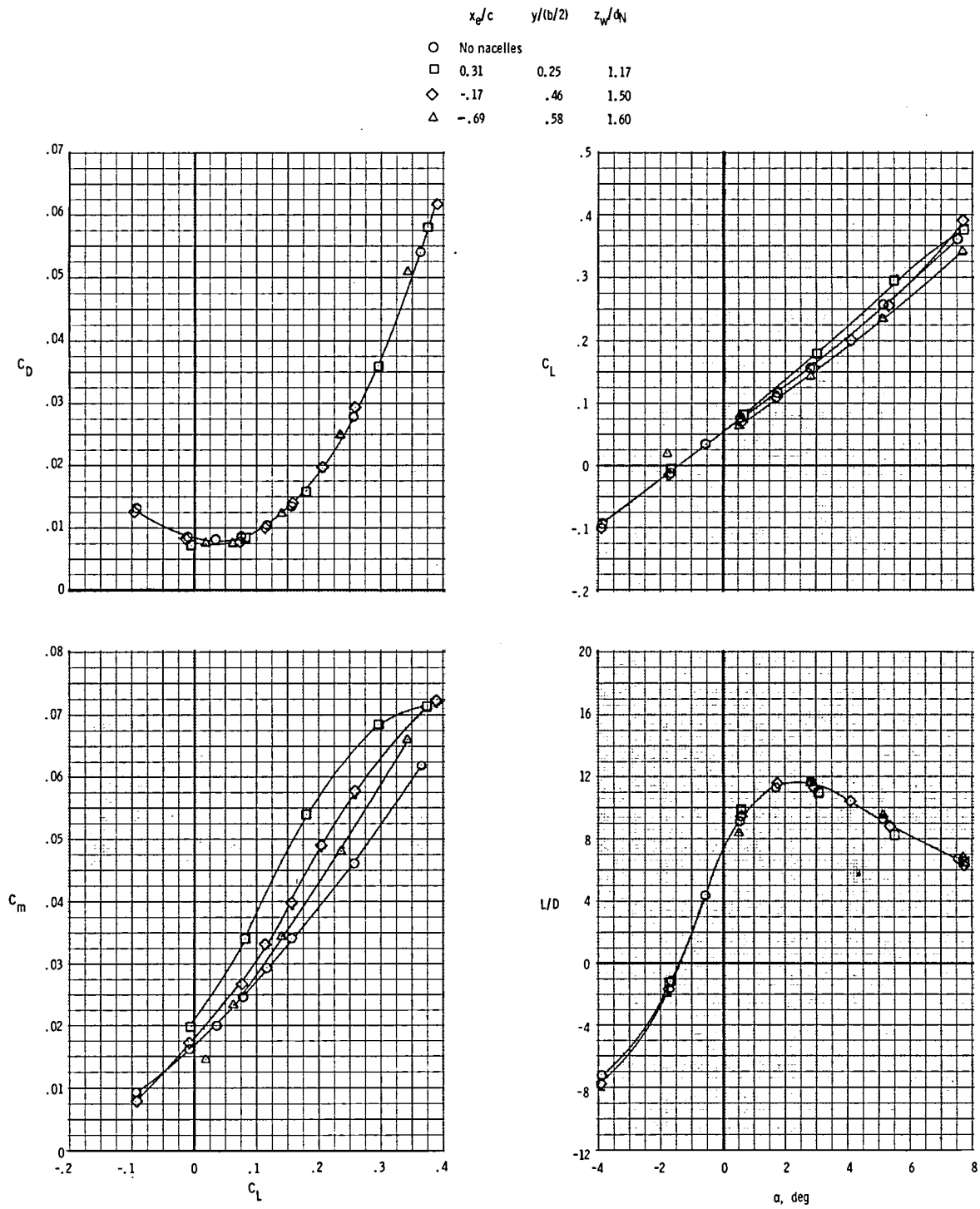

(b) M = 0.80.

Figure 8.- Continued.

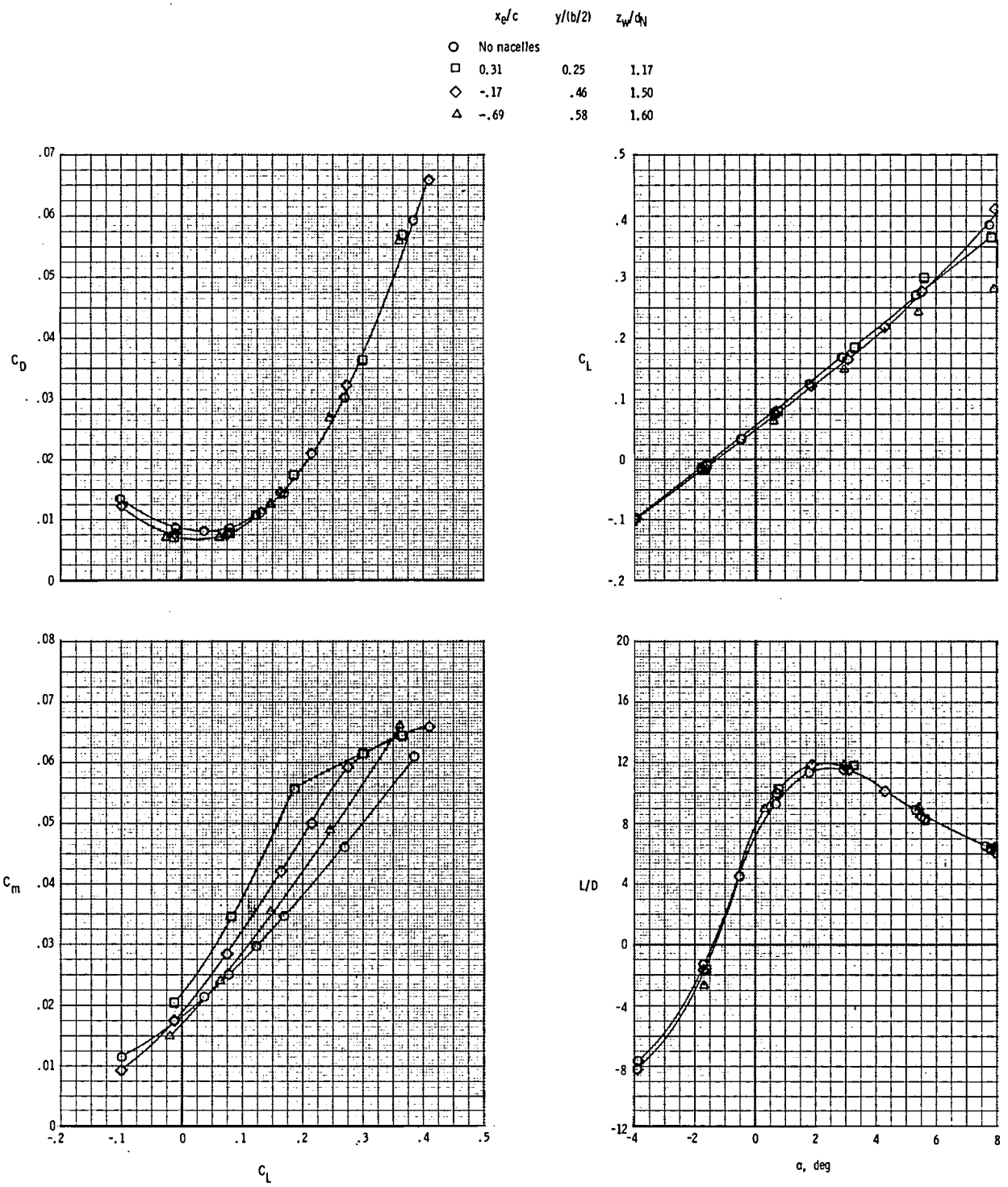

(c) M = 0.90.

Figure 8.- Continued.

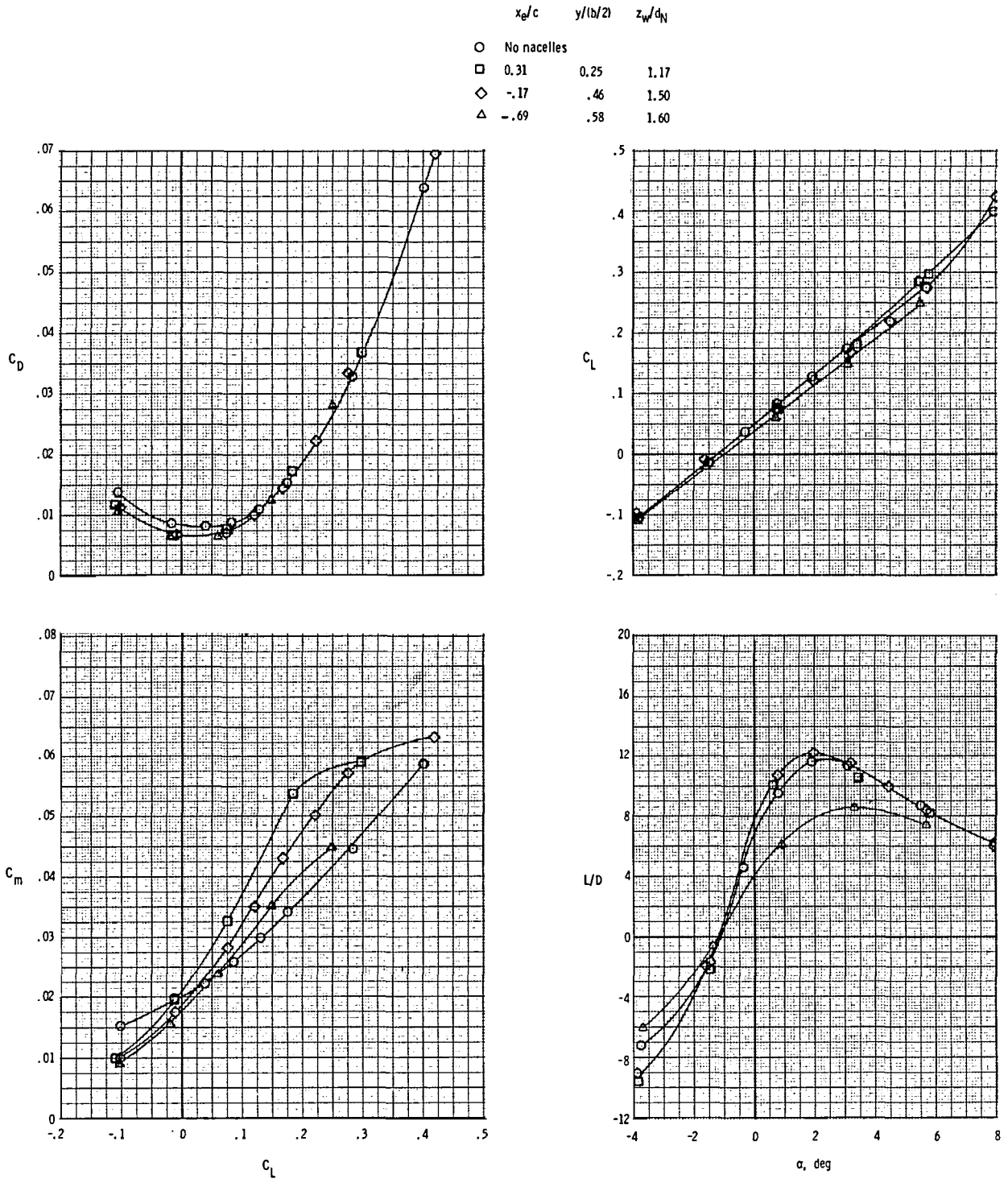

(d) M = 0.95.

Figure 8.- Continued.

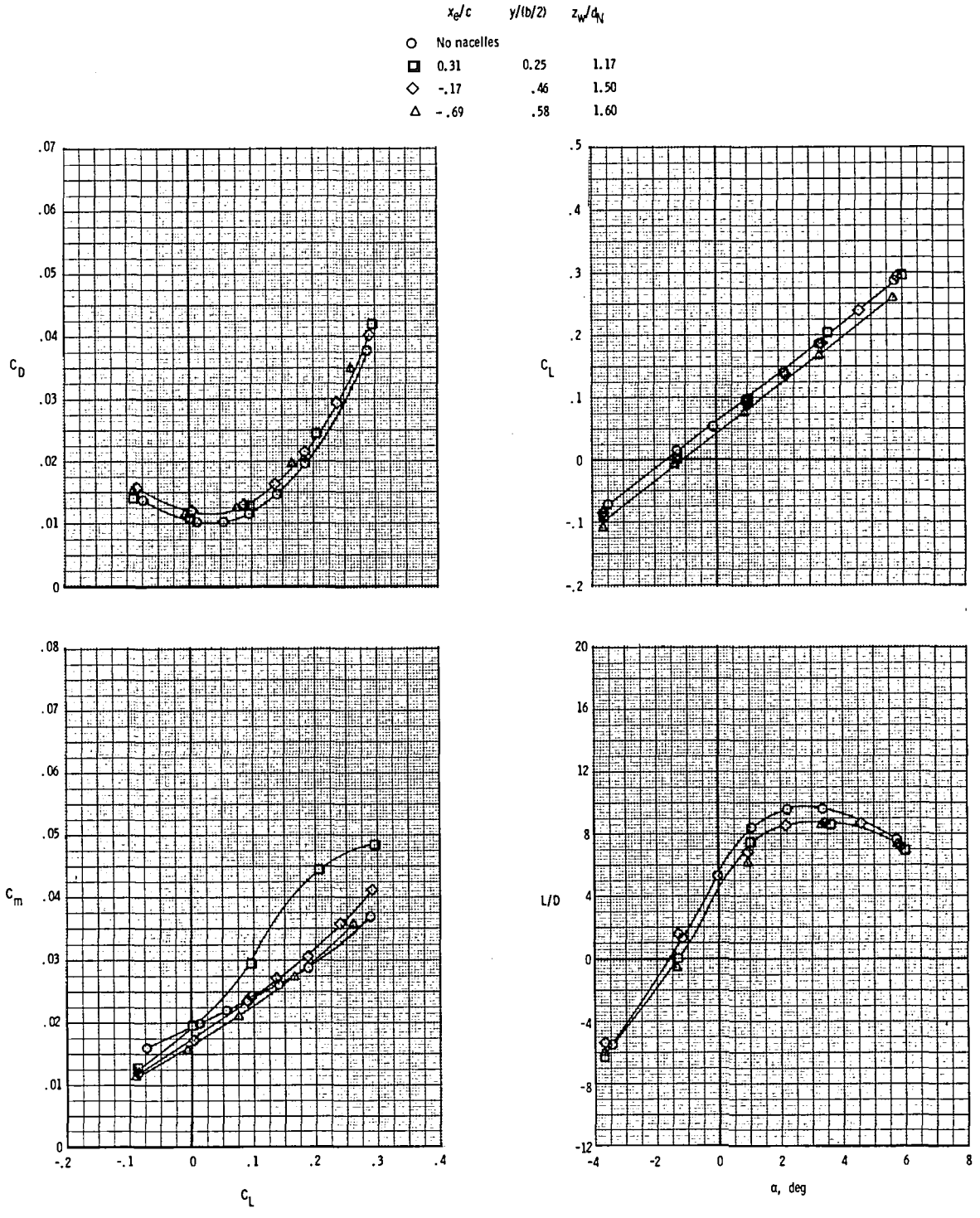

(e) M = 1.20.

Figure 8.- Concluded.

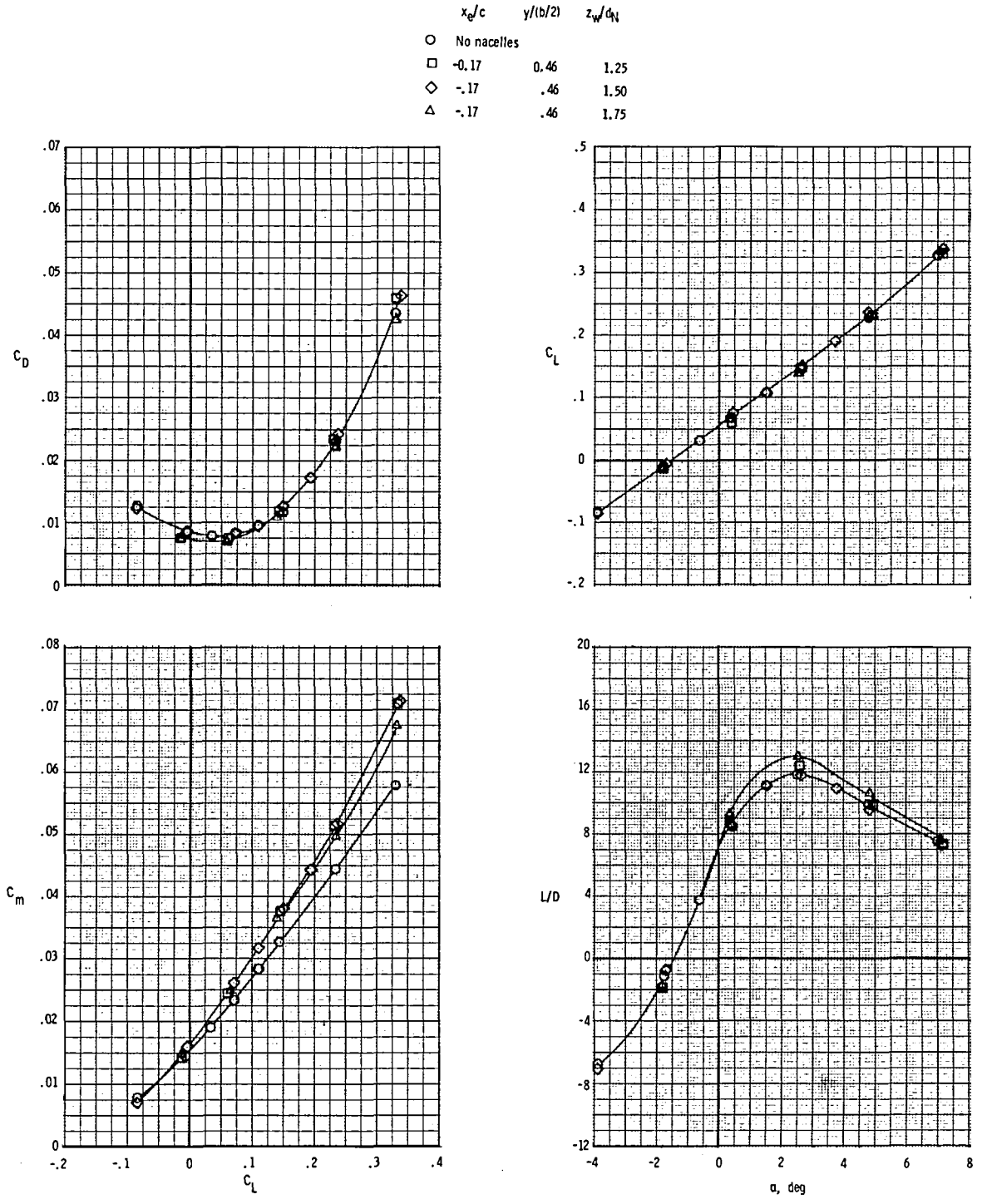

(a) M = 0.60.

Figure 9.- Effects of vertical displacement of nacelle-strut assembly on longitudinal aerodynamic force and moment characteristics with jet off and δ_f at -10°.

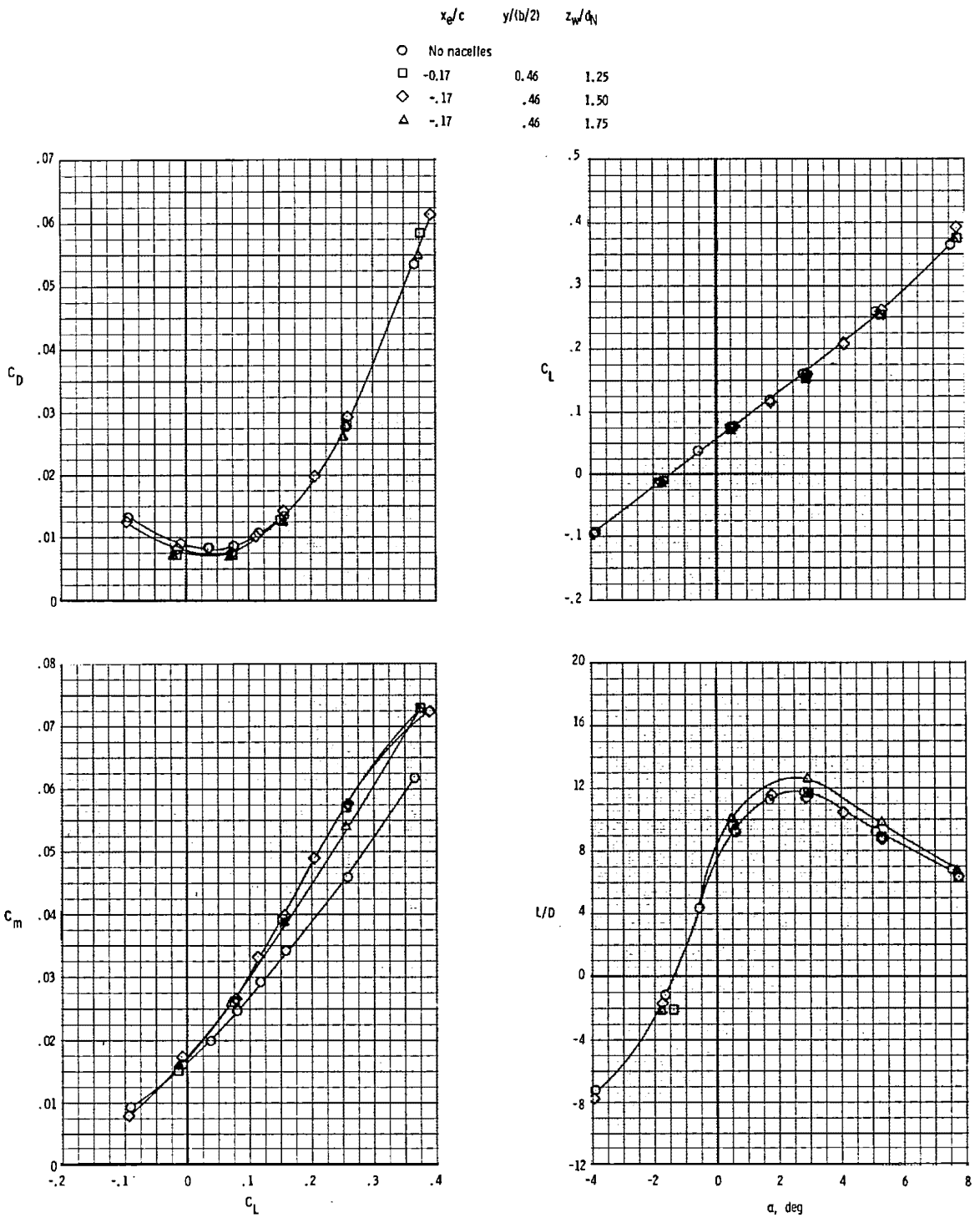

(b) M = 0.80.

Figure 9.- Continued.

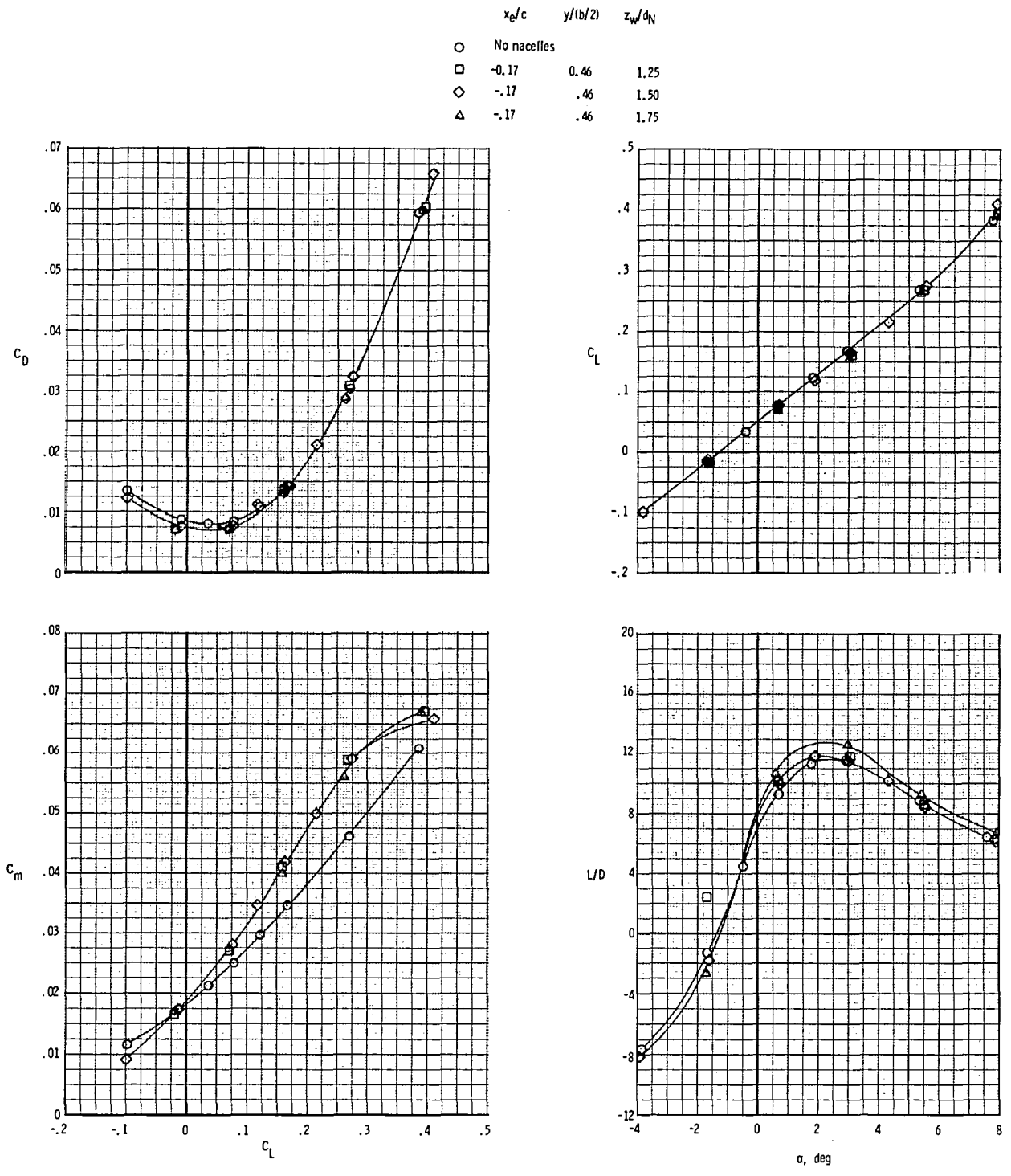

(c) M = 0.90.

Figure 9.- Continued.

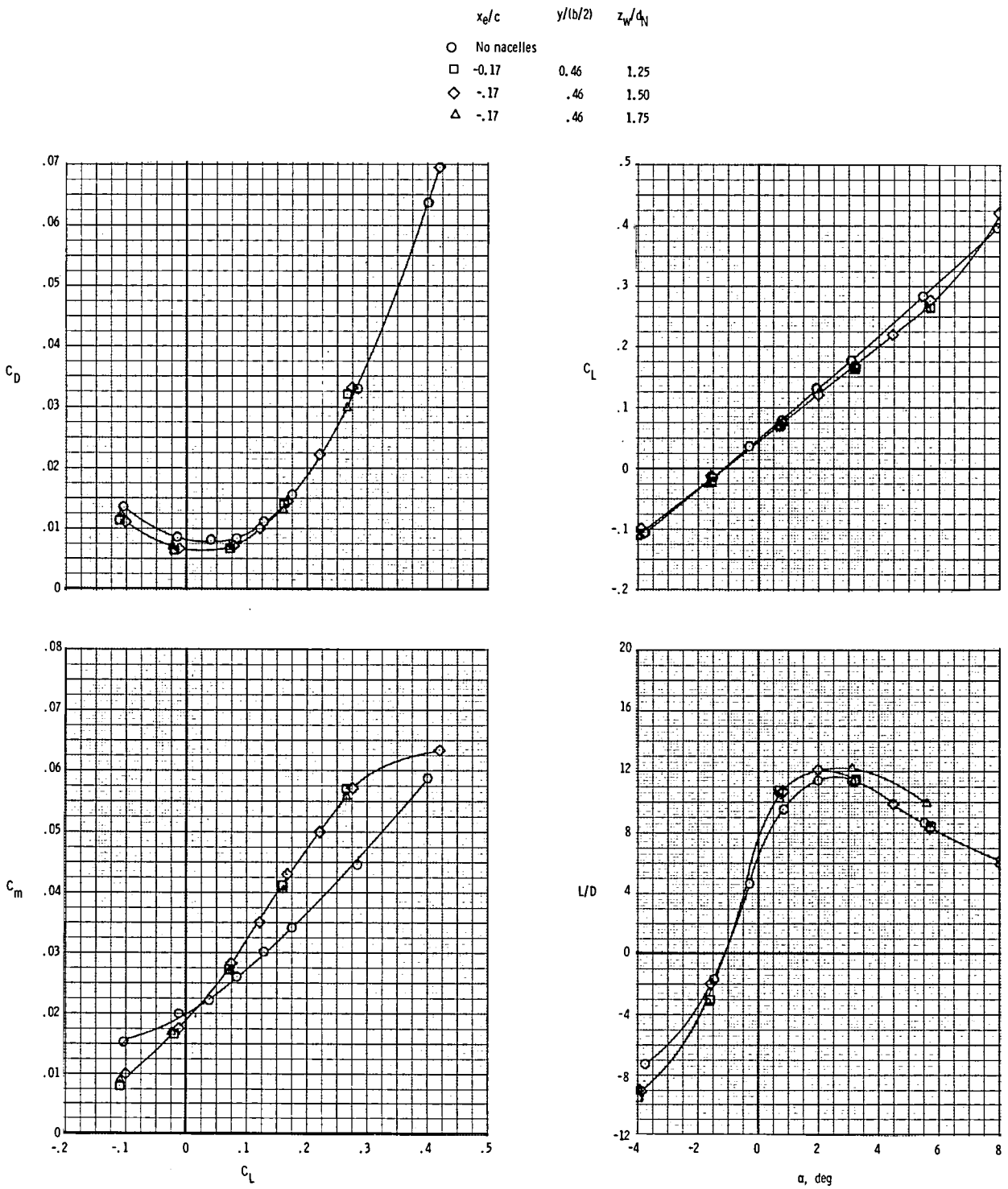

(d) M = 0.95.

Figure 9.- Continued.

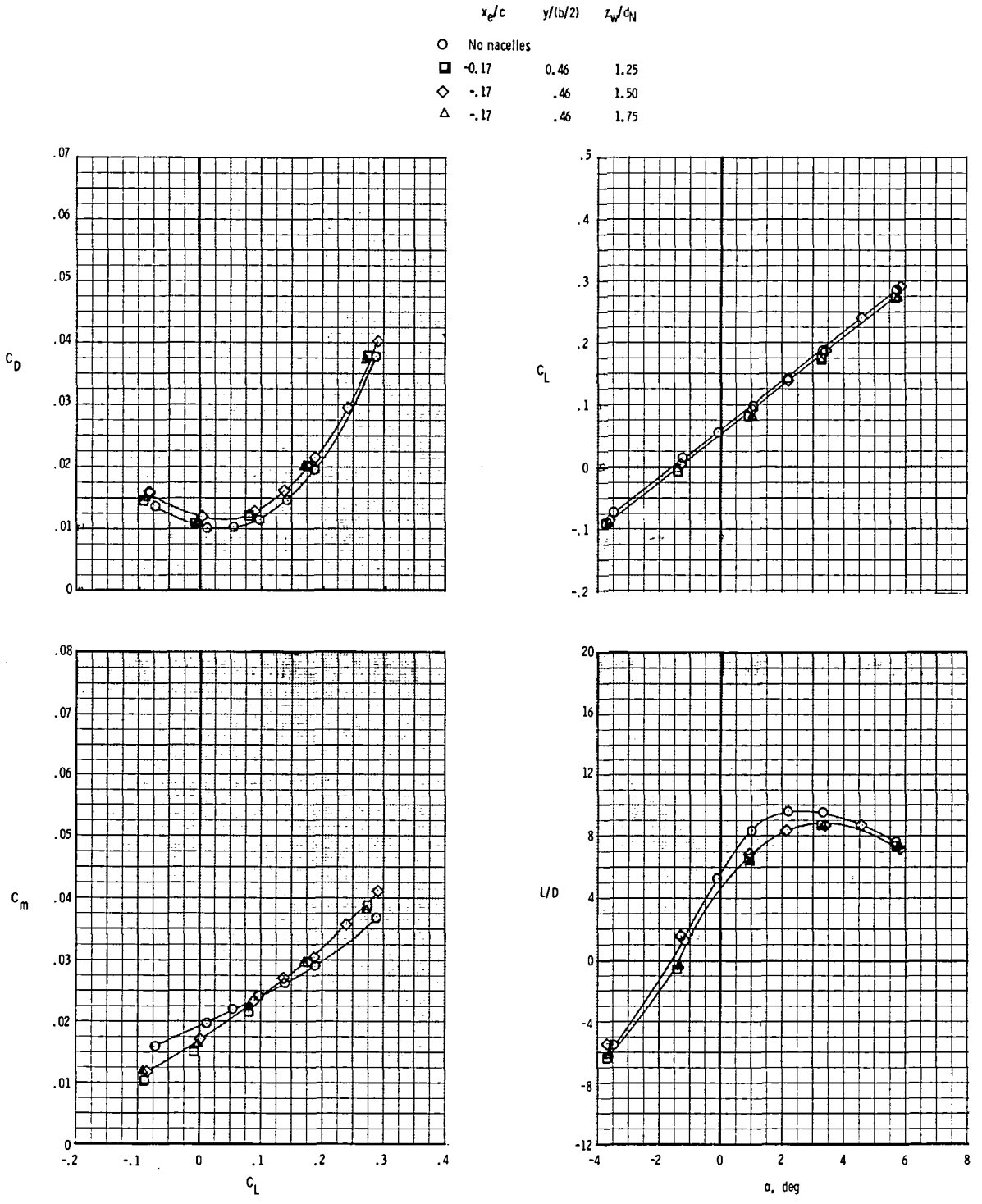

(e) M = 1.20.

Figure 9.- Concluded.

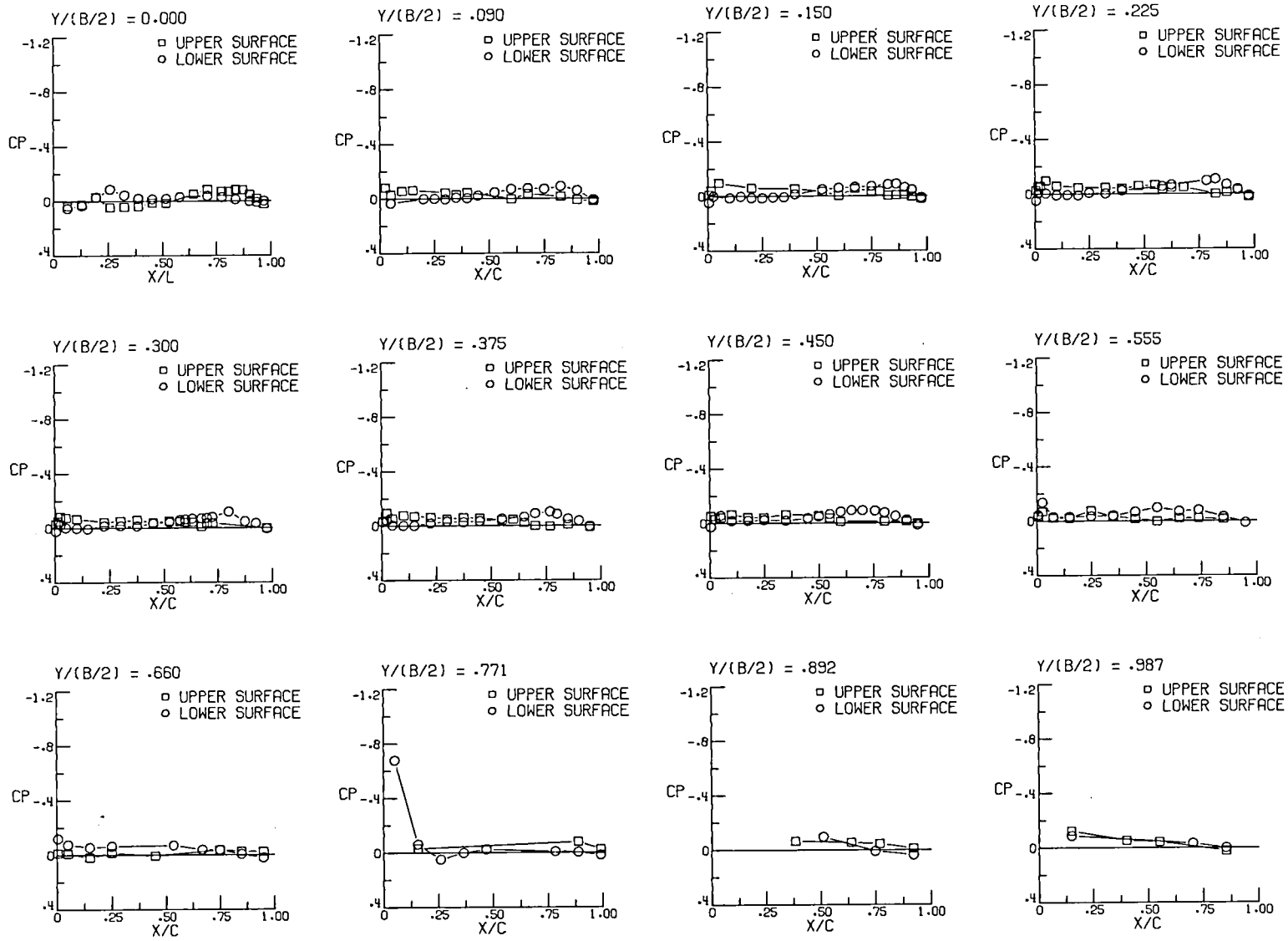

(a) M = 0.60, $\alpha = -2^{o}$.

Figure 10.- Pressure distributions for wing-body configuration without jet nacelles.

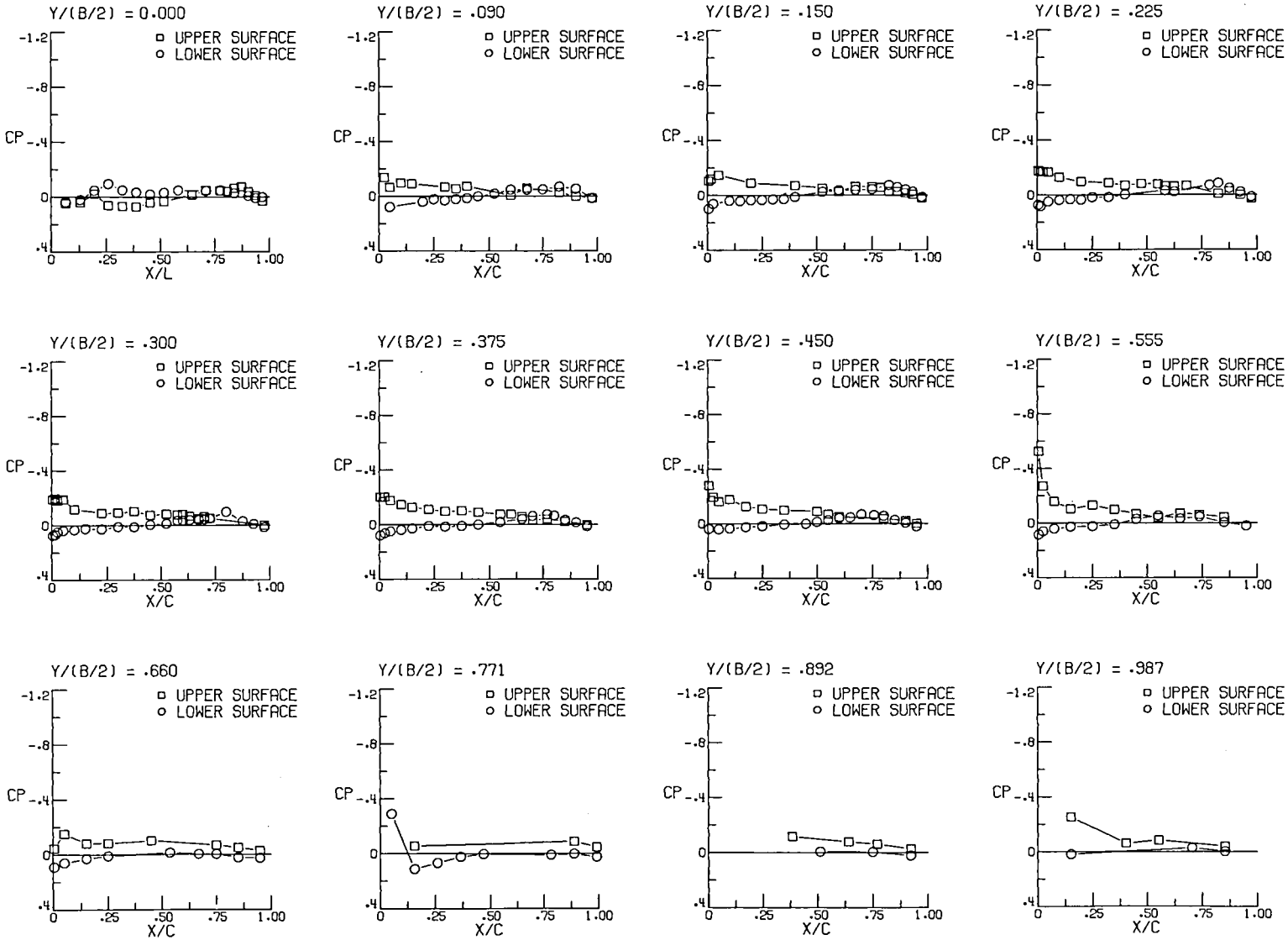

(a) Continued, $\alpha = 0^{o}$.

Figure 10.- Continued.

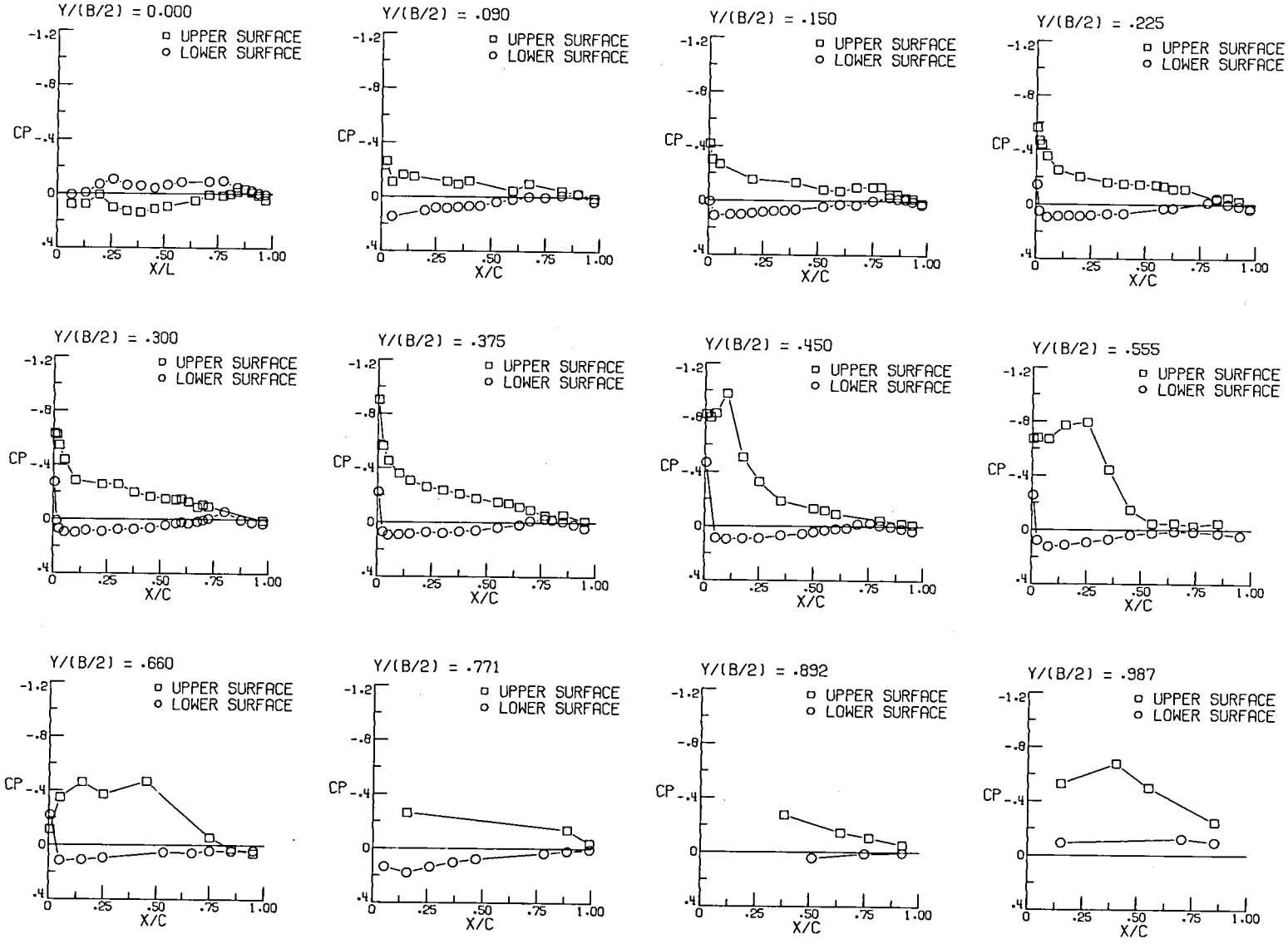

(a) Continued, $\alpha = 4^{o}$.

Figure 10.- Continued.

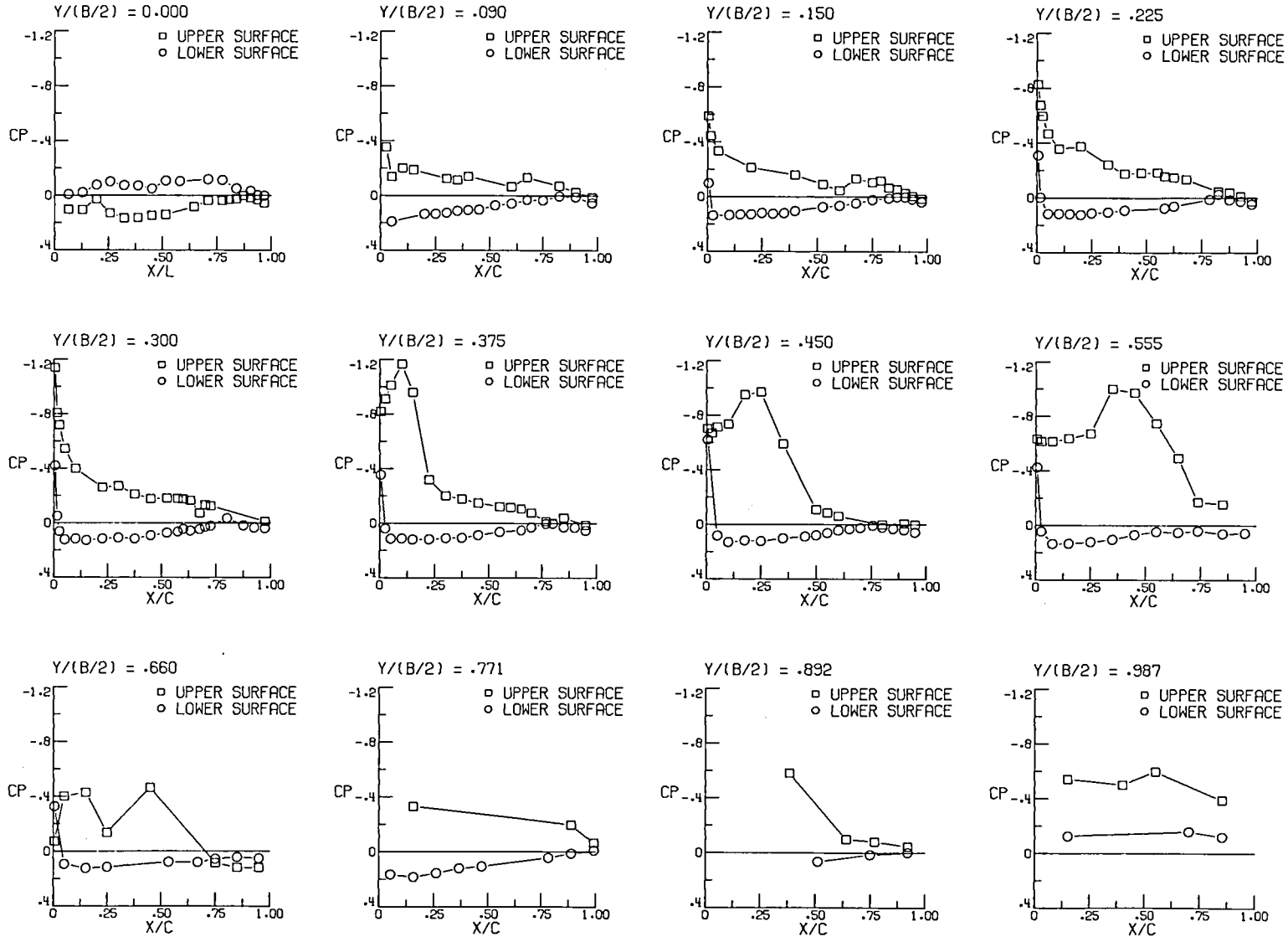

(a) Concluded, $\alpha = 6^{o}$.

Figure 10.- Continued.

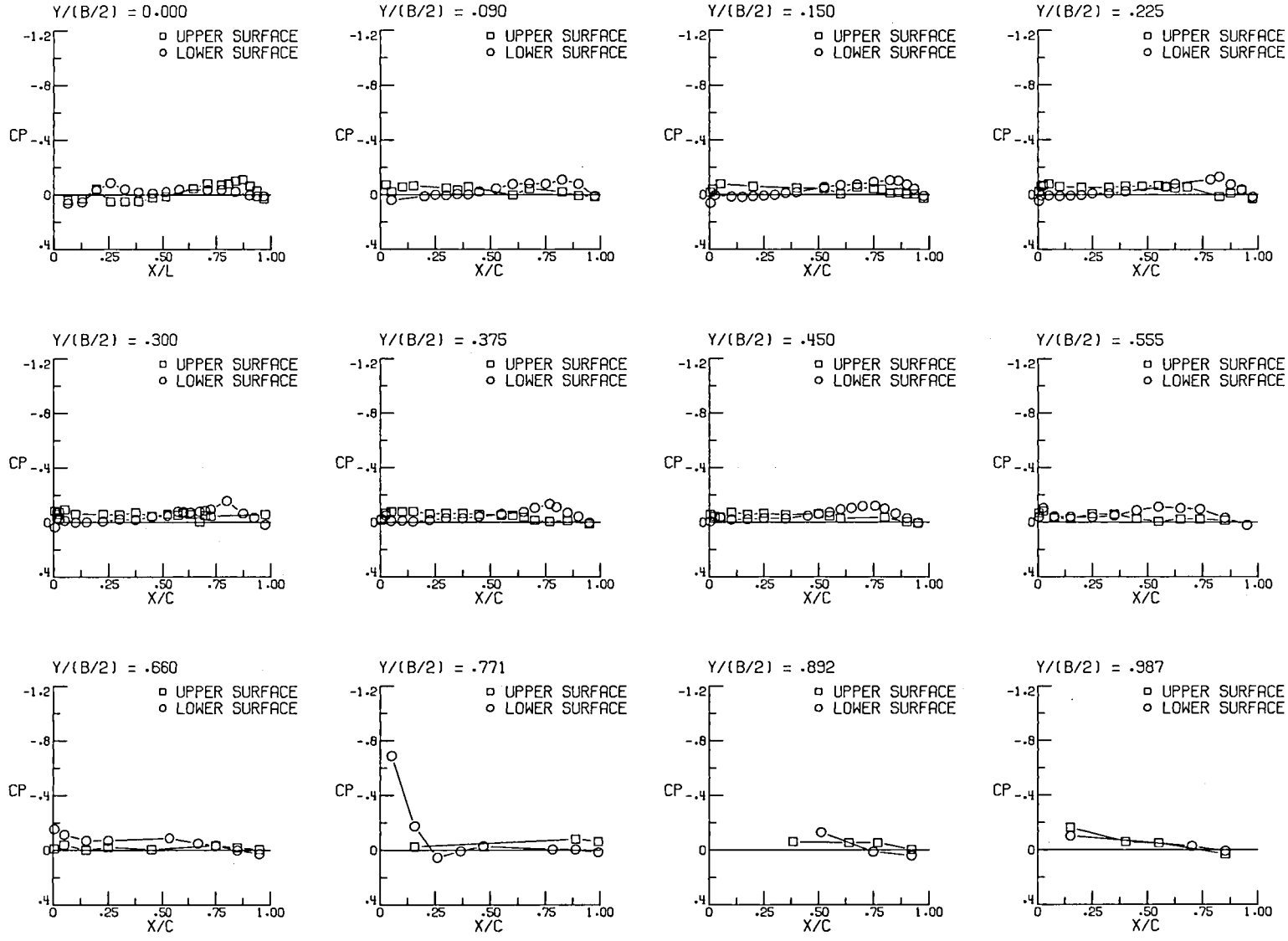

(b) M = 0.80, $\alpha = -2^{o}$.

Figure 10.- Continued.

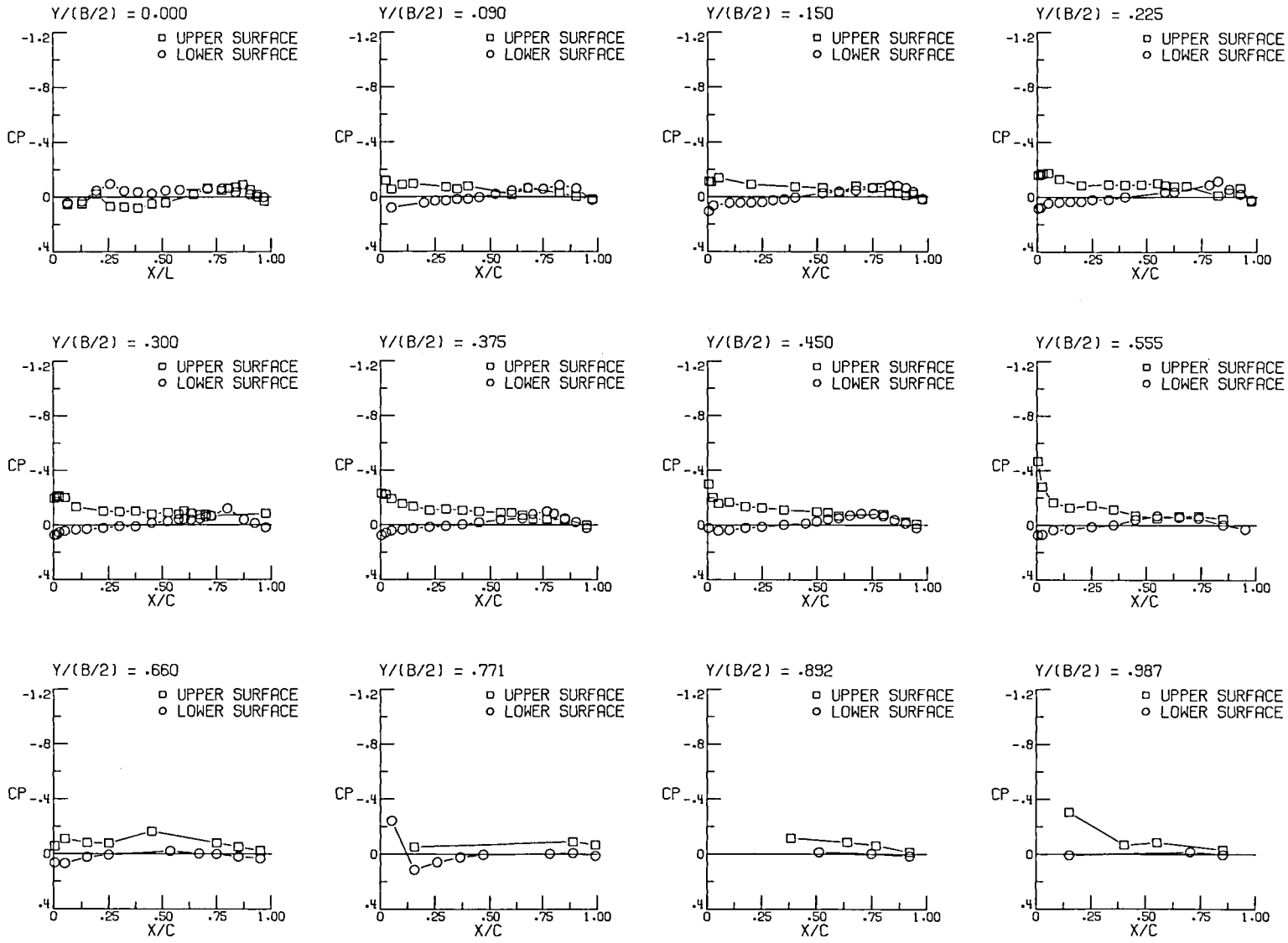

(b) Continued, $\alpha = 0^{o}$.

Figure 10.- Continued.

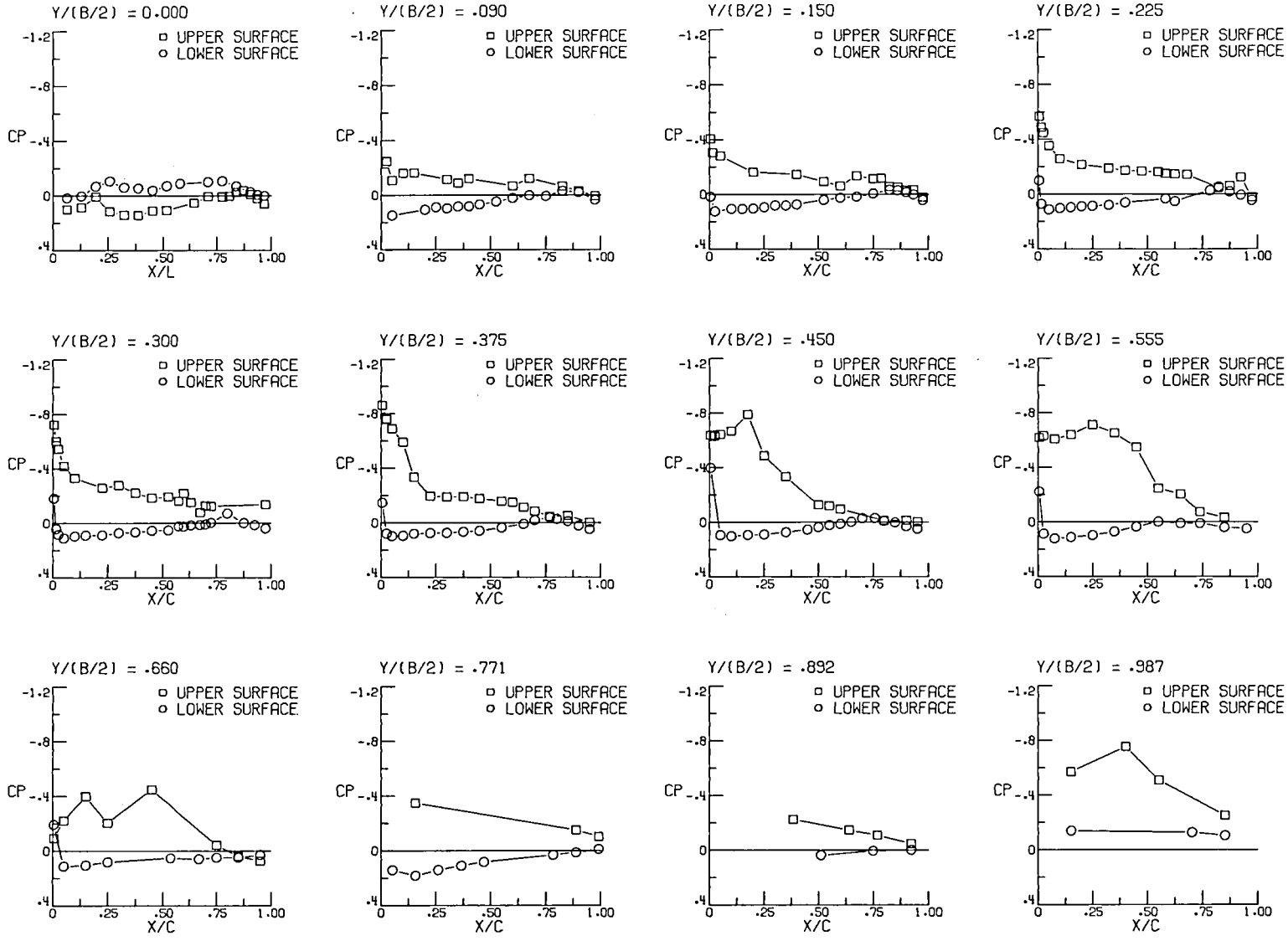

(b) Continued, $\alpha = 4^{o}$.

Figure 10.- Continued.

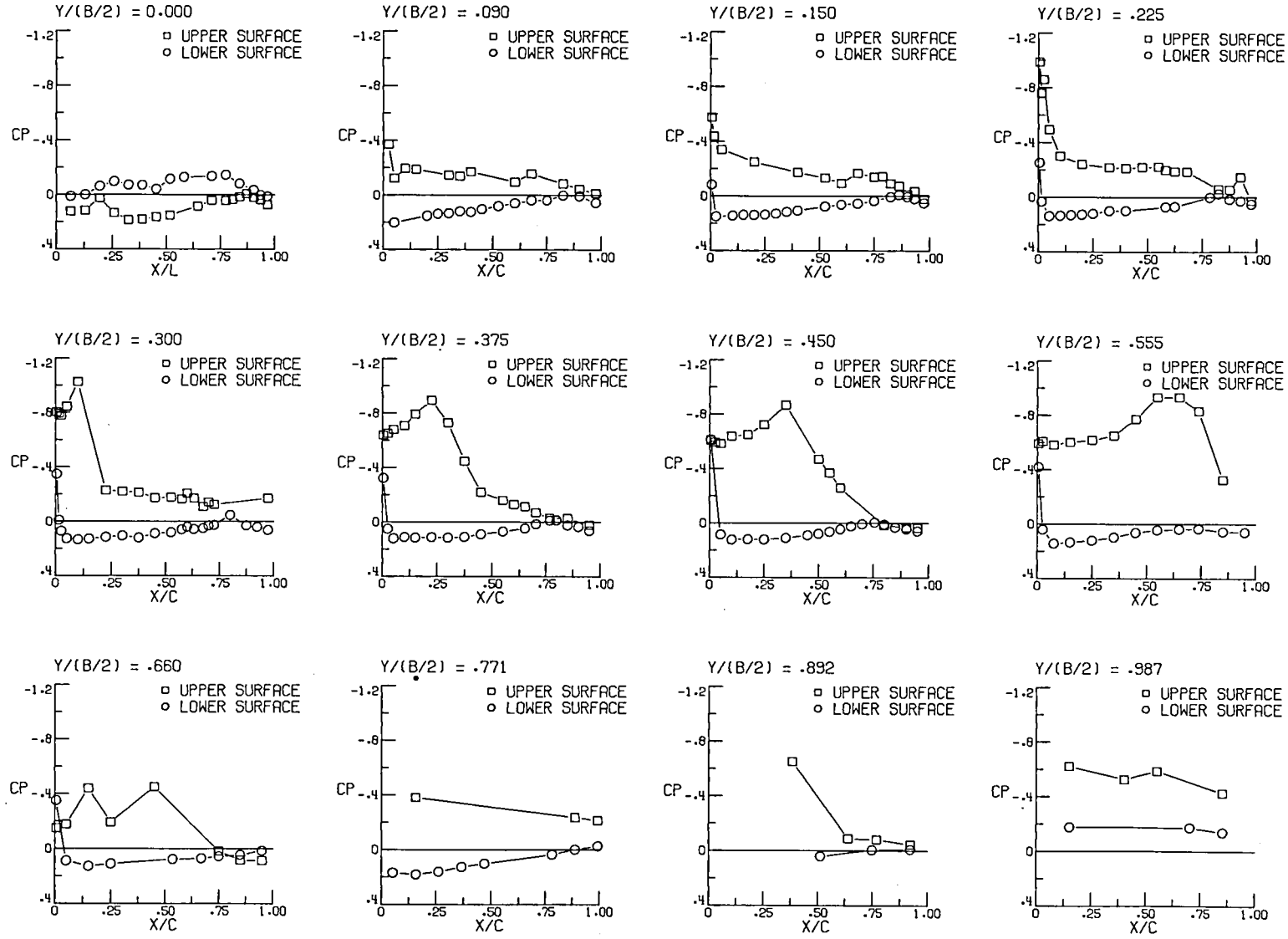

(b) Concluded, $\alpha = 6^{o}$.

Figure 10.- Continued.

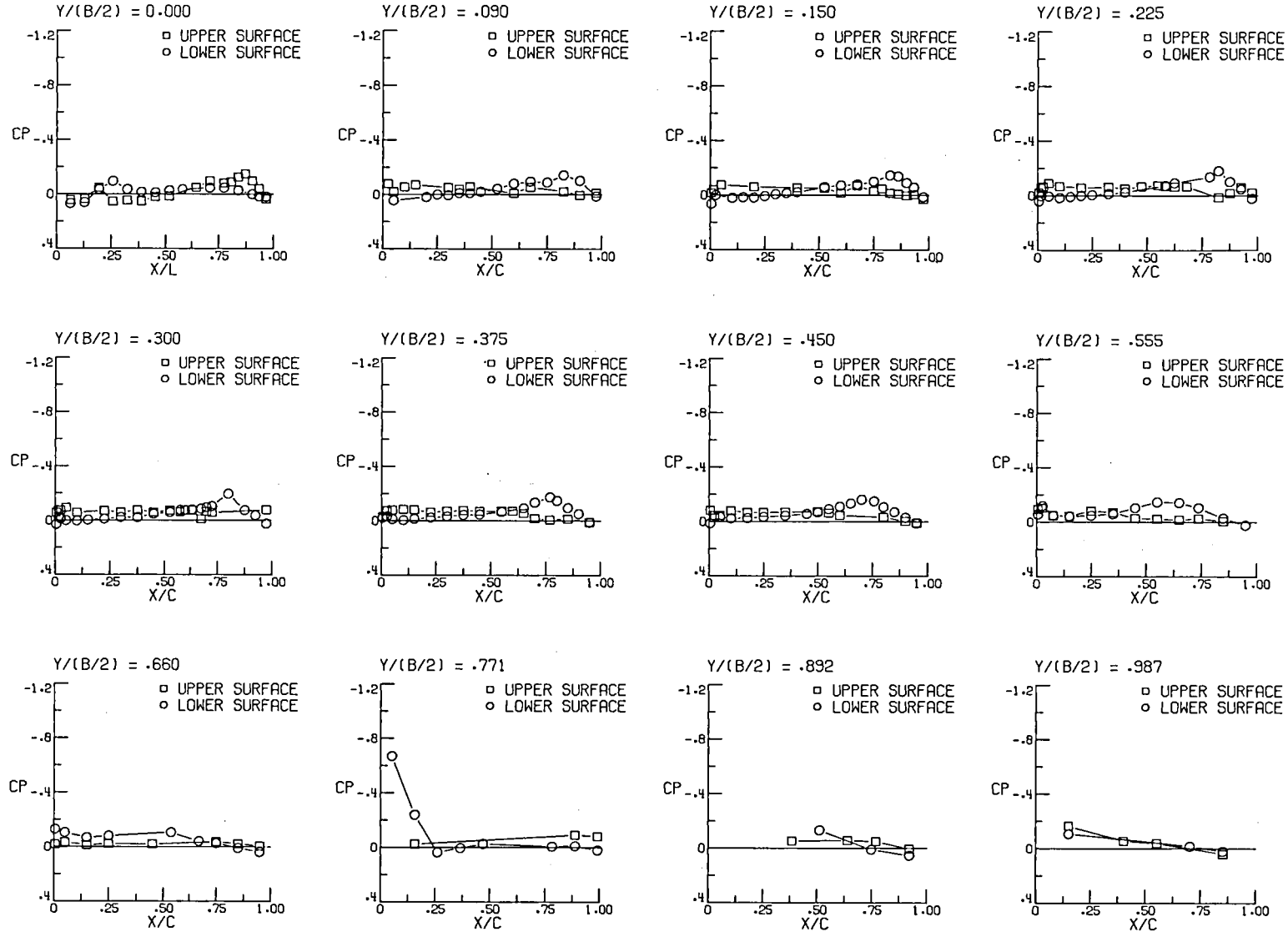

(c) M = 0.90, $\alpha = -2^{o}$.

Figure 10.- Continued.

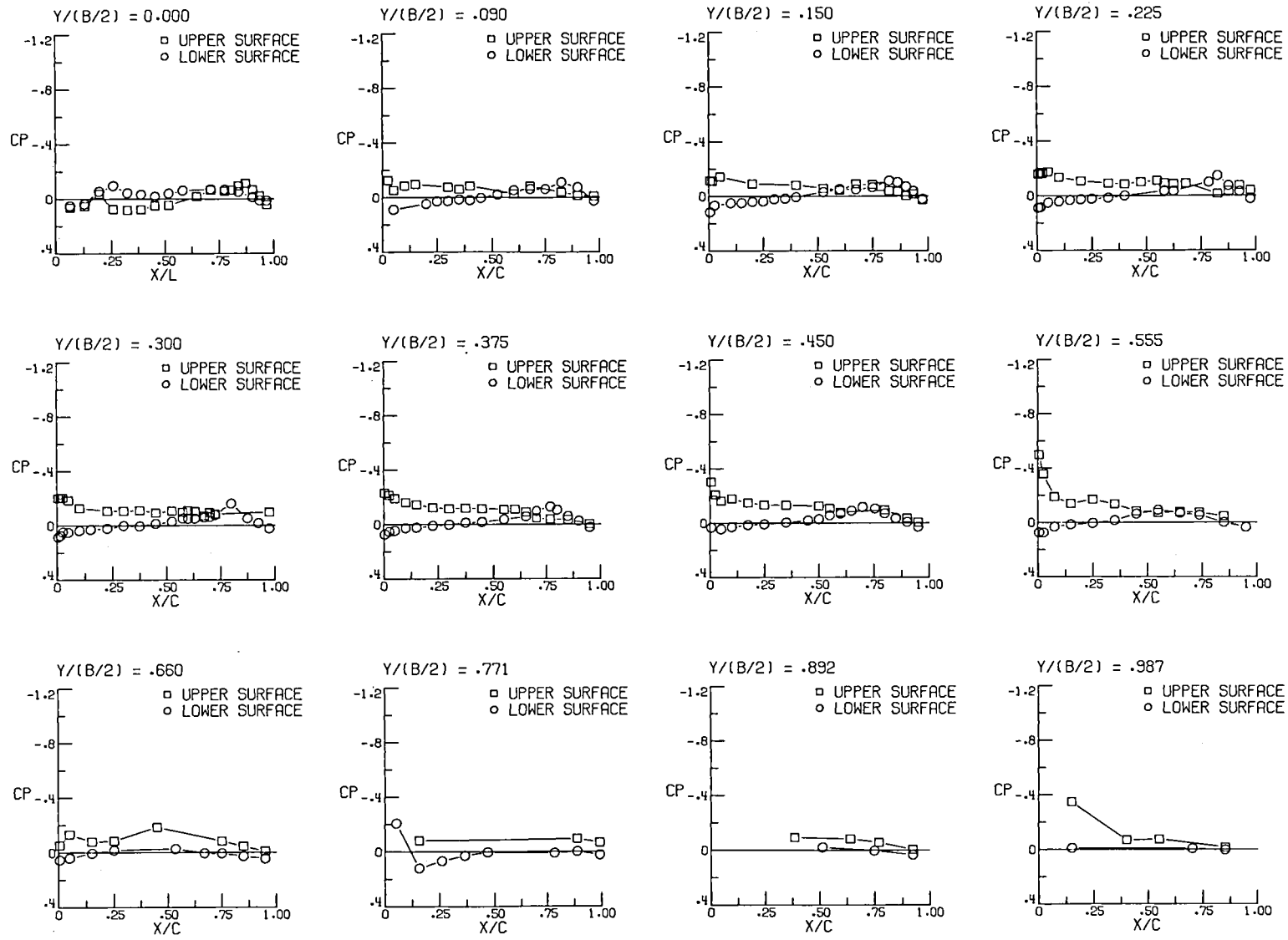

(c) Continued, $\alpha = 0^{o}$.

Figure 10.- Continued.

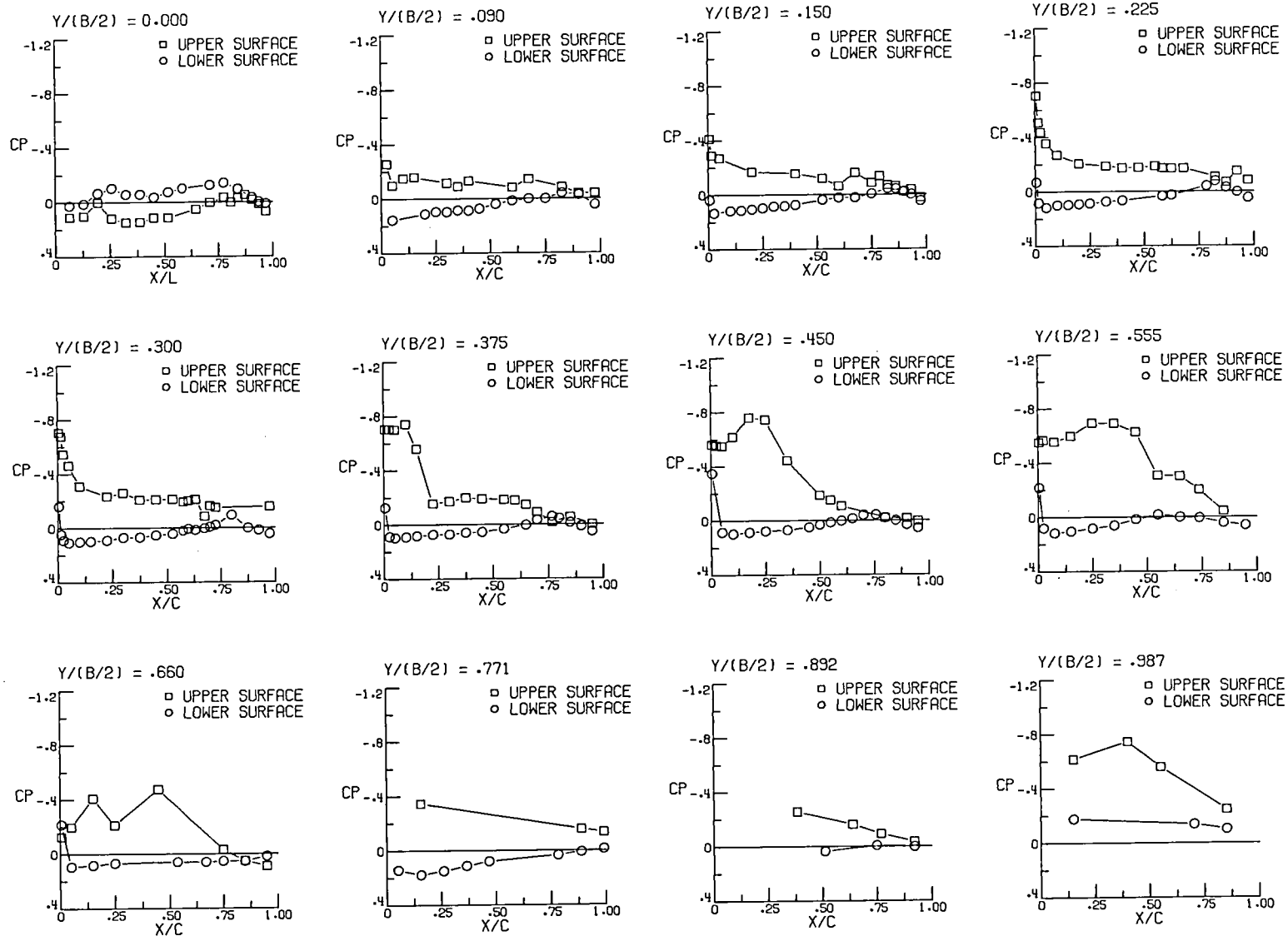

(c) Continued, $\alpha = 4^{\circ}$.

Figure 10.- Continued.

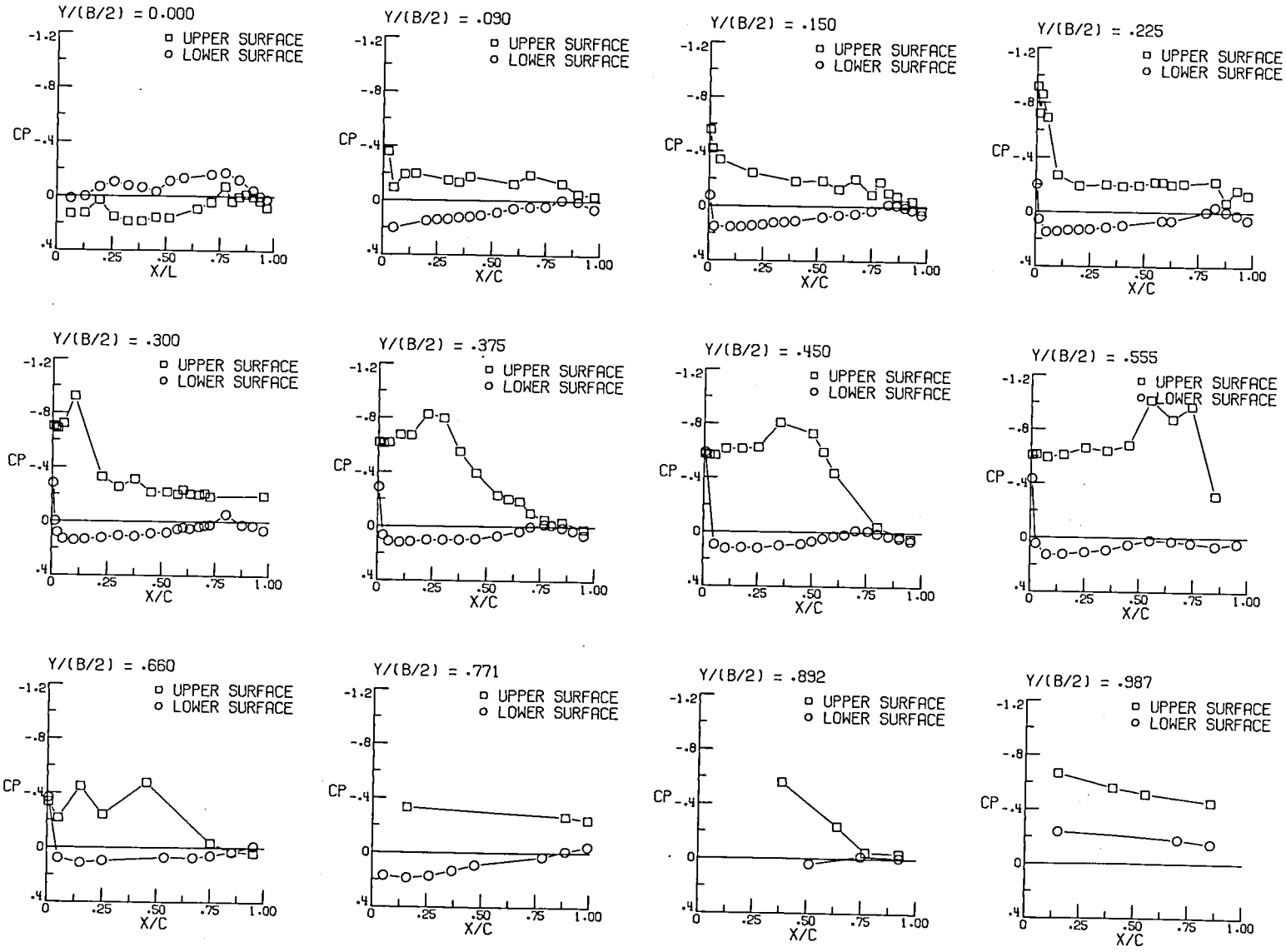

(c) Concluded, $\alpha = 6^{o}$.

Figure 10.- Continued.

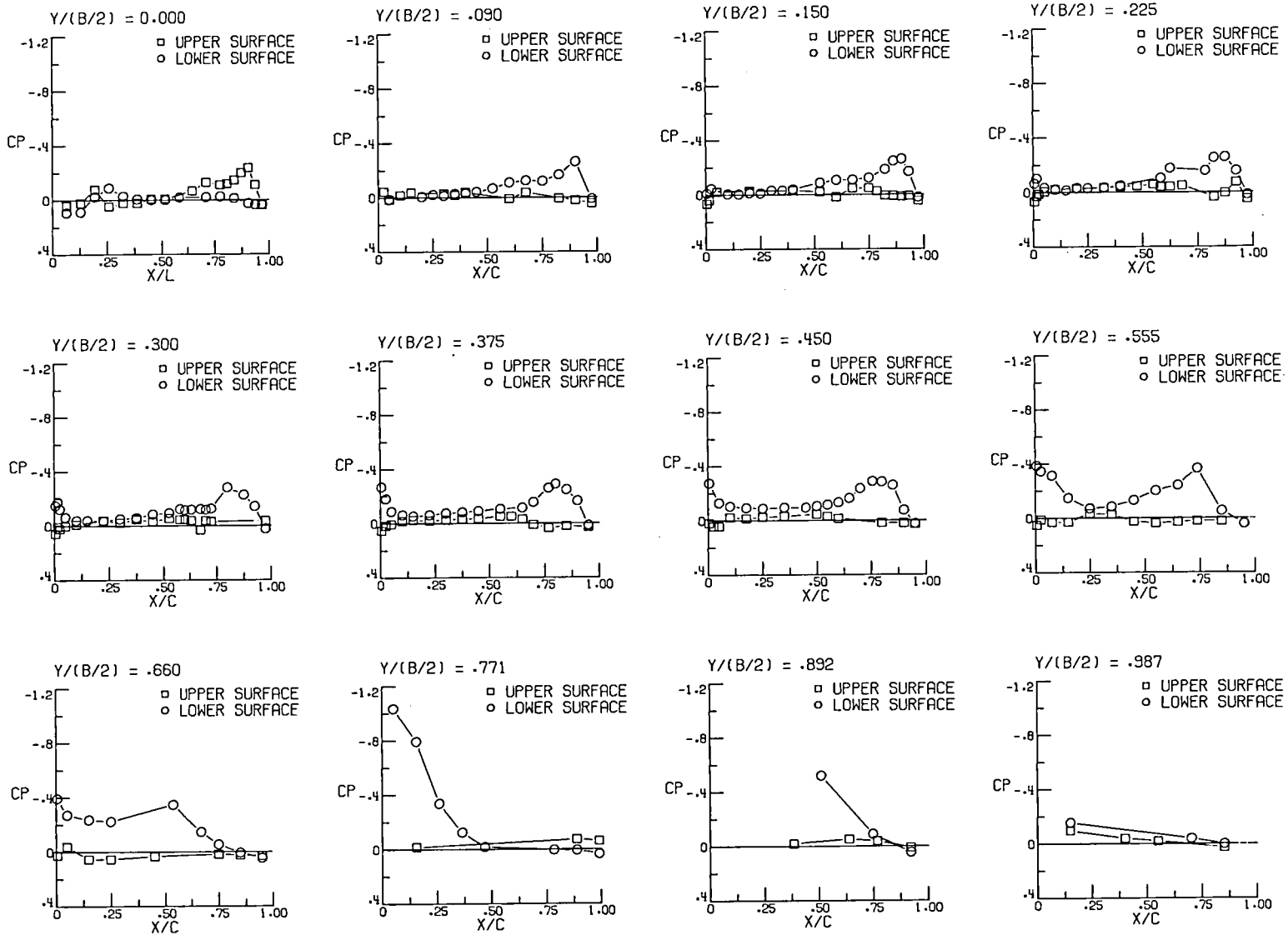

(d) M = 0.95, $\alpha = -4^{\circ}$.

Figure 10.- Continued.

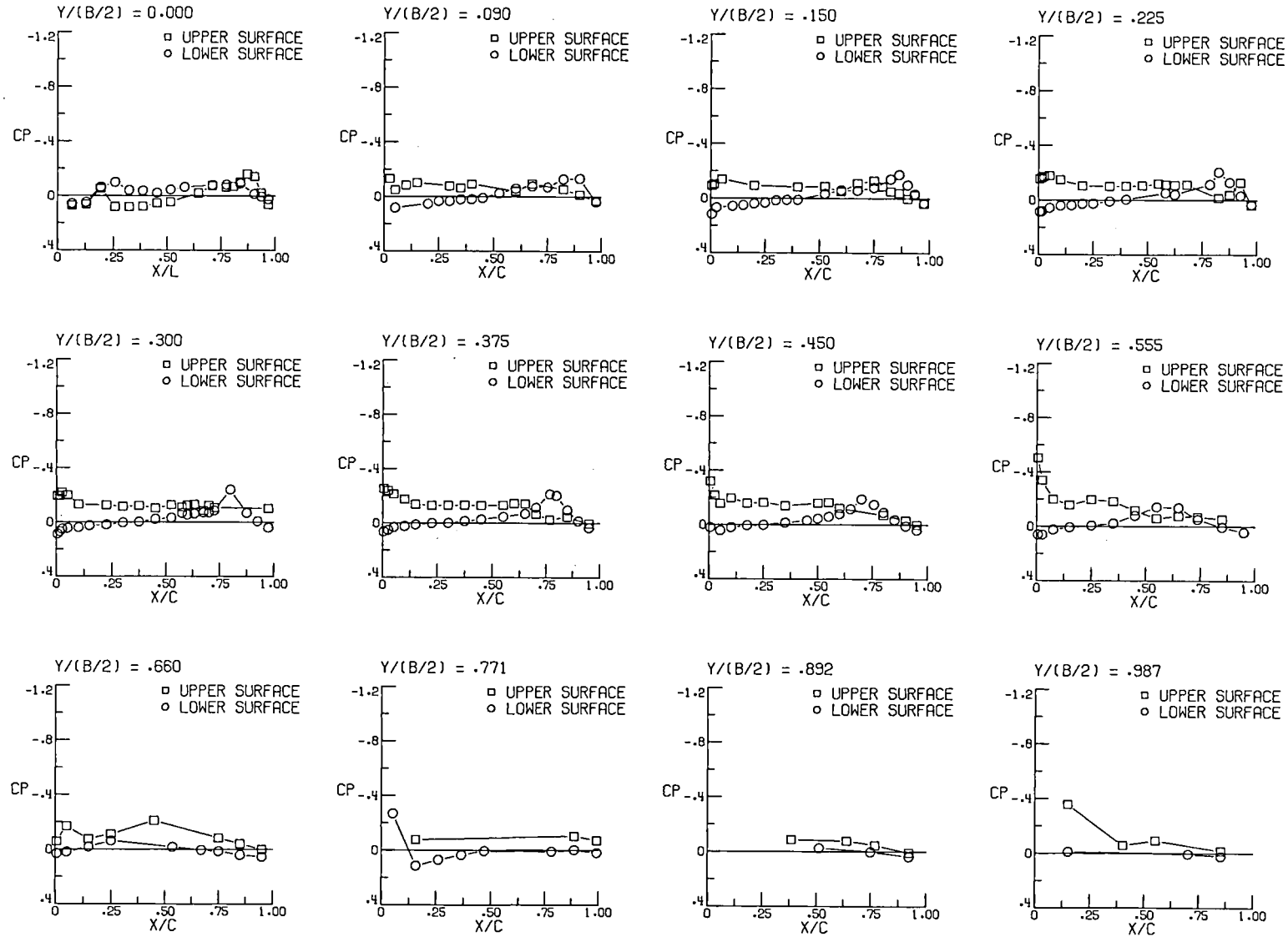

(d) Continued, $\alpha = 0^{o}$.

Figure 10.- Continued.

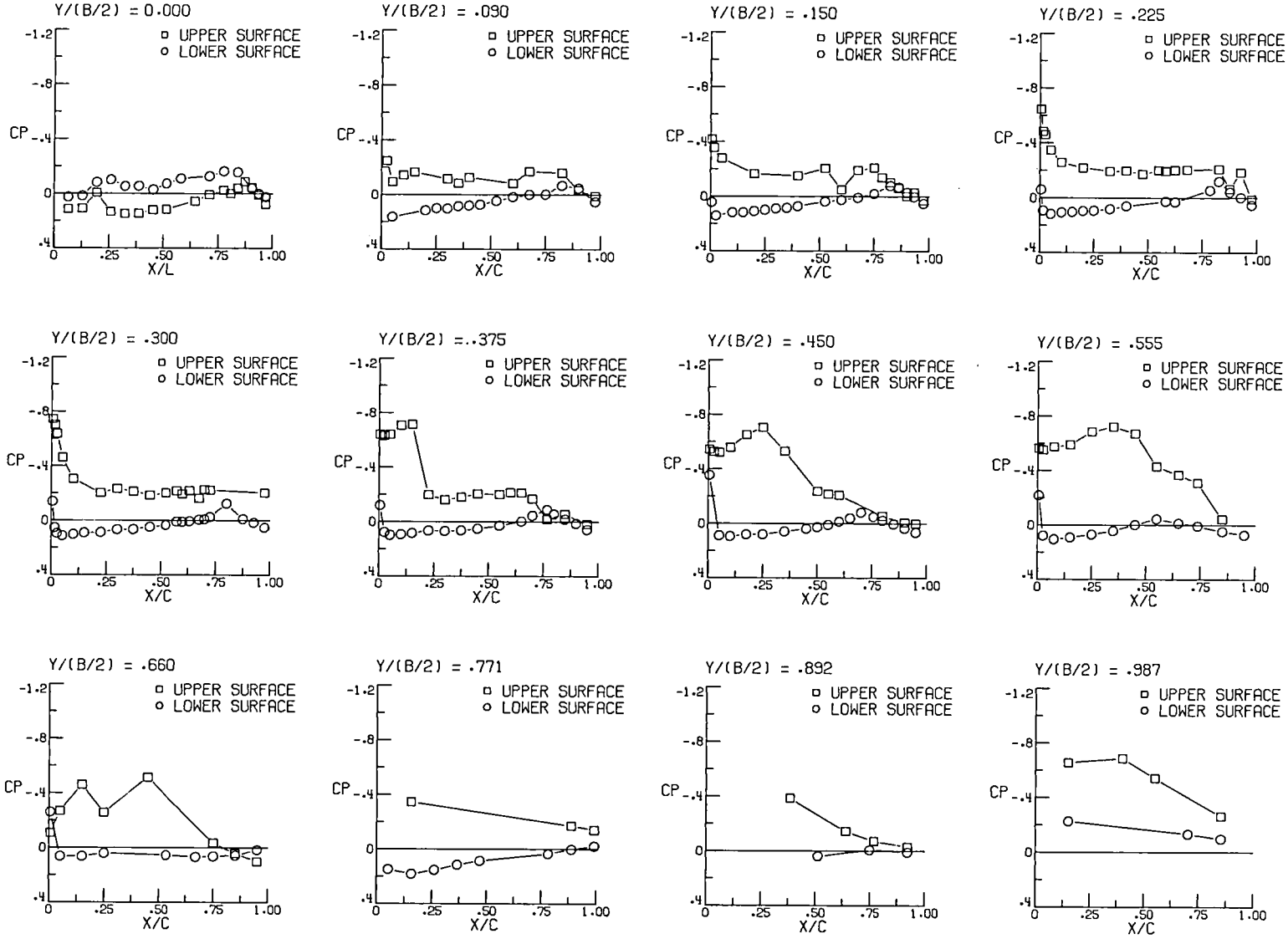

(d) Concluded, $\alpha = 4^{\circ}$.

Figure 10.- Continued.

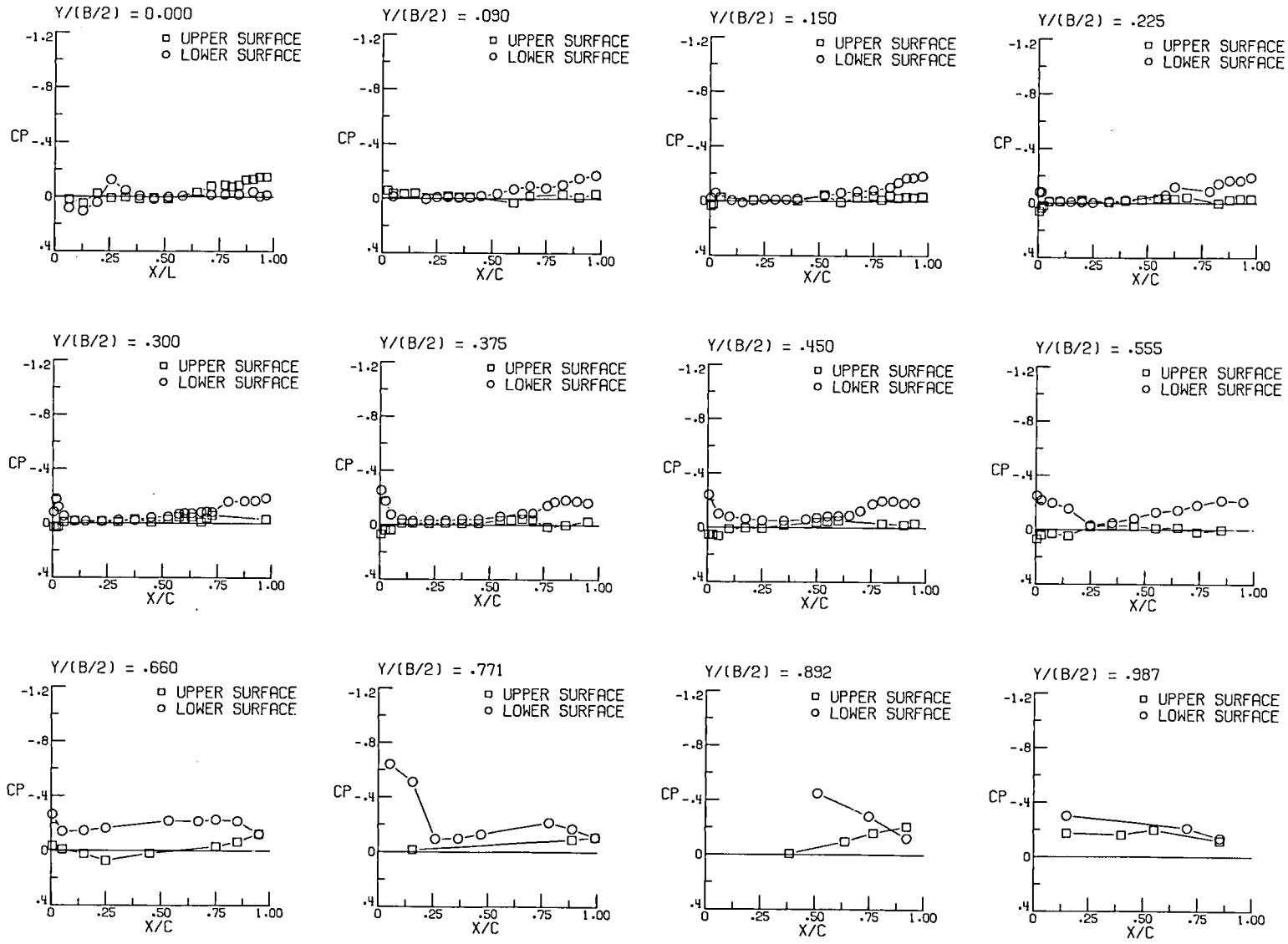

(e) M = 1.20, $\alpha = -4^{\circ}$.

Figure 10.- Continued.

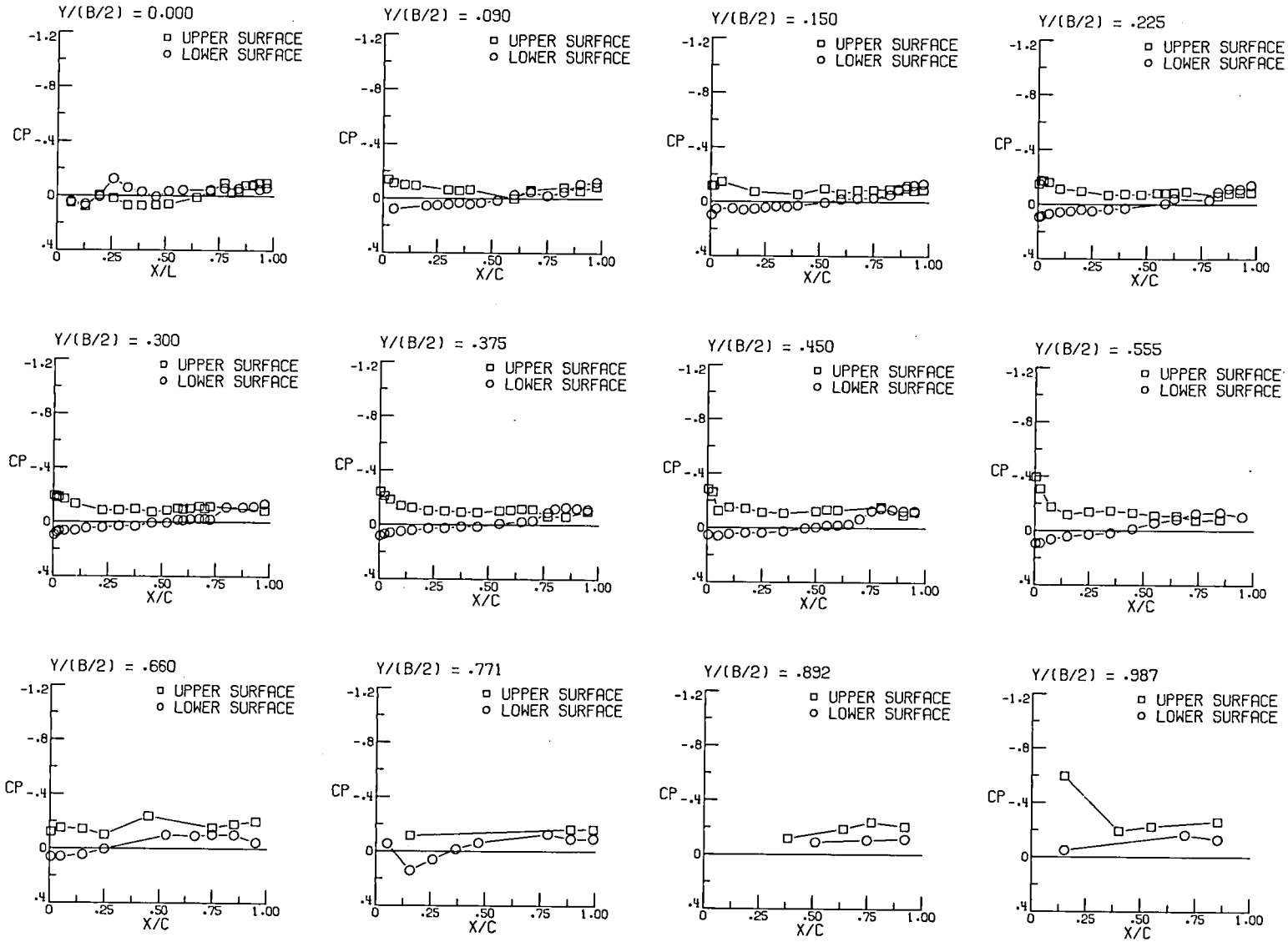

(e) Continued, $\alpha = 0^{o}$.

Figure 10.- Continued.

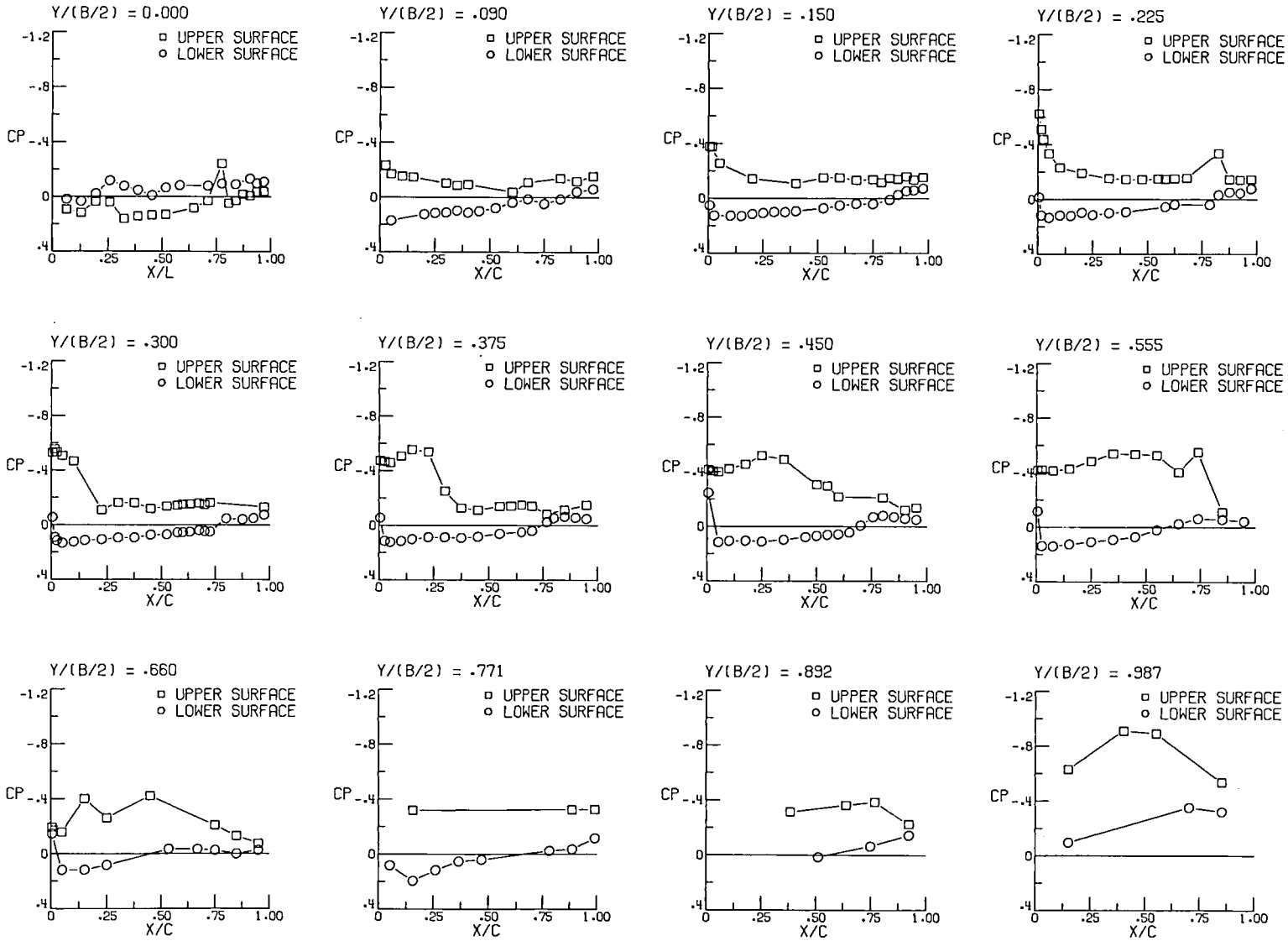

(e) Concluded, $\alpha = 4^{o}$.

Figure 10.- Concluded.

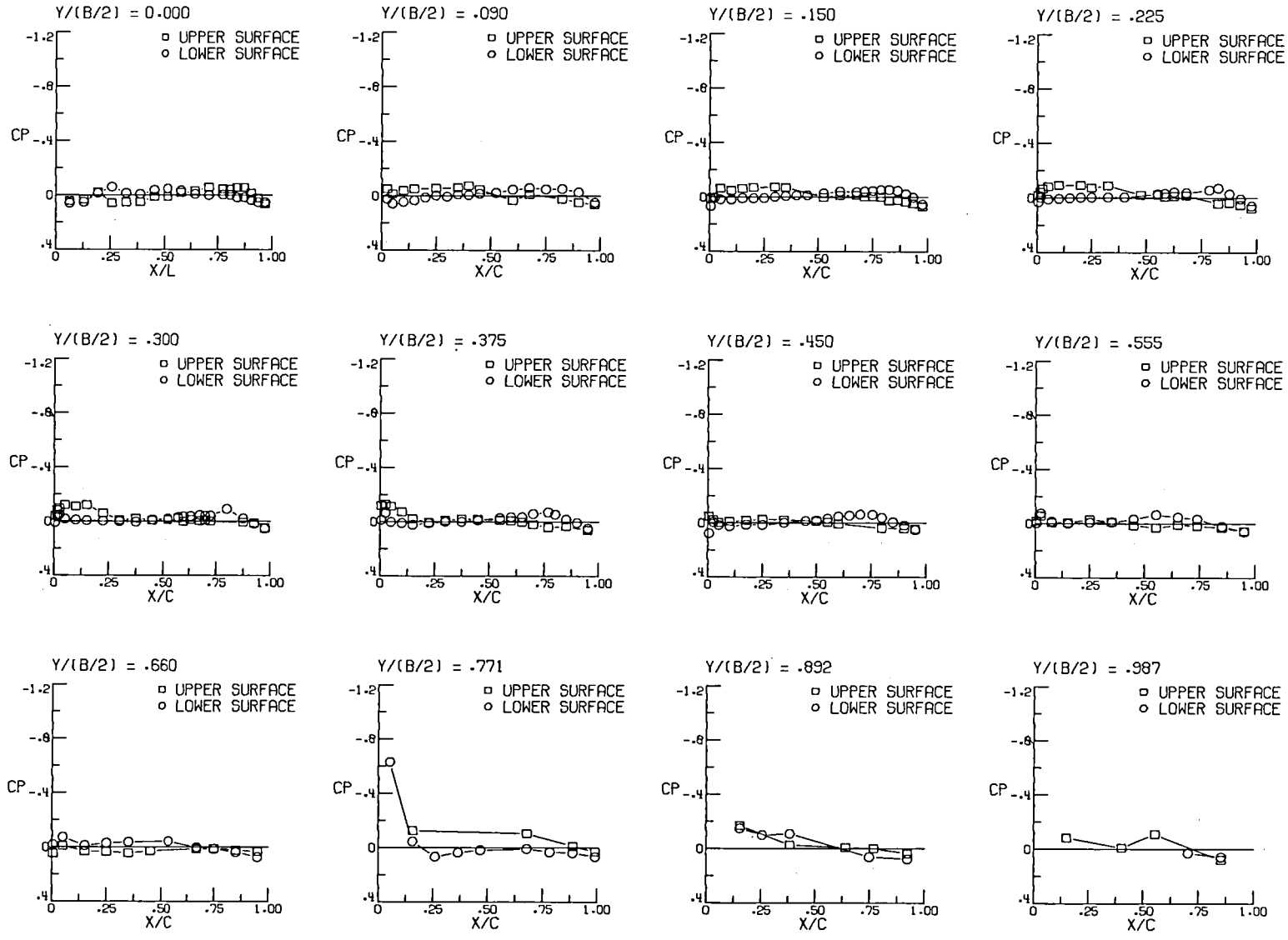

(a) M = 0.60, $\alpha = -2^{o}$, $p_{t,j}/p_{\infty} = 1.0$.

Figure 11.- Pressure distributions for the wing-body configuration with jet nacelle-strut assembly with A/B, $\delta_f = -10^{o}$, $x_e/c = -0.17$, $y/(b/2) = 0.46$, and $z_w/d_N = 1.50$.

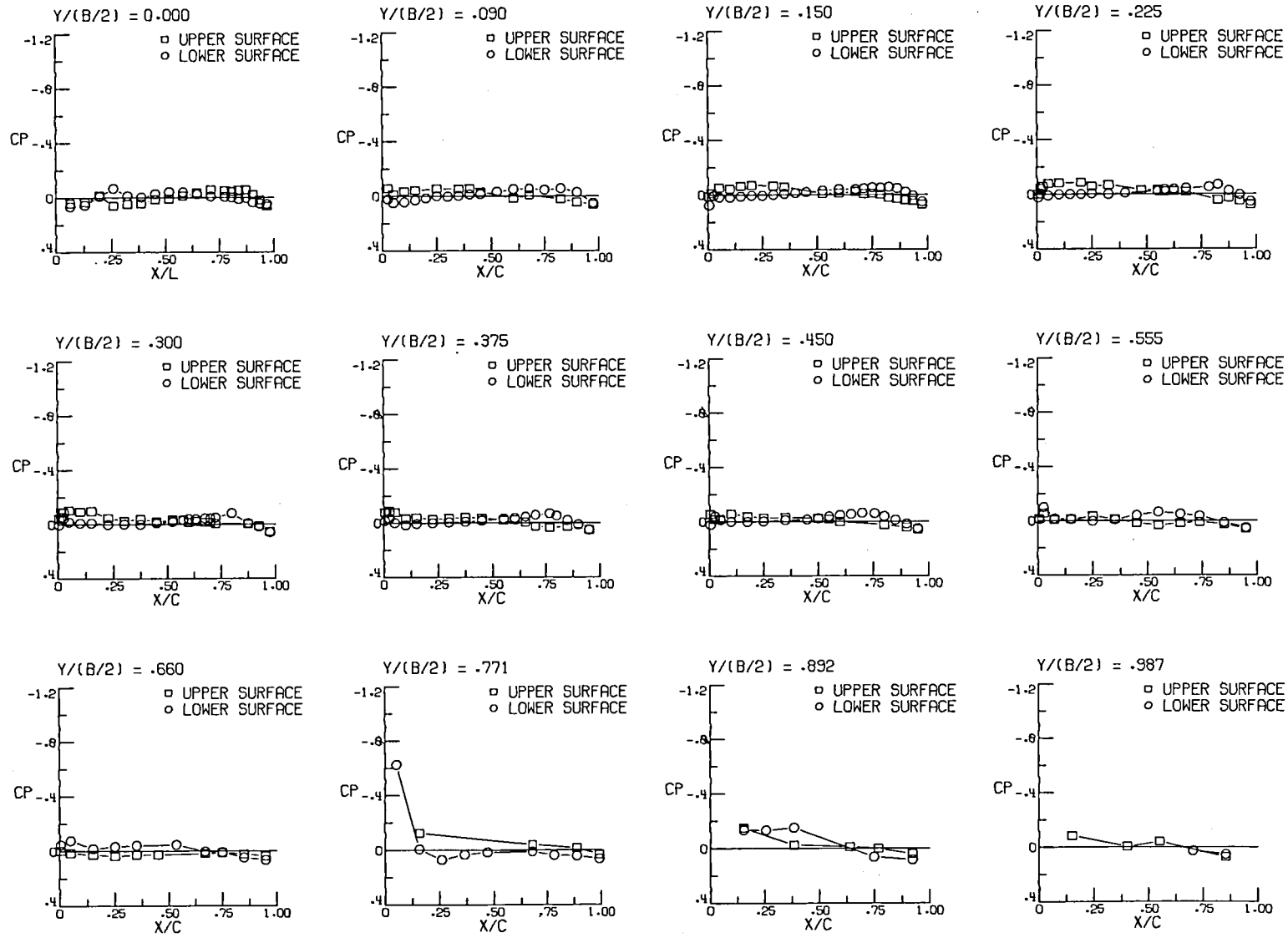

(a) Continued, $\alpha = -2^{o}$, $p_{t,j}/p_{\infty} = 3.0$.

Figure 11.- Continued.

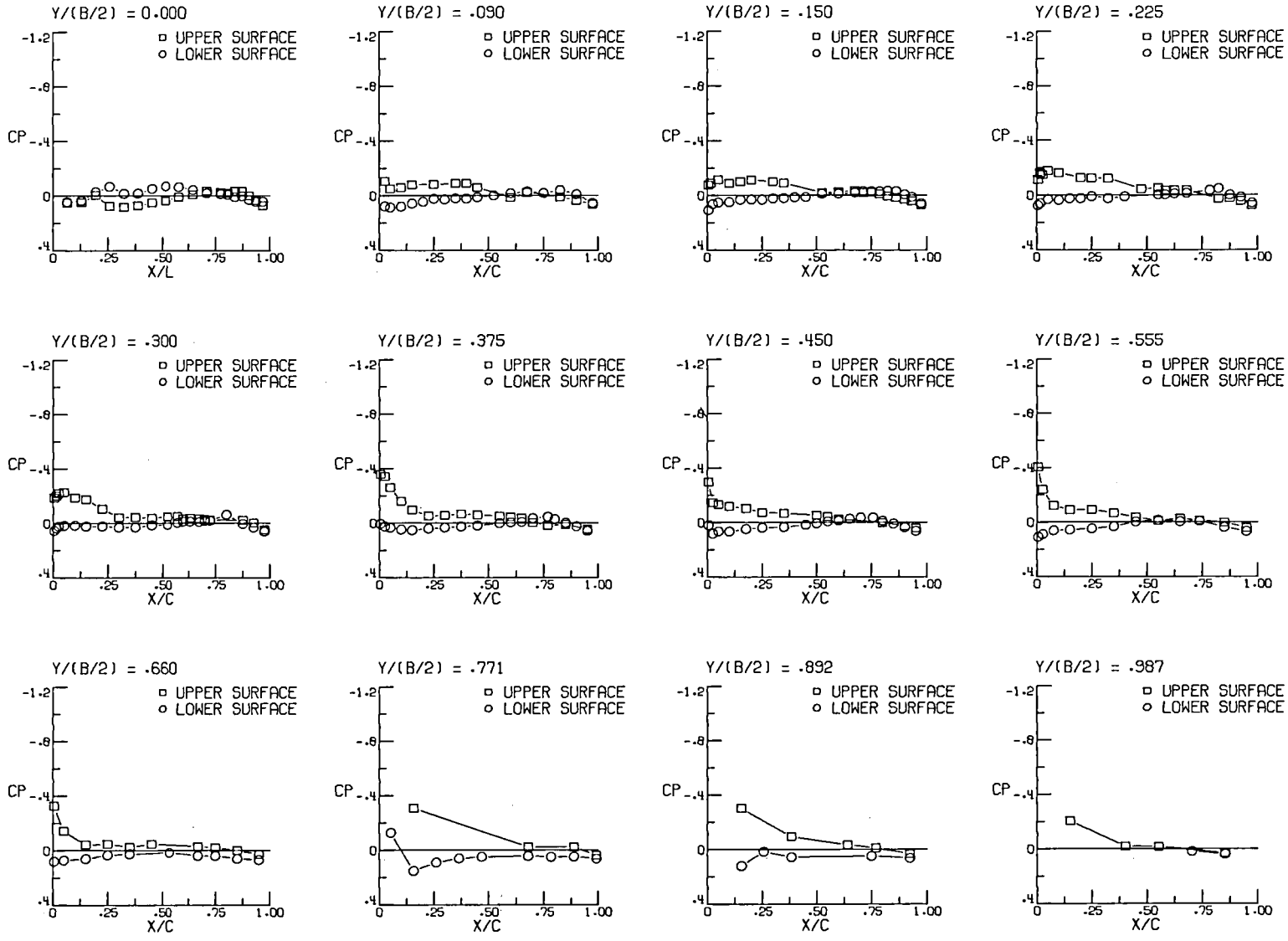

(a) Continued, $\alpha = 0^{o}$, $p_{t,j}/p_{\infty} = 1.0$.

Figure 11.- Continued.

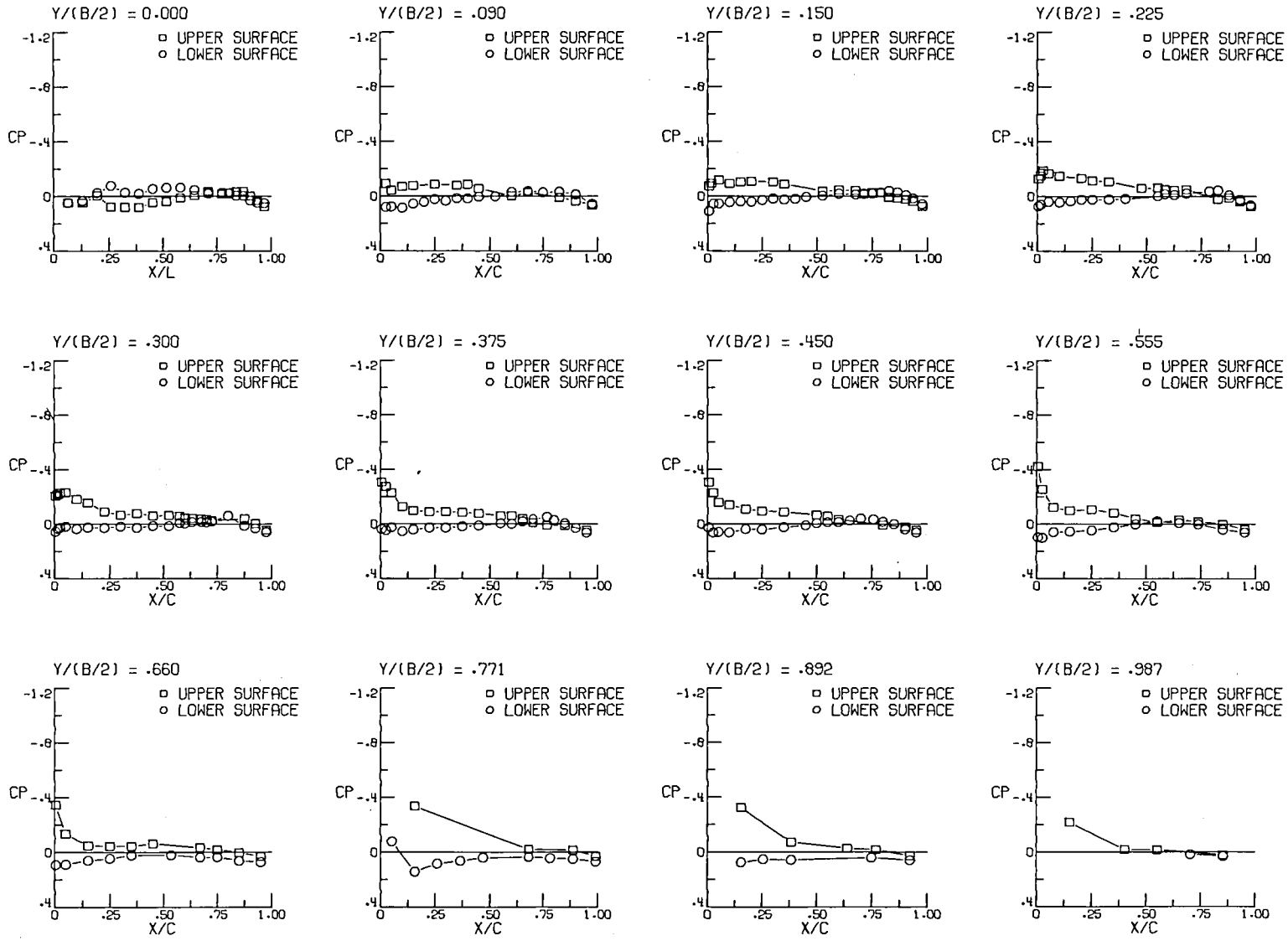

(a) Continued, $\alpha = 0^{o}$, $p_{t,j}/p_{\infty} = 2.9$.

Figure 11.- Continued.

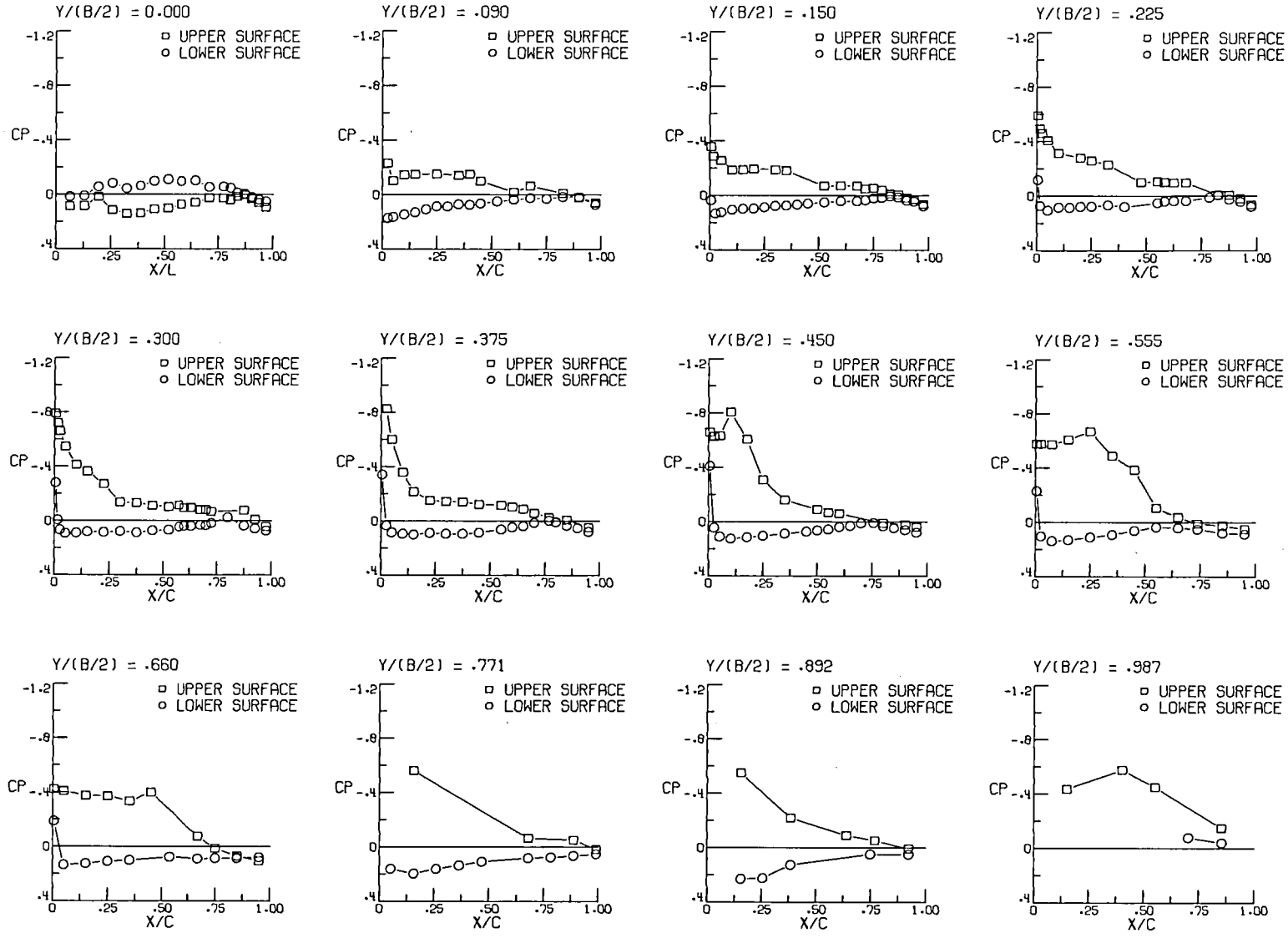

(a) Continued, $\alpha = 4^{o}$, $p_{t,j}/p_{\infty} = 0.9$.

Figure 11.- Continued.

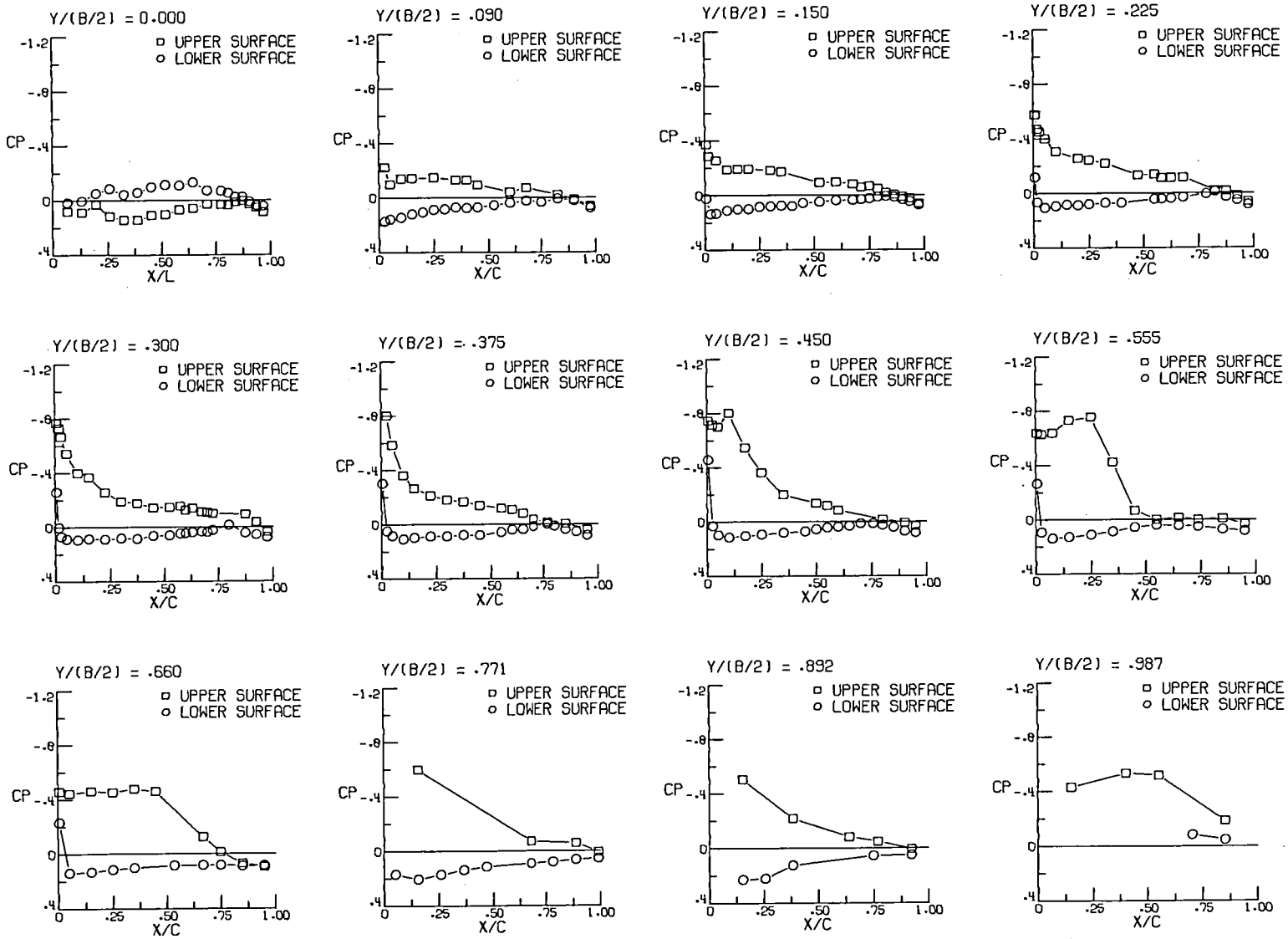

(a) Continued, $\alpha = 4^{o}$, $p_{t,j}/p_{\infty} = 2.9$.

Figure 11.- Continued.

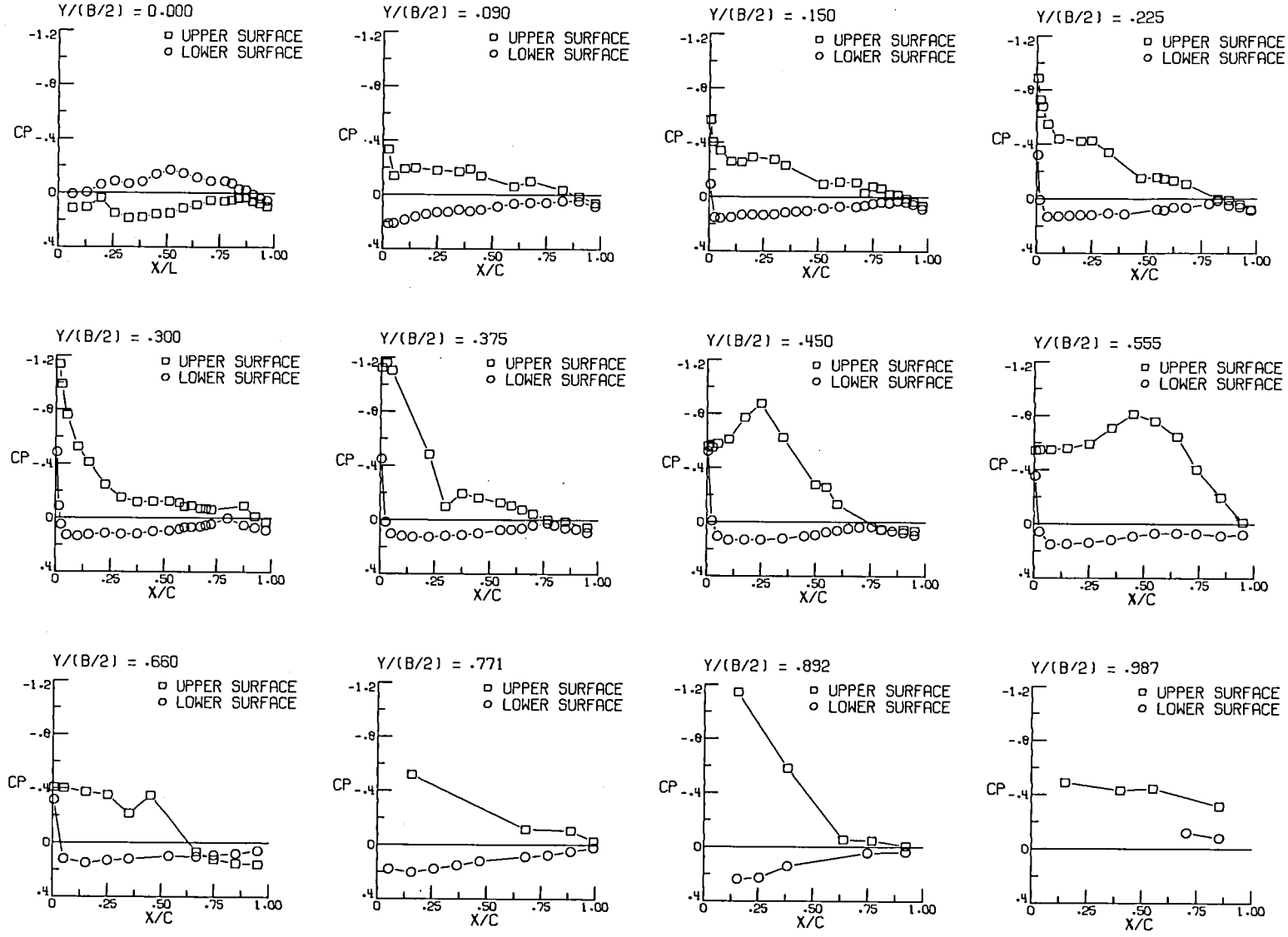

(a) Continued, $\alpha = 6^{\circ}$, $p_{t,j}/p_{\infty} = 1.0$.

Figure 11.- Continued.

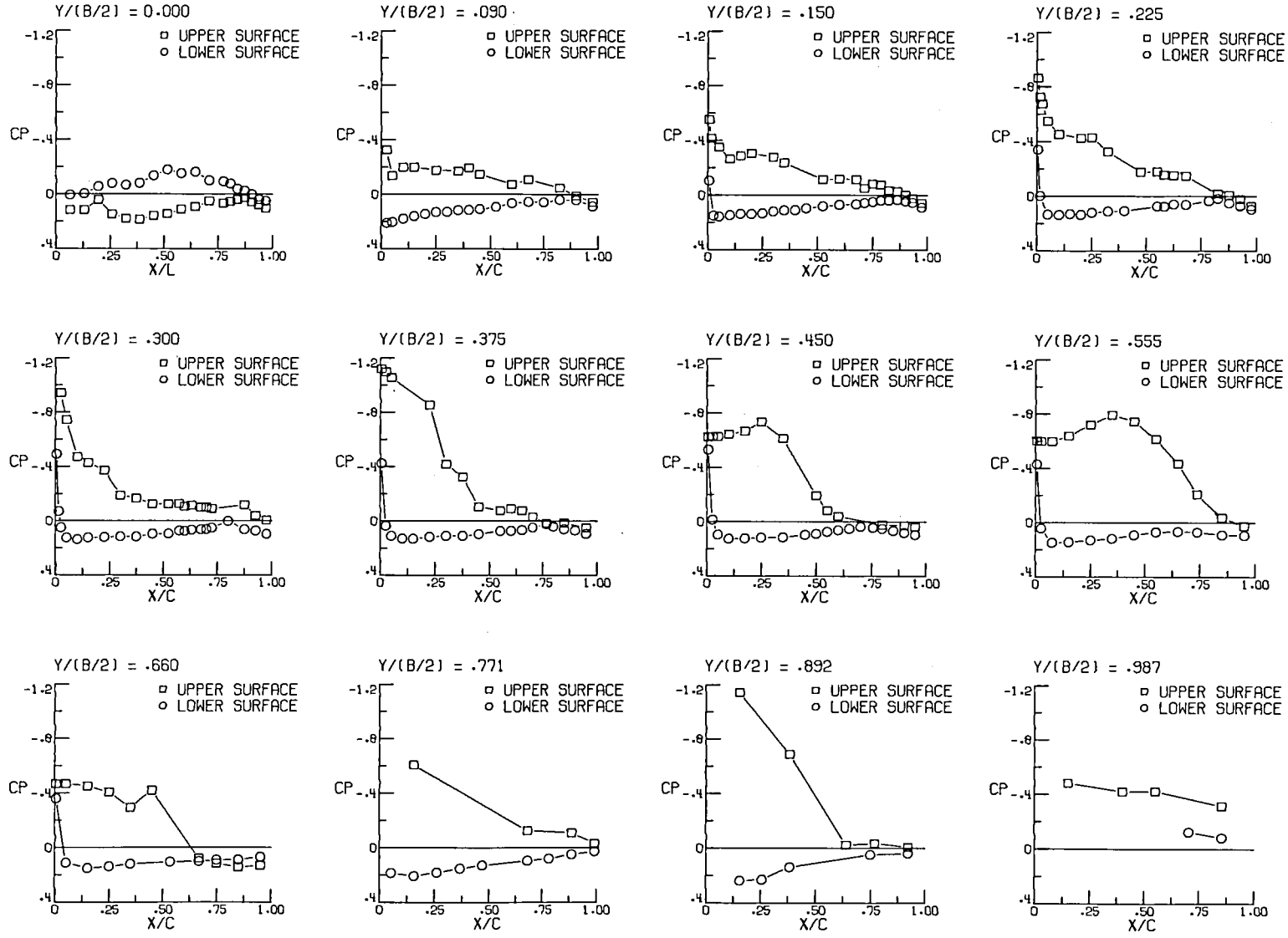

(a) Concluded, $\alpha = 6^{o}$, $p_{t,j}/p_{\infty} = 2.9$.

Figure 11.- Continued.

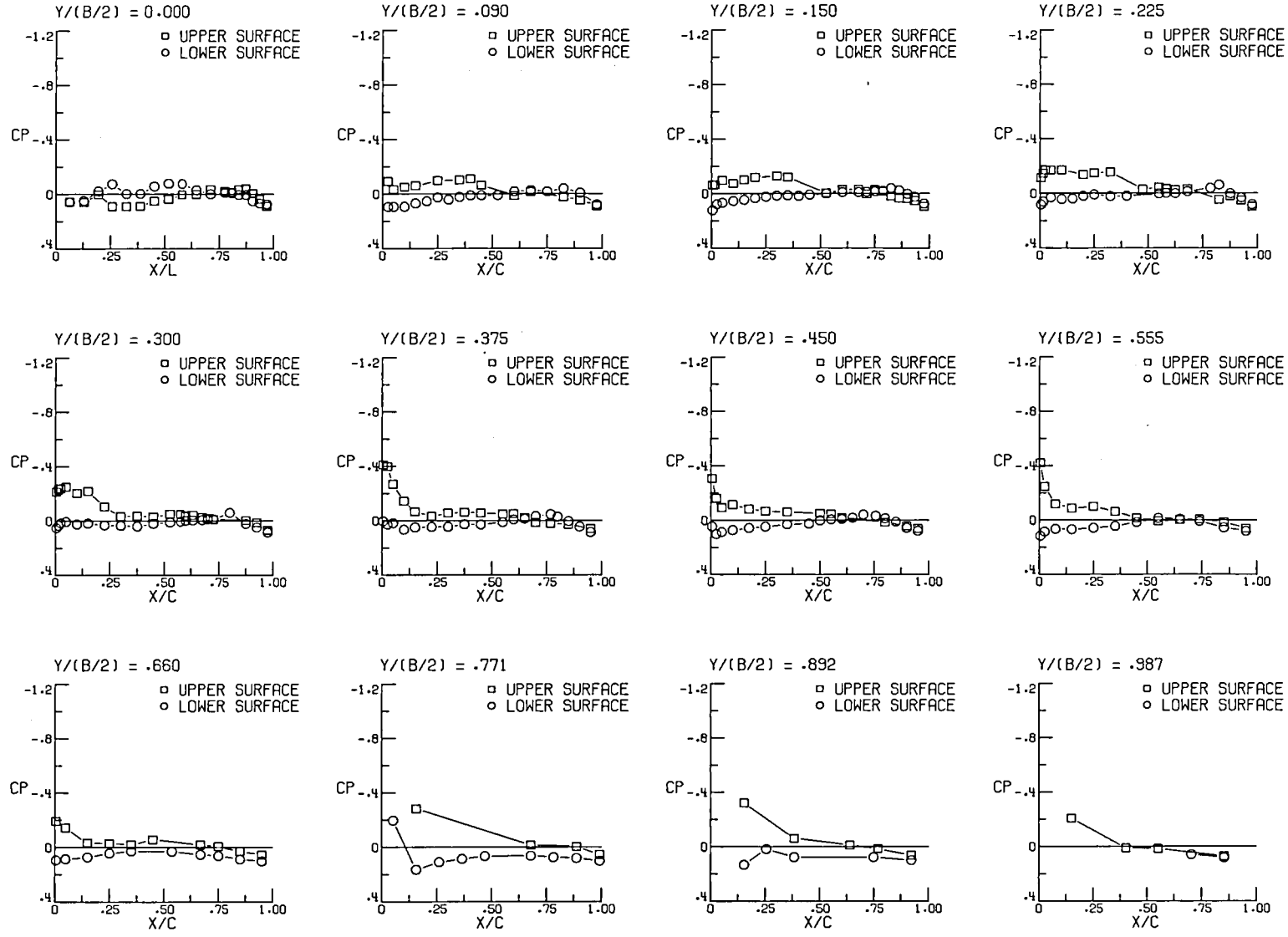

(b) $M = 0.80$, $\alpha = 0^{o}$, $p_{t,j}/p_{\infty} = 1.0$.

Figure 11.- Continued.

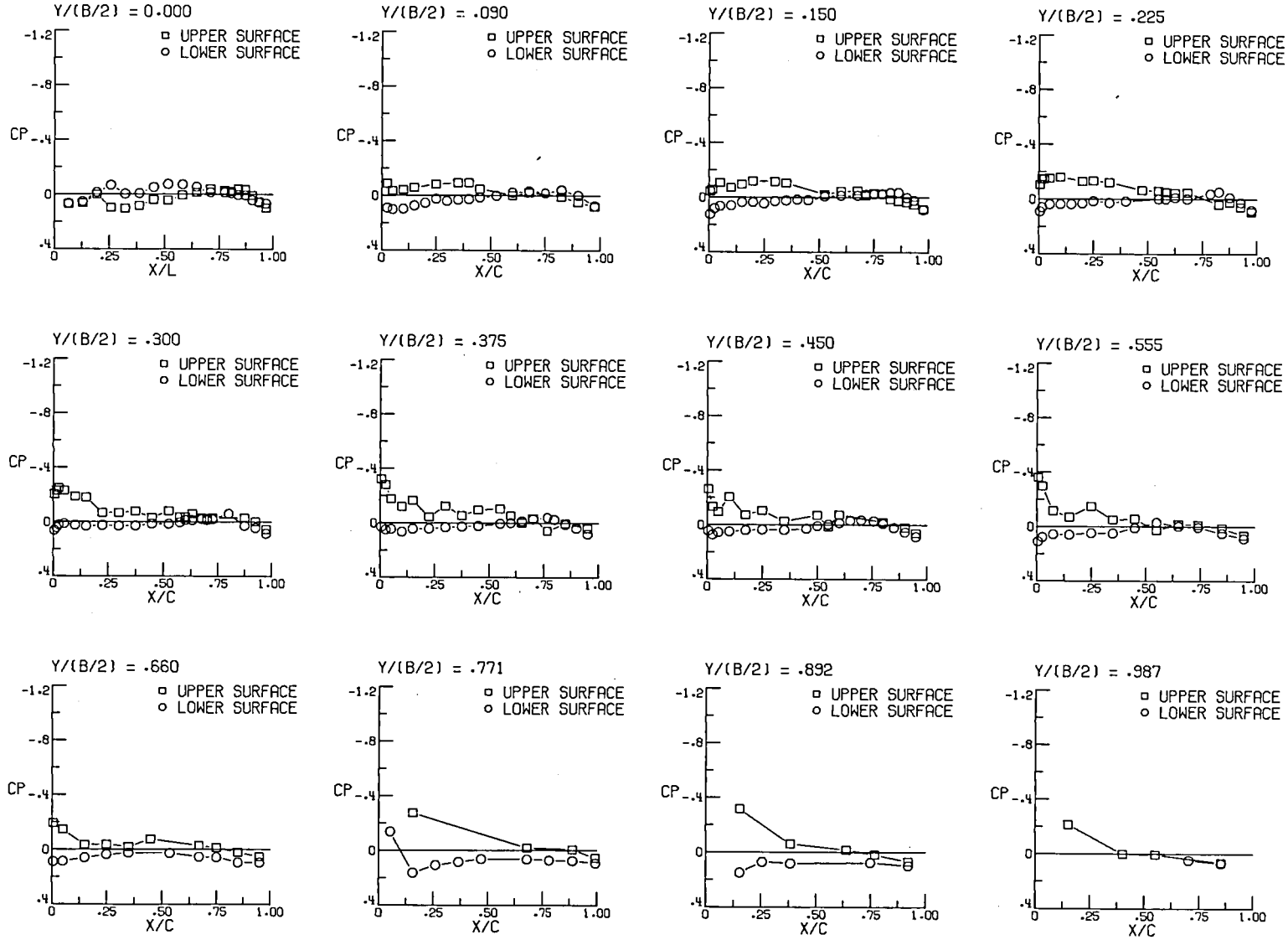

(b) Continued, $\alpha = 0^{o}$, $p_{t,j}/p_{\infty} = 5.1$.

Figure 11.- Continued.

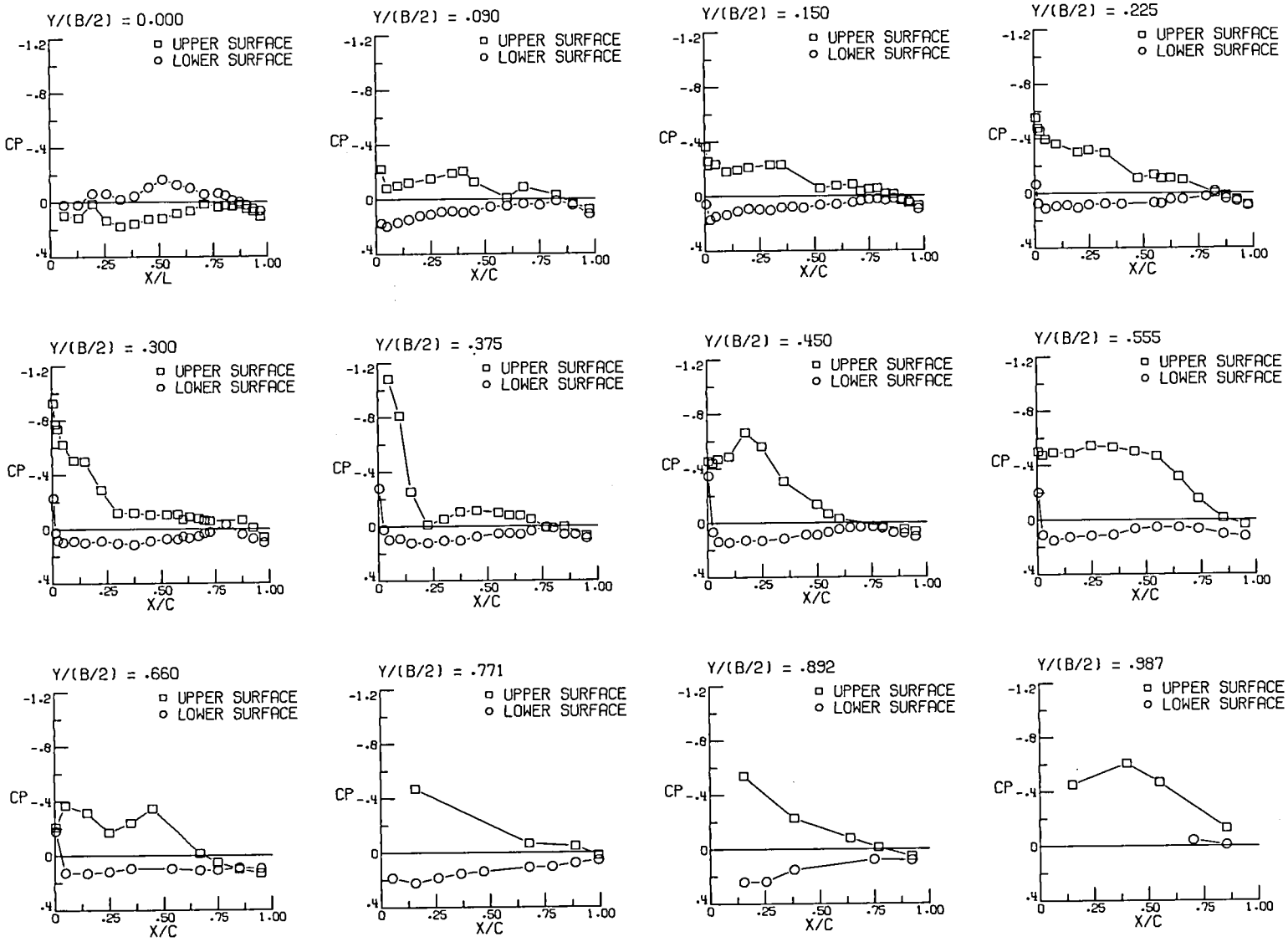

(b) Continued, $\alpha = 4^{o}$, $p_{t,j}/p_{\infty} = 0.9$.

Figure 11.- Continued.

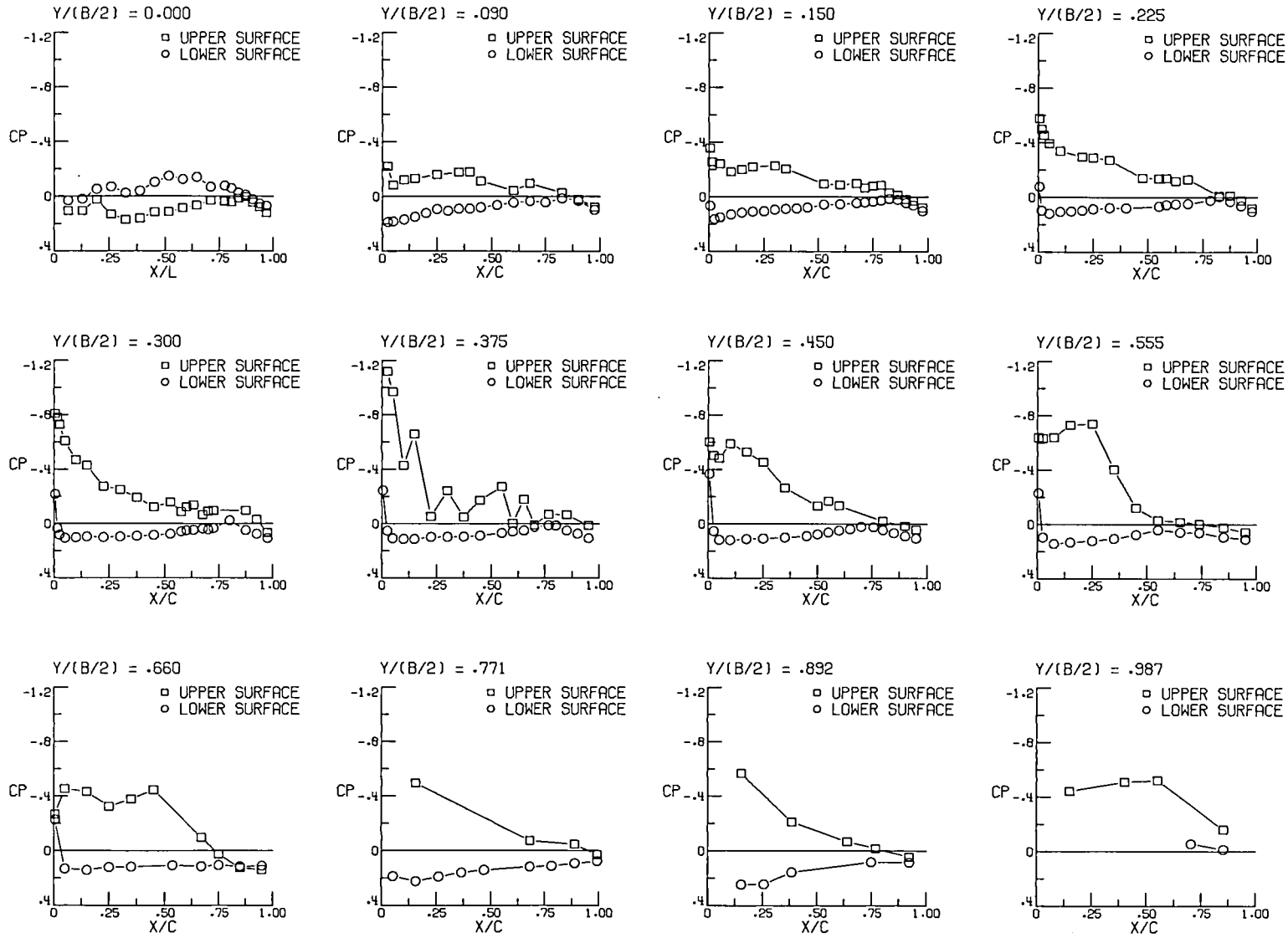

(b) Continued, $\alpha = 4^{o}$, $p_{t,j}/p_{\infty} = 5.0$.

Figure 11.- Continued.

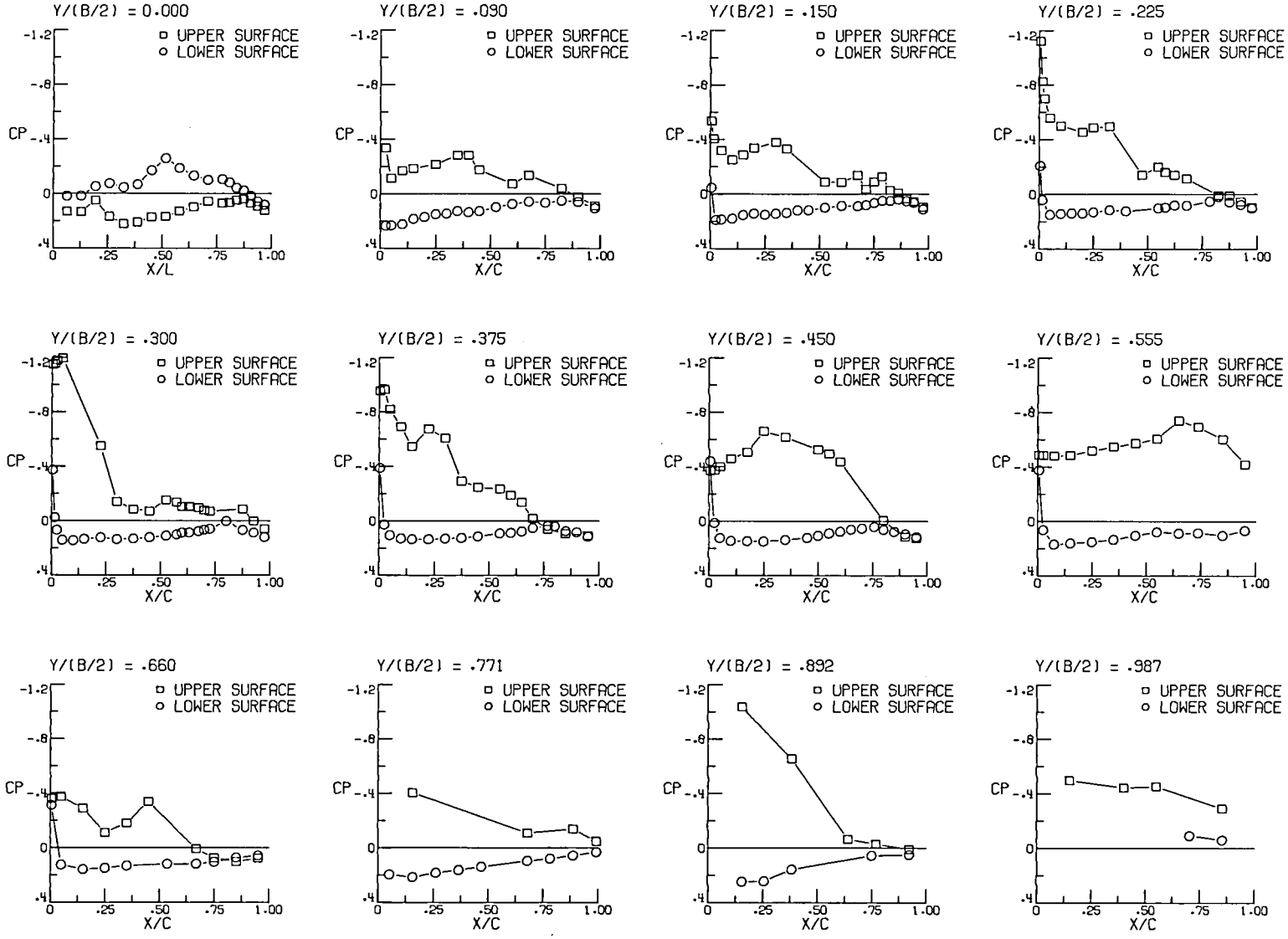

(b) Continued, $\alpha = 6^{o}$, $p_{t,j}/p_{\infty} = 0.8$.

Figure 11.- Continued.

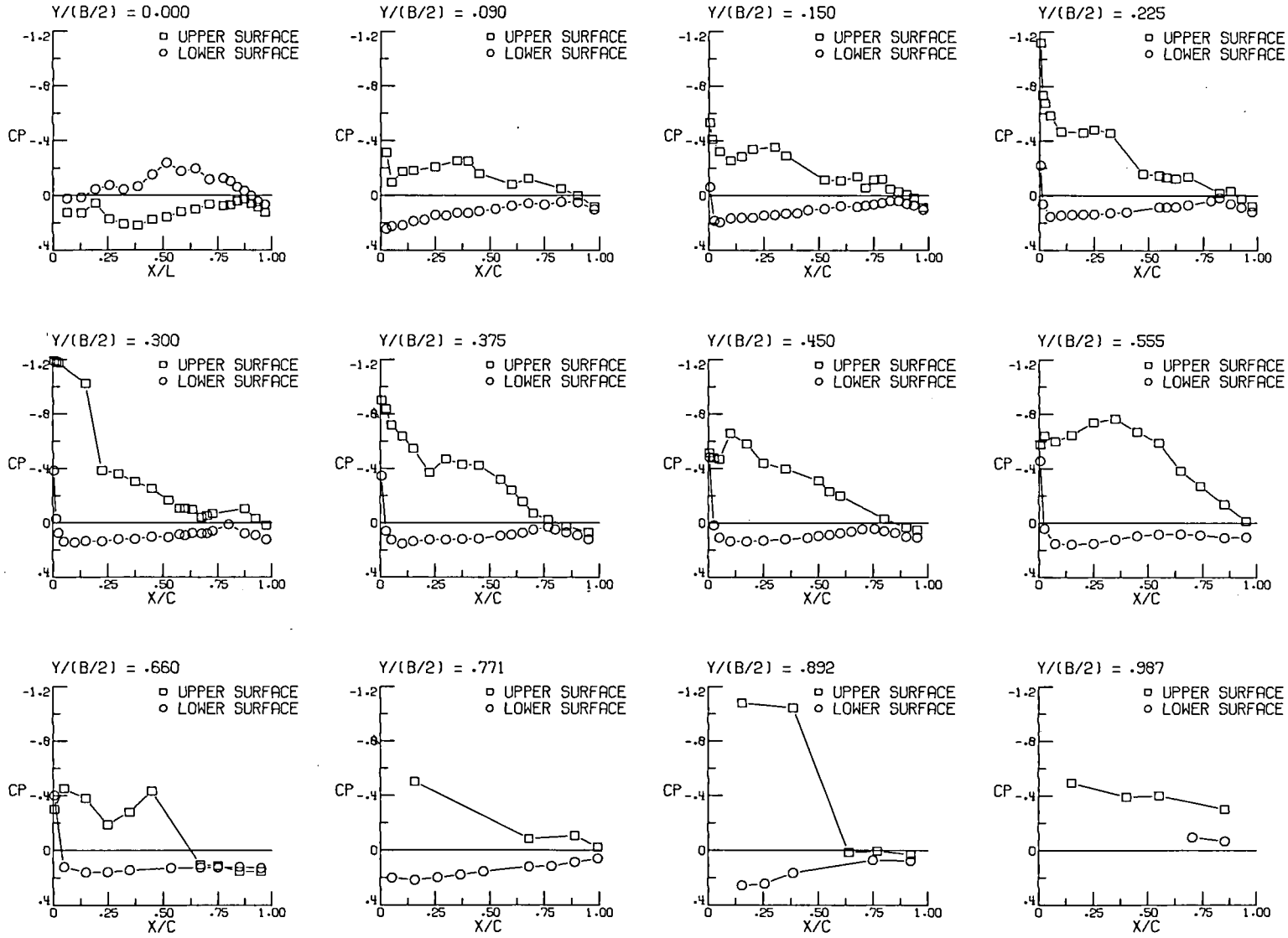

(b) Continued, $\alpha = 6^{o}$, $p_{t,j}/p_{\infty} = 5.1$.

Figure 11.- Continued.

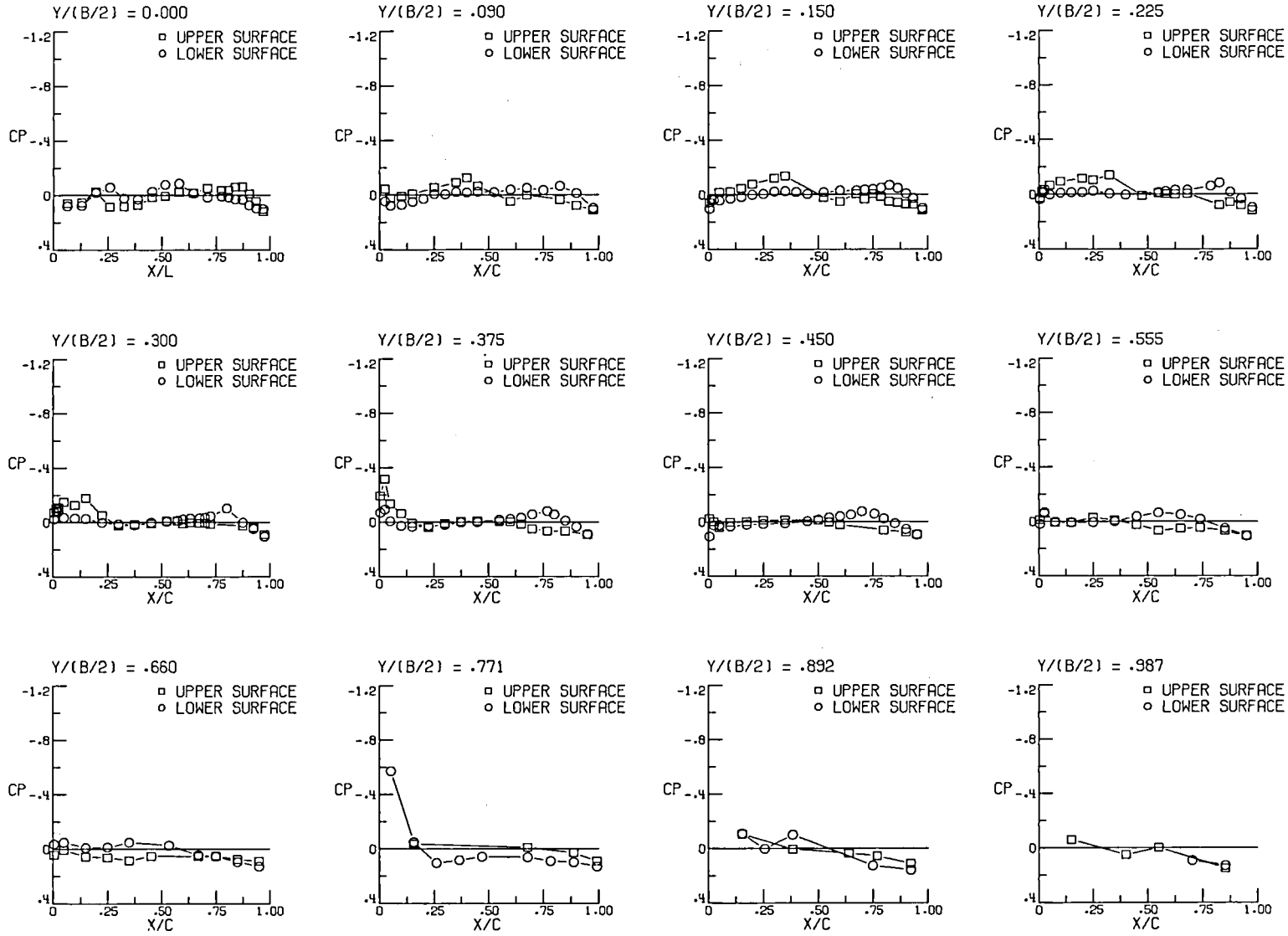

(c) M = 0.90, $\alpha = -2^{o}$, $p_{t,j}/p_{\infty} = 1.0$.

Figure 11.- Continued.

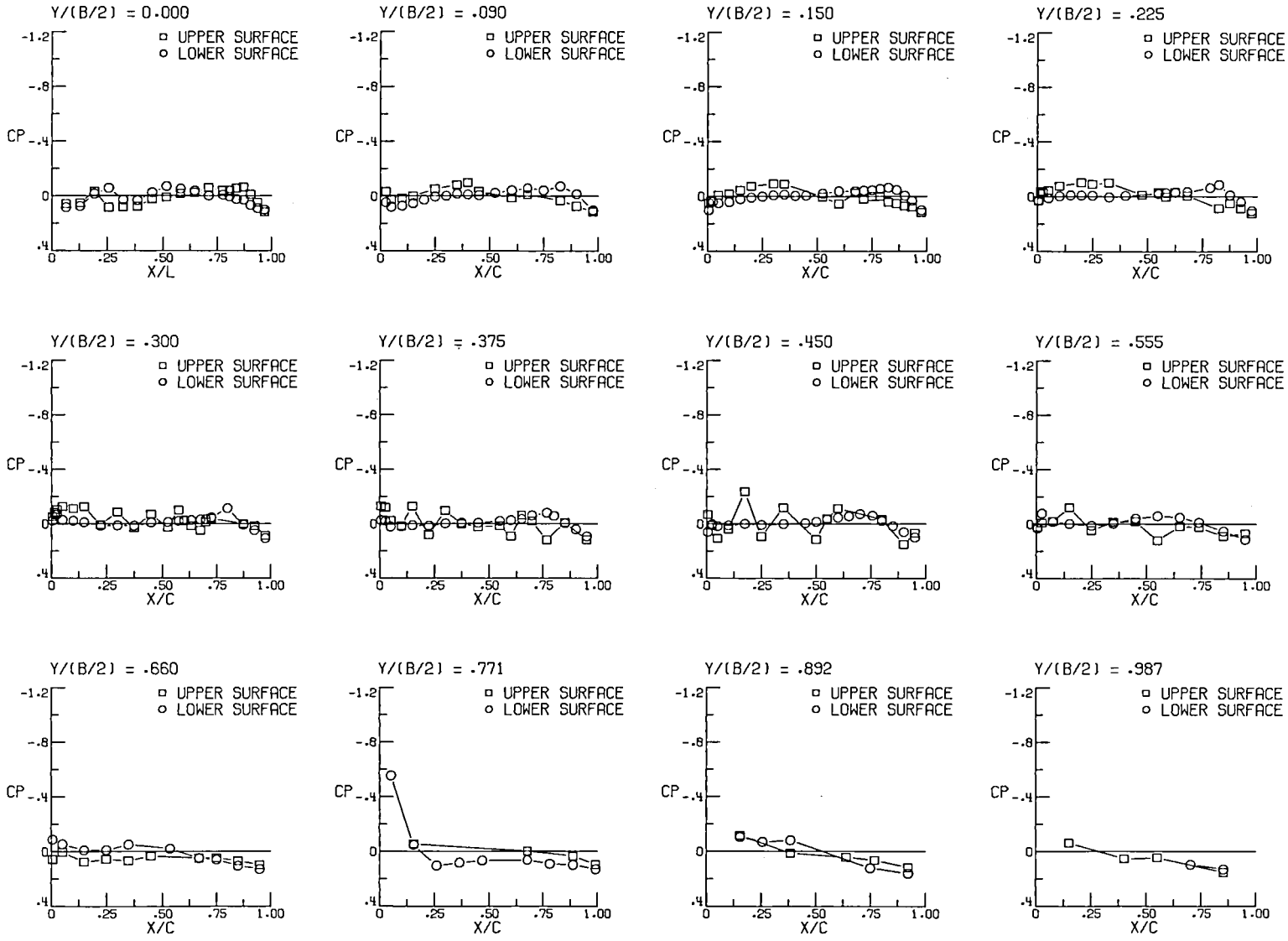

(c) Continued, $\alpha = -2^{o}$, $p_{t,j}/p_{\infty} = 6.1$.

Figure 11.- Continued.

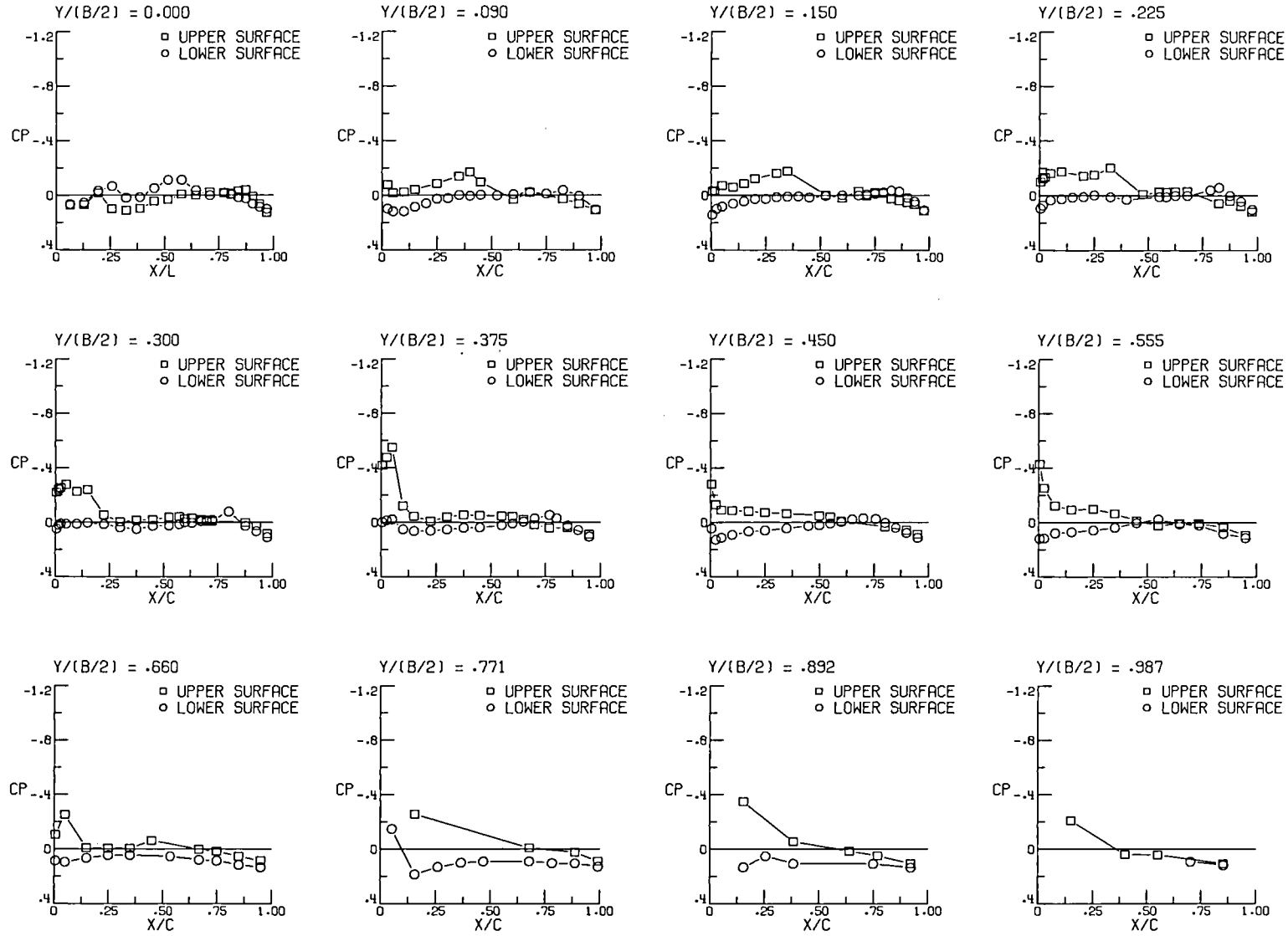

(d) Continued, $\alpha = 0^{o}$, $p_{t,j}/p_{\infty} = 1.0$.

Figure 11.- Continued.

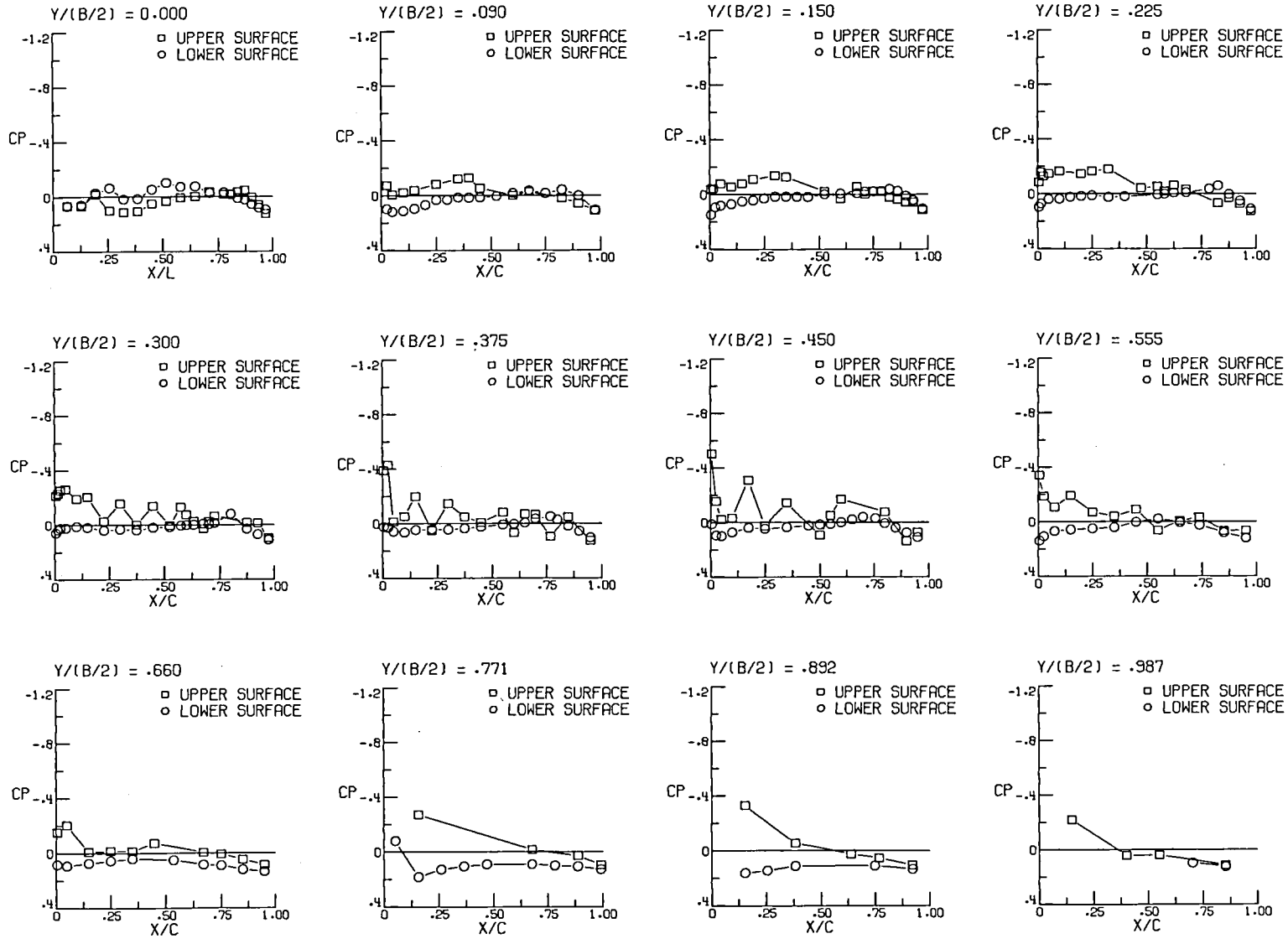

(c) Continued, $\alpha = 0^{o}$, $p_{t,j}/p_{\infty} = 5.9$.

Figure 11.- Continued.

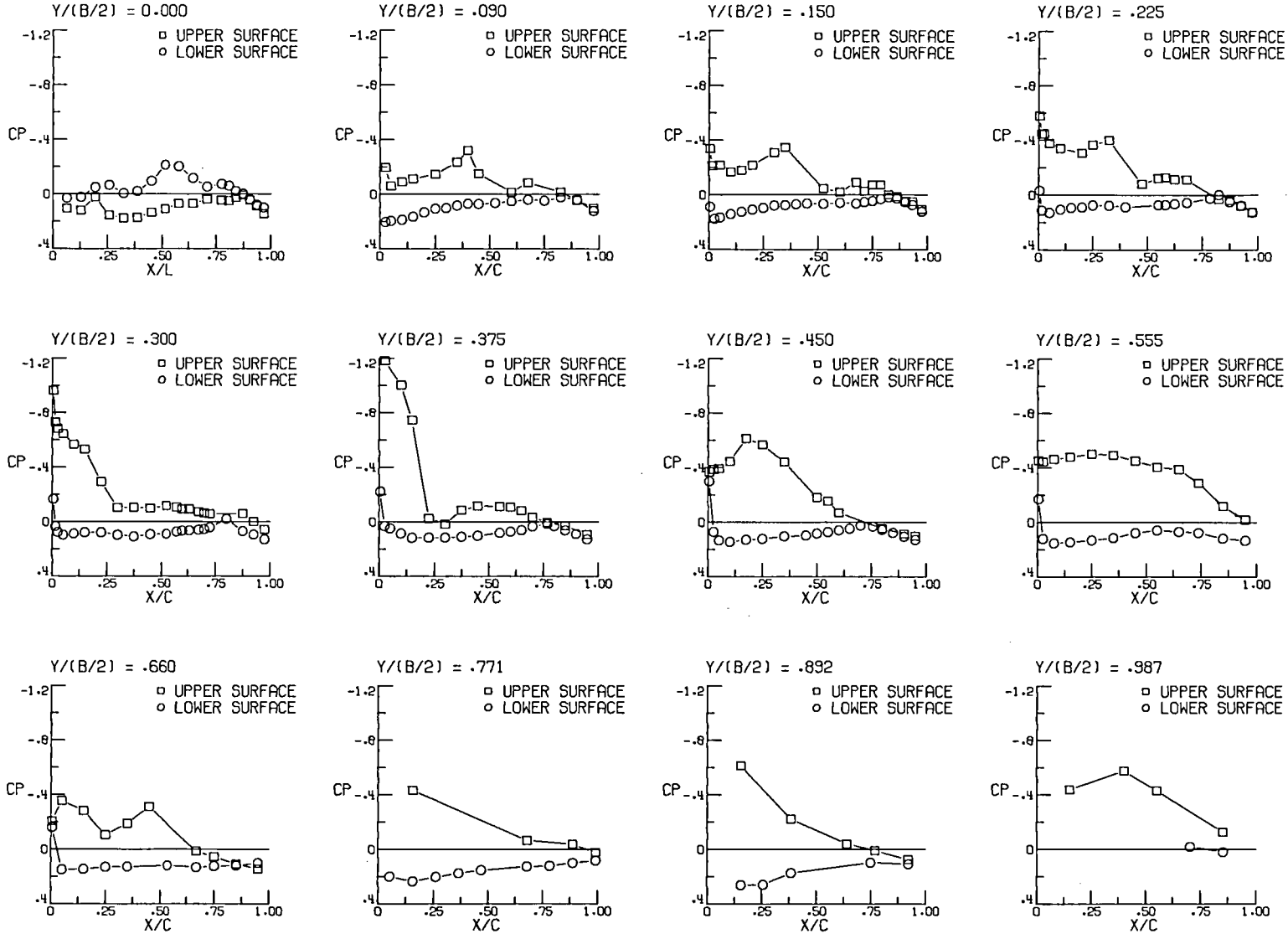

(c) Continued, $\alpha = 4^{o}$, $p_{t,j}/p_{\infty} = 0.9$.

Figure 11.- Continued.

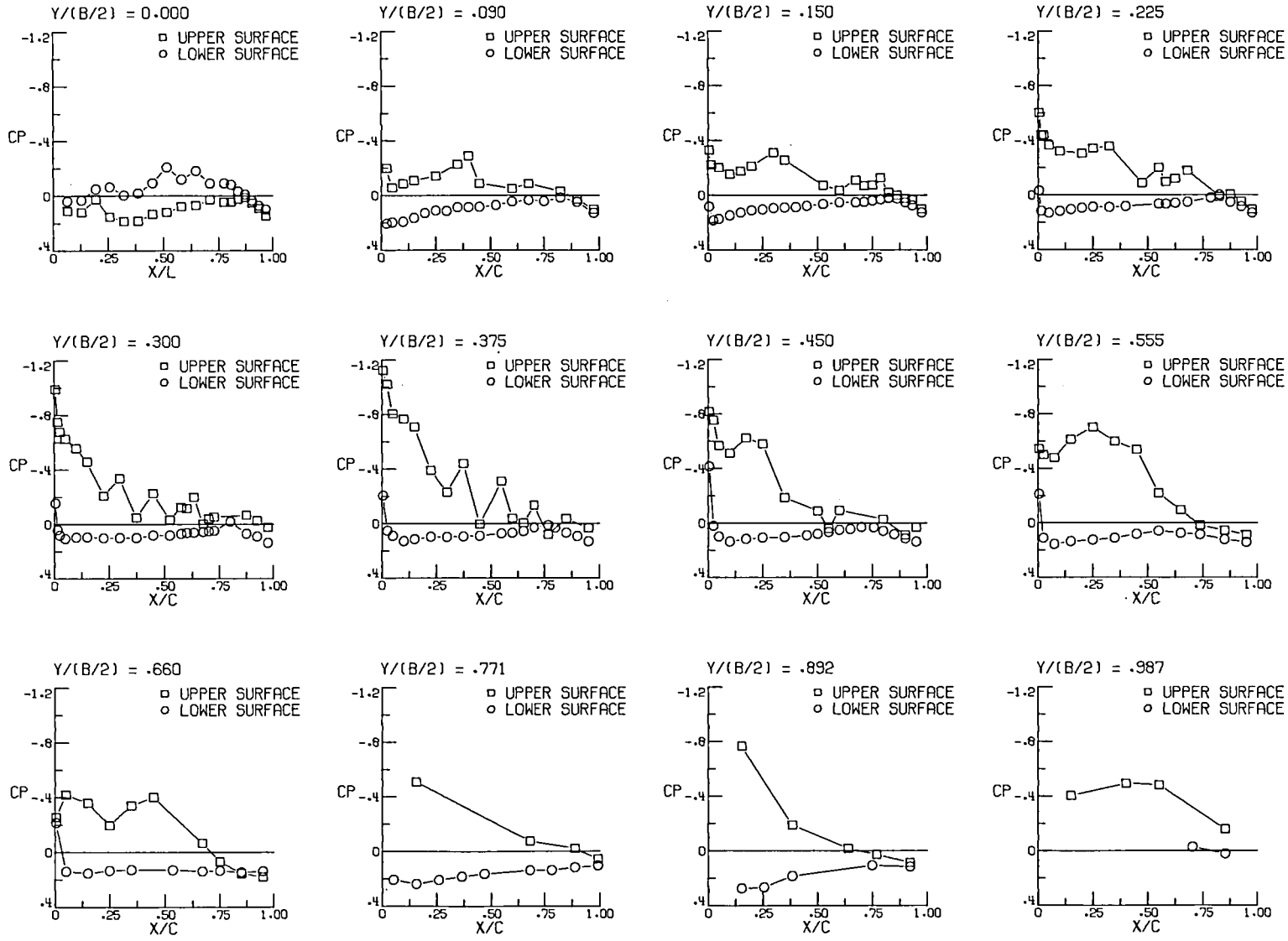

(c) Continued, $\alpha = 4^{o}$, $p_{t,j}/p_{\infty} = 6.0$.

Figure 11.- Continued.

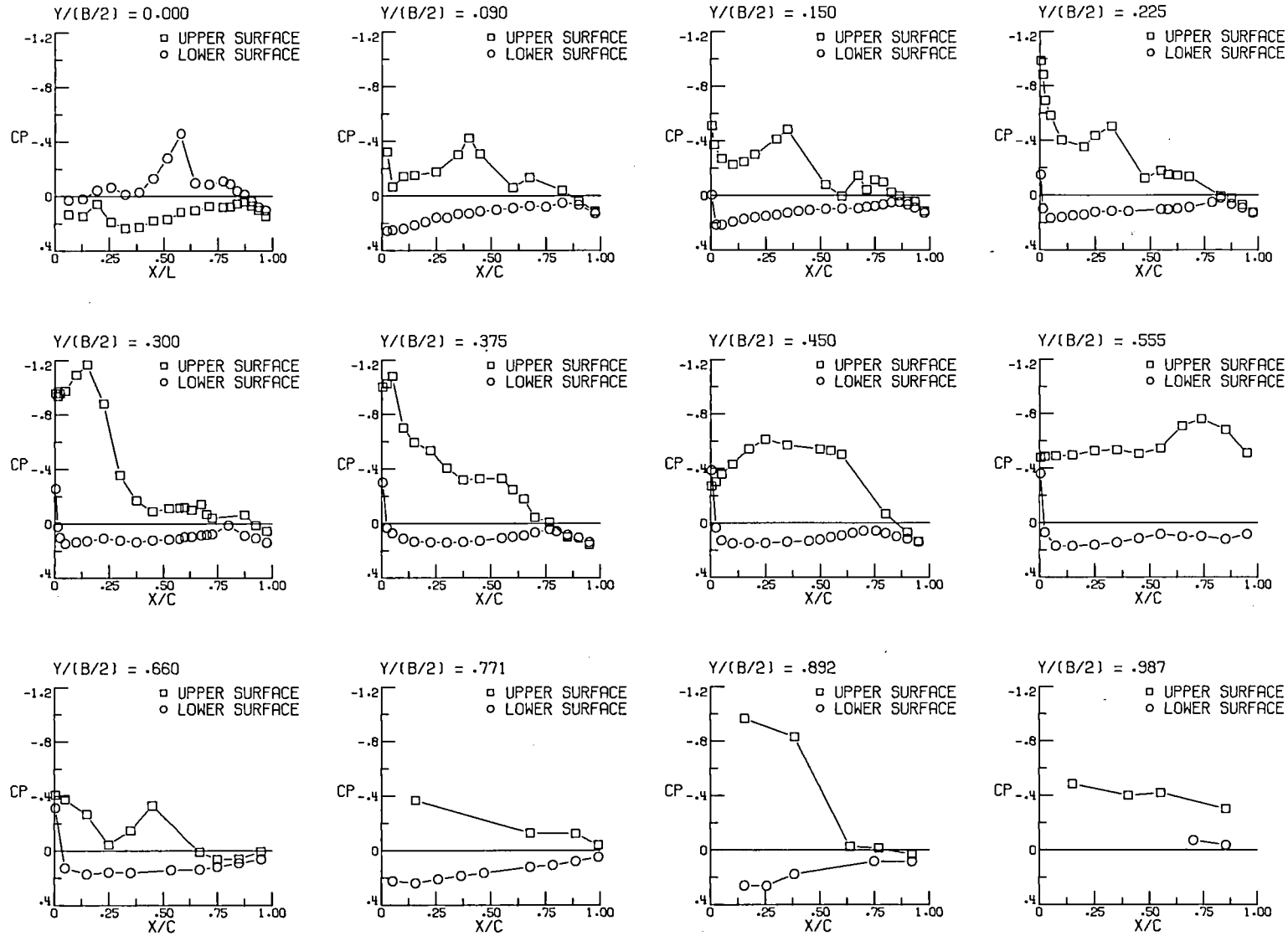

(c) Continued, $\alpha = 6^{o}$, $p_{t,j}/p_{\infty} = 0.7$.

Figure 11.- Continued.

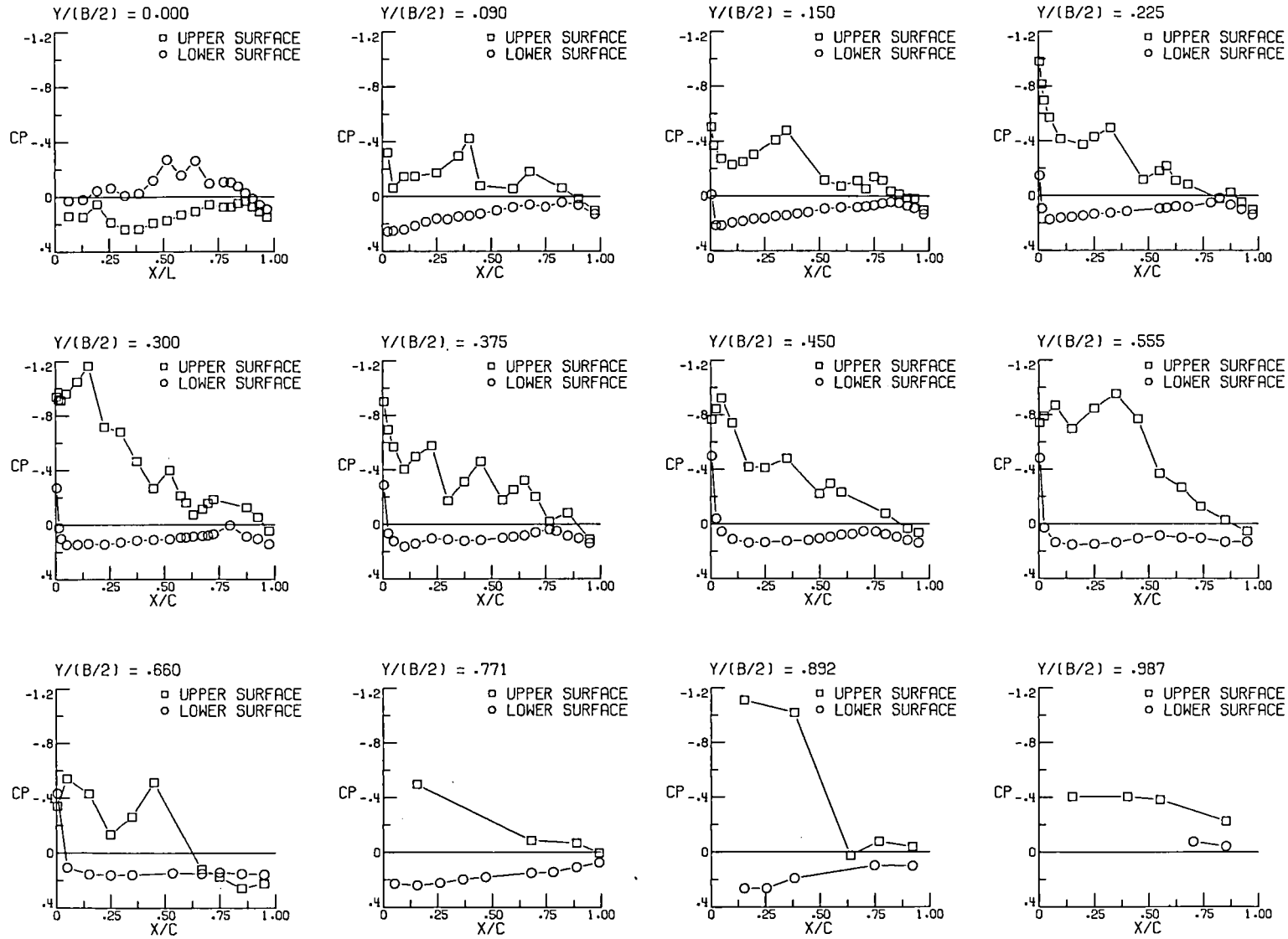

(c) Concluded, $\alpha = 6^{o}$, $p_{t,j}/p_{\infty} = 8.2$.

Figure 11.- Continued.

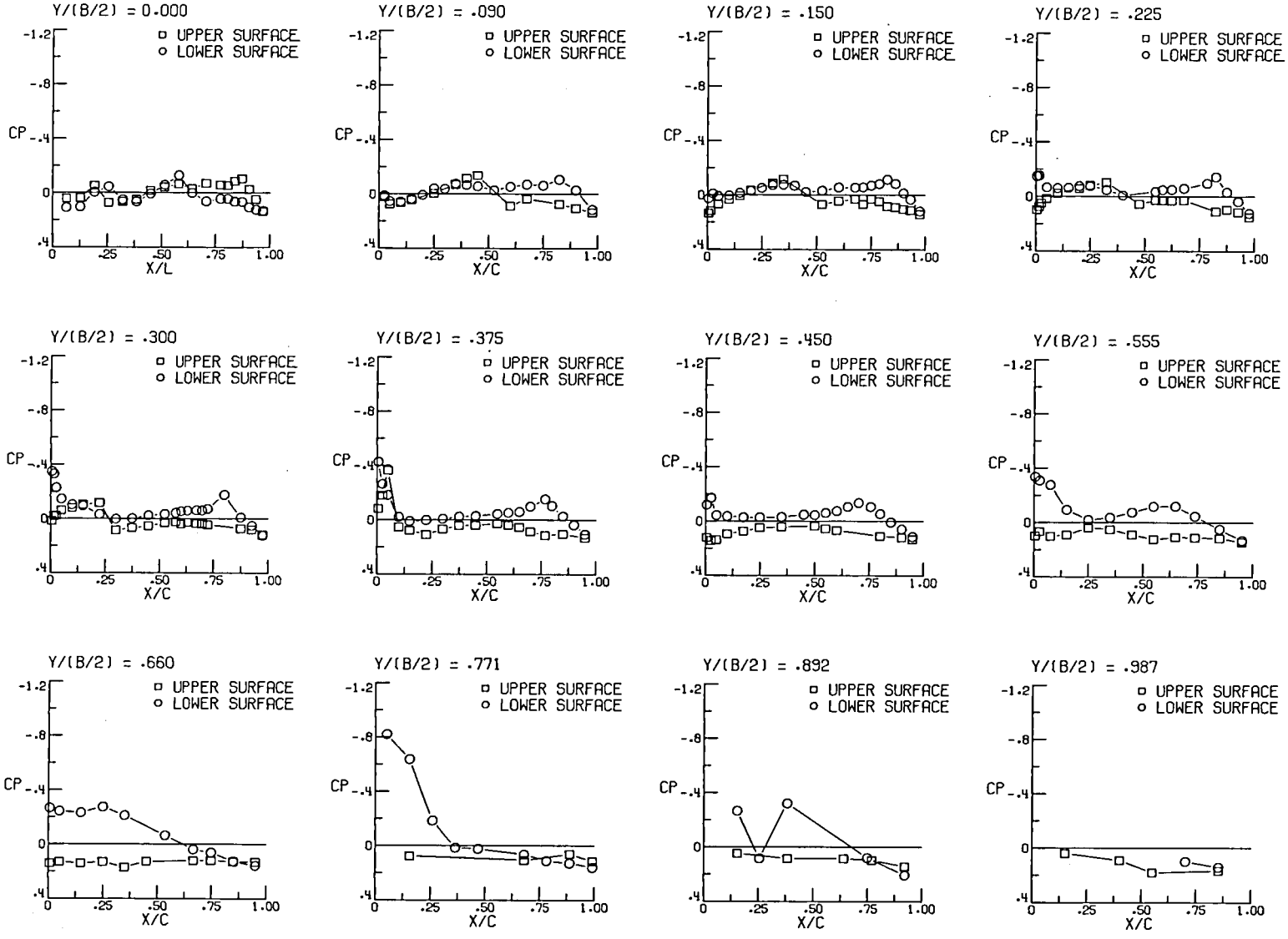

(d) $M = 0.95$, $\alpha = -4^{\circ}$, $p_{t,j}/p_{\infty} = 1.0$.

Figure 11.- Continued.

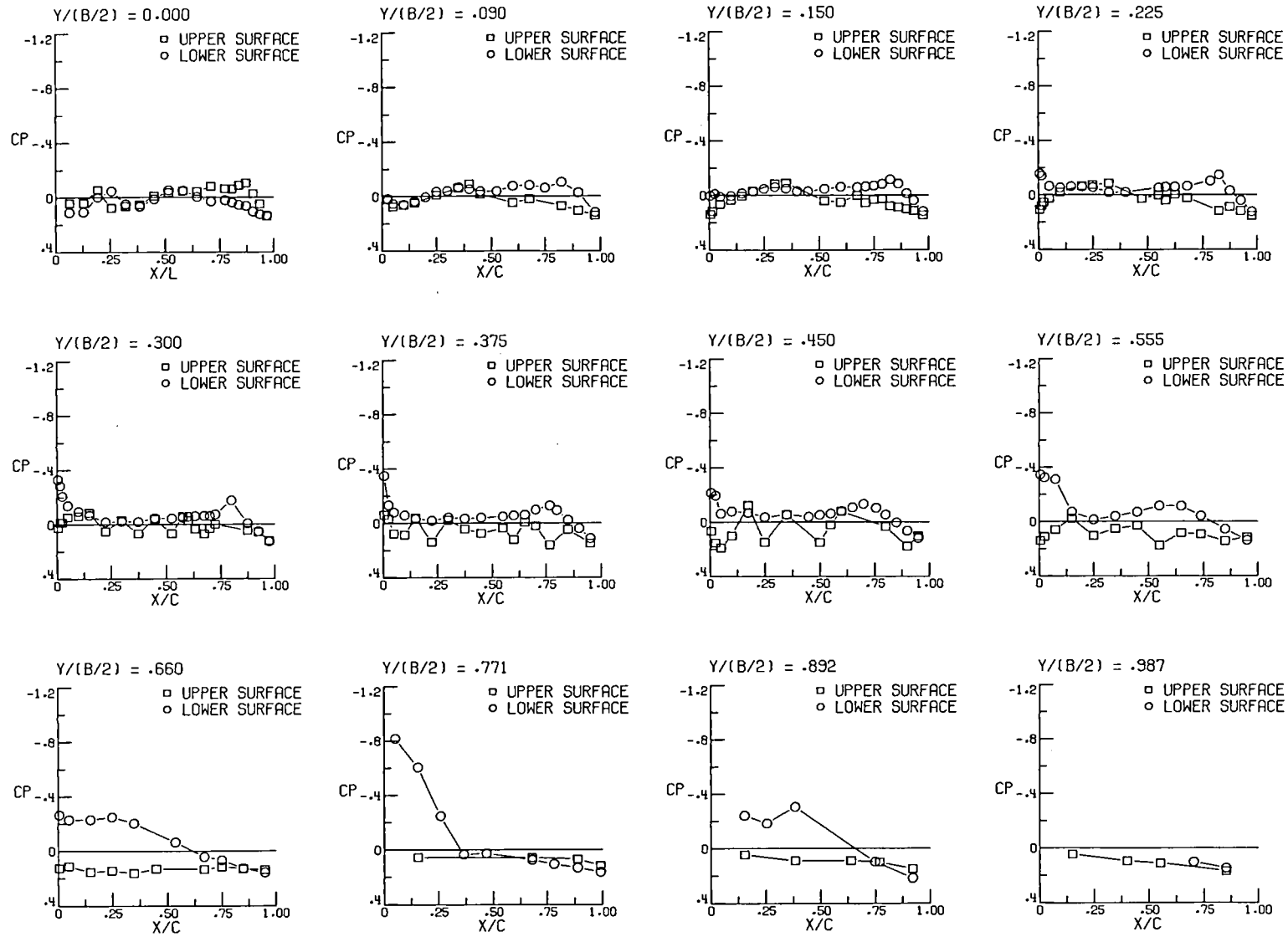

(d) Continued, $\alpha = -4^{o}$, $p_{t,j}/p_{\infty} = 6.1$.

Figure 11.- Continued.

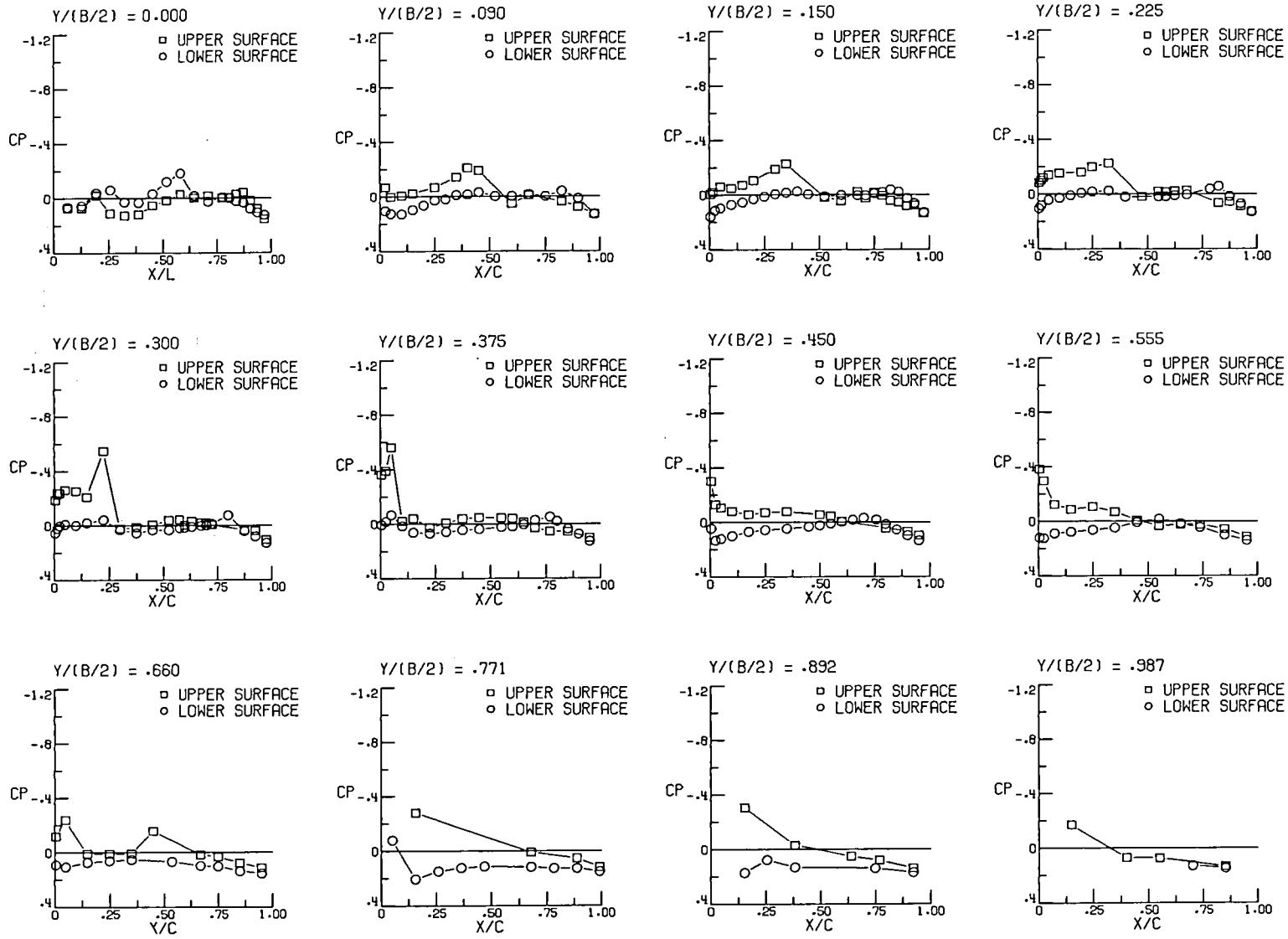

(d) Continued, $\alpha = 0^{o}$, $p_{t,j}/p_{\infty} = 1.0$.

Figure 11.- Continued.

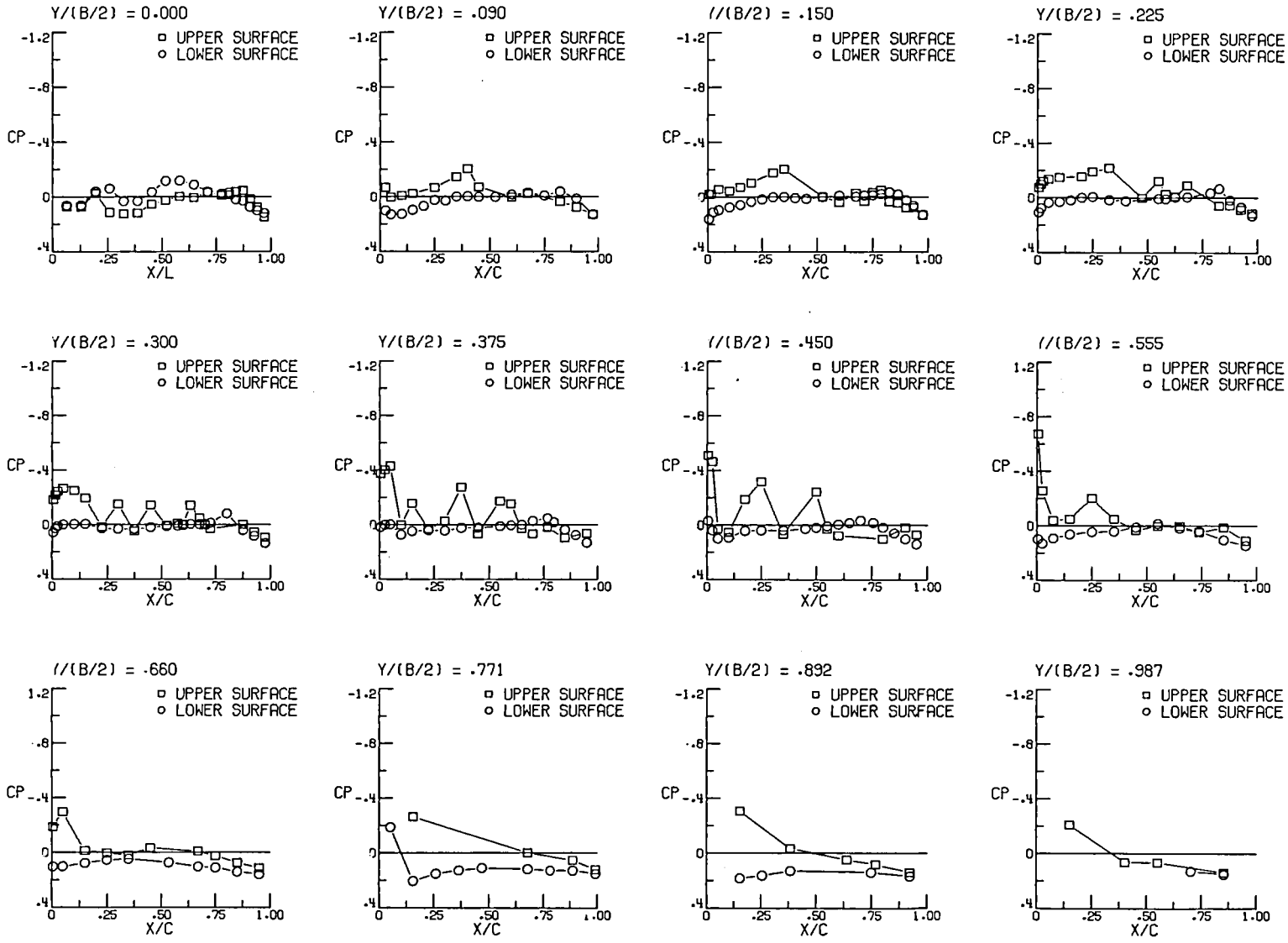

(d) Continued, $\alpha = 0^{o}$, $p_{t,j}/p_{\infty} = 6.1$.

Figure 11.- Continued.

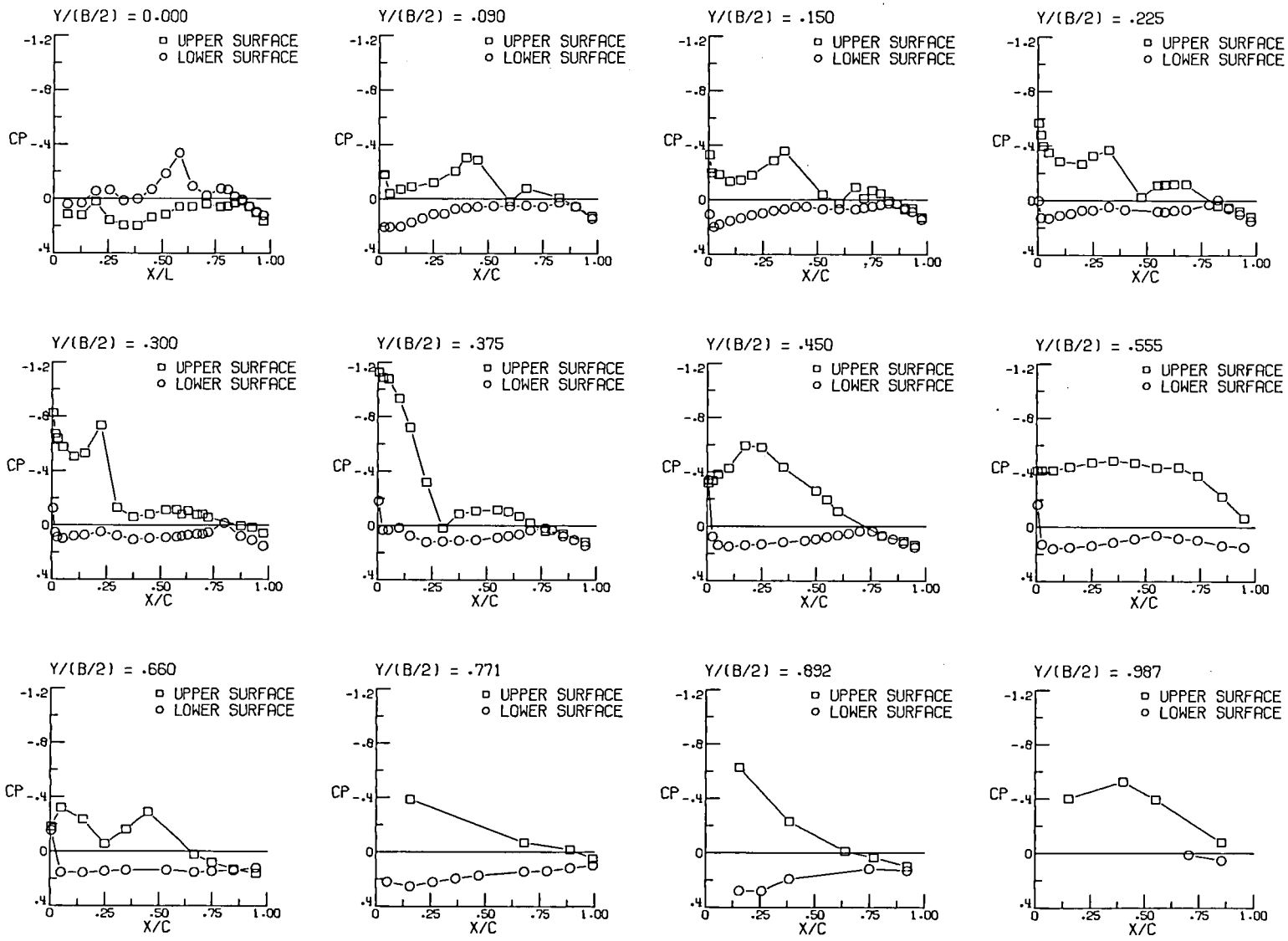

(d) Continued, $\alpha = 4^{o}$, $p_{t,j}/p_{\infty} = 0.8$.

Figure 11.- Continued.

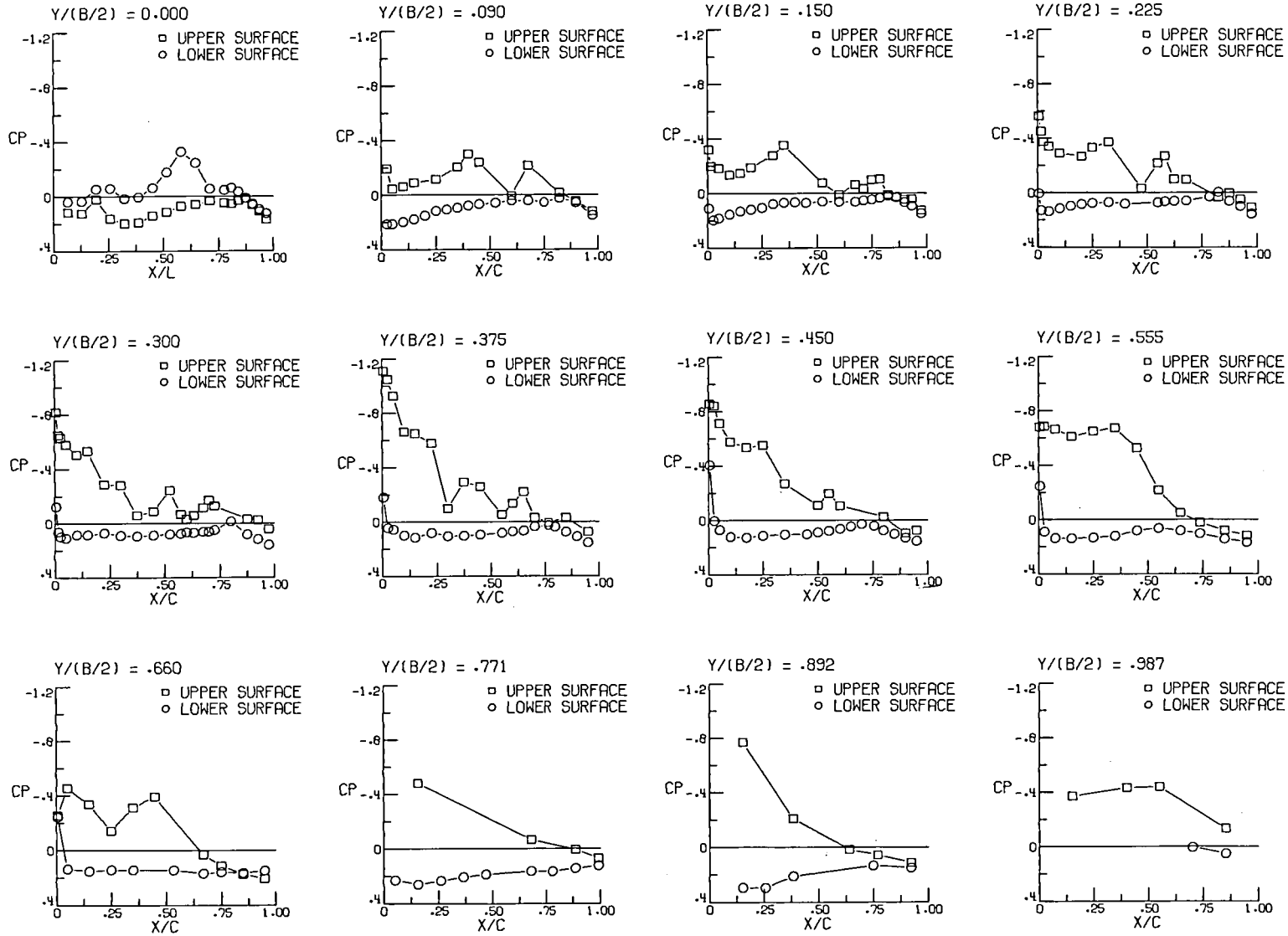

(d) Continued, $\alpha = 4^{o}$, $p_{t,j}/p_{\infty} = 6.1$.

Figure 11.- Continued.

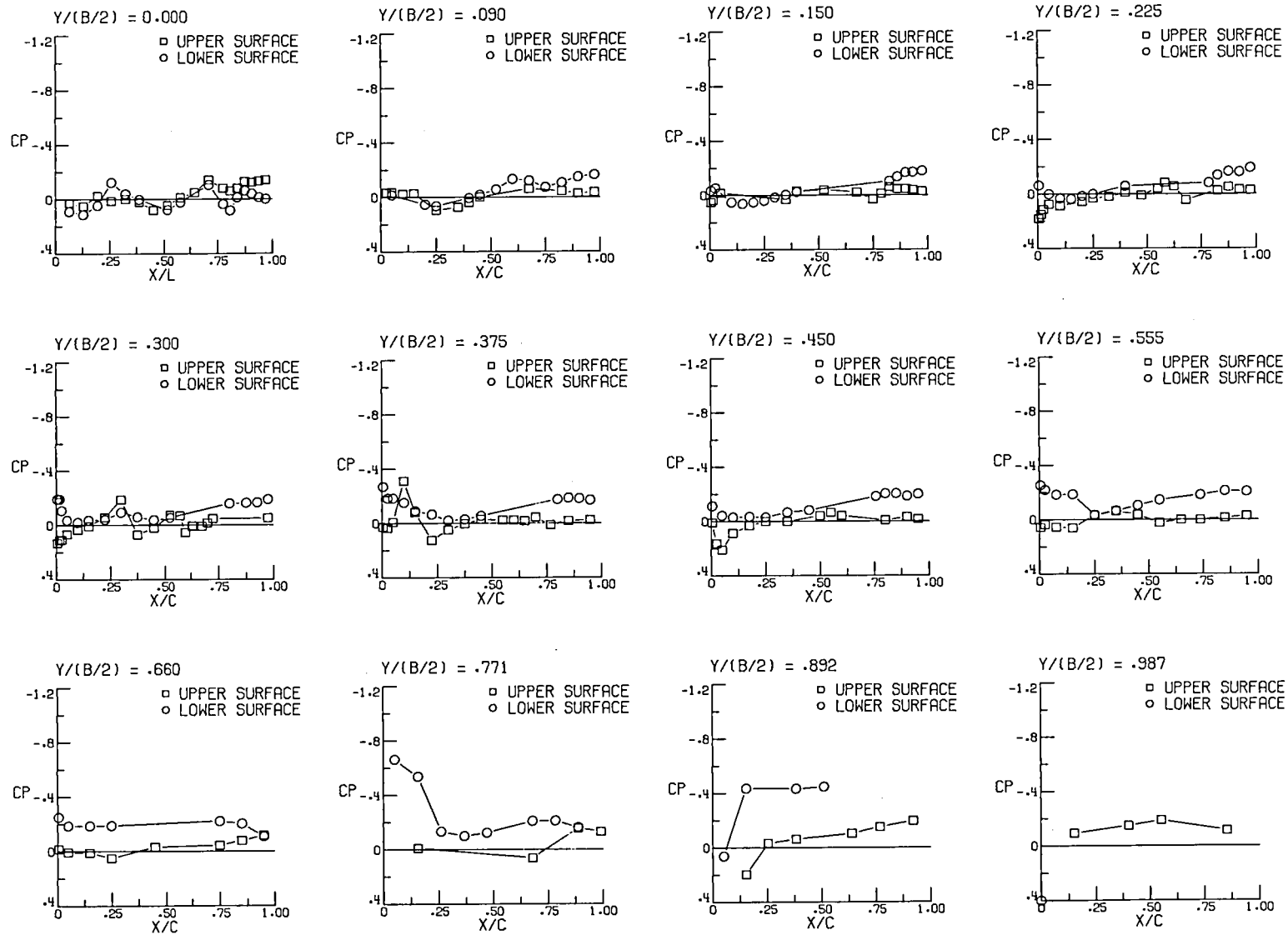

(e) M = 1.20, $\alpha = -4^{o}$, $p_{t,j}/p_{\infty} = 0.9$.

Figure 11.- Continued.

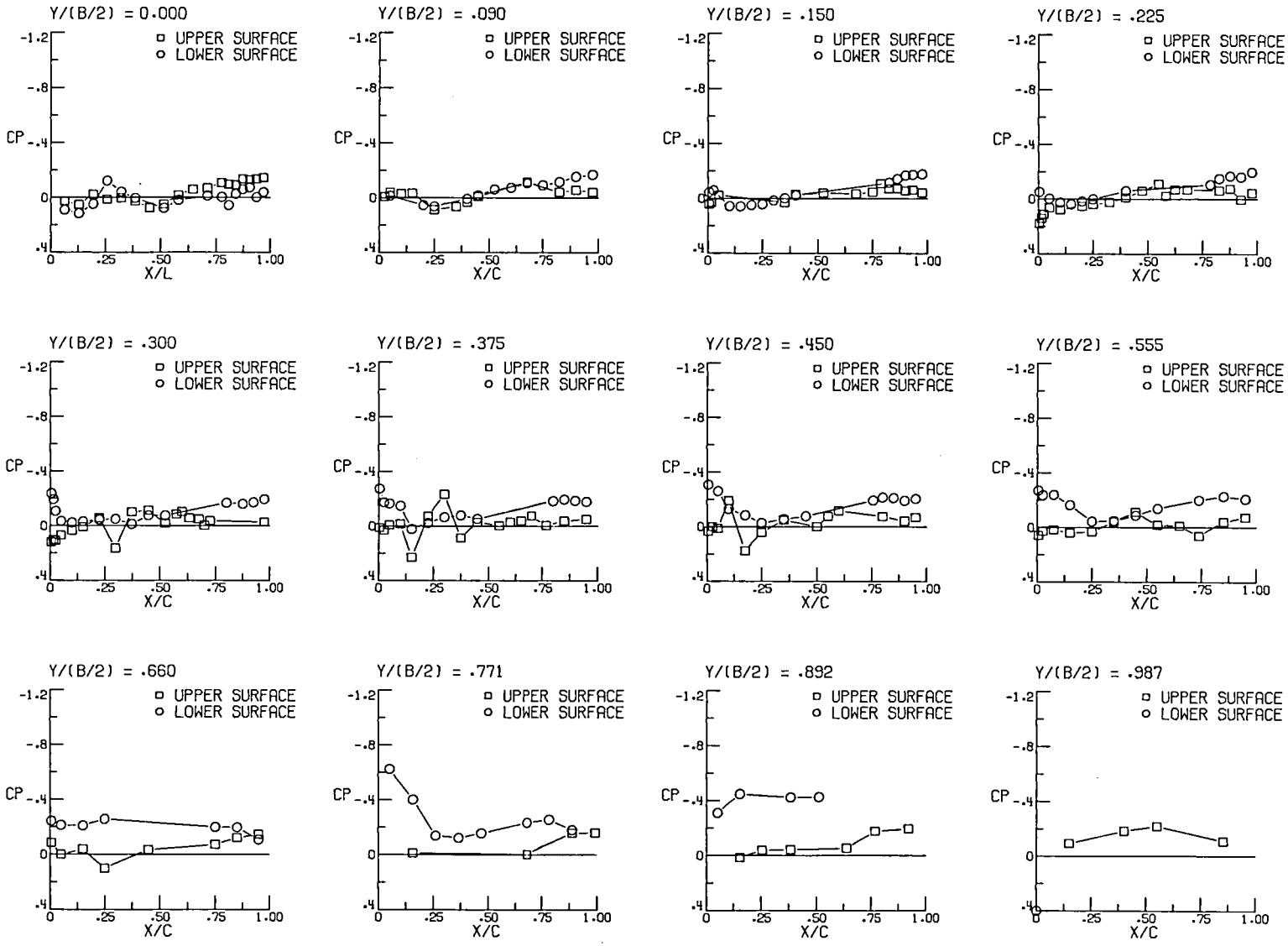

(e) Continued, $\alpha = -4^{o}$, $p_{t,j}/p_{\infty} = 9.1$.

Figure 11.- Continued.

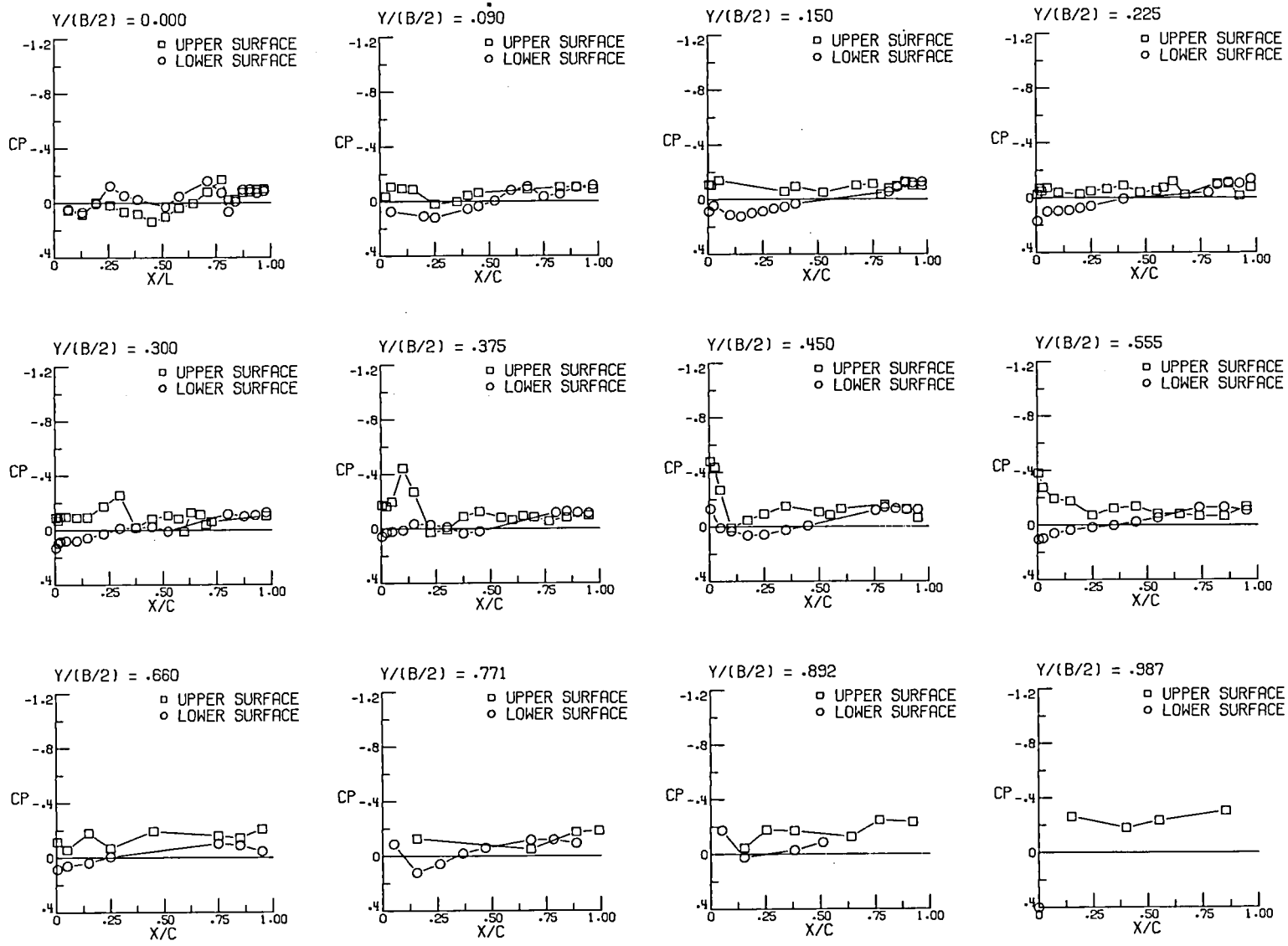

(e) Continued, $\alpha = 0^{o}$, $p_{t,j}/p_{\infty} = 0.8$.

Figure 11.- Continued.

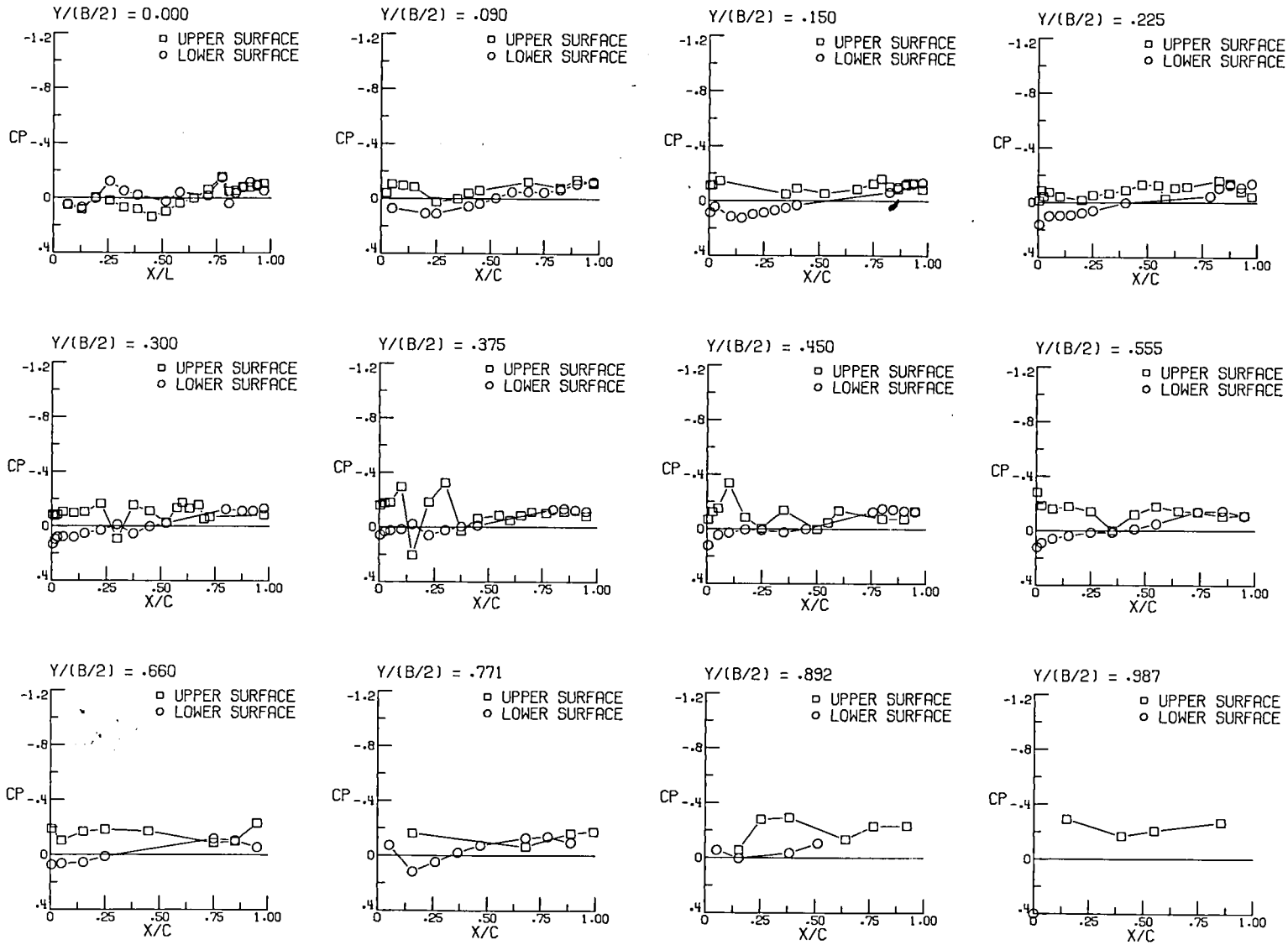

(e) Continued, $\alpha = 0^{o}$, $p_{t,j}/p_{\infty} = 9.0$.

Figure 11.- Continued.

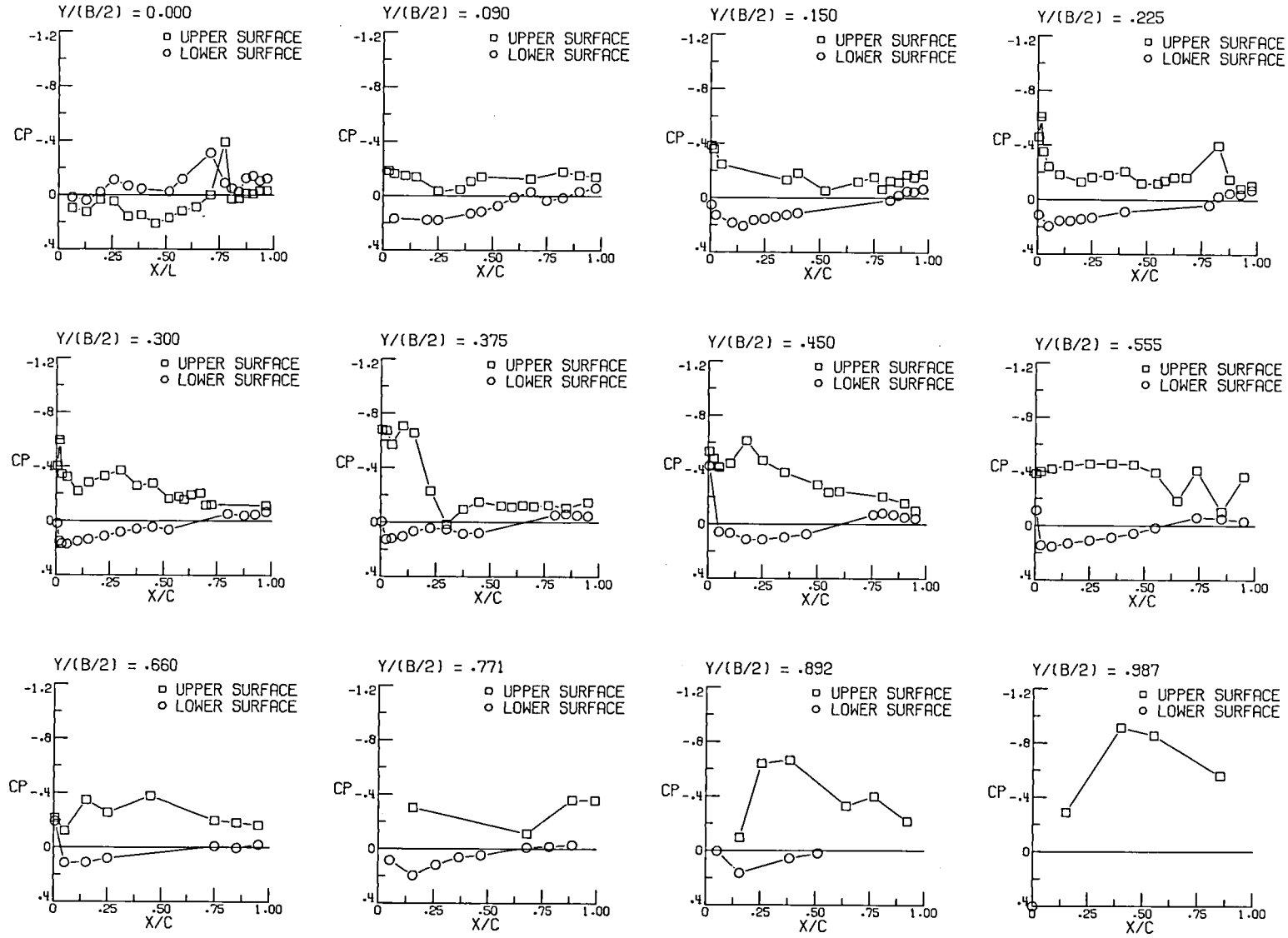

(e) Continued, $\alpha = 4^{o}$, $p_{t,j}/p_{\infty} = 0.6$.

Figure 11.- Continued.

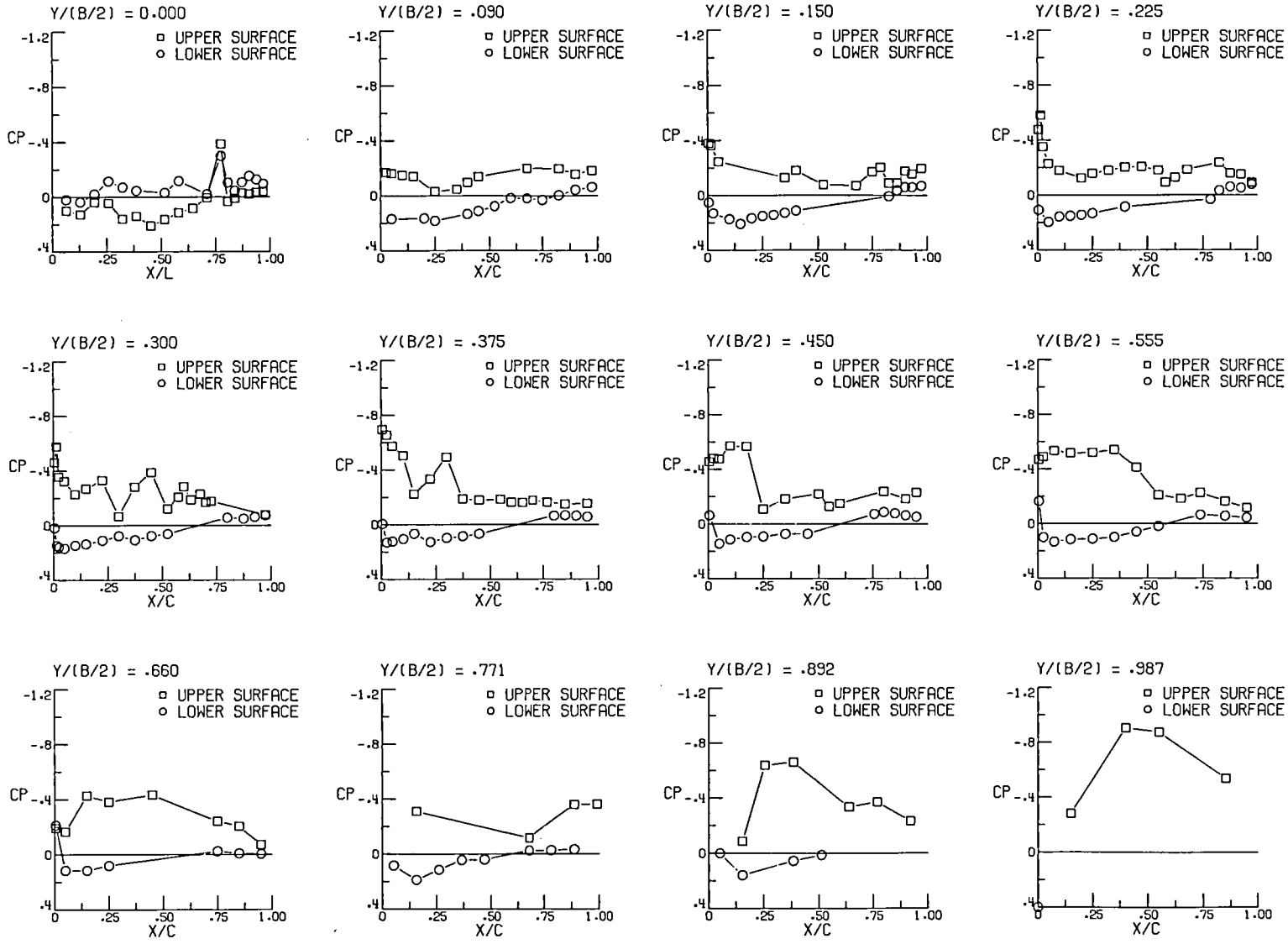

(e) Concluded, $\alpha = 4^{o}$, $p_{t,j}/p_{\infty} = 9.3$.

Figure 11.- Concluded.

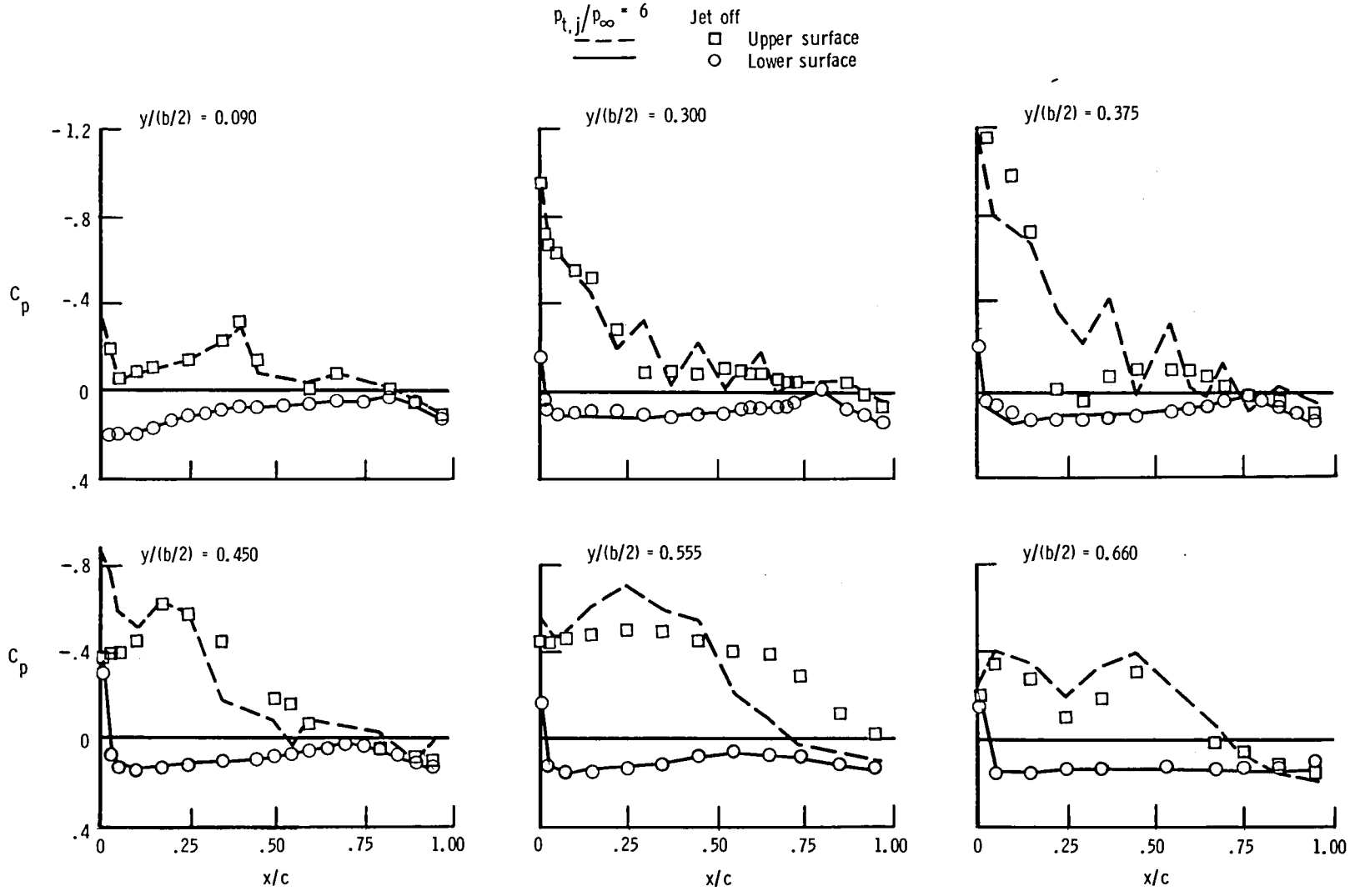

(a) M = 0.90.

Figure 12.- Effect of jet exhaust flow on wing pressure distributions with A/B, $\delta_f = -10^o$, $\alpha = 4^o$, $x_e/c = -0.17$, $y/(b/2) = 0.46$, and $z_w/d_N = 1.50$.

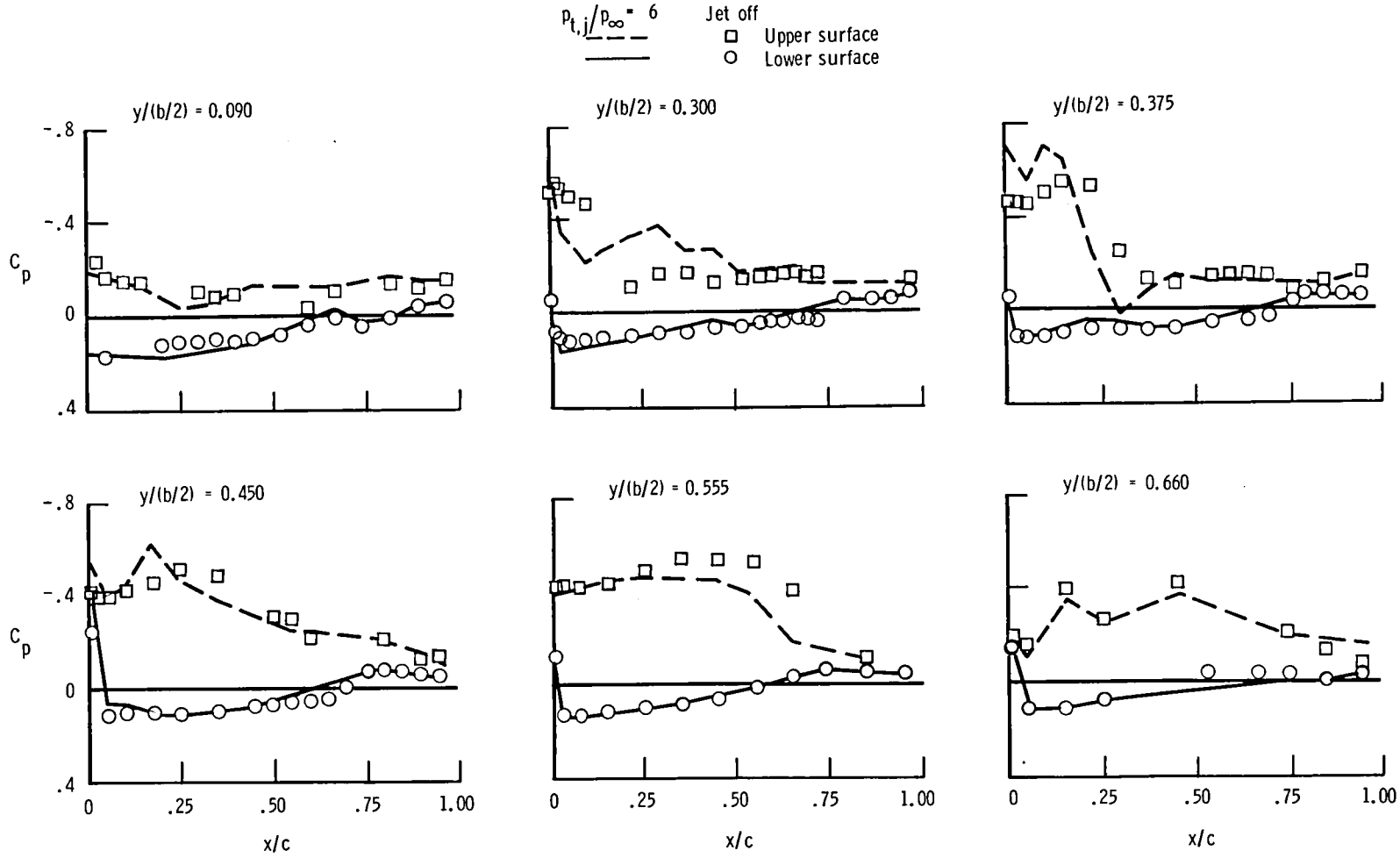

(b) M = 1.20.

Figure 12.- Concluded.

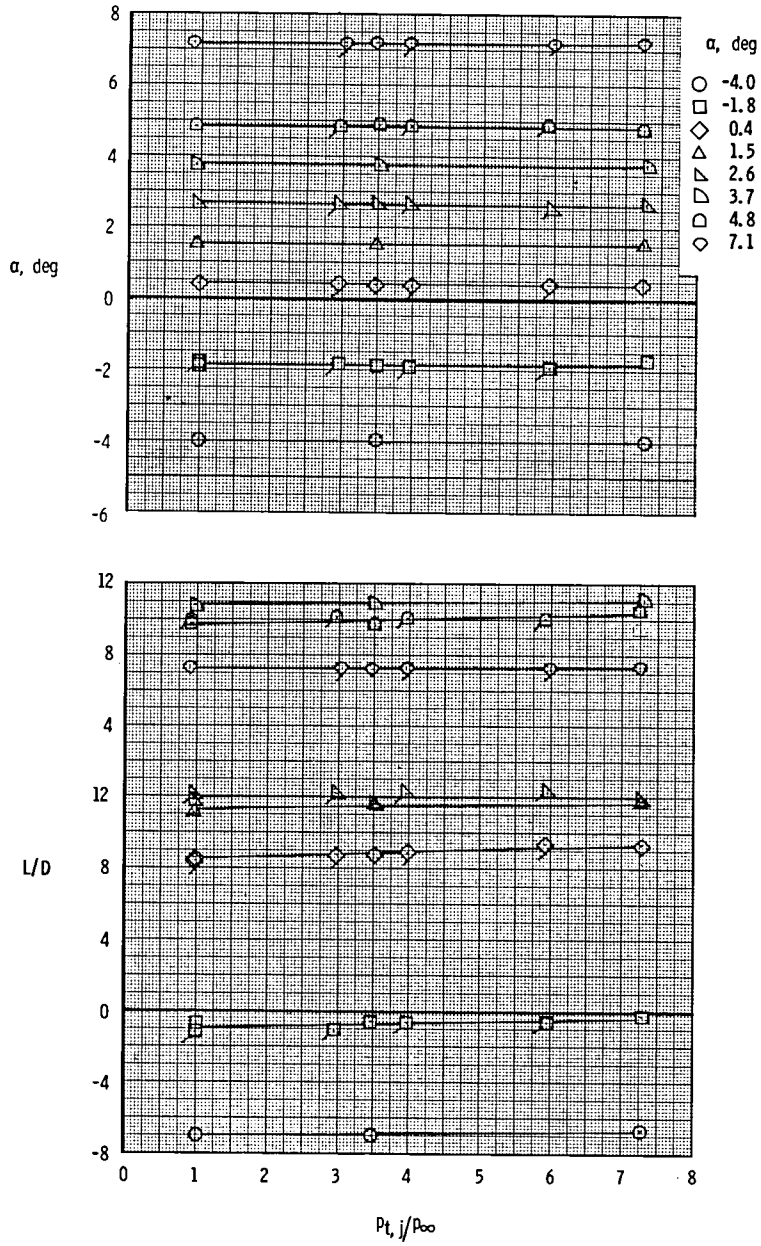

(a) M = 0.60.

Figure 13.- Variation of longitudinal aerodynamic characteristics with jet total-pressure ratio at $x_e/c = -0.17$, $y/(b/2) = 0.46$, and $z_w/d_N = 1.50$. A/B; $\delta_f = -10^o$. (Flagged symbols indicate repeat test points.)

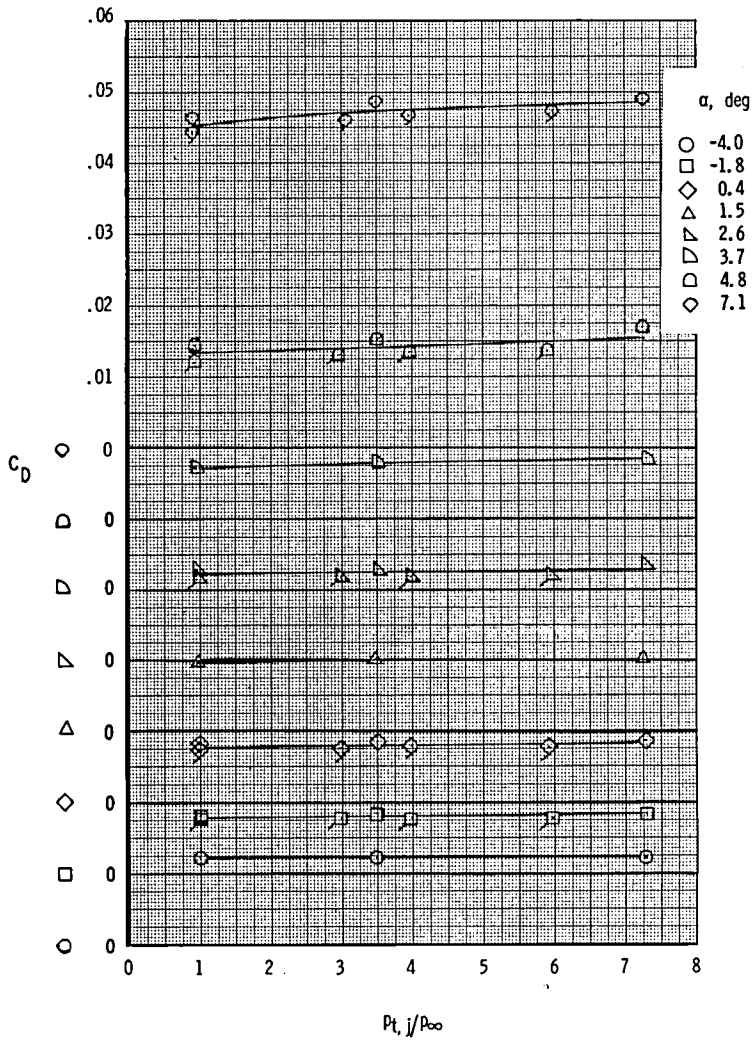

(a) Continued.

Figure 13.- Continued.

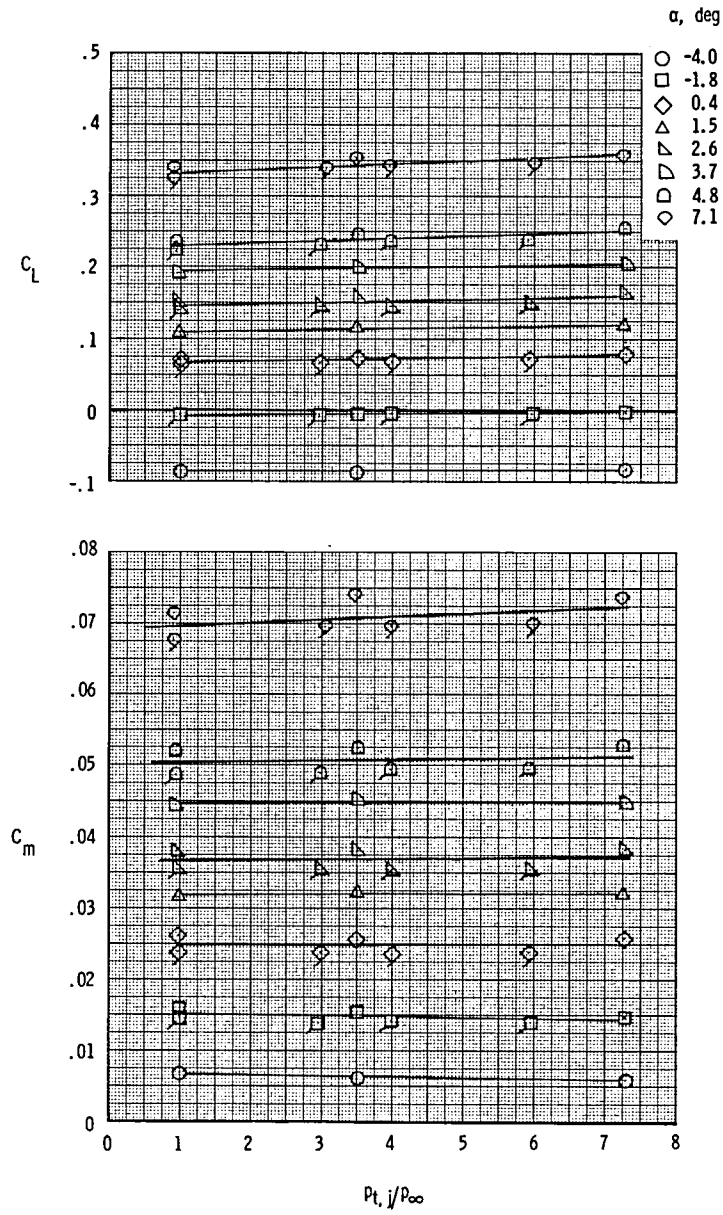

(a) Concluded.

Figure 13.- Continued.

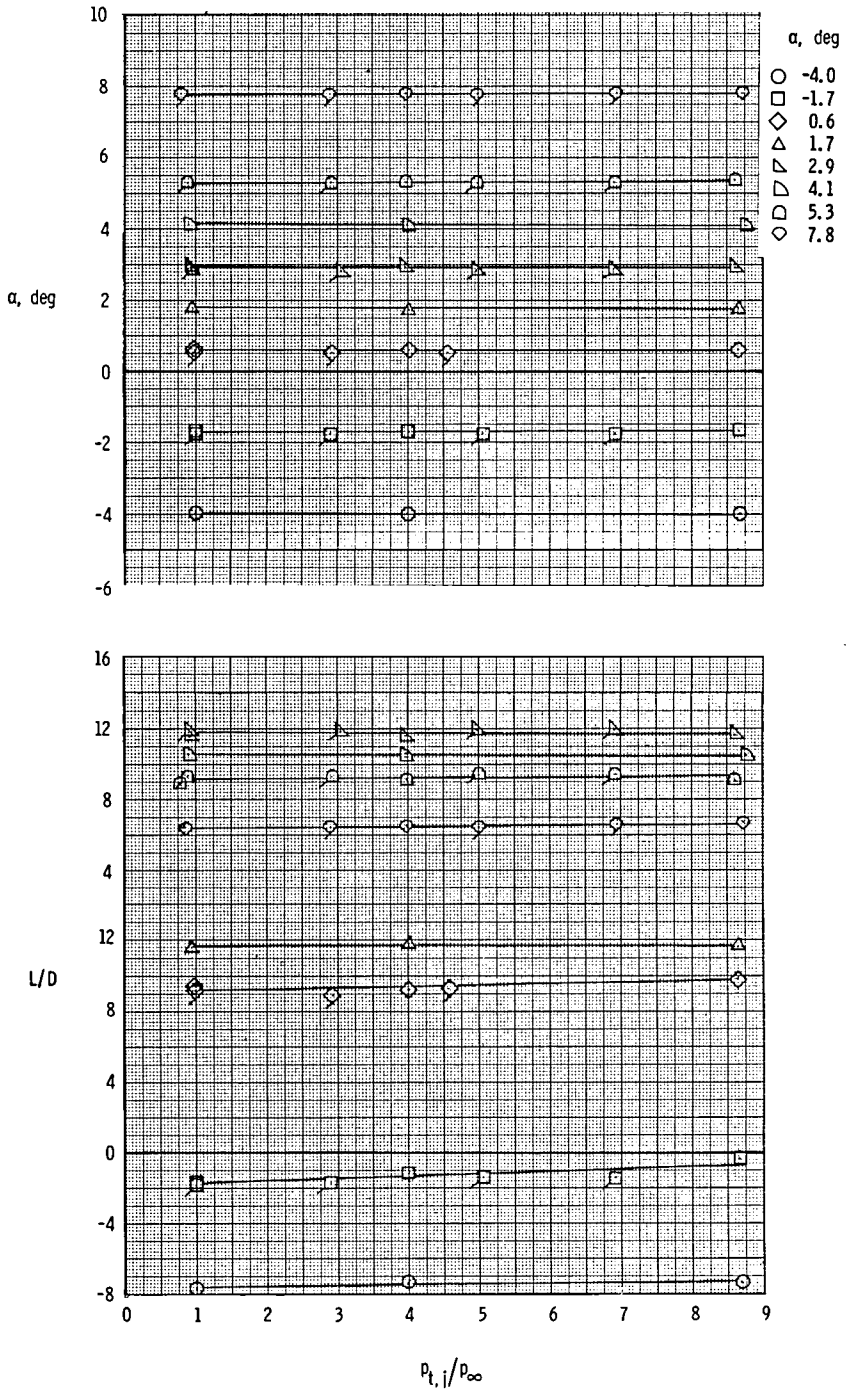

(b) M = 0.80.

Figure 13.- Continued.

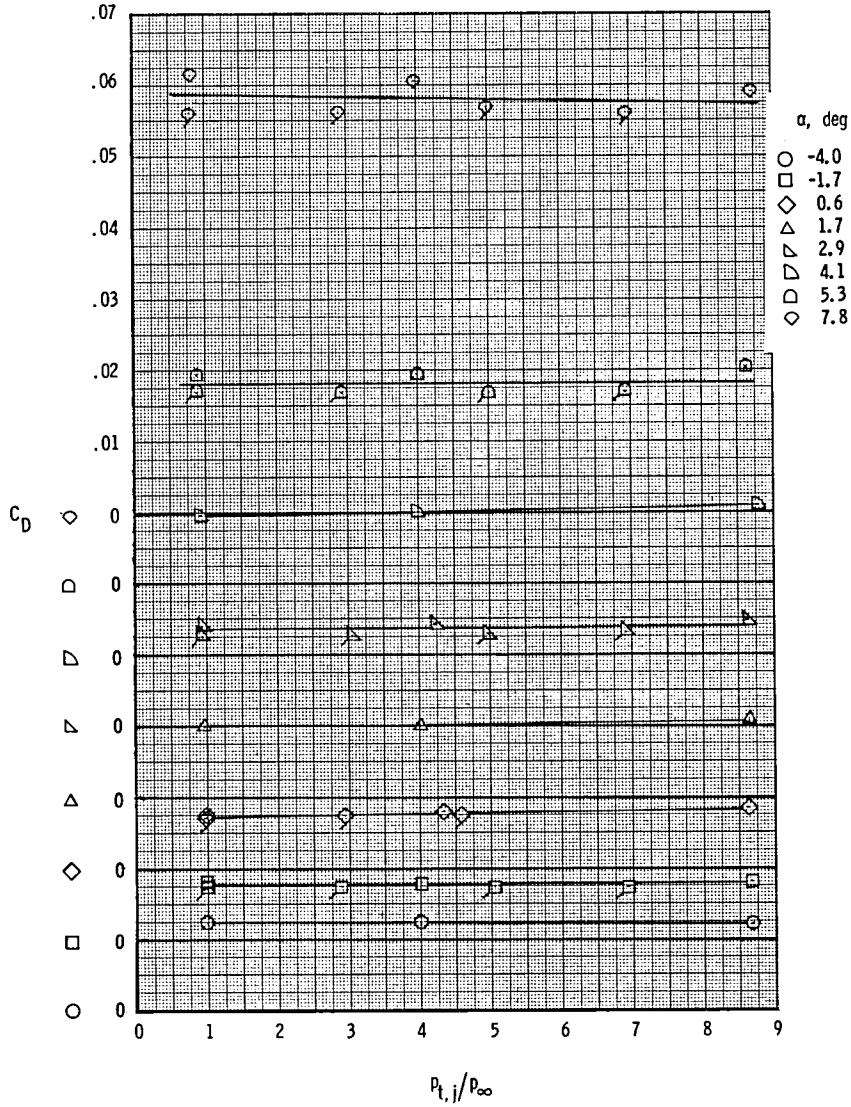

(b) Continued.

Figure 13.- Continued.

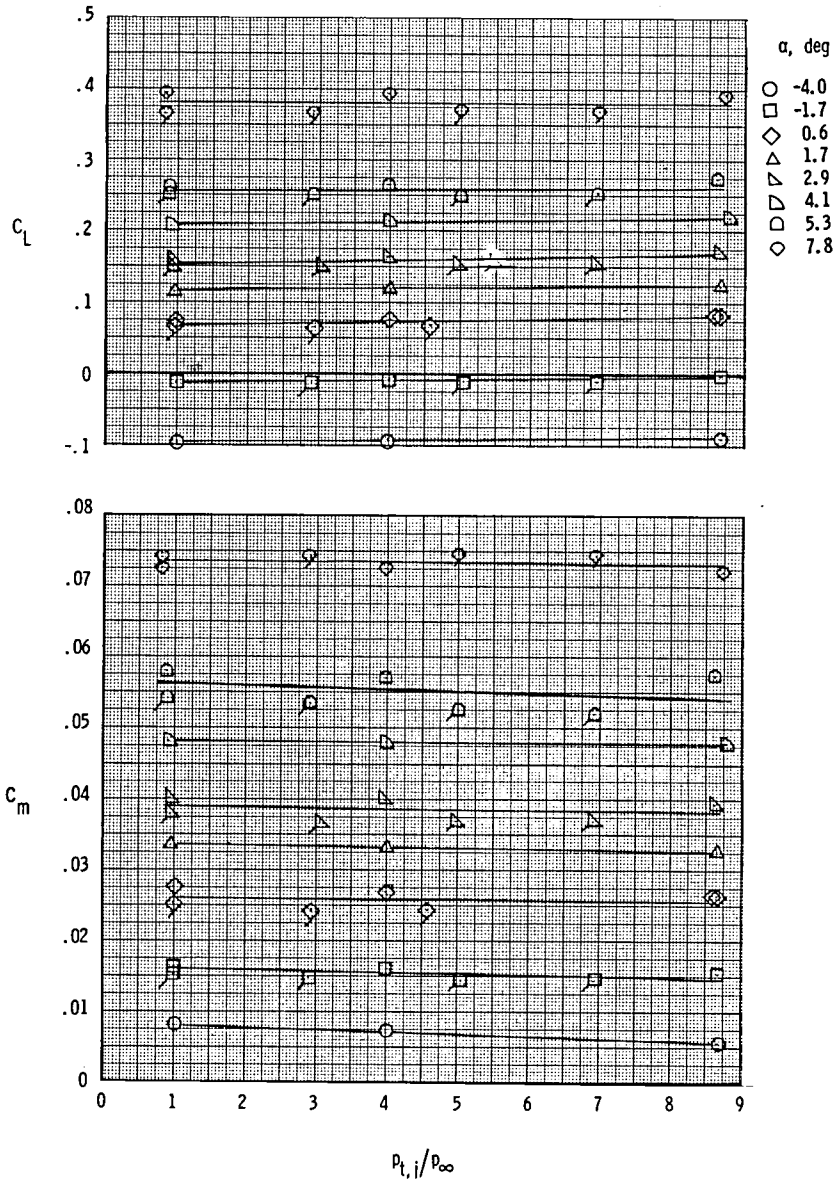

(b) Concluded.

Figure 13.- Continued.

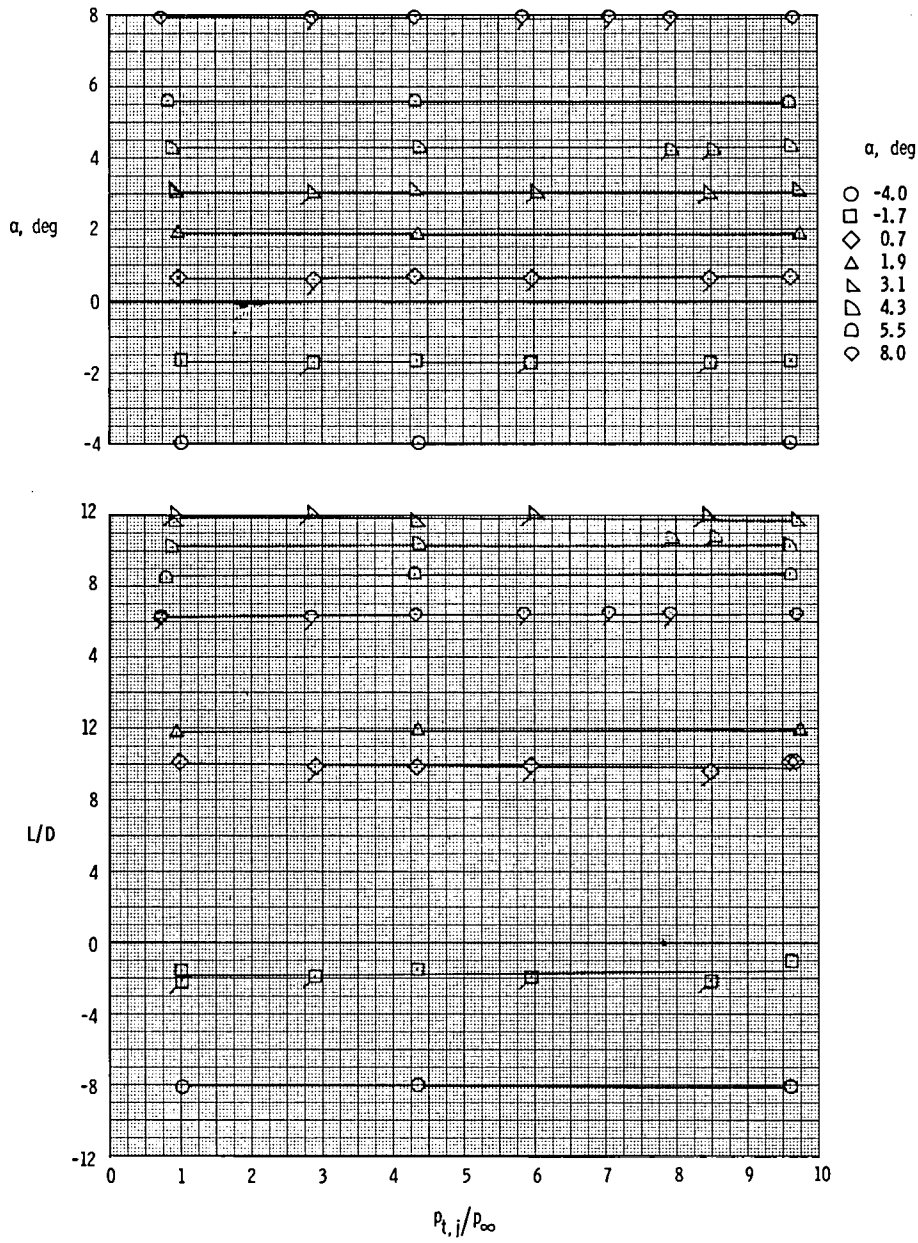

(c) M = 0.90.

Figure 13.- Continued.

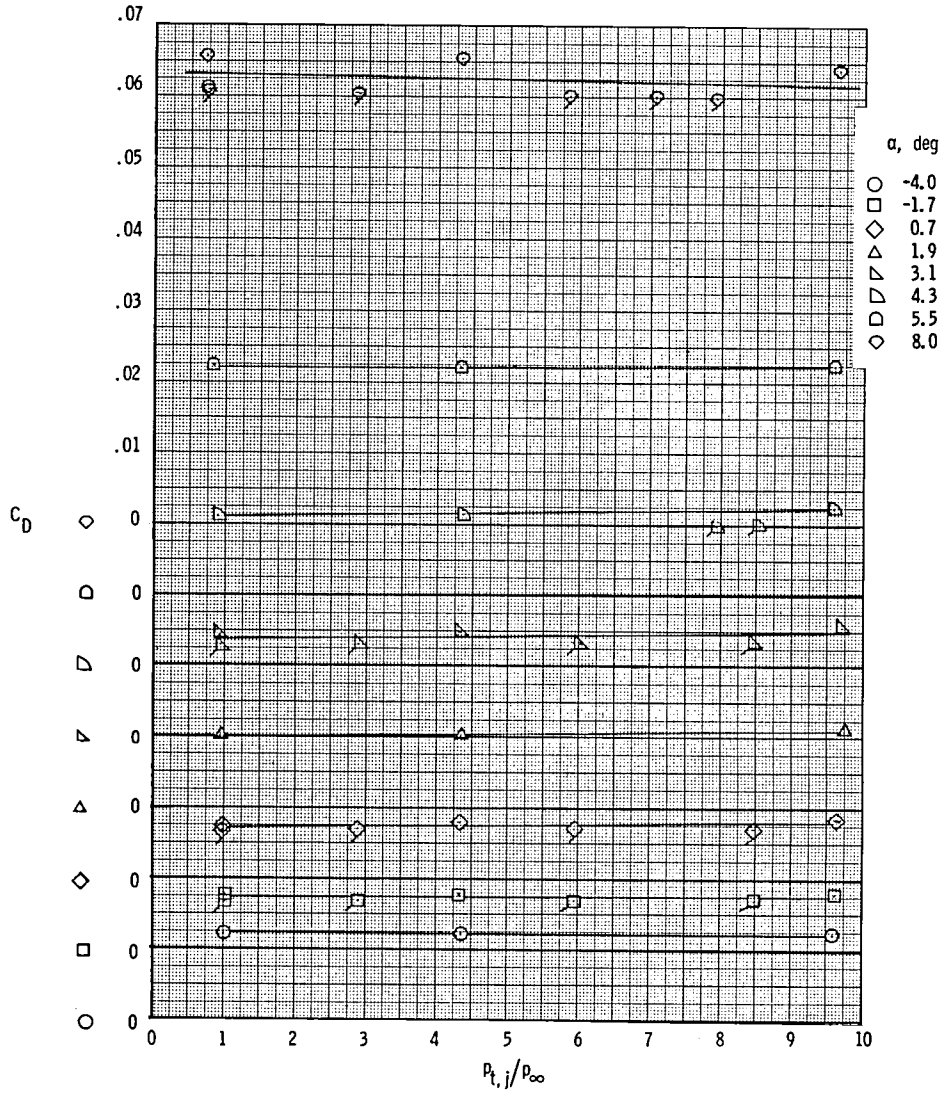

(c) Continued.

Figure 13.- Continued.

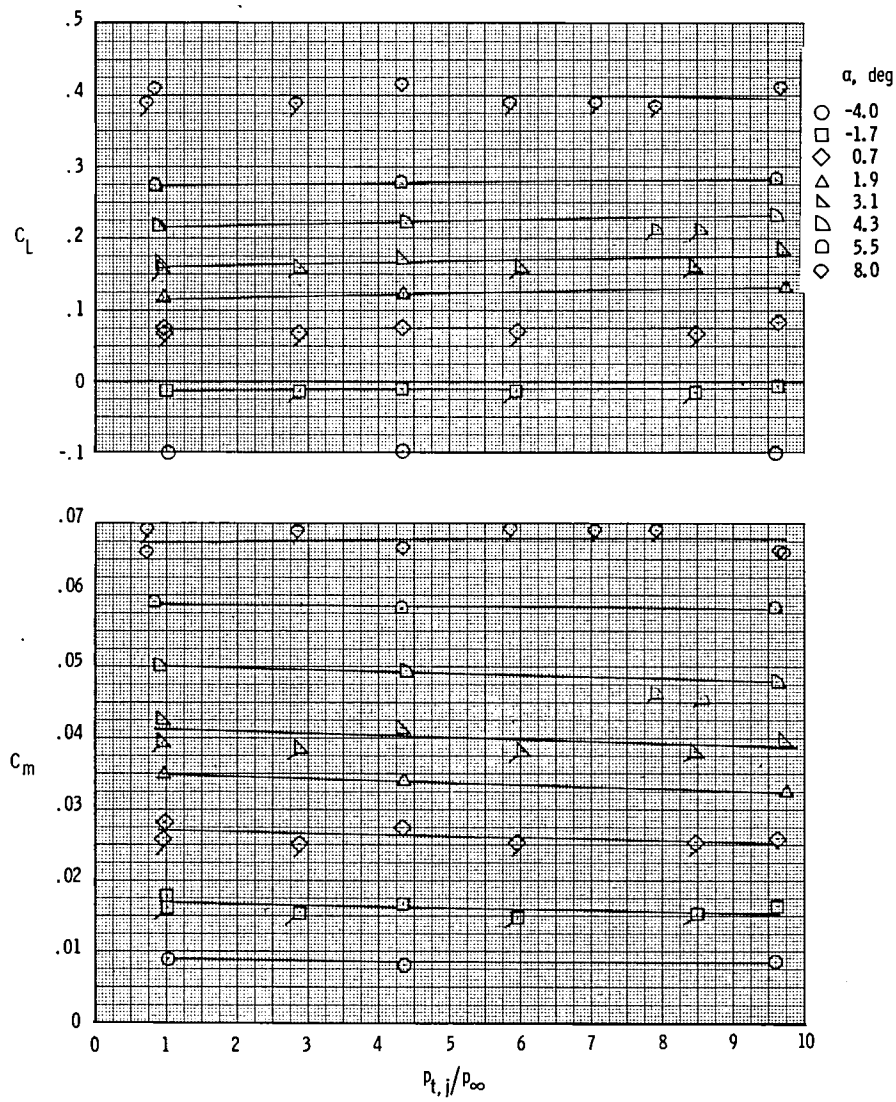

(c) Concluded.

Figure 13.- Continued.

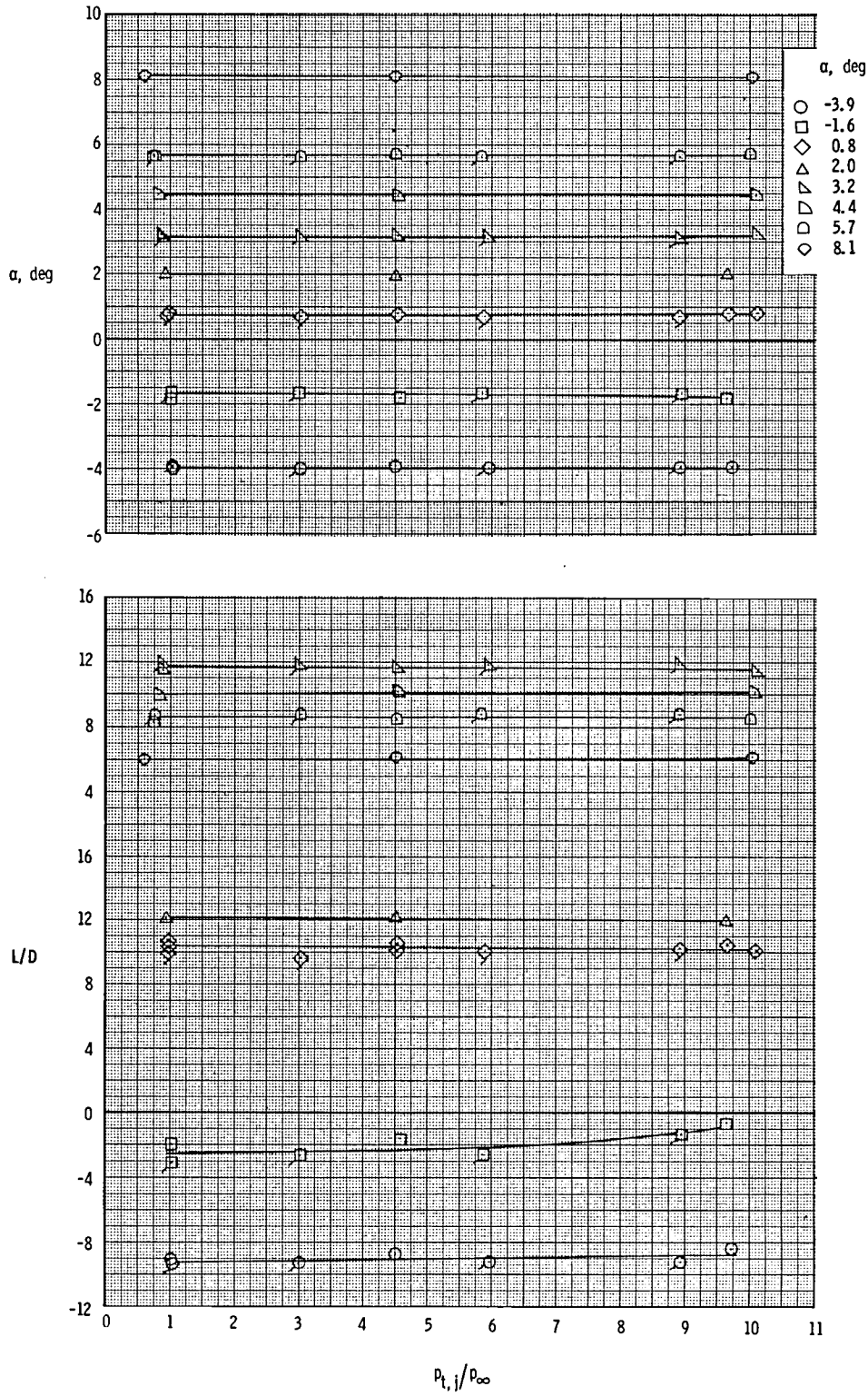

(d) M = 0.95.

Figure 13.- Continued.

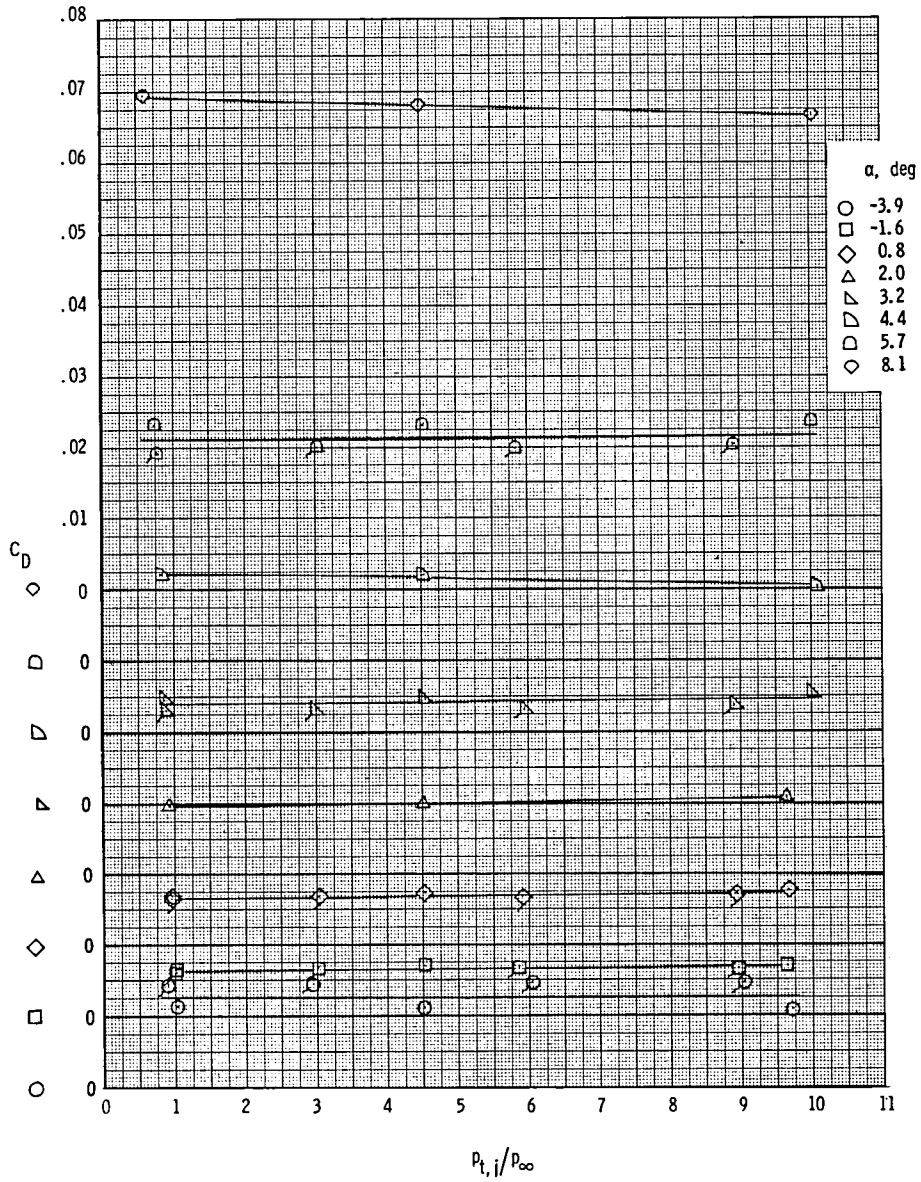

(d) Continued.

Figure 13.- Continued.

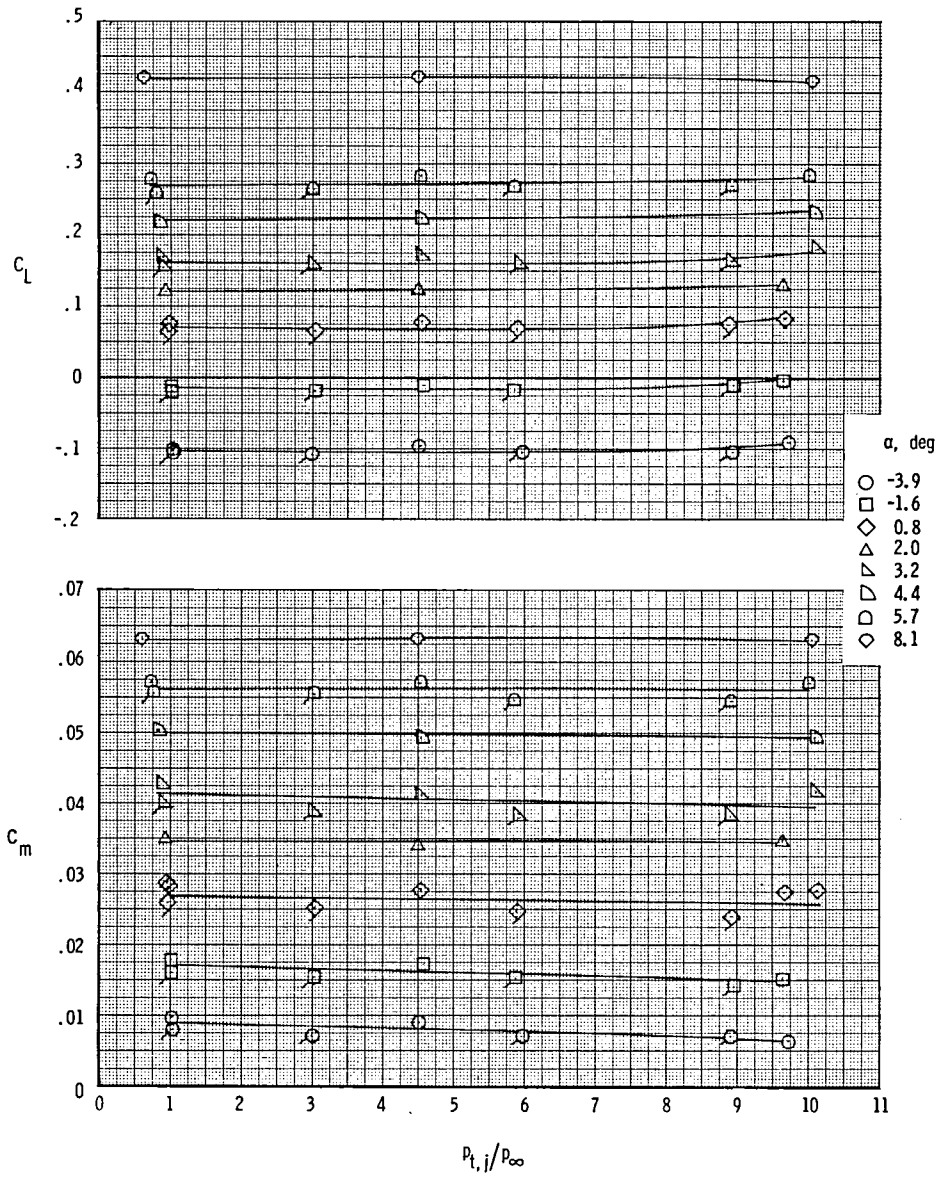

(d) Concluded.

Figure 13.- Continued.

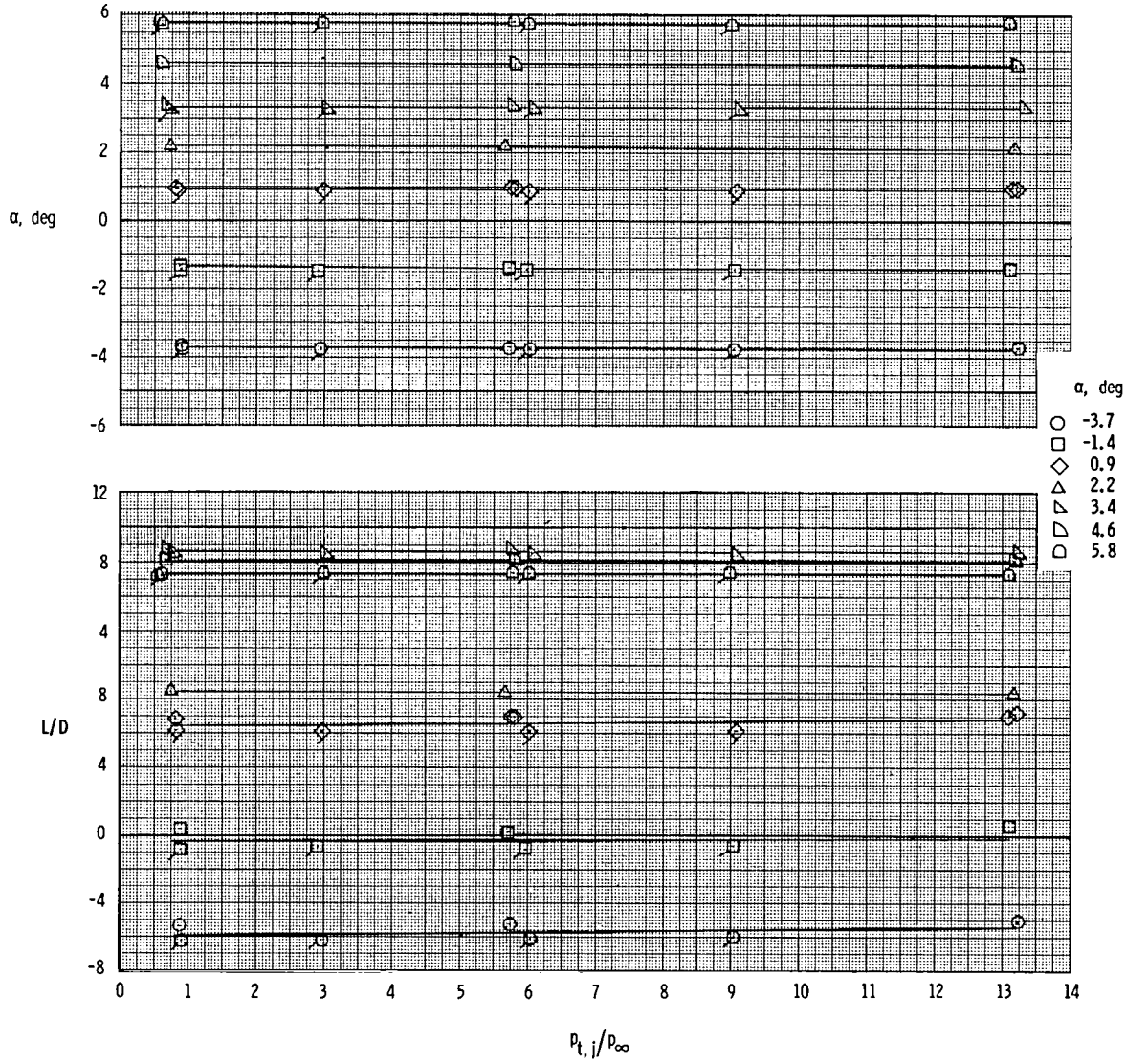

(e) M = 1.20.

Figure 13.- Continued.

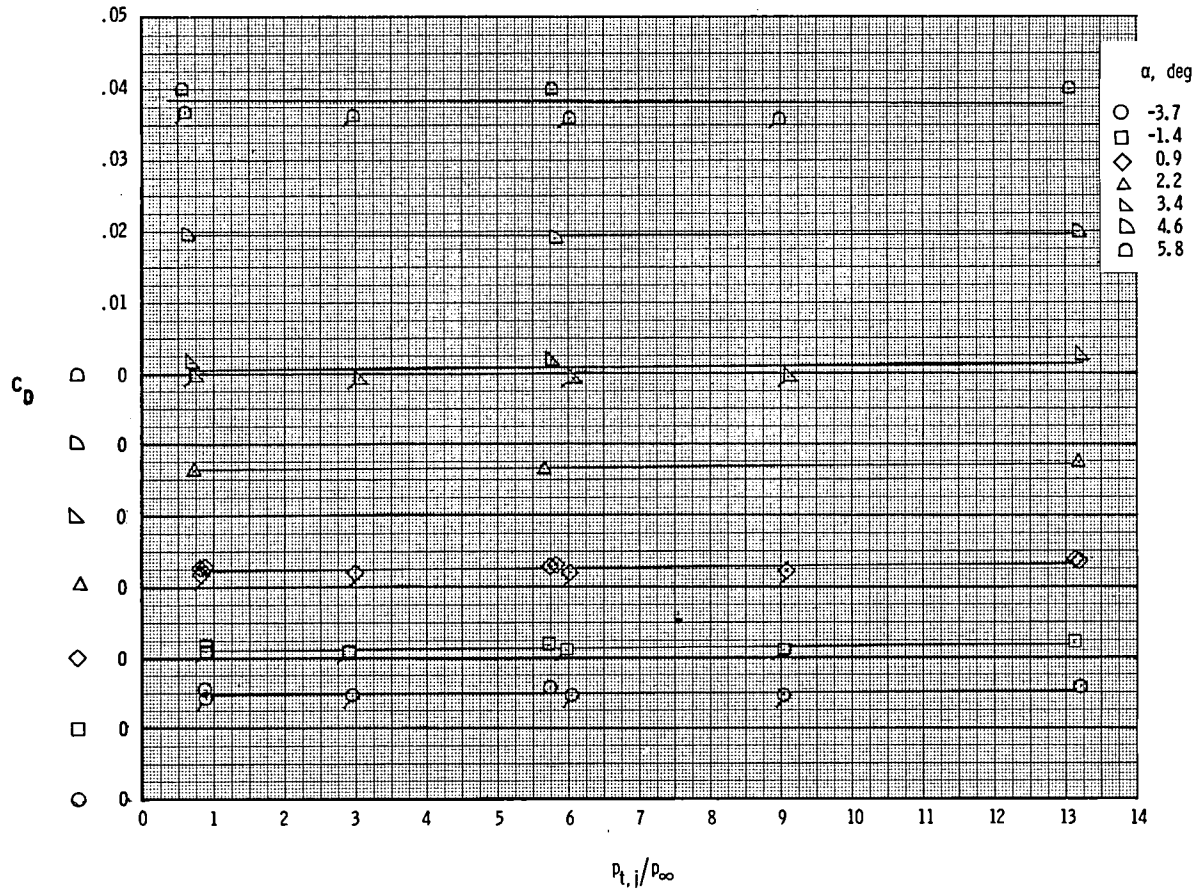

(e) Continued.

Figure 13.- Continued.

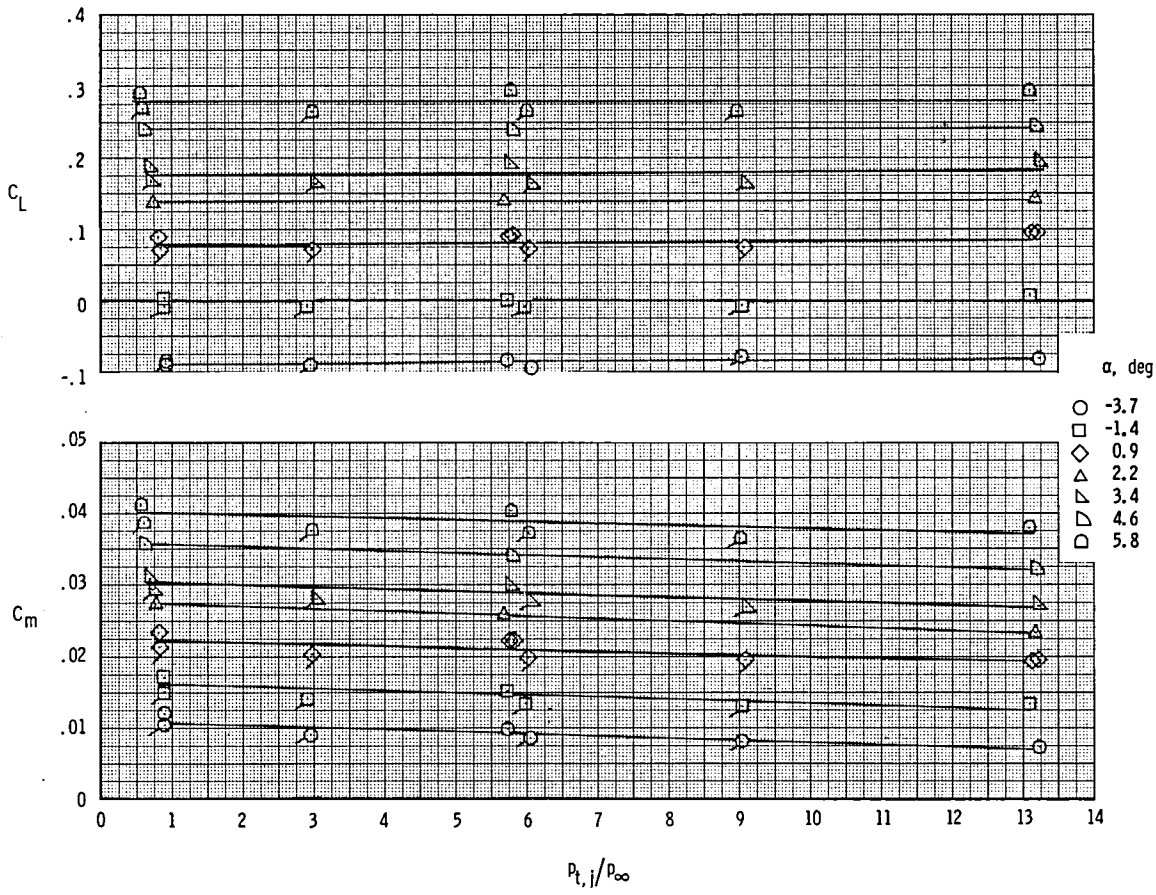

(e) Concluded.

Figure 13.- Concluded.

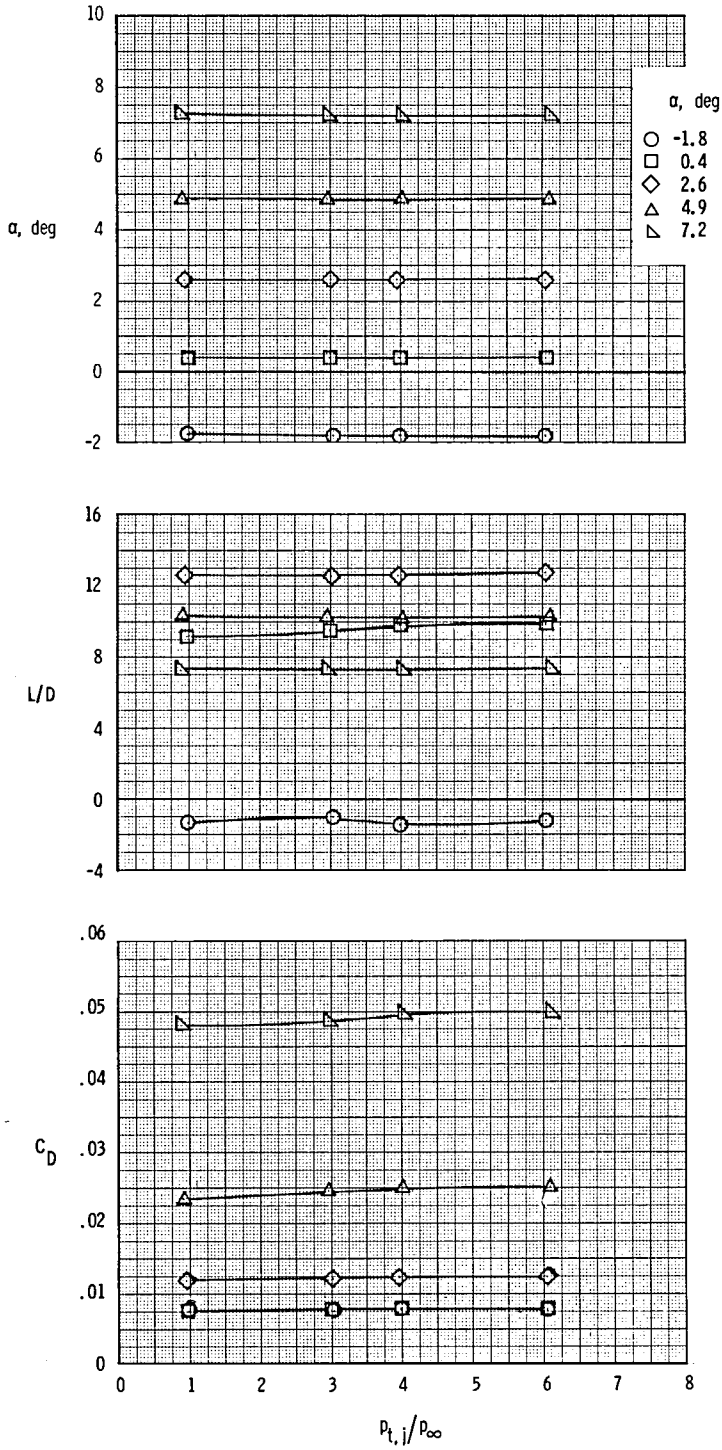

(a) M = 0.60.

Figure 14.- Variation of longitudinal aerodynamic characteristics with jet total-pressure ratio at $x_e/c = 0.10$, $y/(b/2) = 0.46$, and $z_w/d_N = 1.47$. A/B; $\delta_f = -10^o$.

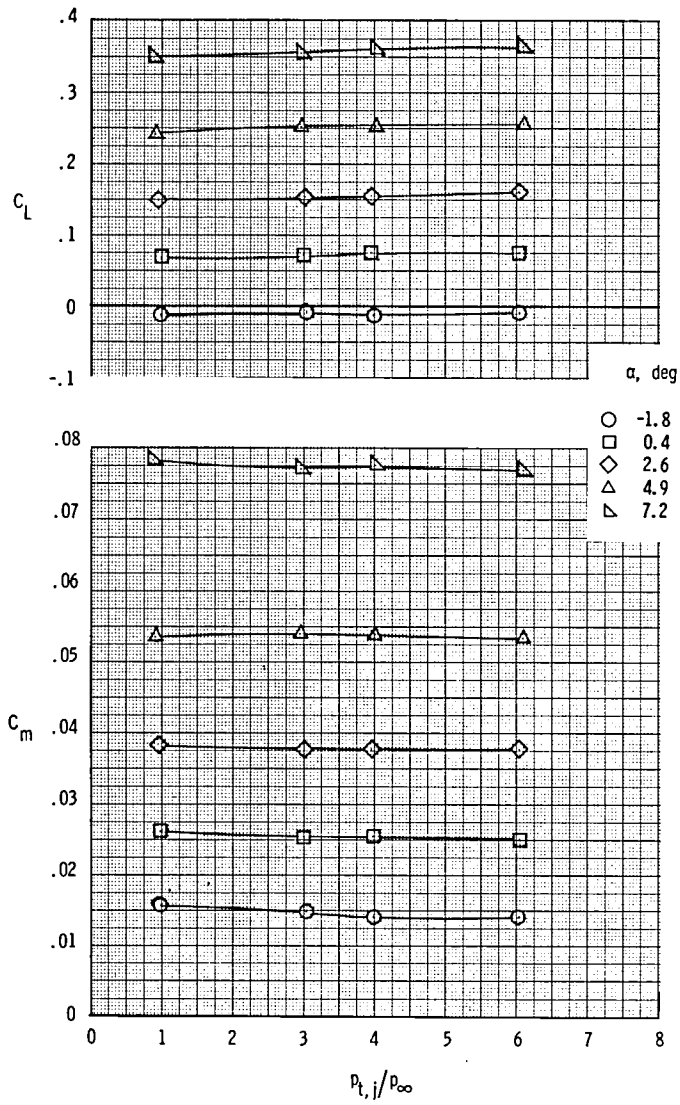

(a) Concluded.

Figure 14.- Continued.

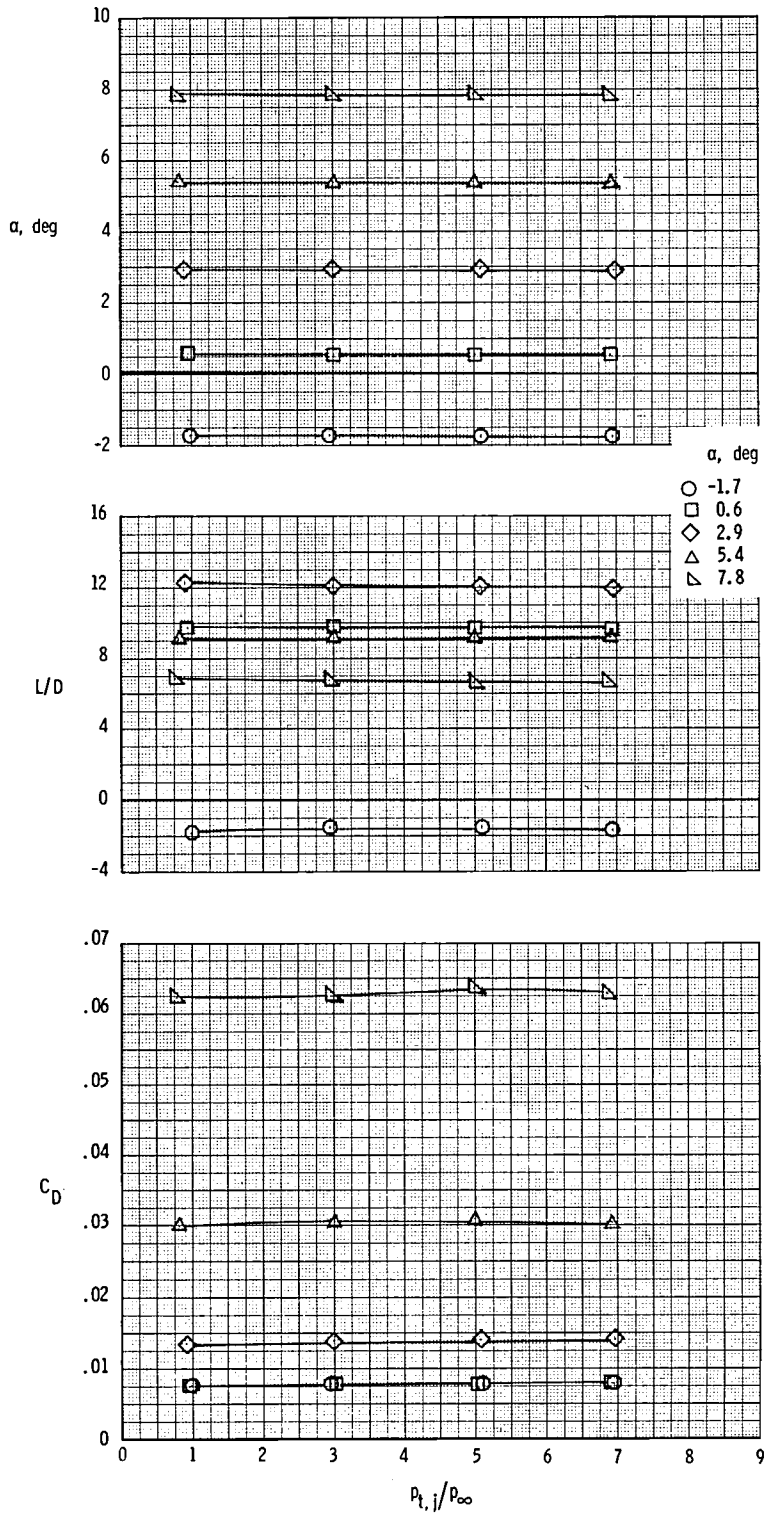

(b) M = 0.80.

Figure 14.- Continued.

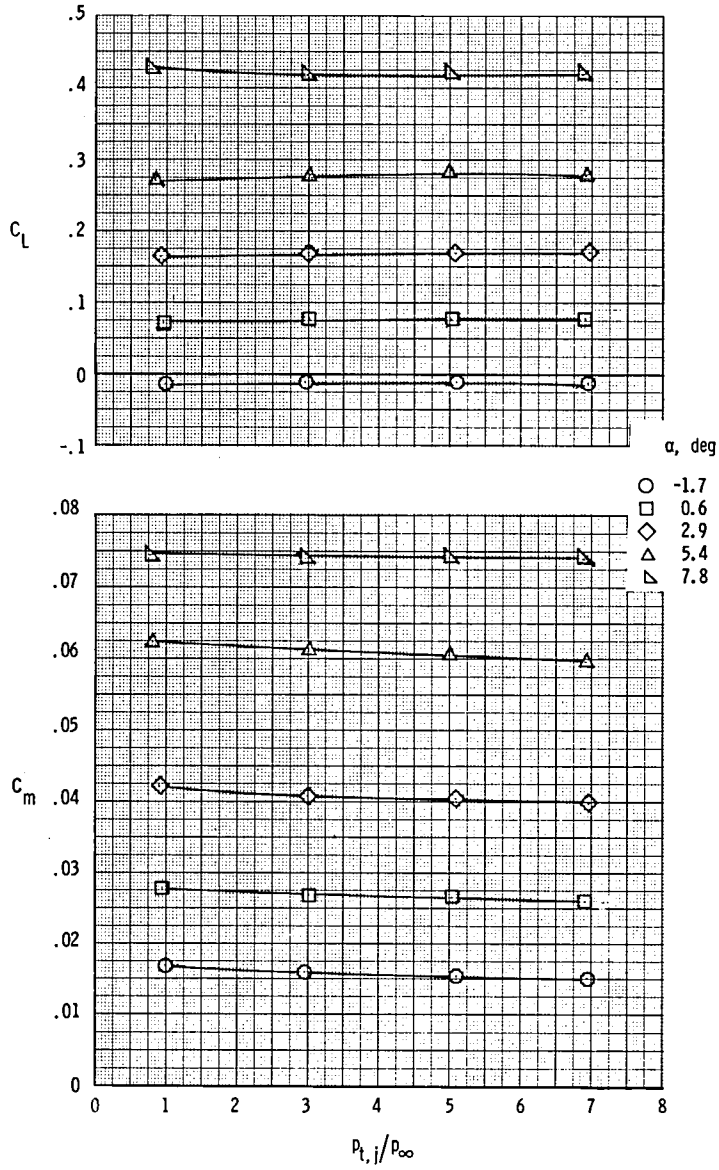

(b) Concluded.

Figure 14.- Continued.

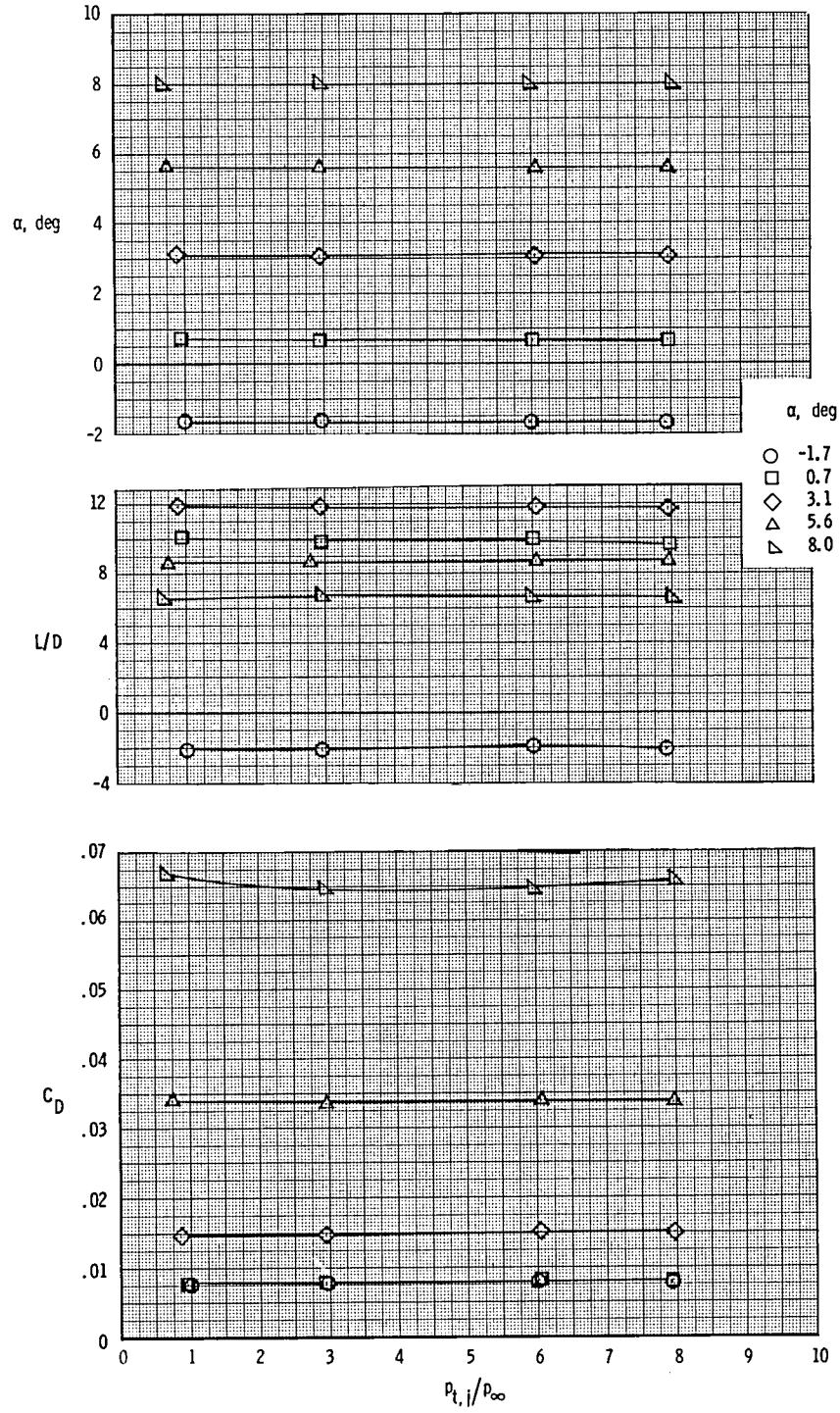

(c) M = 0.90.

Figure 14.- Continued.

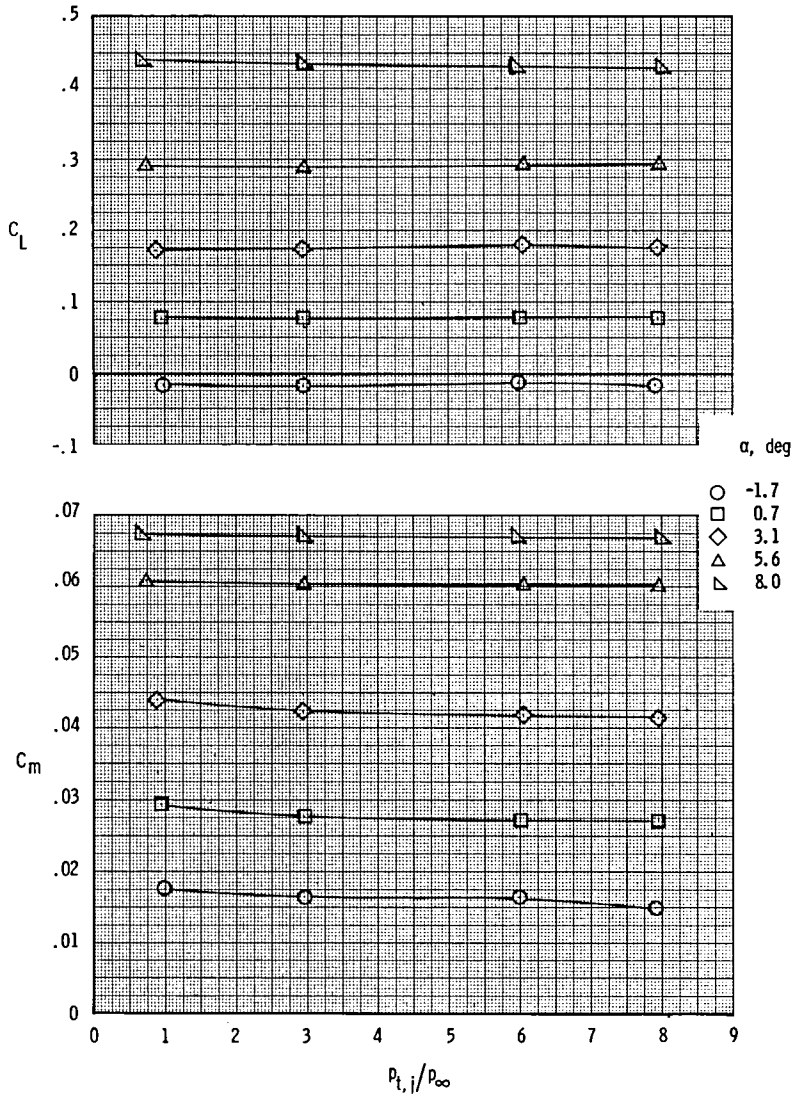

(c) Concluded.

Figure 14.- Continued.

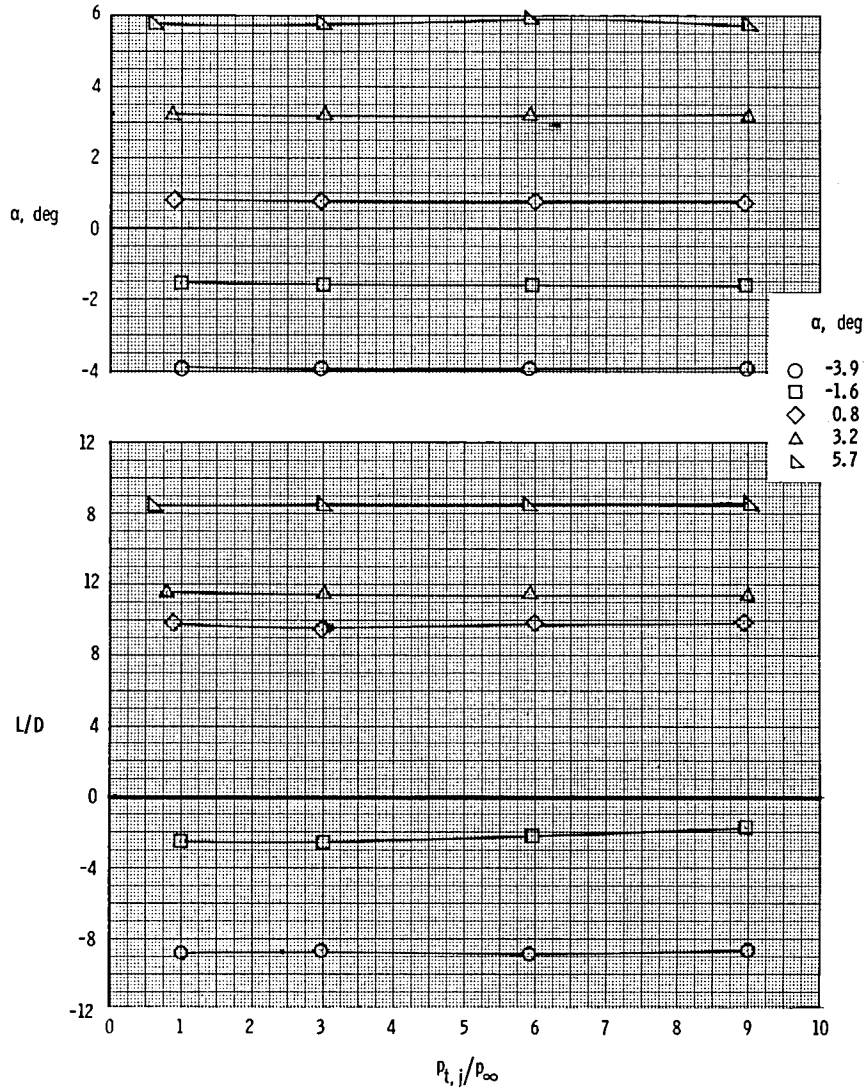

(d) M = 0.95.

Figure 14.- Continued.

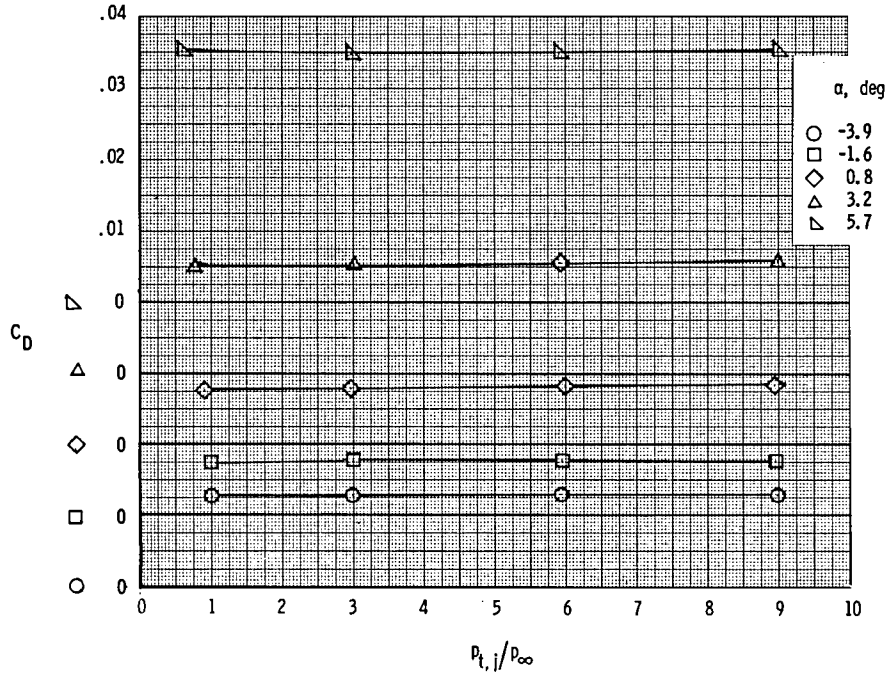

(d) Continued.

Figure 14.- Continued.

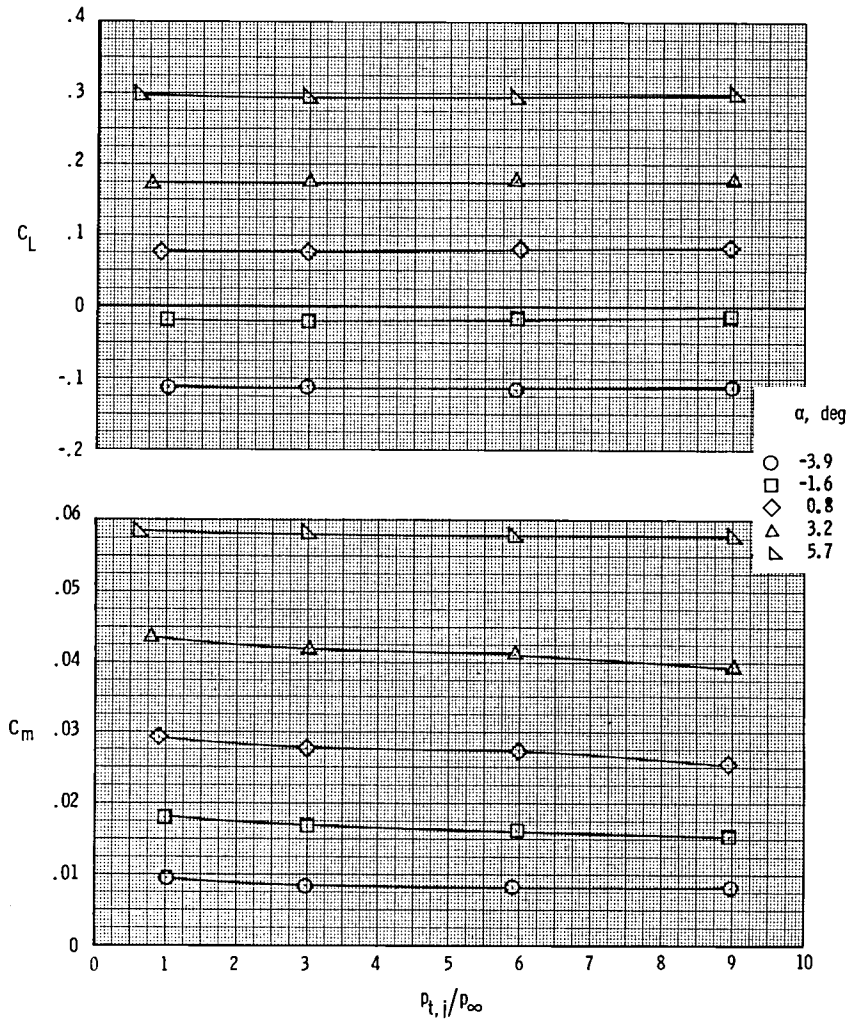

(d) Concluded.

Figure 14.- Continued.

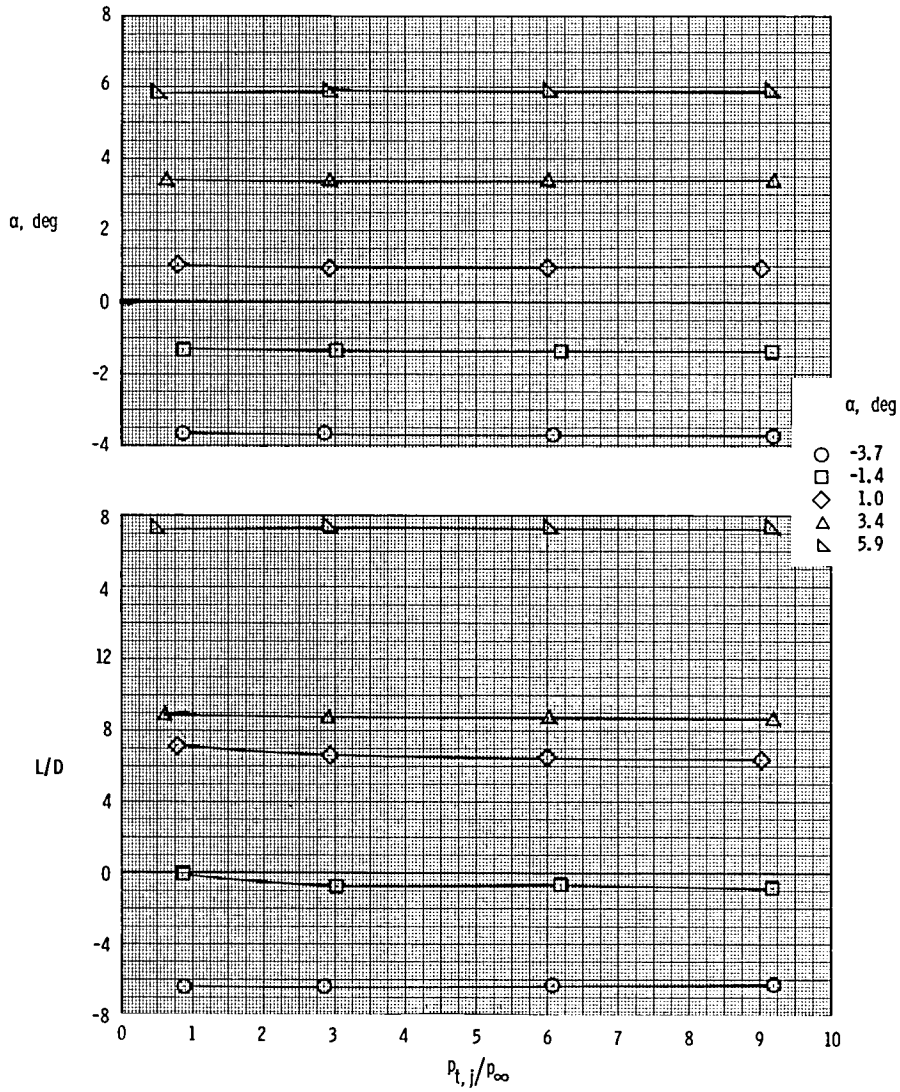

(e) M = 1.20.

Figure 14.- Continued.

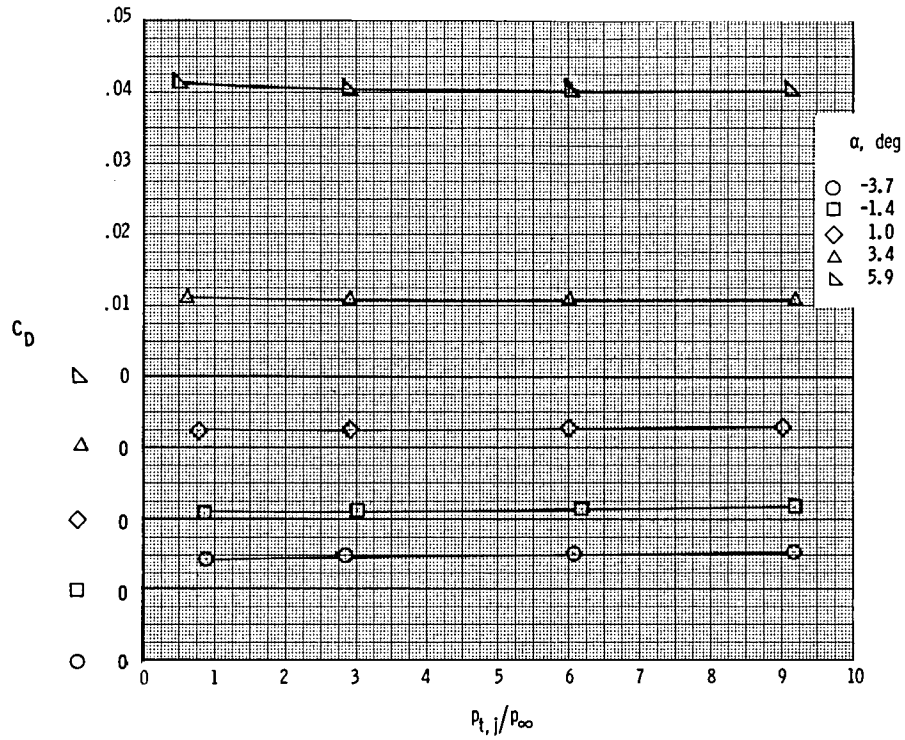

(e) Continued.

Figure 14.- Continued.

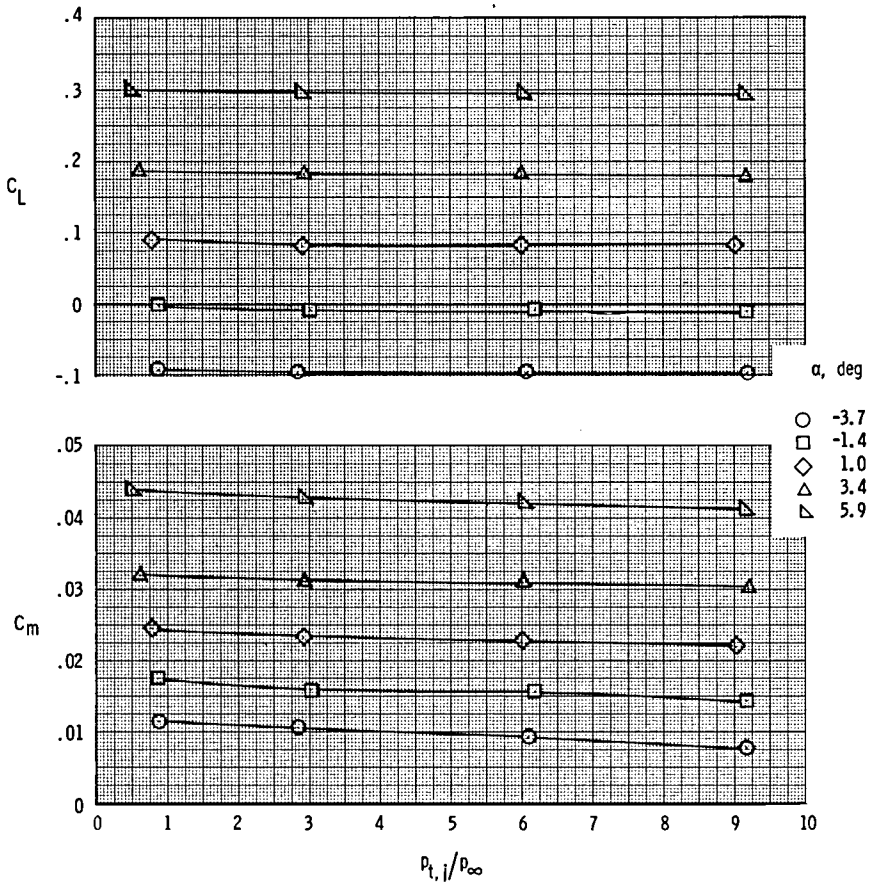

(e) Concluded.

Figure 14.- Concluded.

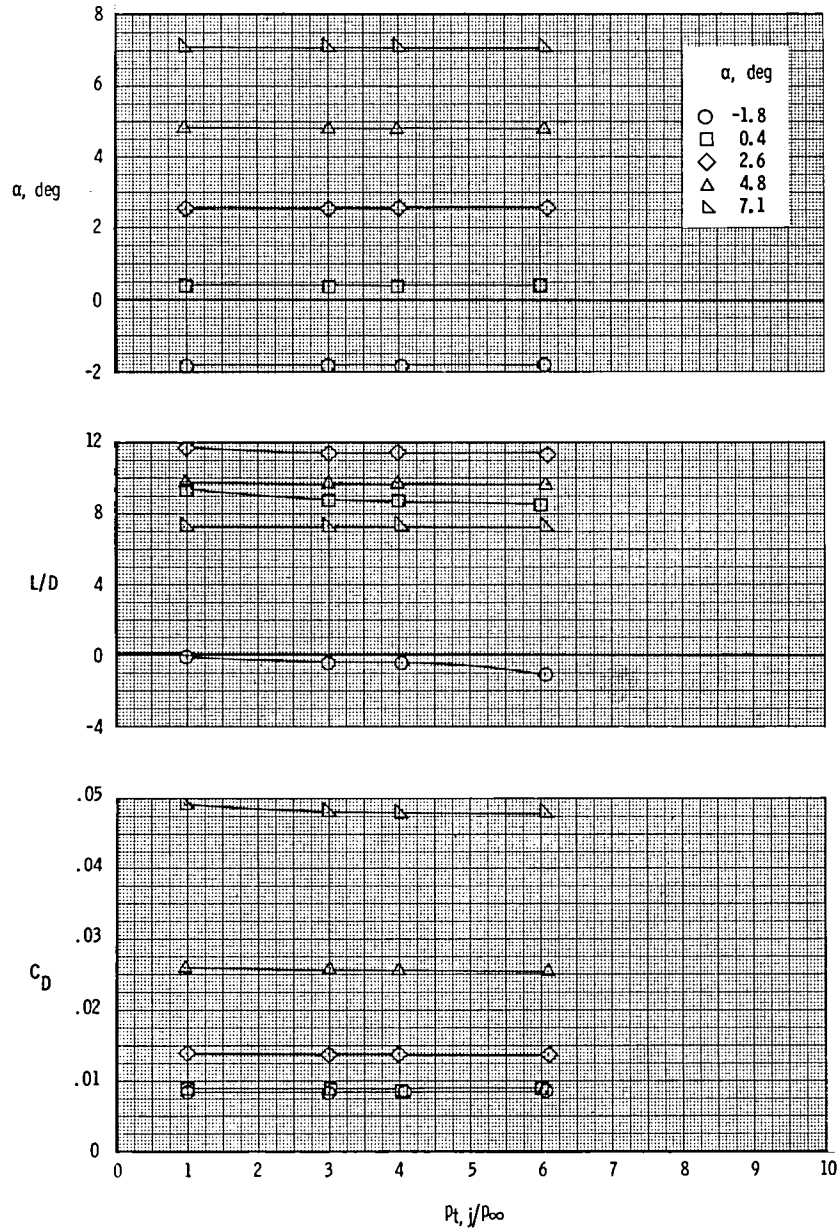

(a) M = 0.60.

Figure 15.- Variation of longitudinal aerodynamic characteristics with jet total-pressure ratio at $x_e/c = 0.82$, $y/(b/2) = 0.46$, and $z_w/d_N = 1.63$. A/B; $\delta_f = -10^o$.

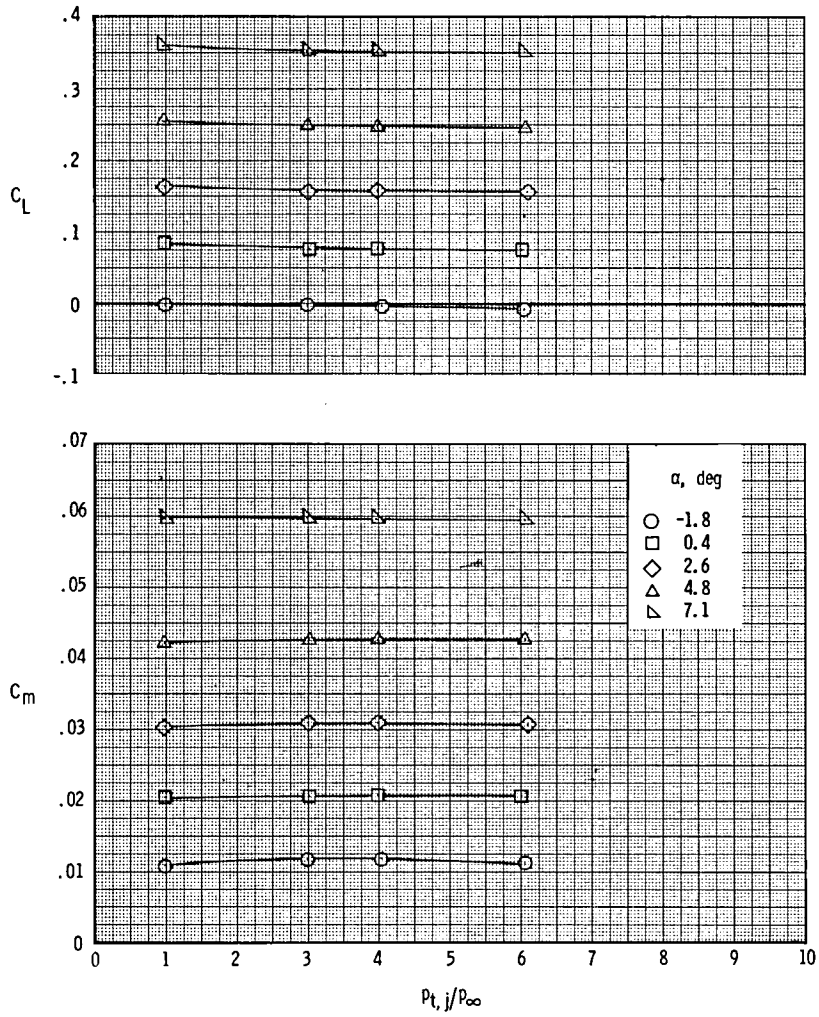

(a) Concluded.

Figure 15.- Continued.

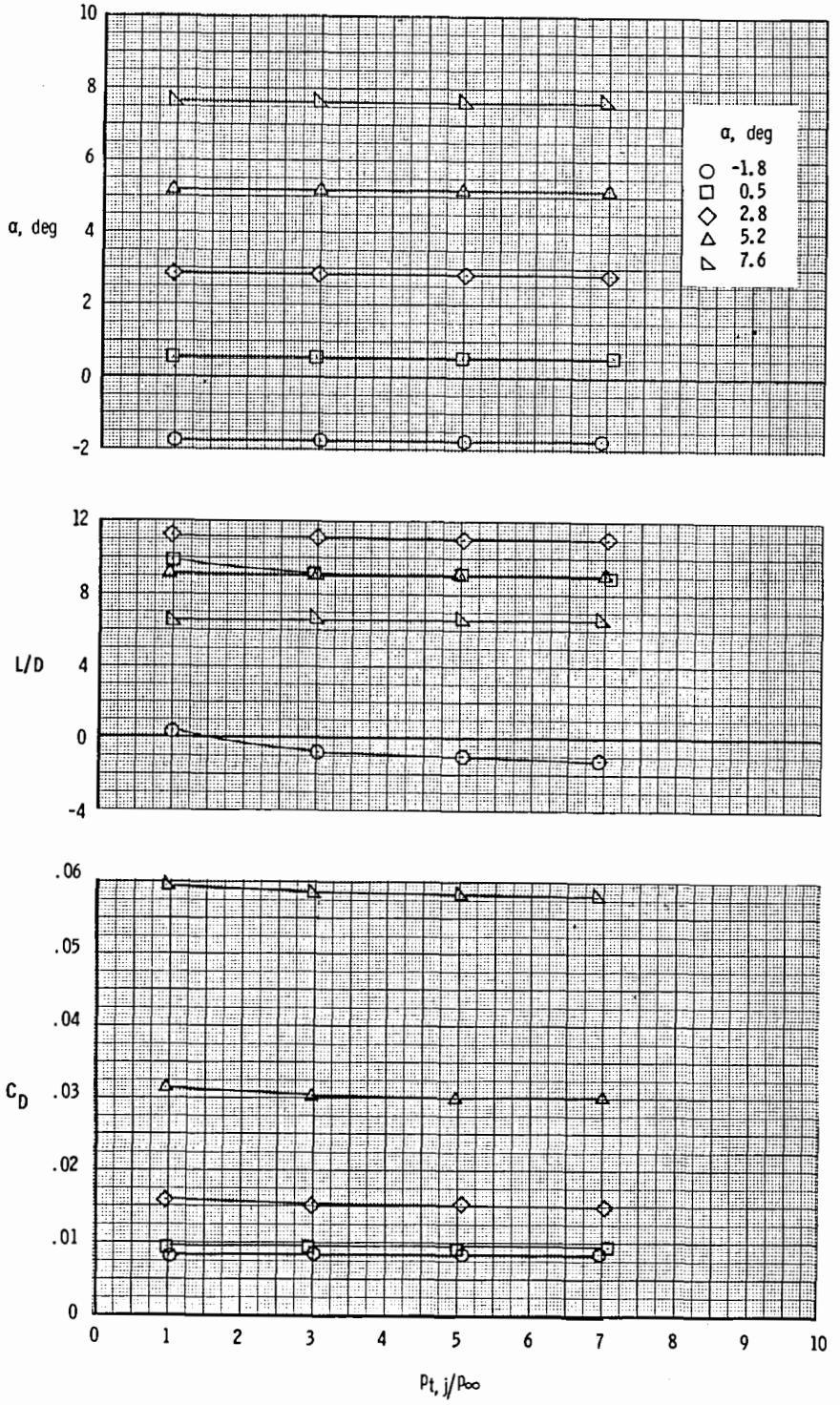

(b) M = 0.80.

Figure 15.- Continued.

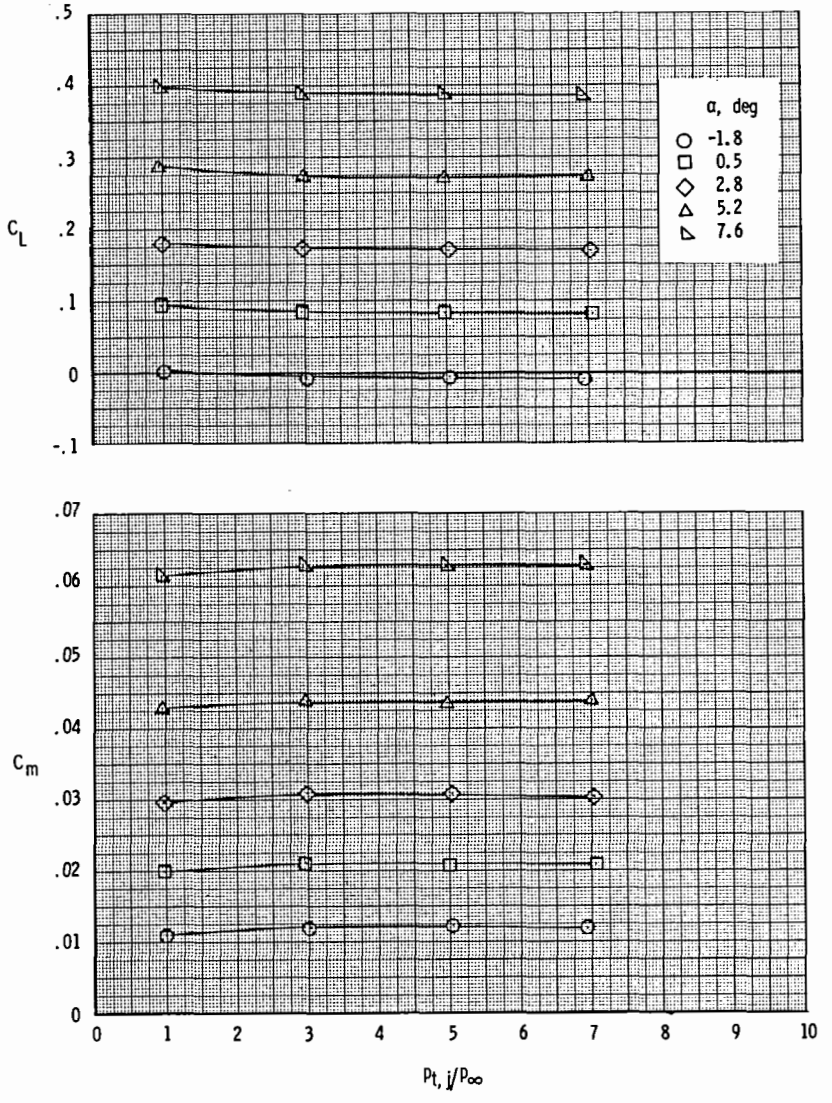

(b) Concluded.

Figure 15.- Continued.

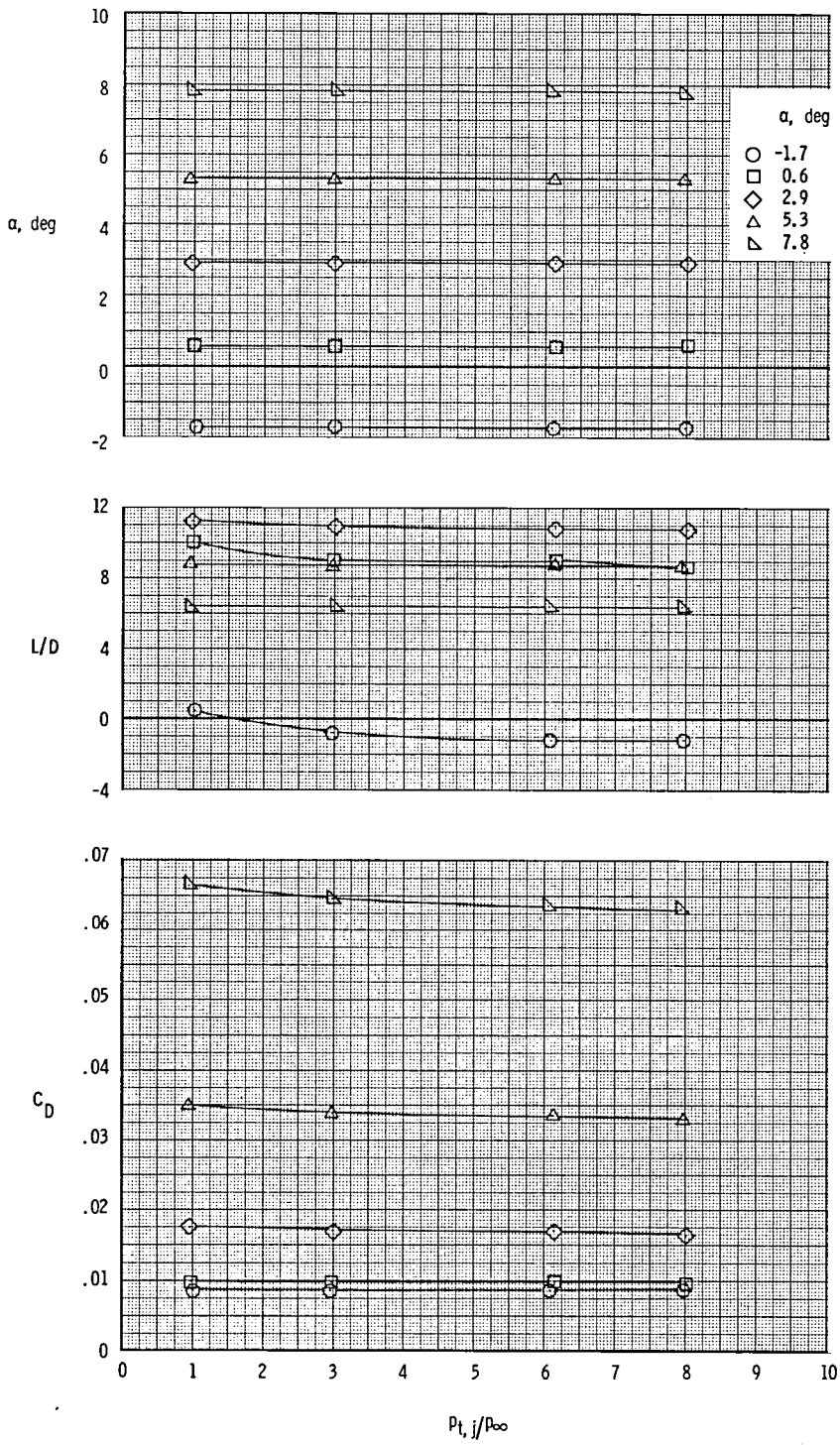

(c) M = 0.90.

Figure 15.- Continued.

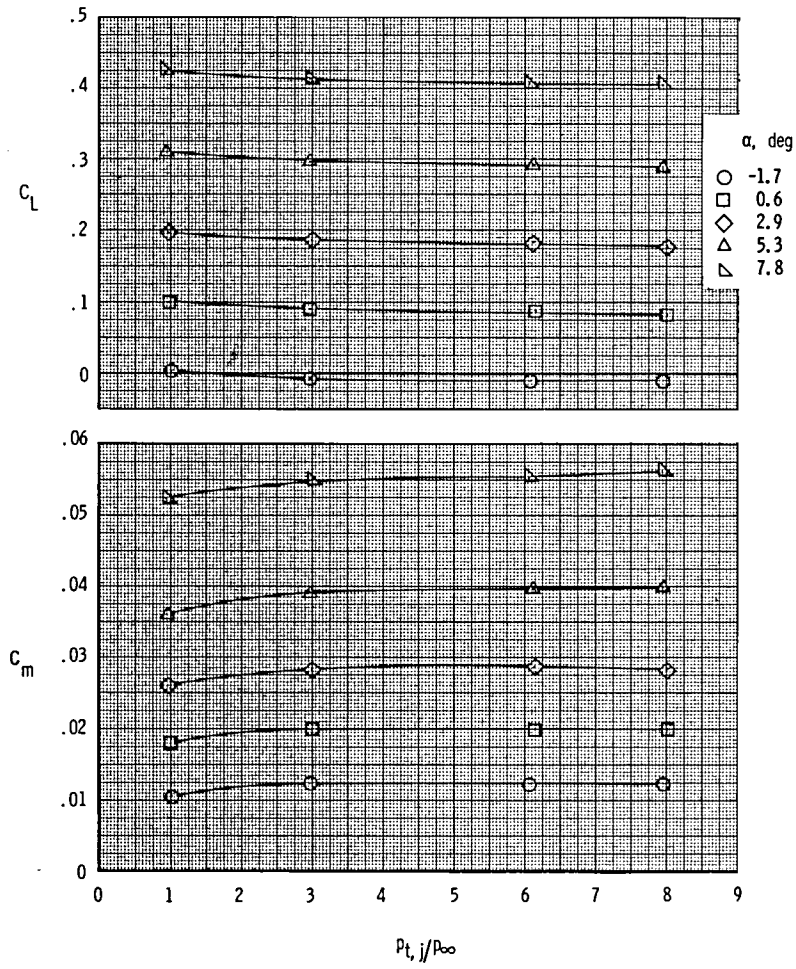

(c) Concluded.

Figure 15.- Continued.

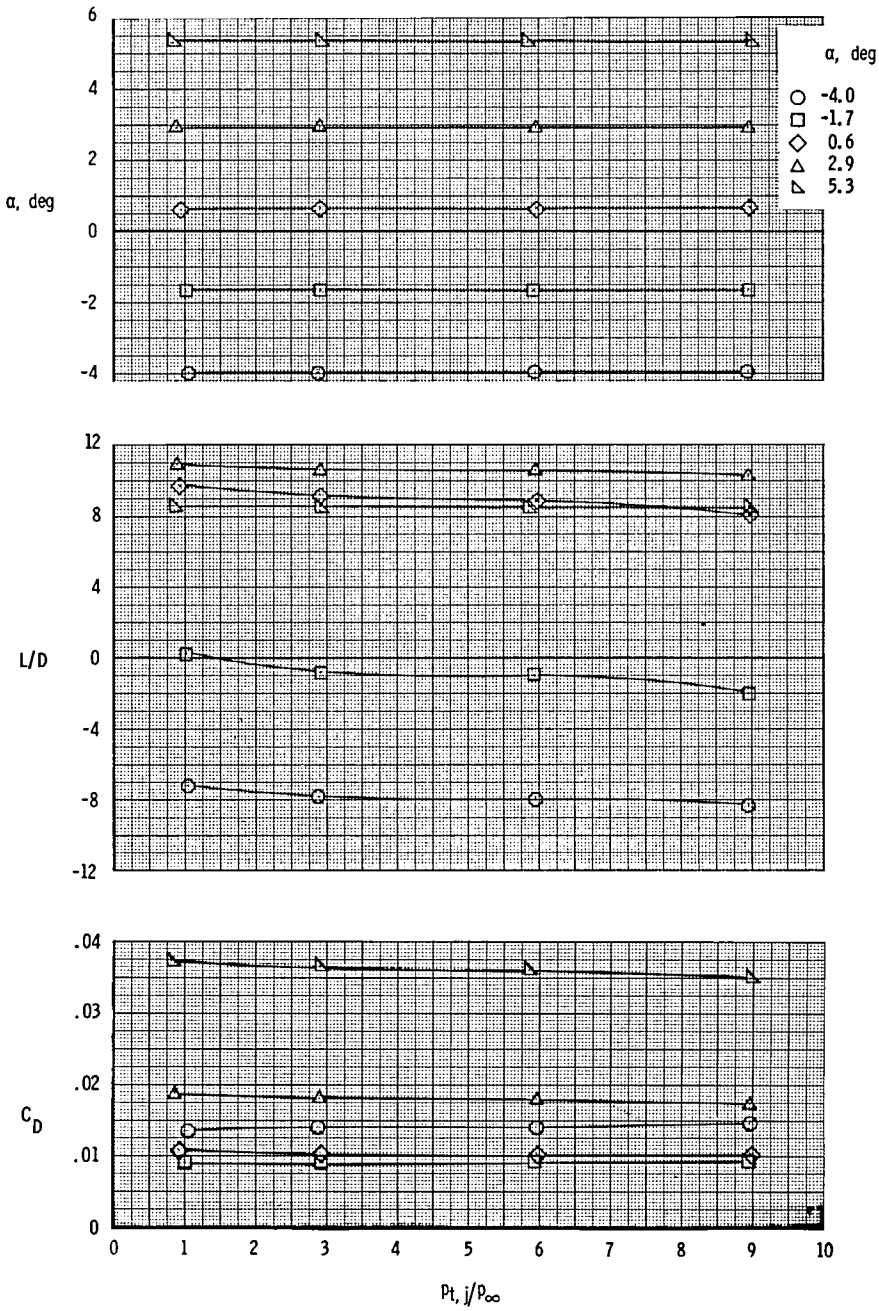

(d) M = 0.95.

Figure 15.- Continued.

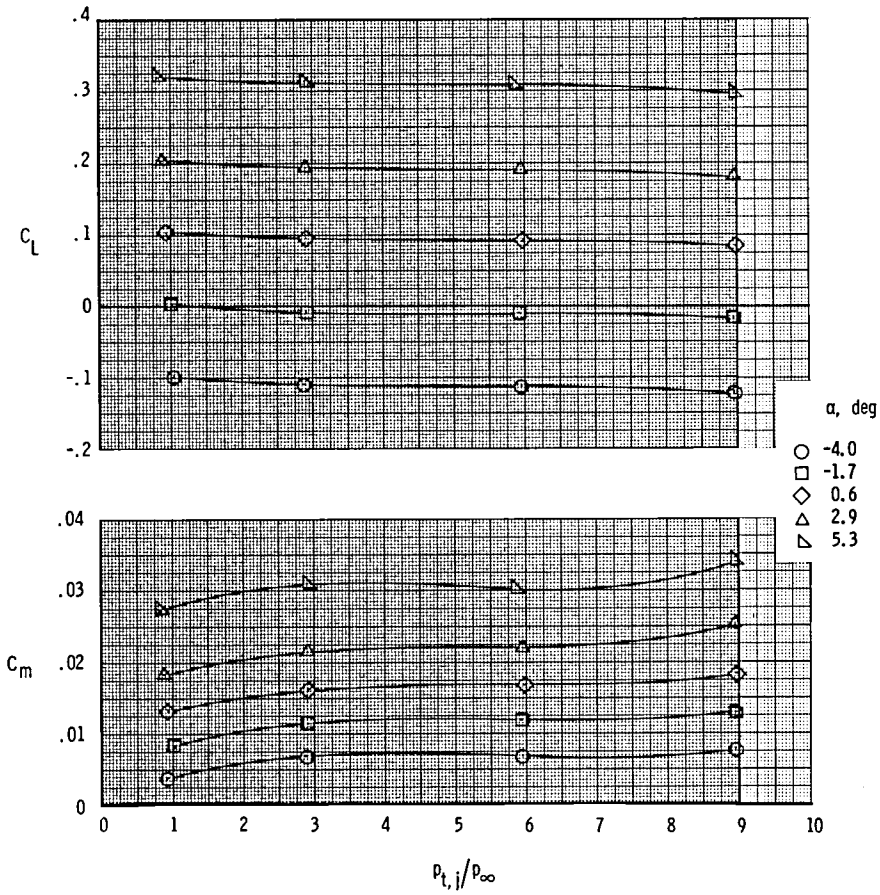

(d) Concluded.

Figure 15.- Continued.

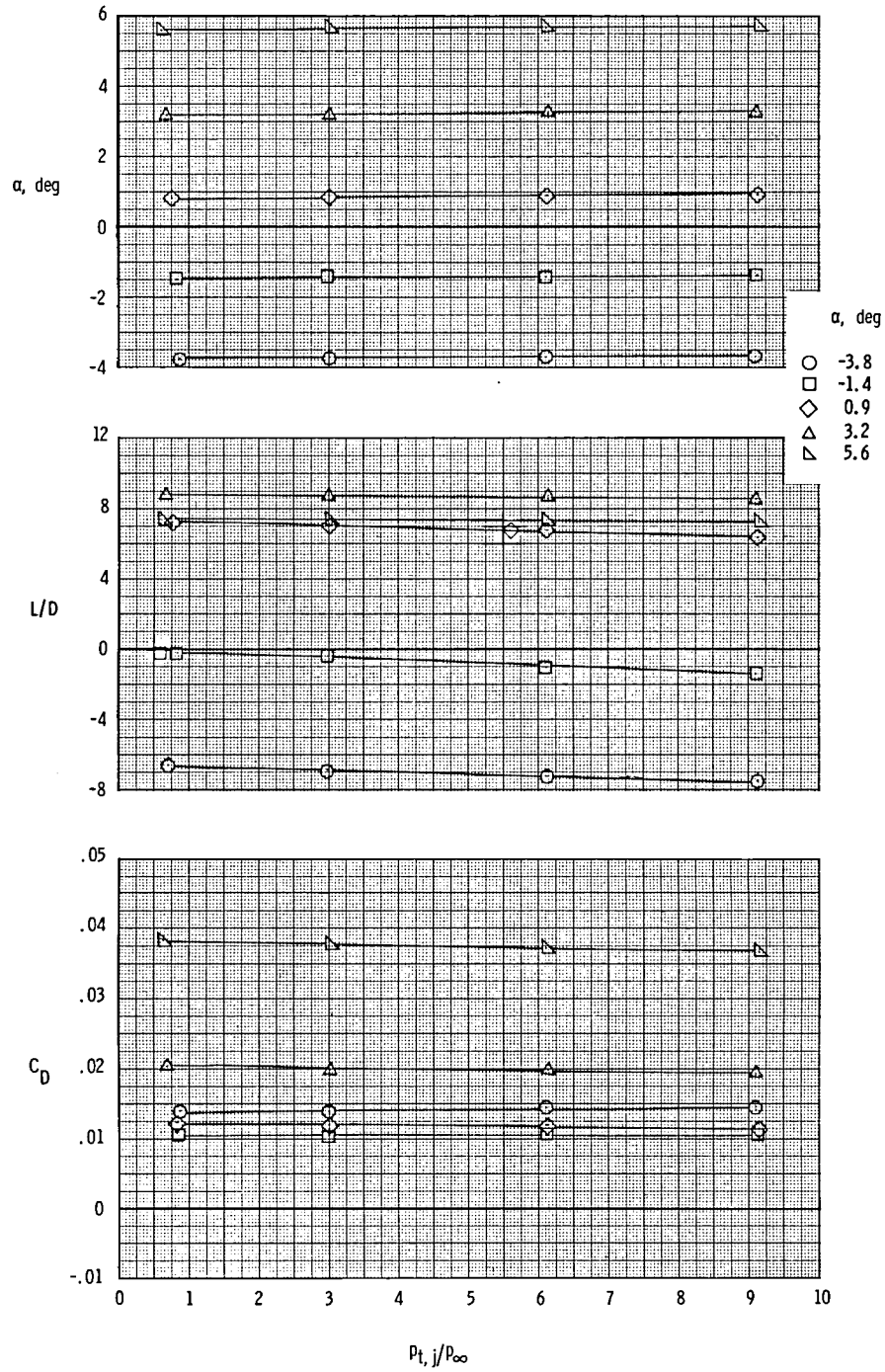

(e) M = 1.20.

Figure 15.- Continued.

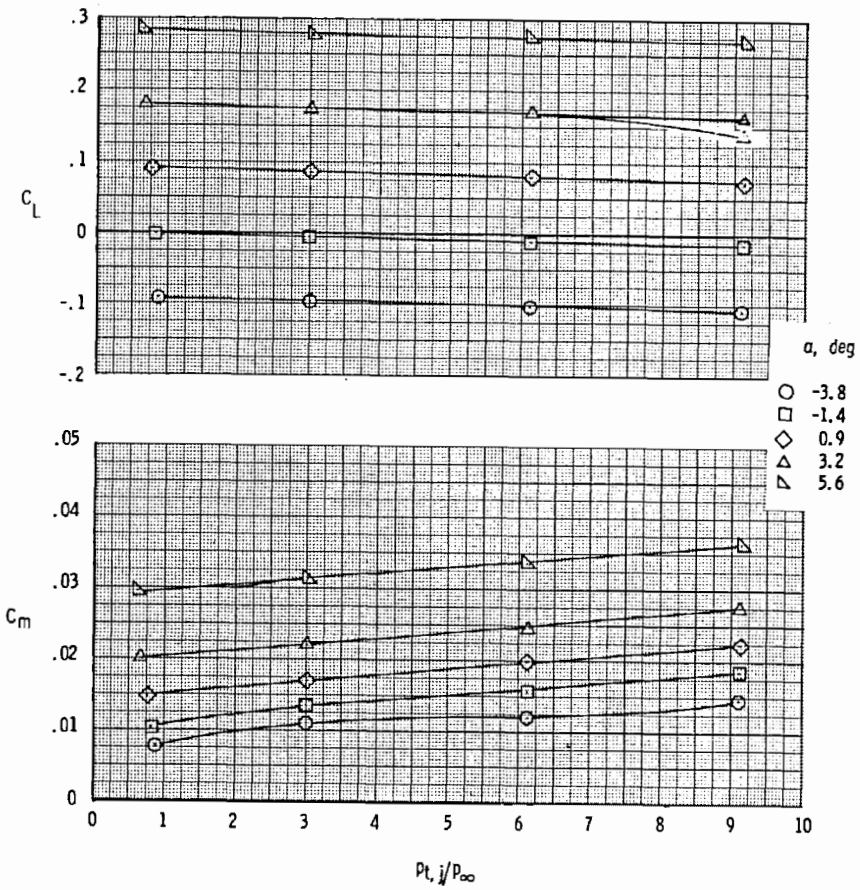

(e) Concluded.

Figure 15.- Concluded.

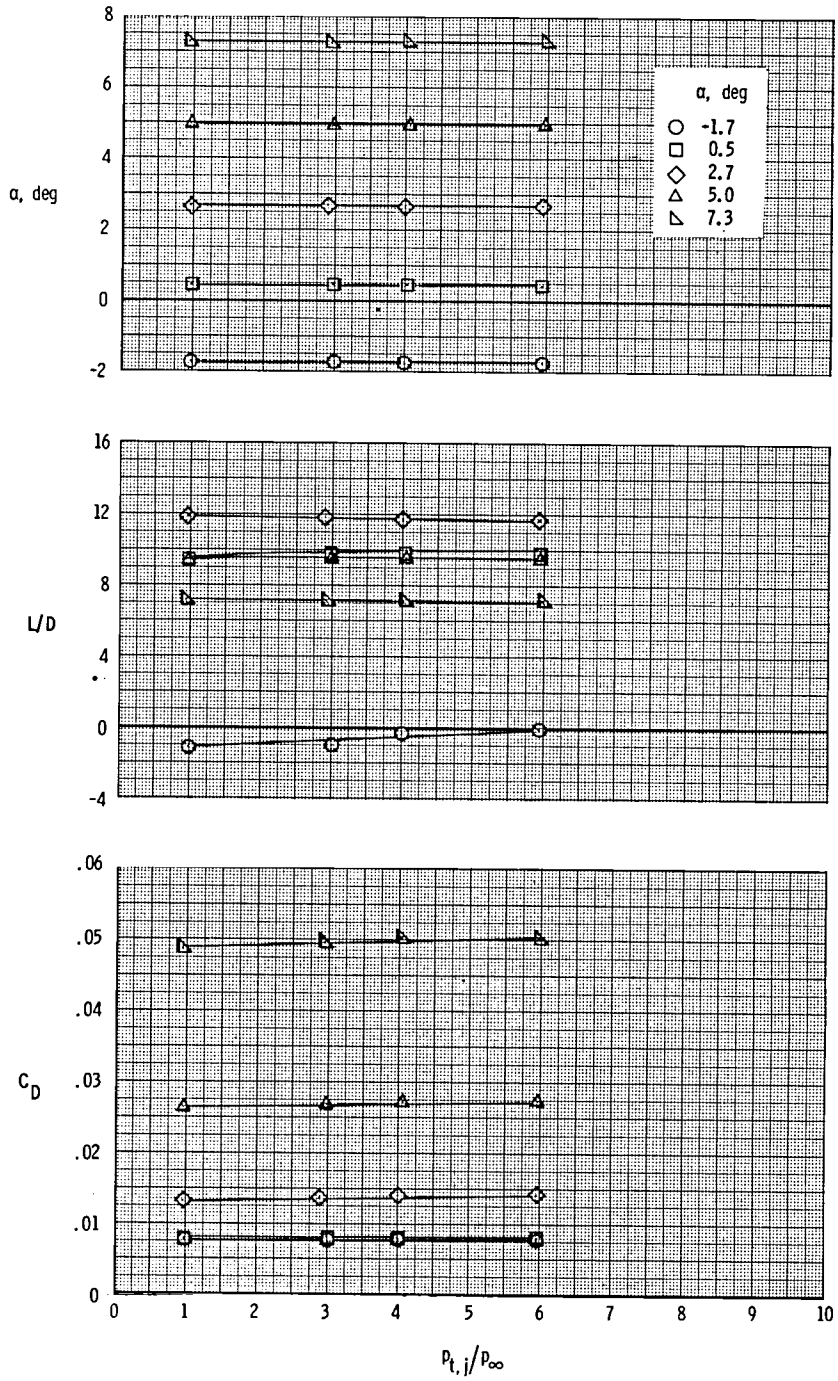

(a) M = 0.60.

Figure 16.- Variation of longitudinal aerodynamic characteristics with jet total-pressure ratio at $x_e/c = 0.31$, $y/(b/2) = 0.25$, and $z_w/d_N = 1.17$. A/B; $\delta_f = -10^o$.

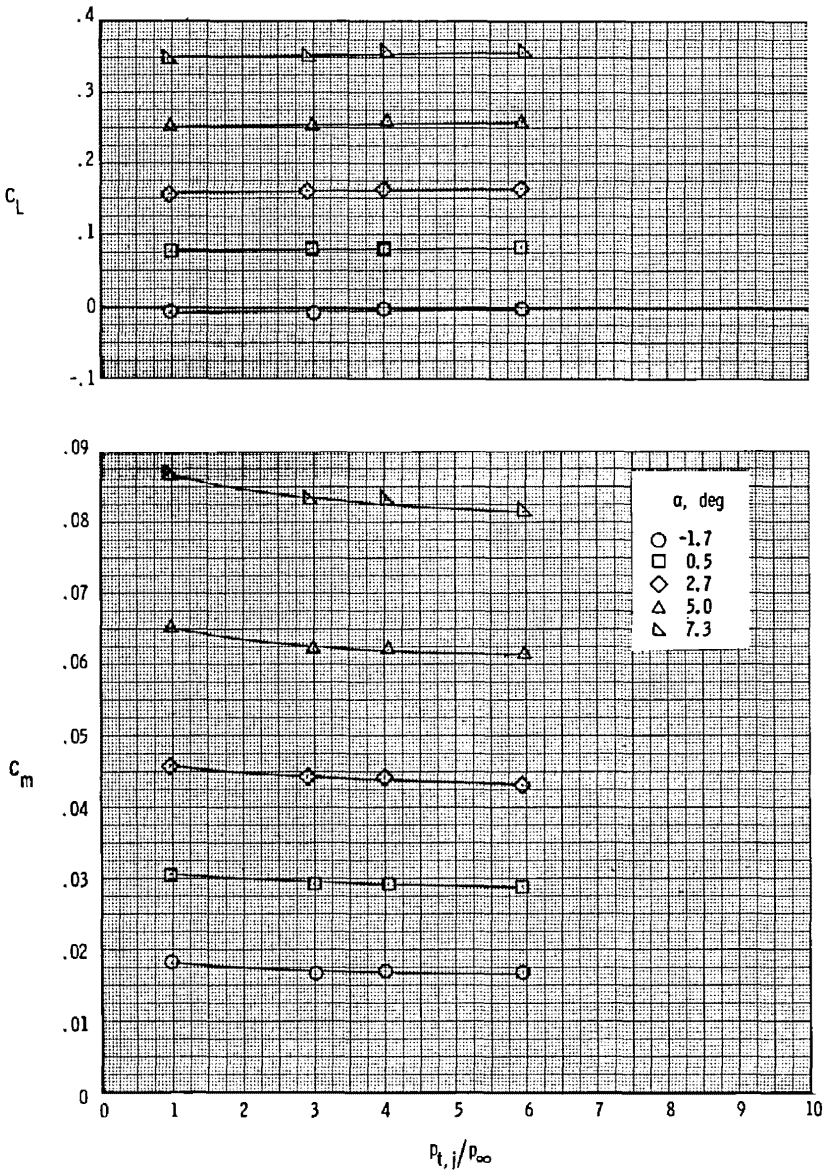

(a) Concluded.

Figure 16.- Continued.

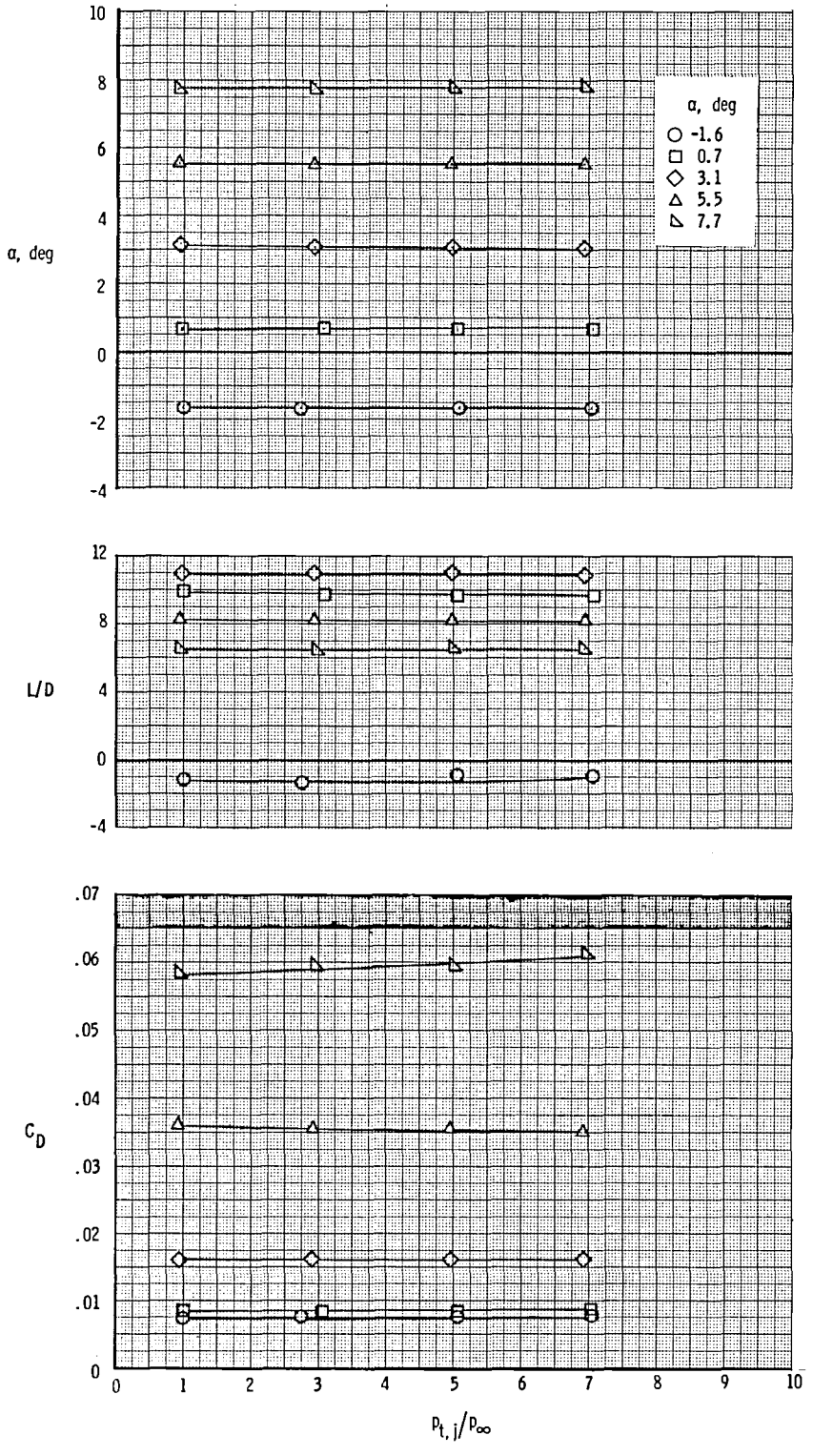

(b) M = 0.80.

Figure 16.- Continued.

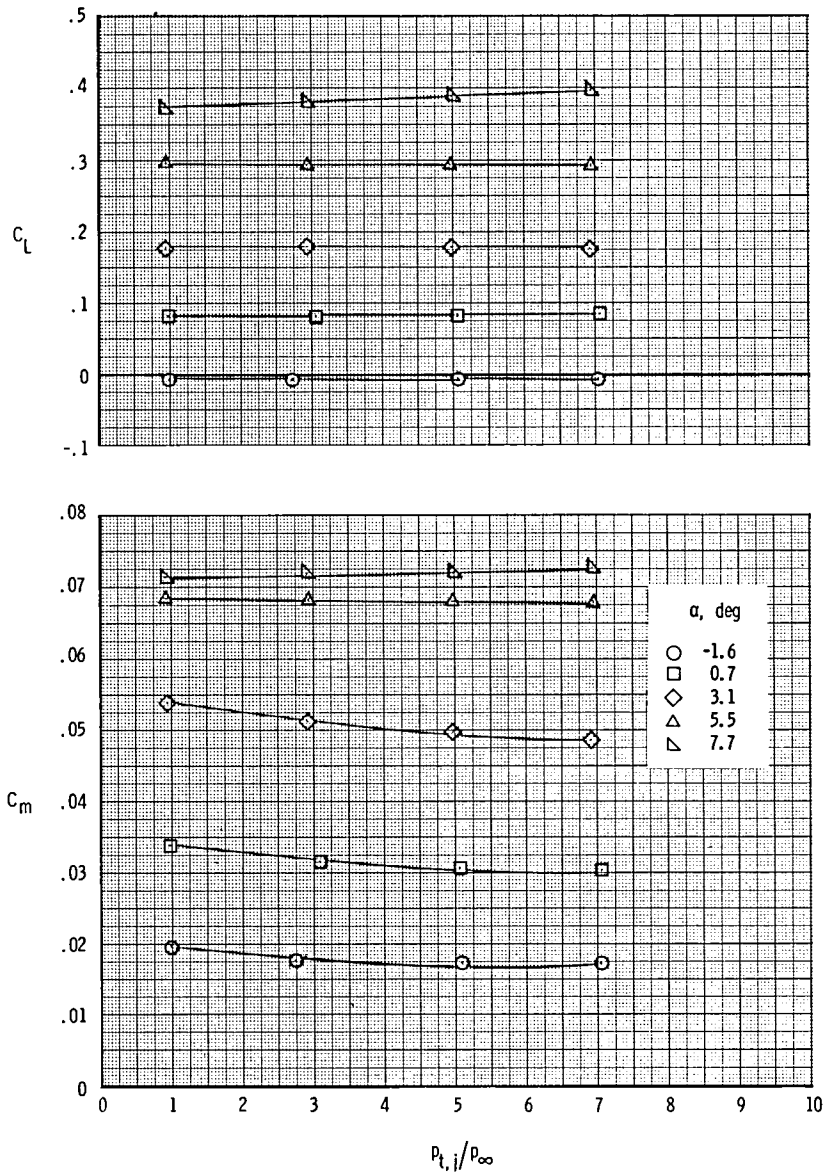

(b) Concluded.

Figure 16.- Continued.

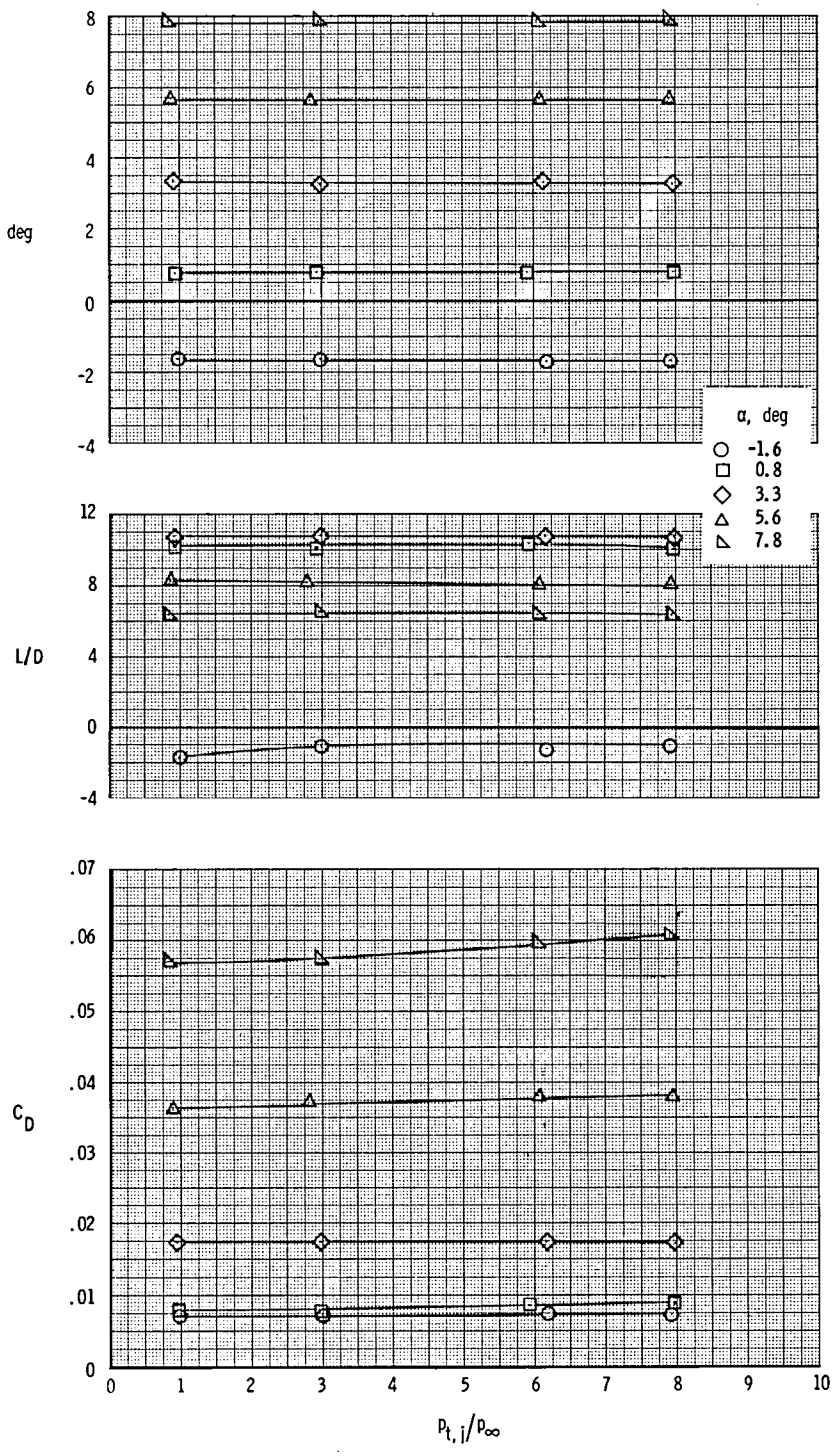

(c) M = 0.90.

Figure 16.- Continued.

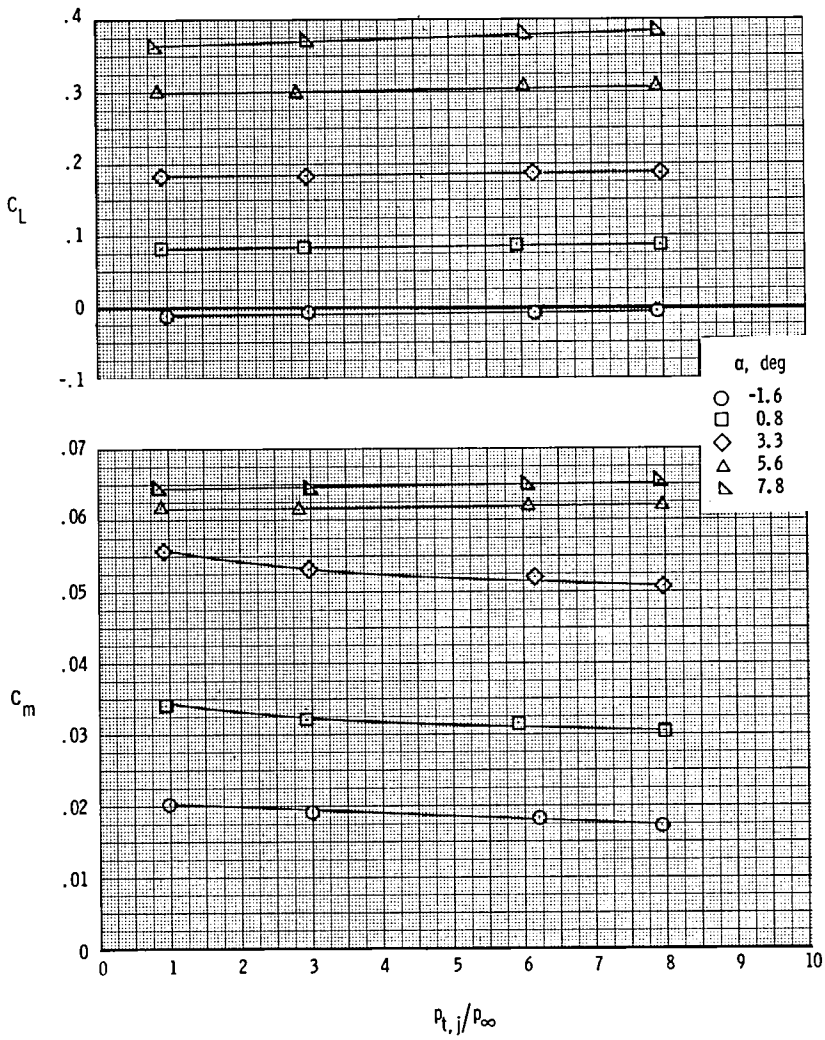

(c) Concluded.

Figure 16.- Continued.

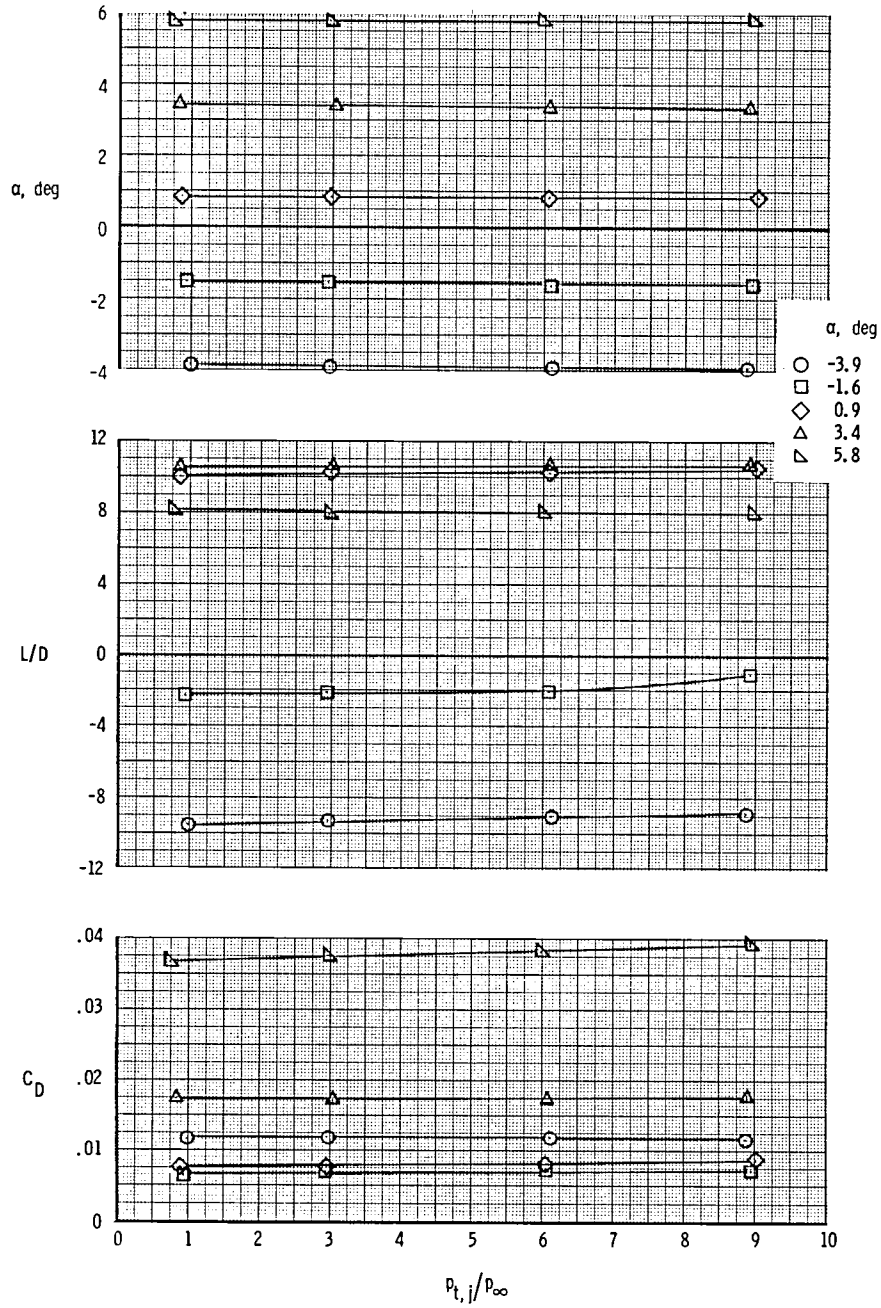

(d) M = 0.95.

Figure 16.- Continued.

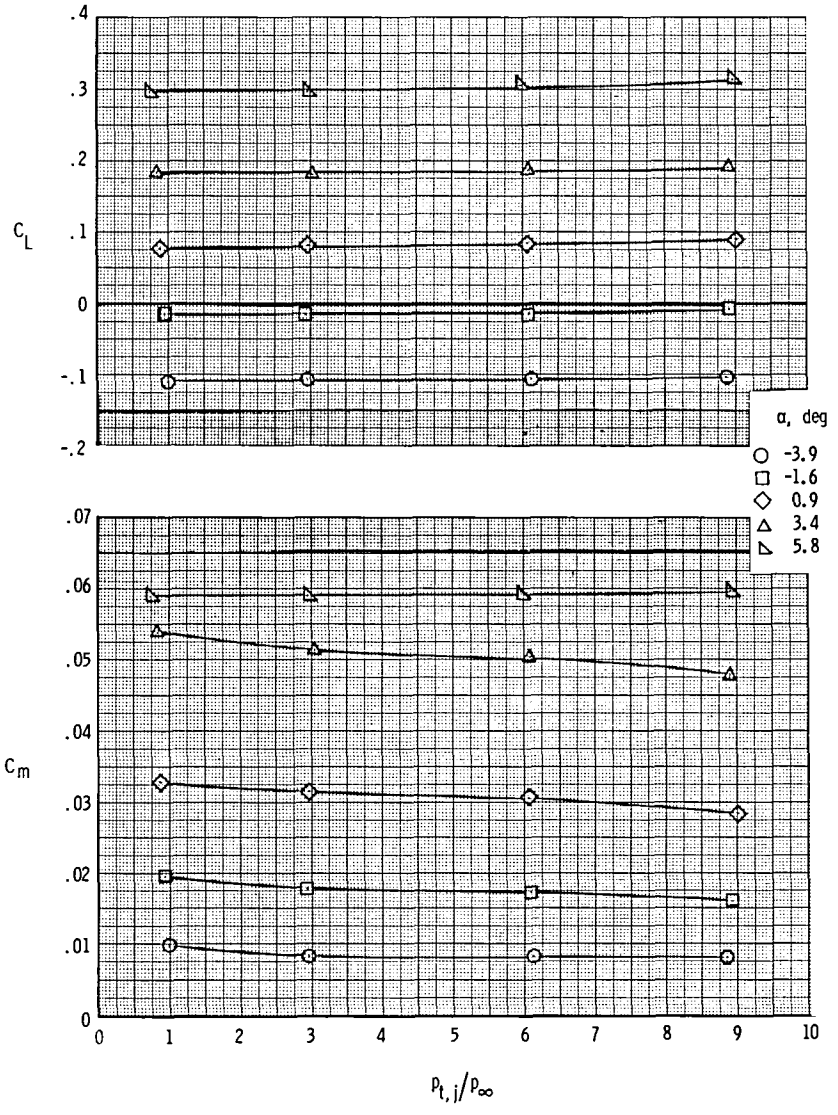

(d) Concluded.

Figure 16.- Continued.

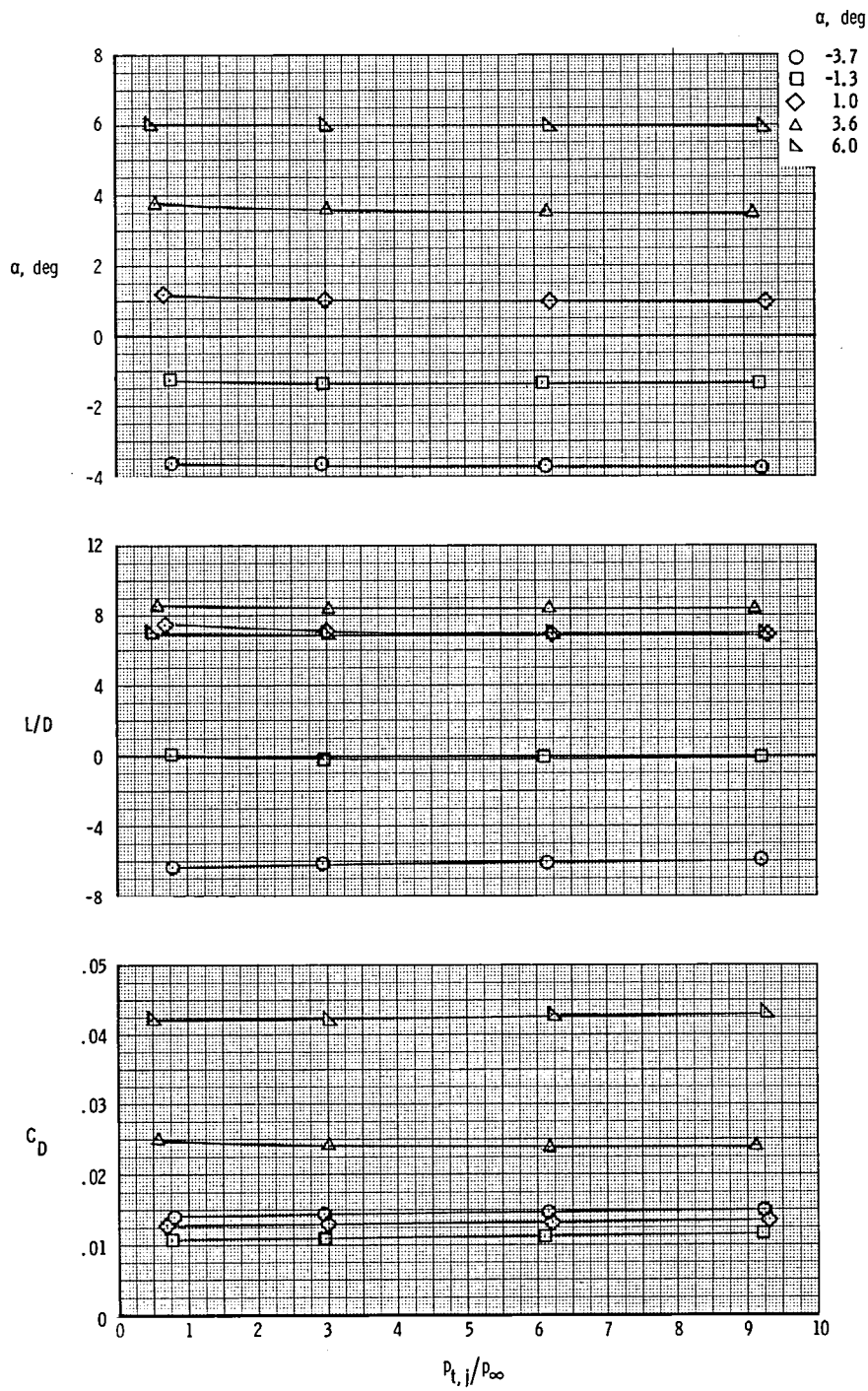

(e) M = 1.20.

Figure 16.- Continued.

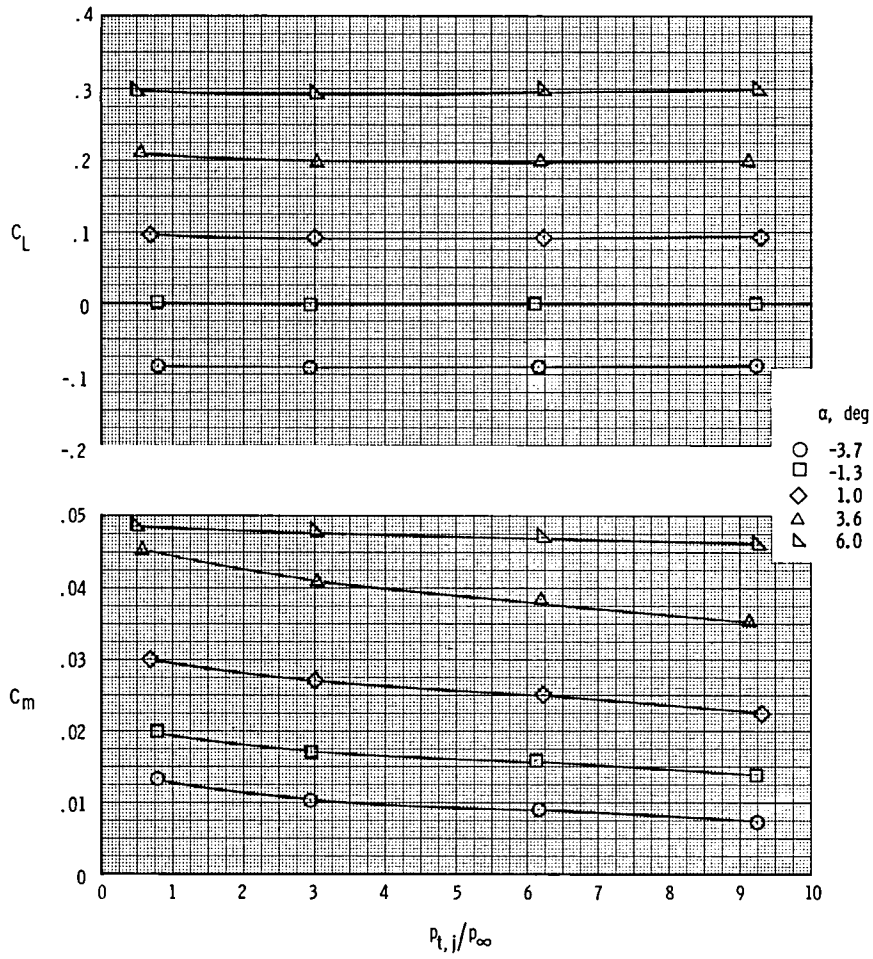

(e) Concluded.

Figure 16.- Concluded.

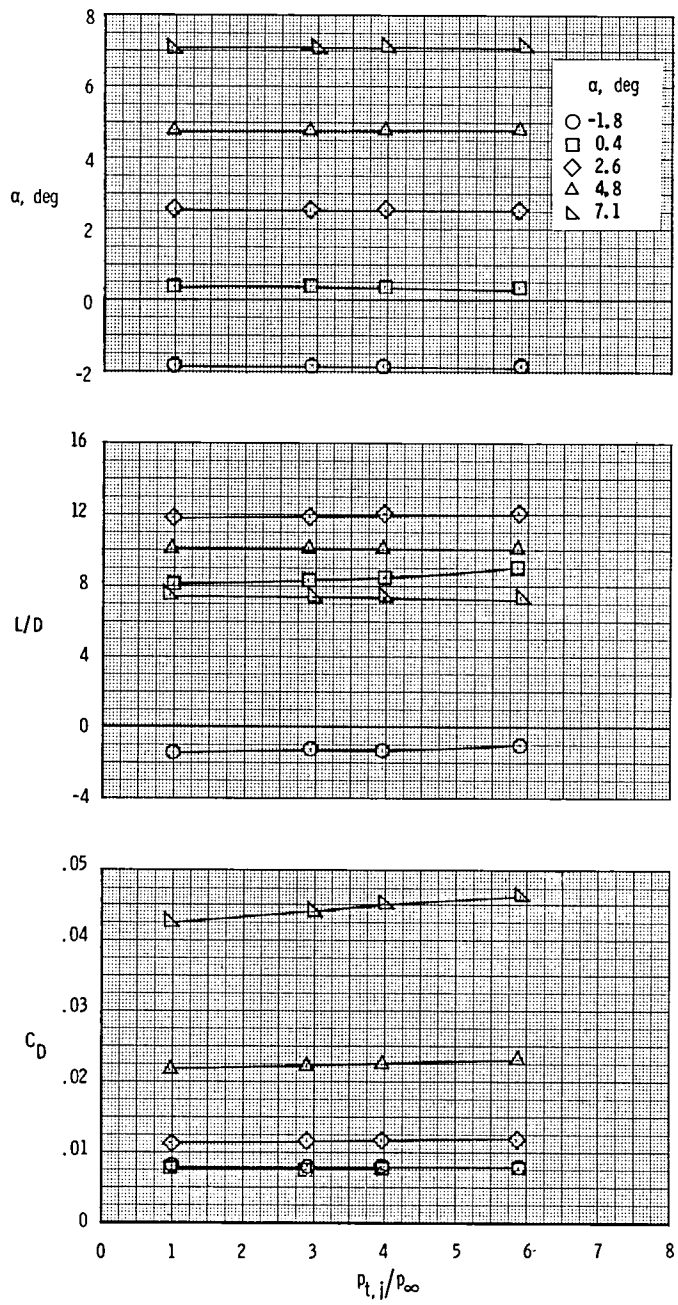

(a) M = 0.60.

Figure 17.- Variation of longitudinal aerodynamic characteristics with jet total-pressure ratio at $x_e/c = -0.69$, $y/(b/2) = 0.58$, and $z_w/d_N = 1.60$. A/B; $\delta_f = -10^o$.

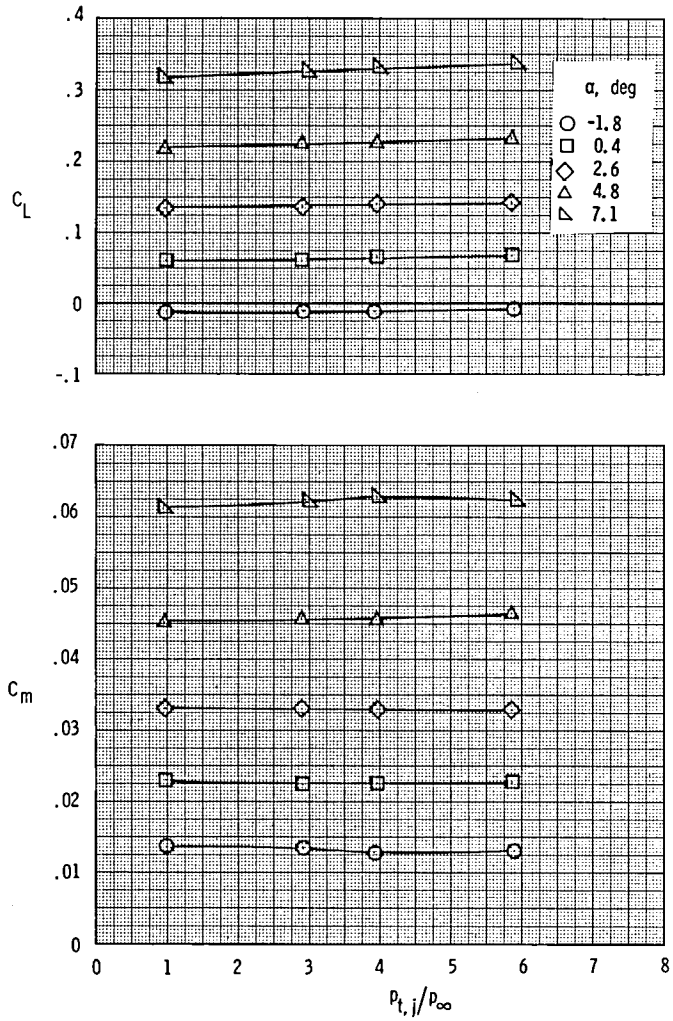

(a) Concluded.

Figure 17.- Continued.

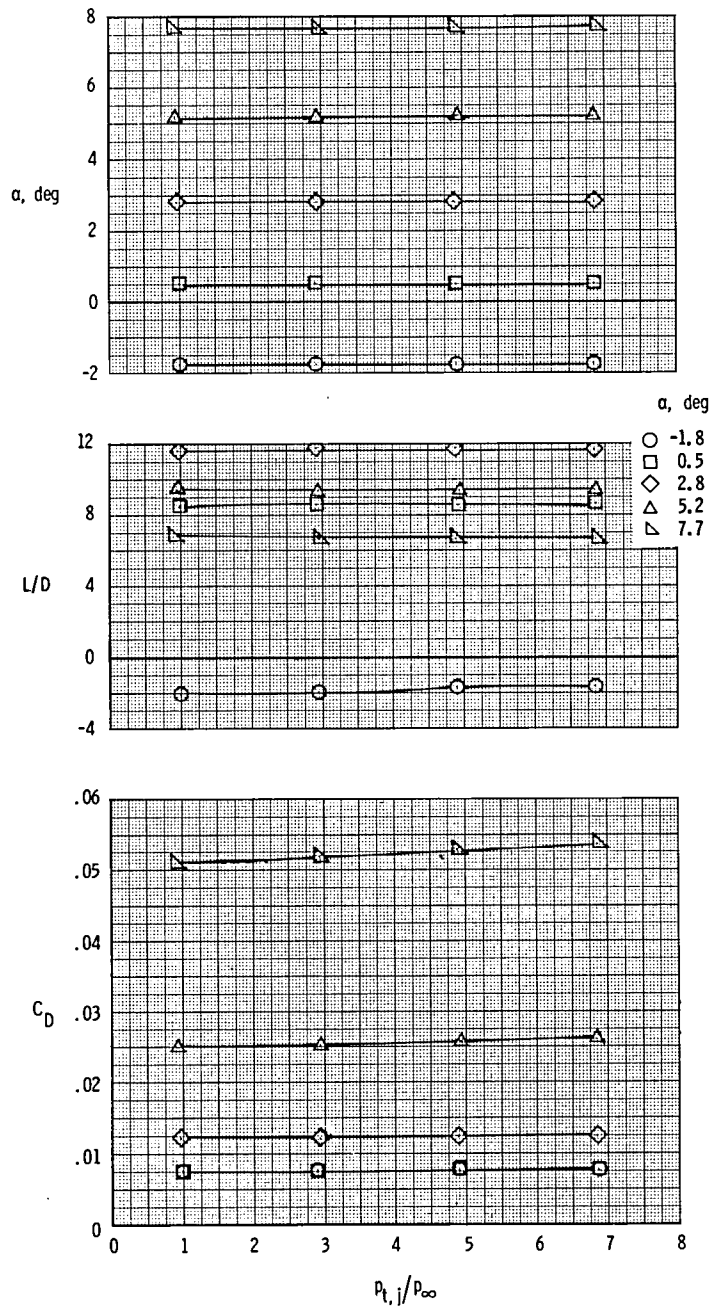

(b) M = 0.80.

Figure 17.- Continued.

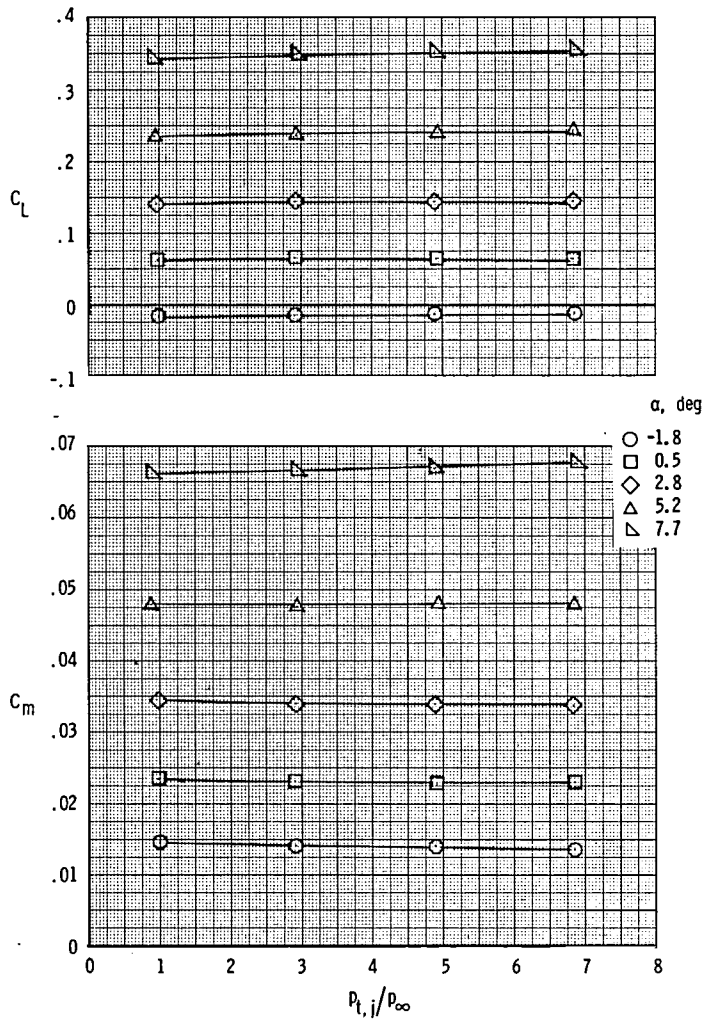

(b) Concluded.

Figure 17.- Continued.

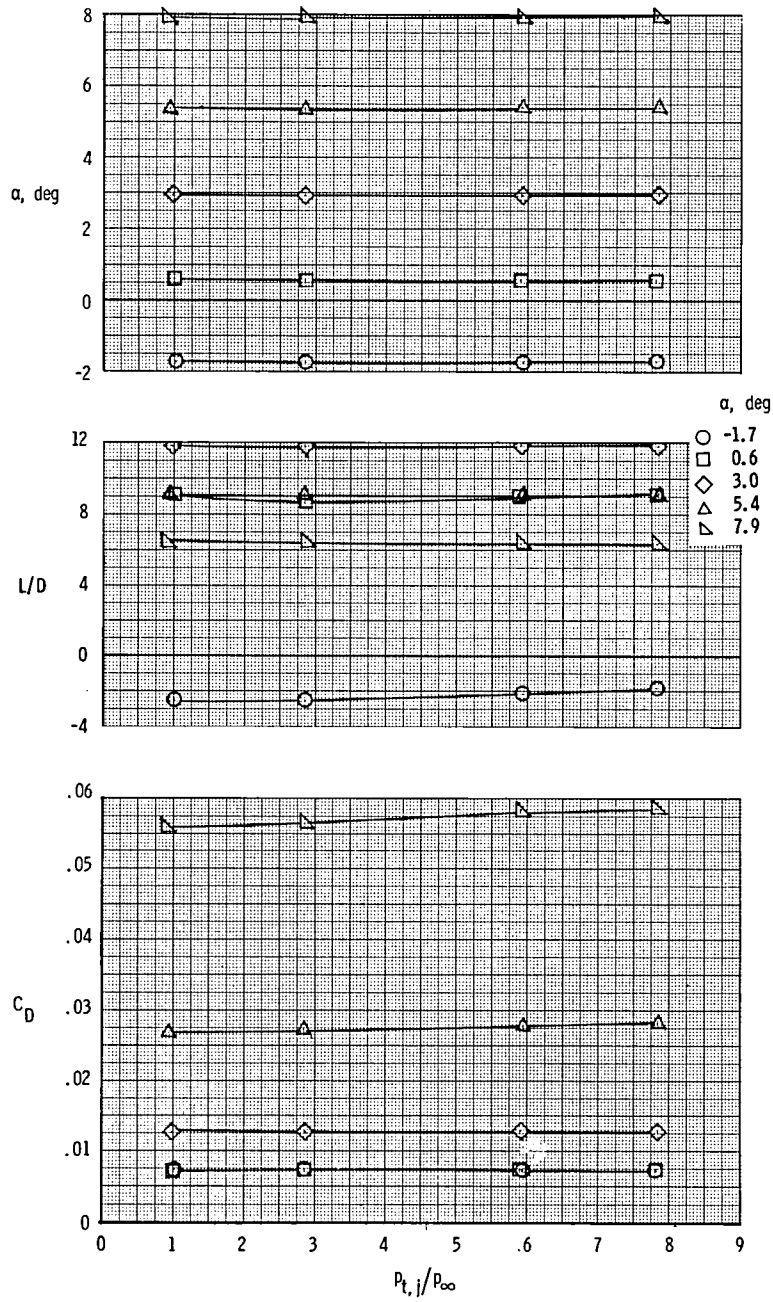

(c) M = 0.90.

Figure 17.- Continued.

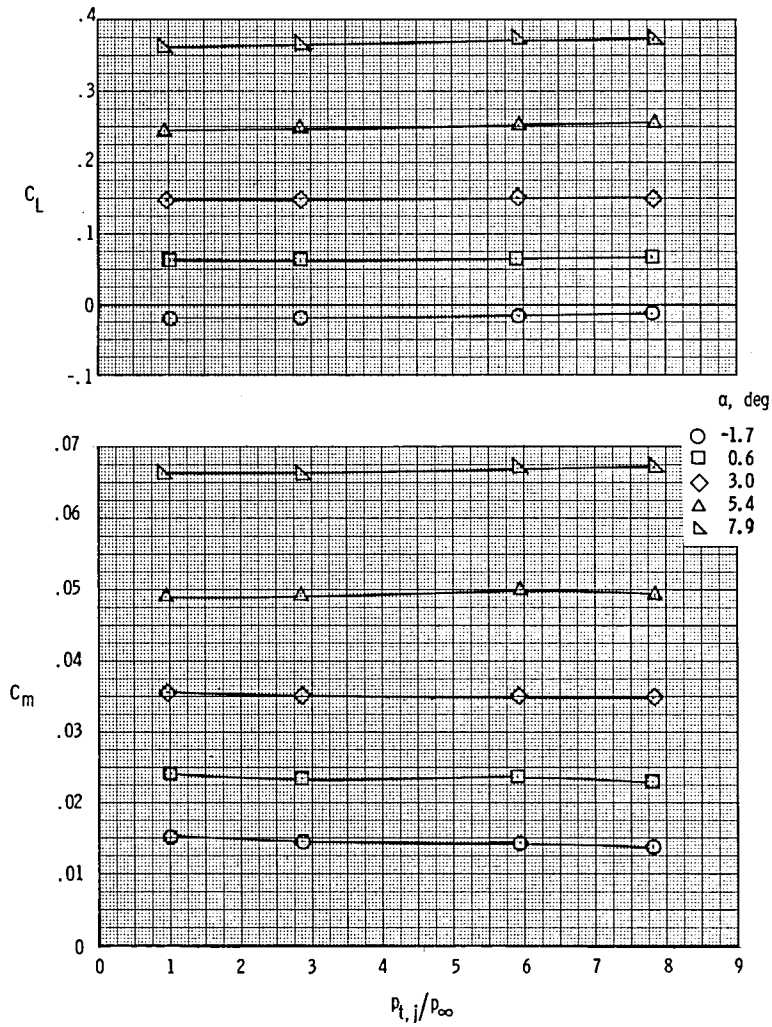

(c) Concluded.

Figure 17.- Continued.

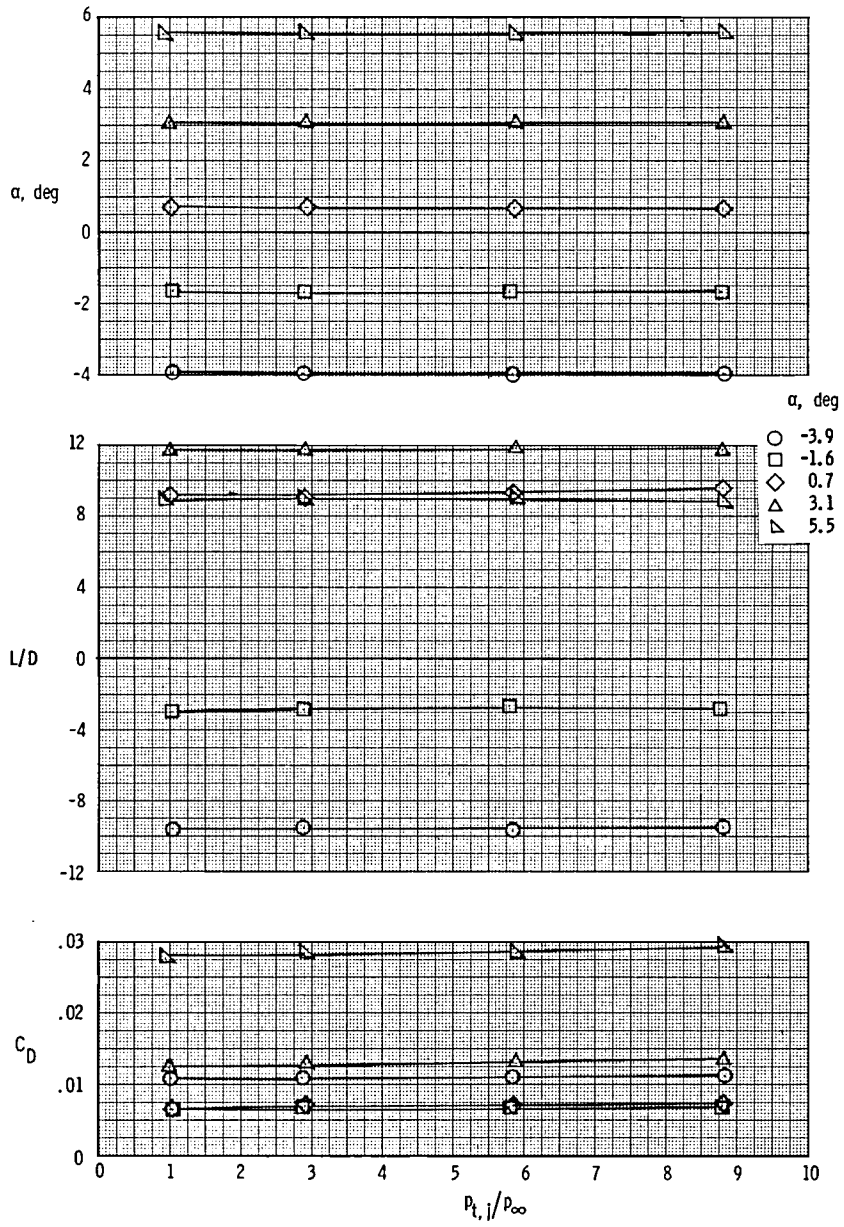

(d) M = 0.95.

Figure 17.- Continued.

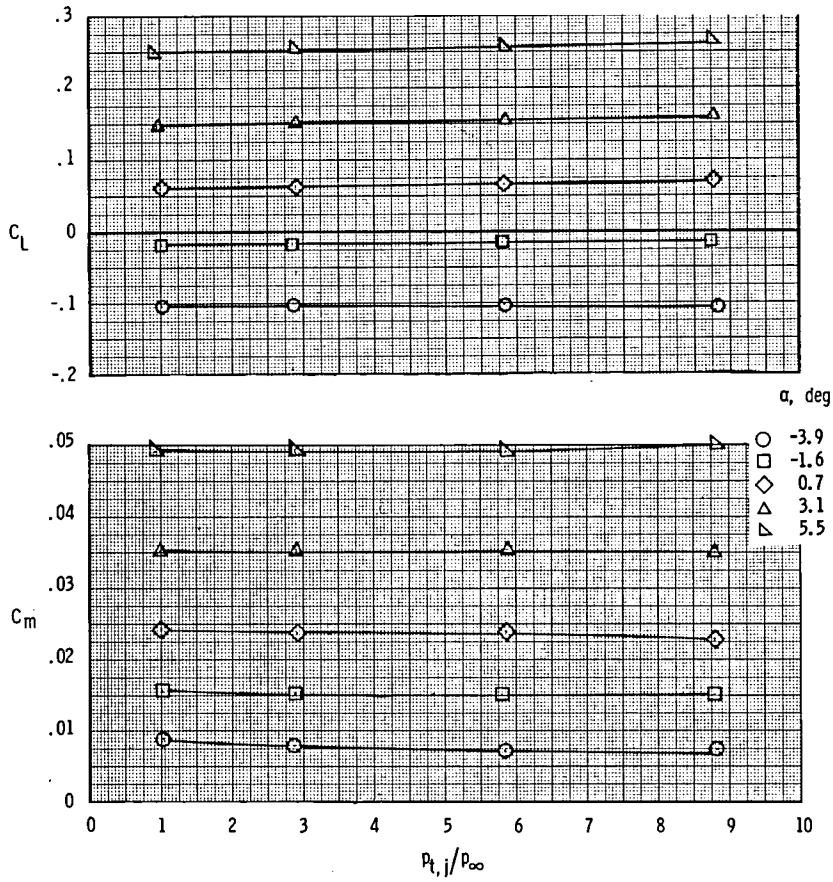

(d) Concluded.

Figure 17.- Continued.

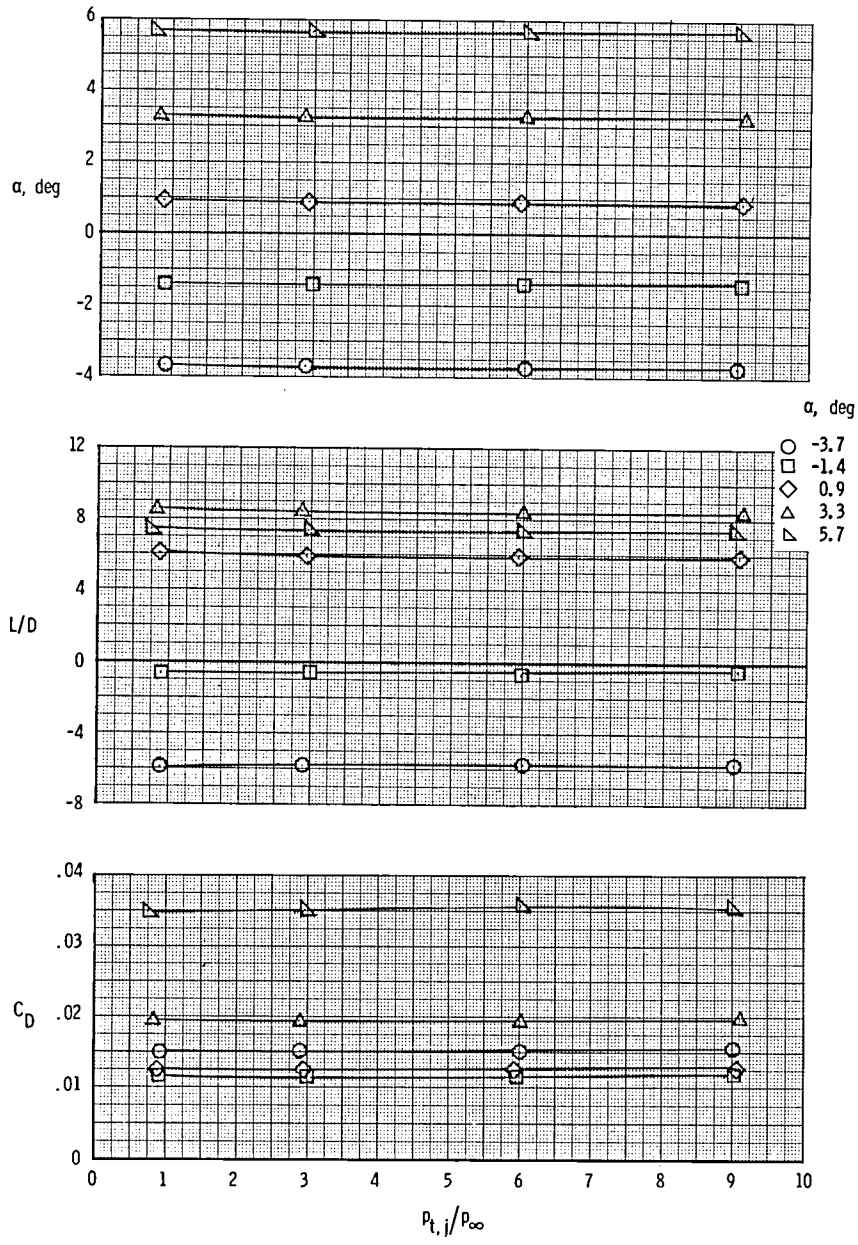

(e) M = 1.20.

Figure 17.- Continued.

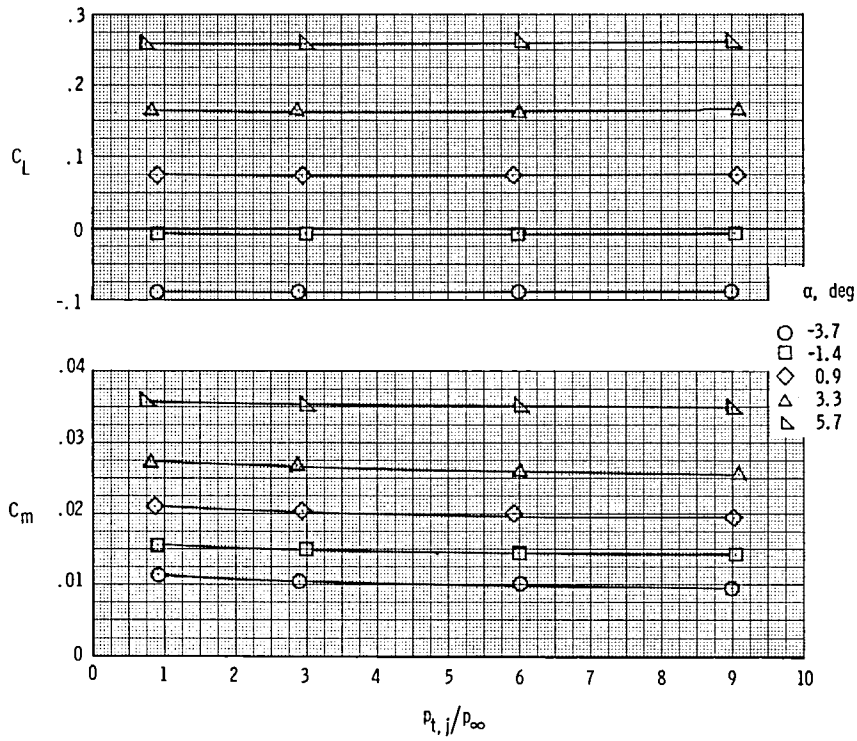

(e) Concluded.

Figure 17.- Concluded.

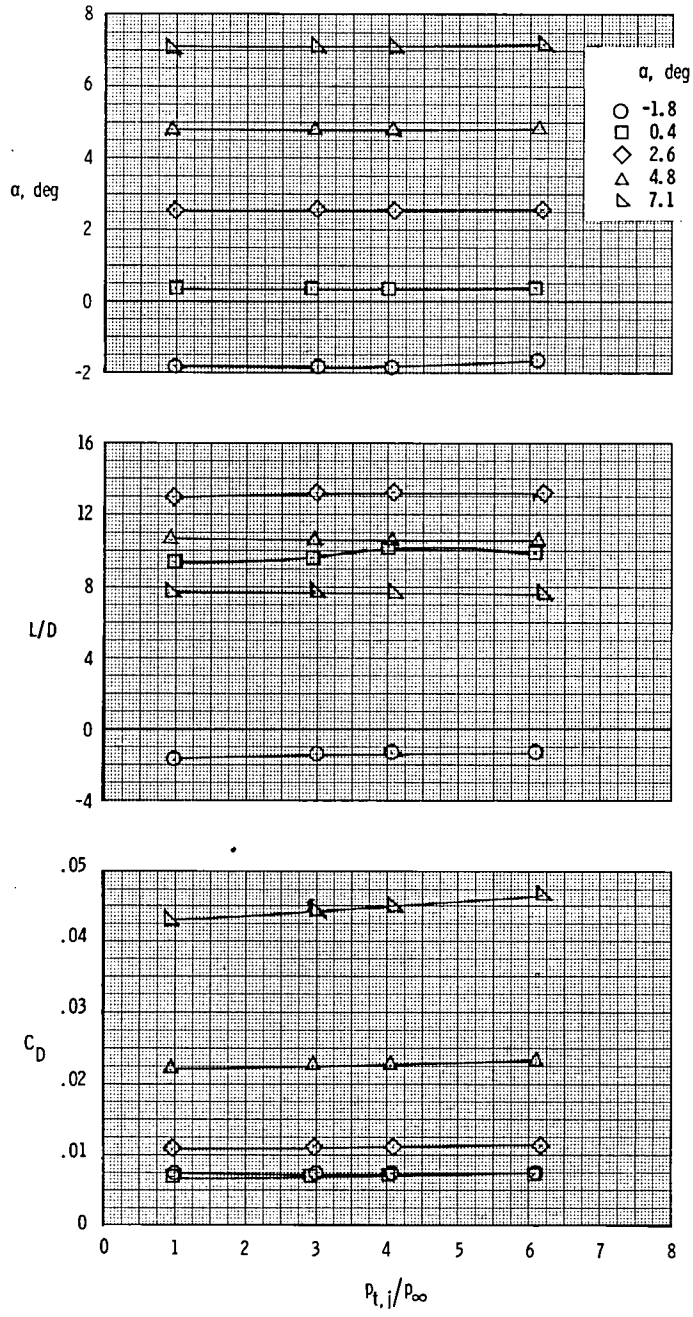

(a) M = 0.60.

Figure 18.- Variation of longitudinal aerodynamic characteristics with jet total-pressure ratio at $x_e/c = 0.17$, $y/(b/2) = 0.46$, and $z_w/d_N = 1.75$. A/B; $\delta_f = -10^o$.

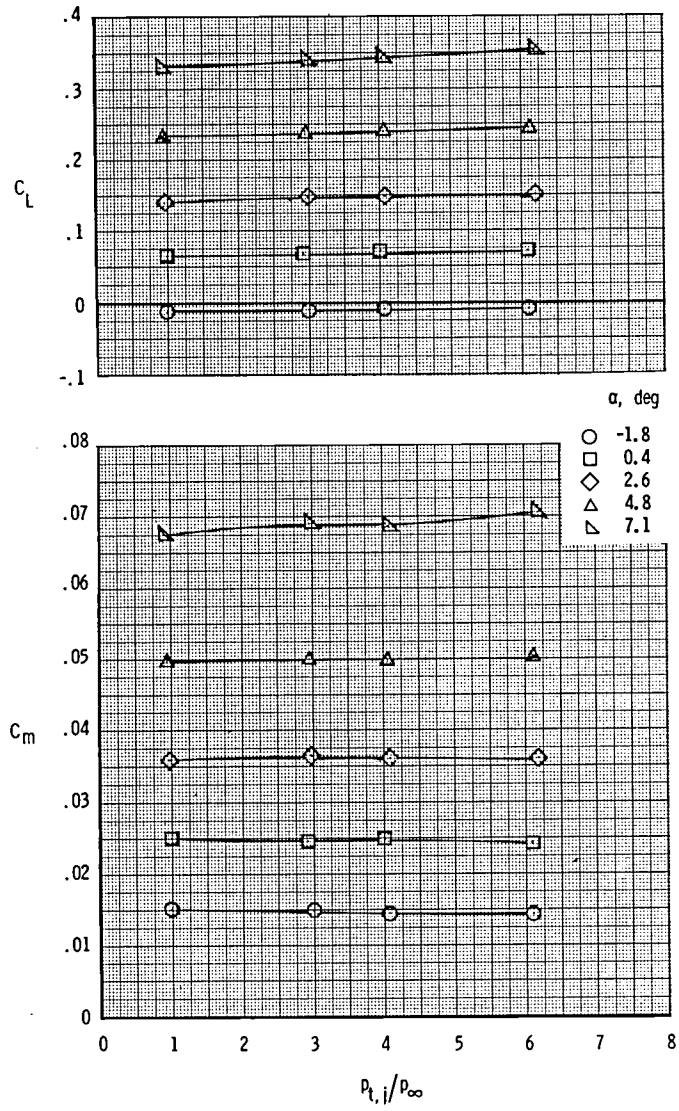

(a) Concluded.

Figure 18.- Continued.

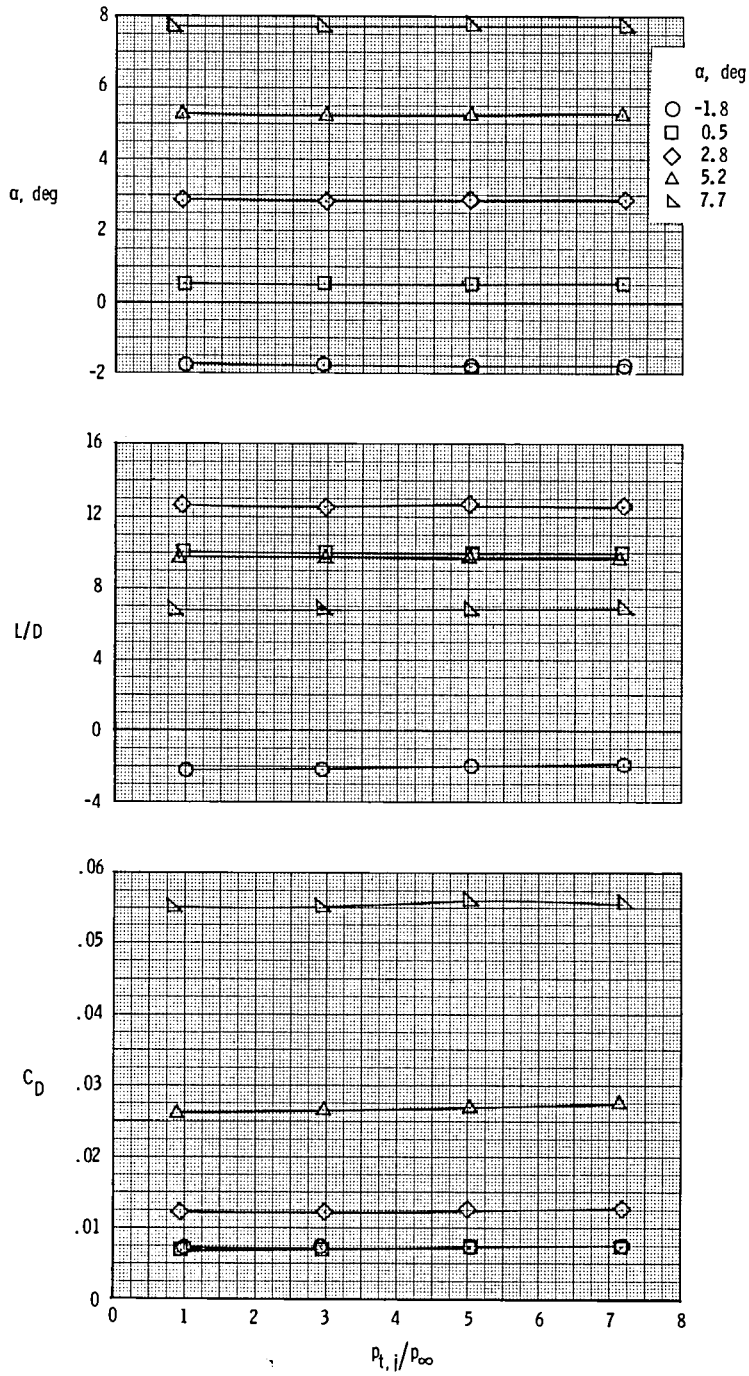

(b) M = 0.80.

Figure 18.- Continued.

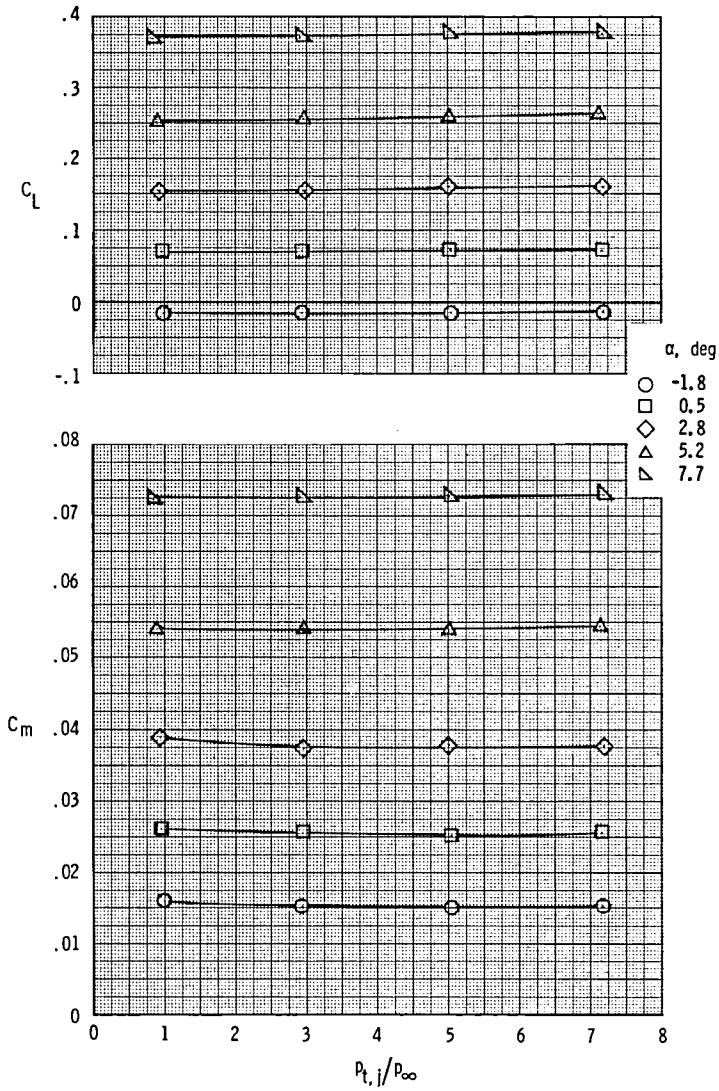

(b) Concluded.

Figure 18.- Continued.

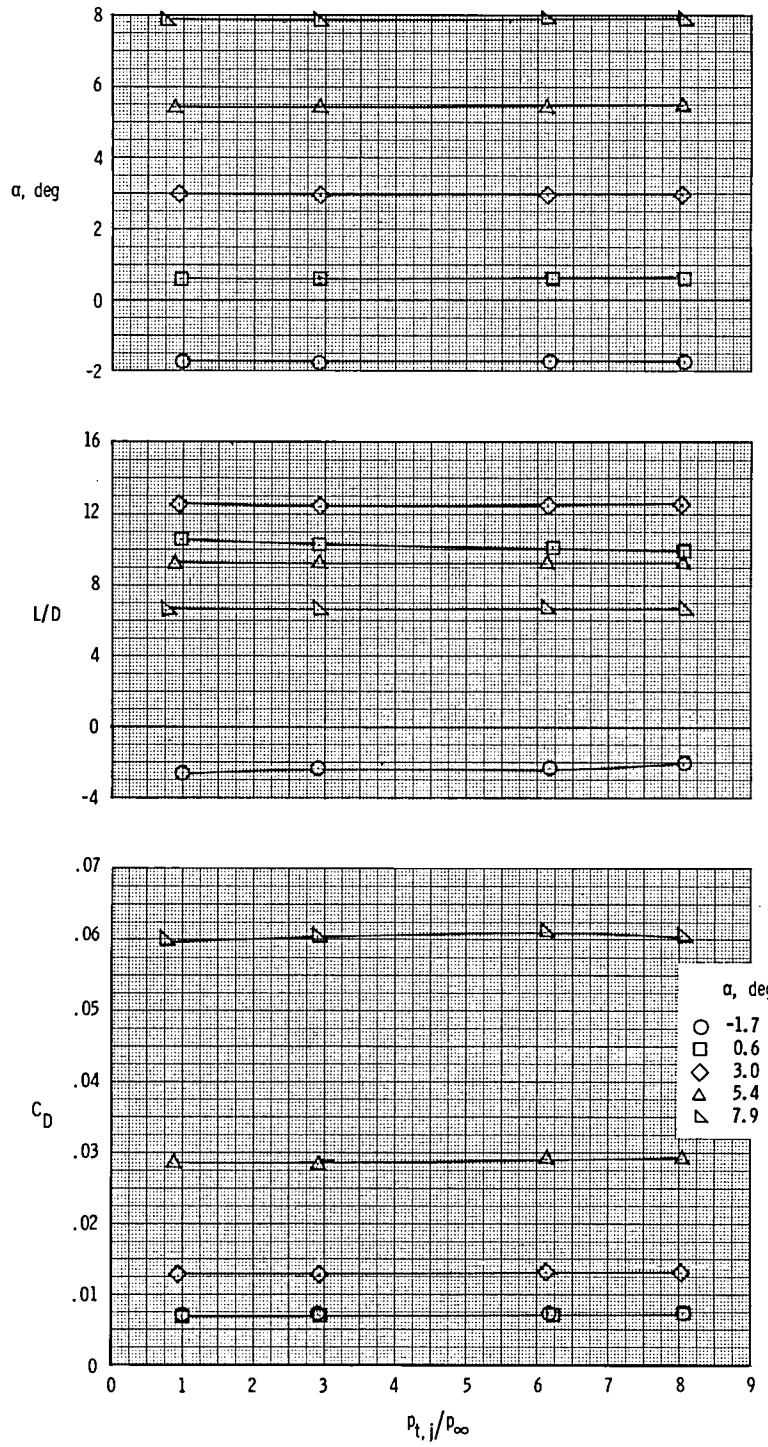

(c) M = 0.90.

Figure 18.- Continued.

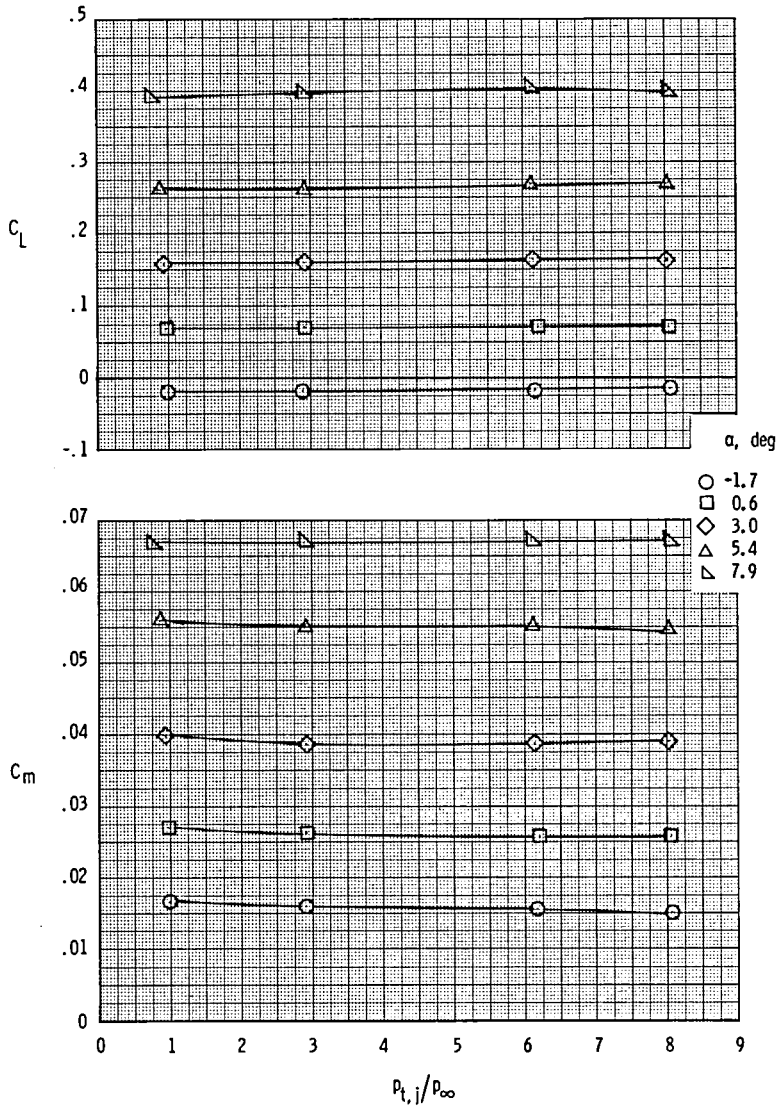

(c) Concluded.

Figure 18.- Continued.

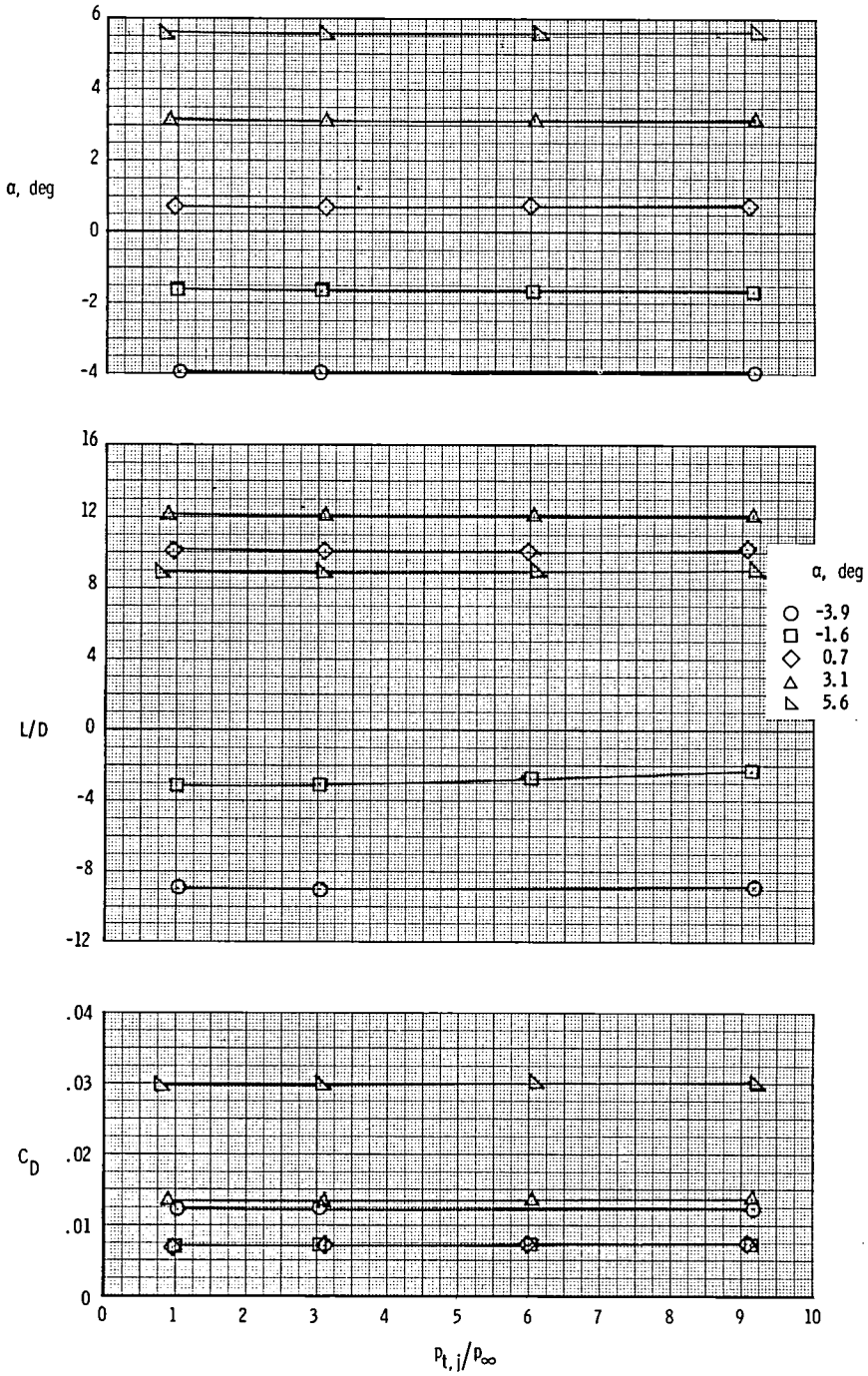

(d) M = 0.95.

Figure 18.- Continued.

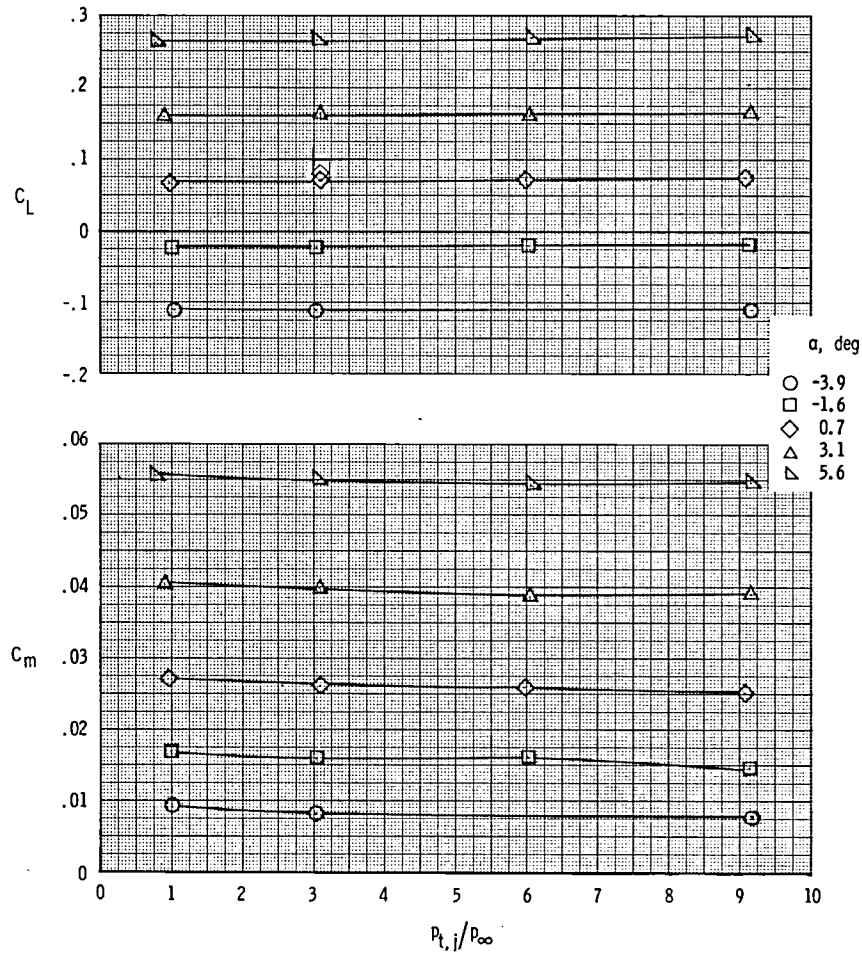

(d) Concluded.

Figure 18.- Continued.

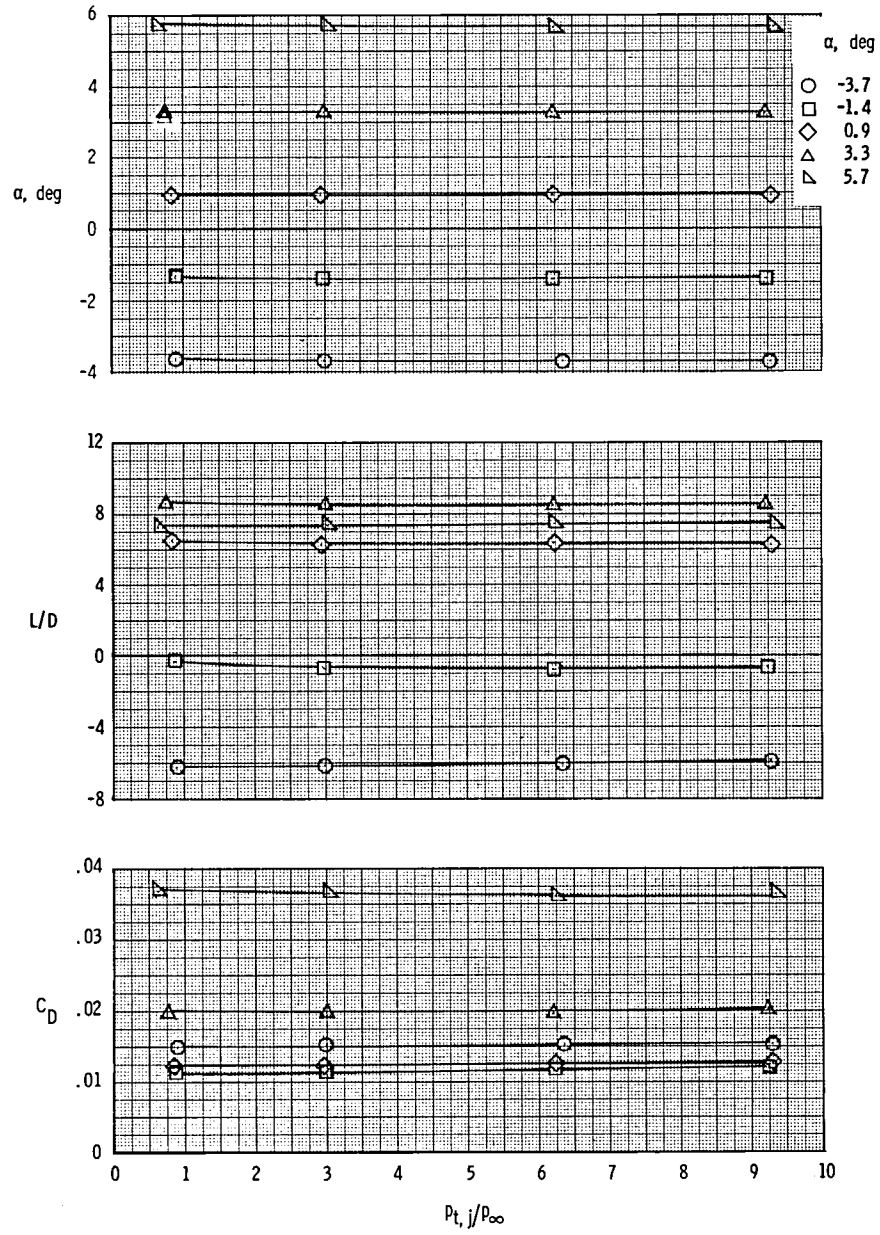

(e) M = 1.20.

Figure 18.- Continued.

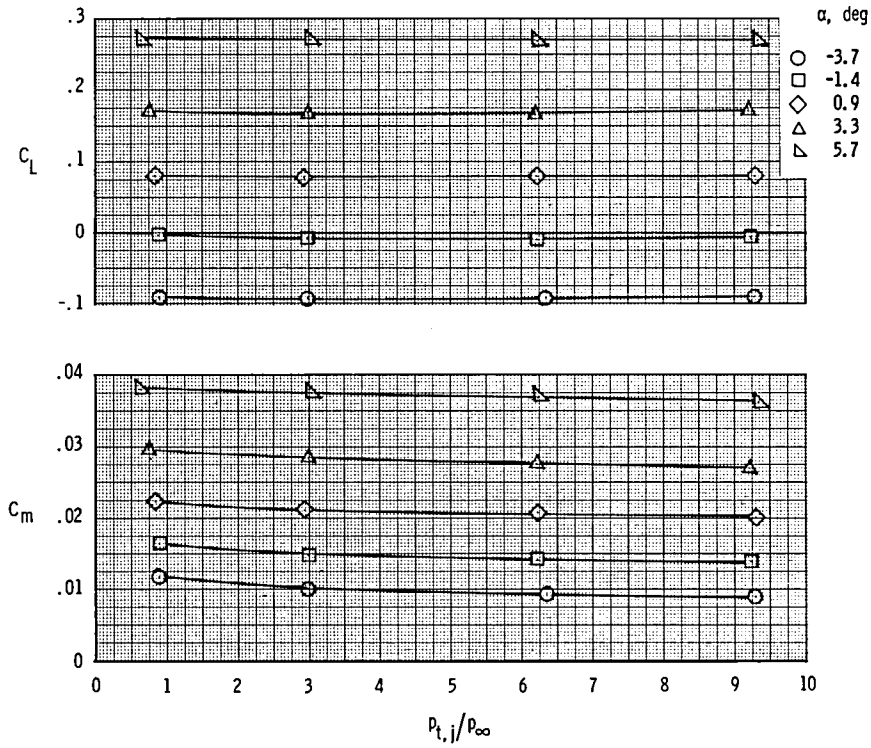

(e) Concluded.

Figure 18.- Concluded.

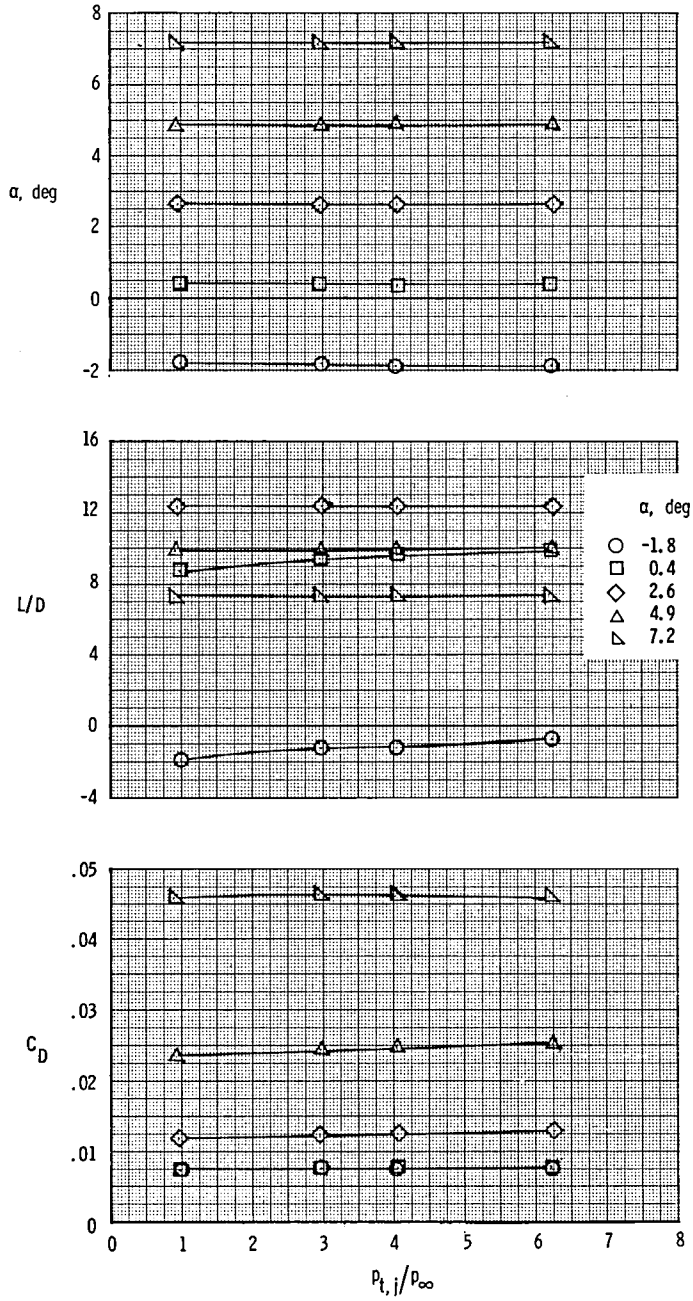

(a) M = 0.60.

Figure 19.- Variation of longitudinal aerodynamic characteristics with jet total-pressure ratio at $x_e/c = -0.17$, $y/(b/2) = 0.46$, and $z_w/d_N = 1.25$. A/B; $\delta_f = -10^o$.

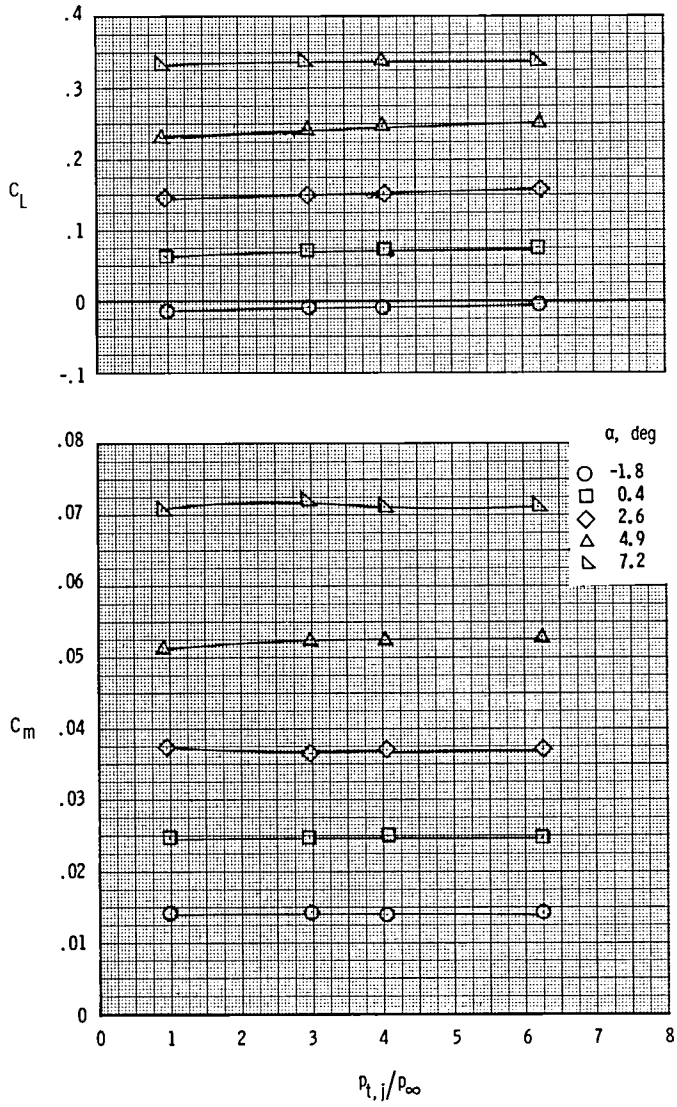

(a) Concluded.

Figure 19.- Continued.

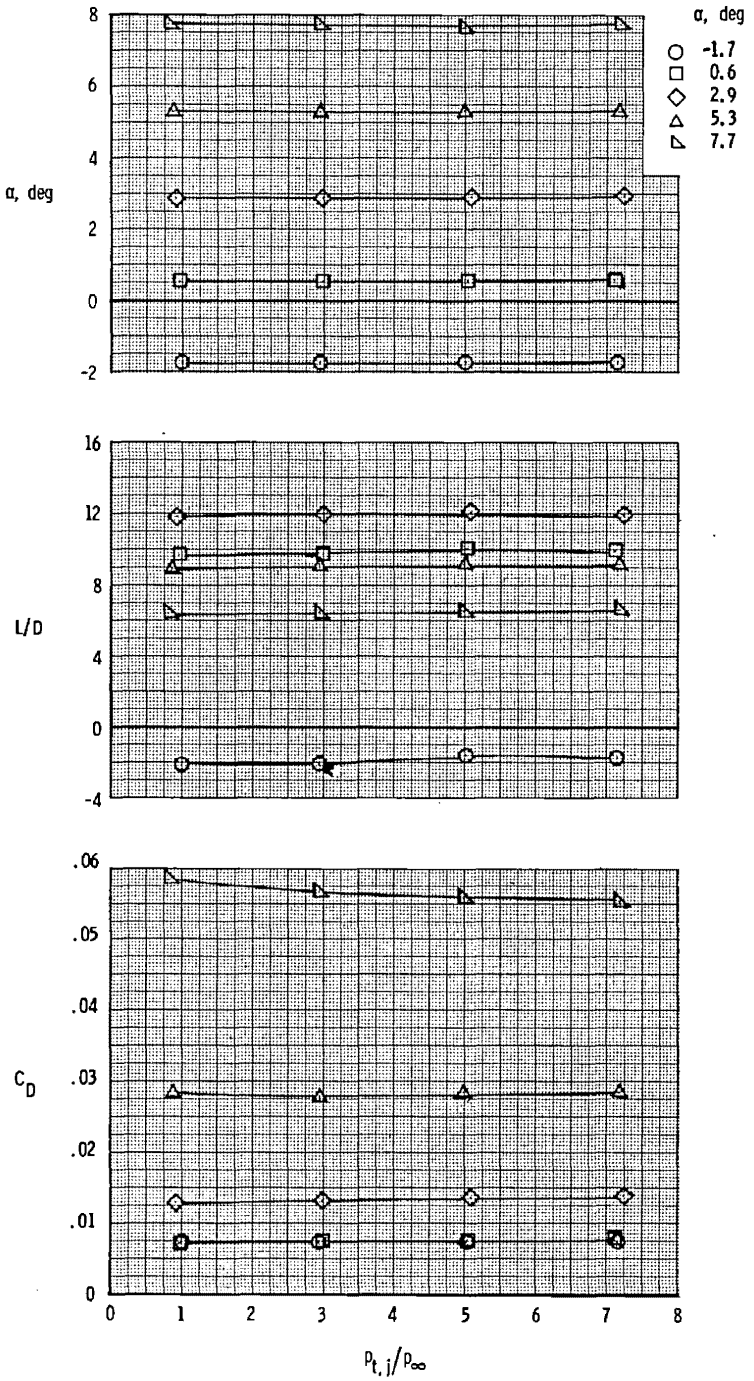

(b) M = 0.80.

Figure 19.- Continued.

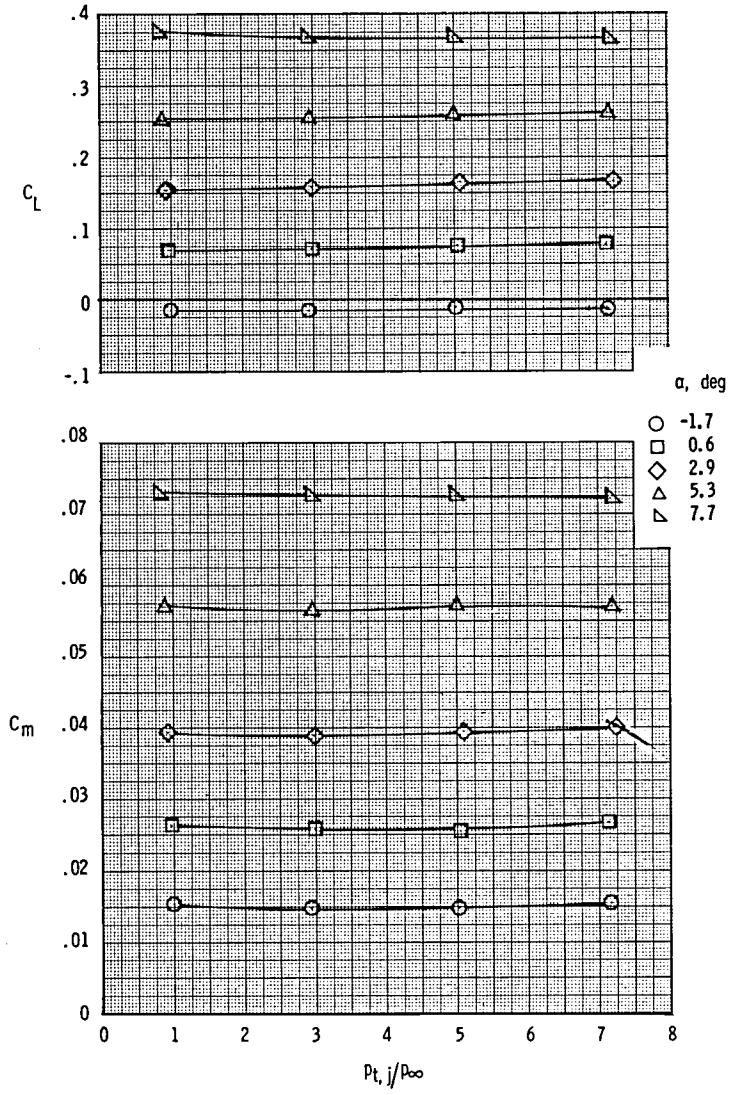

(b) Concluded.

Figure 19.- Continued.

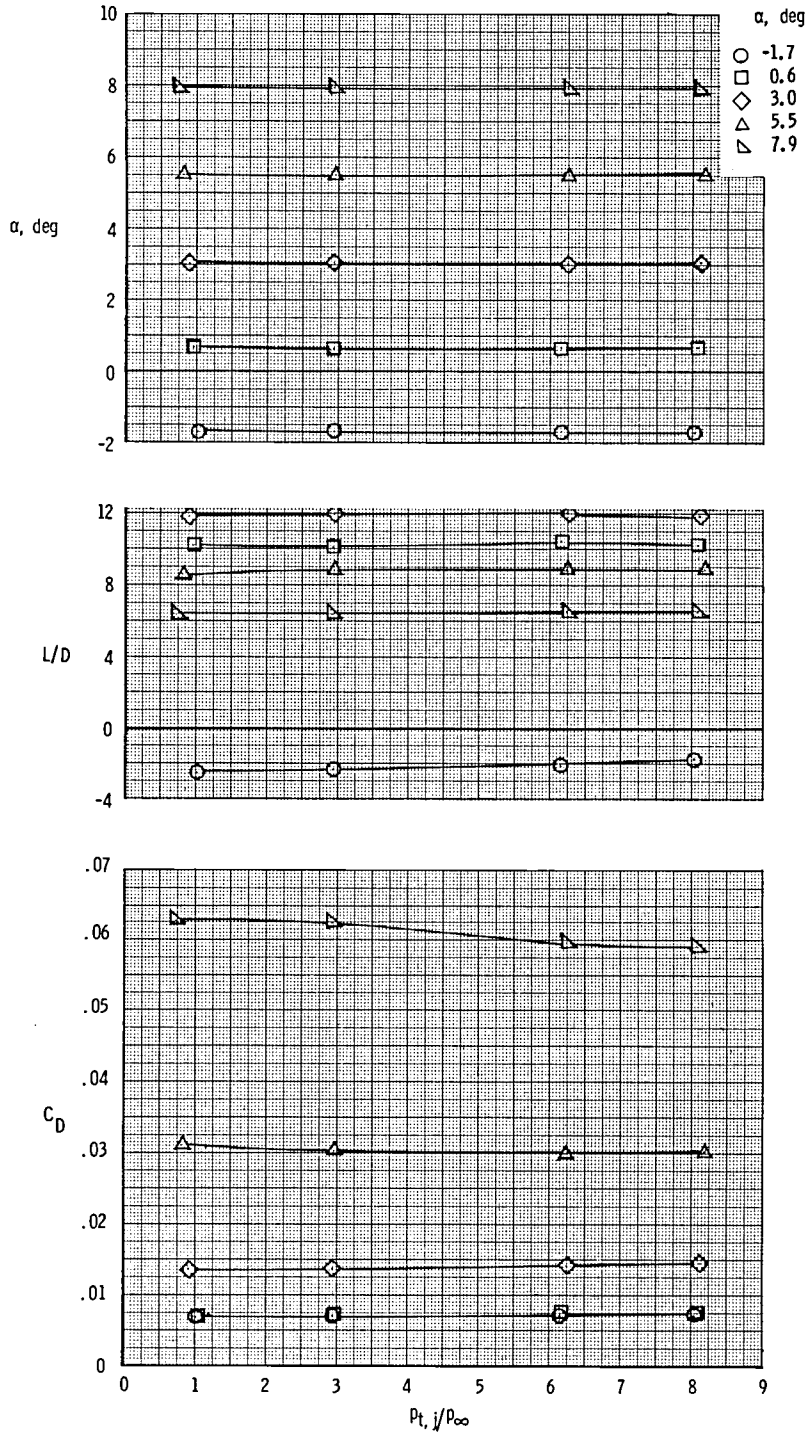

(c) M = 0.90.

Figure 19.- Continued.

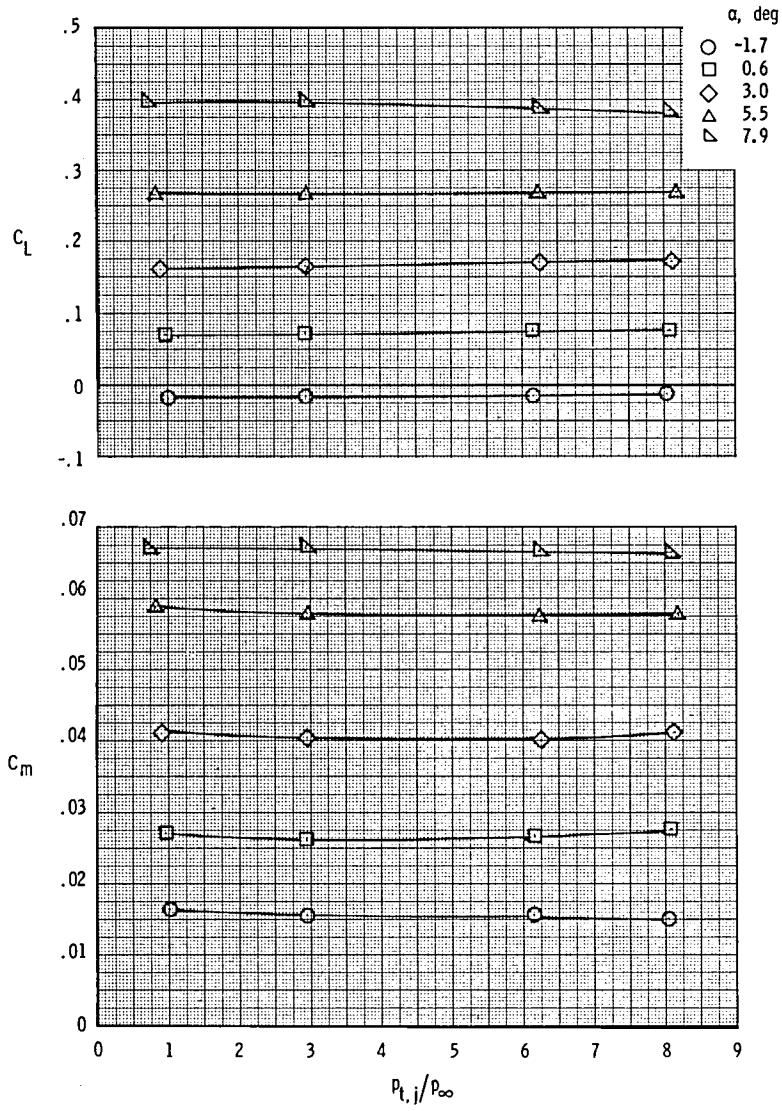

(c) Concluded.

Figure 19.- Continued.

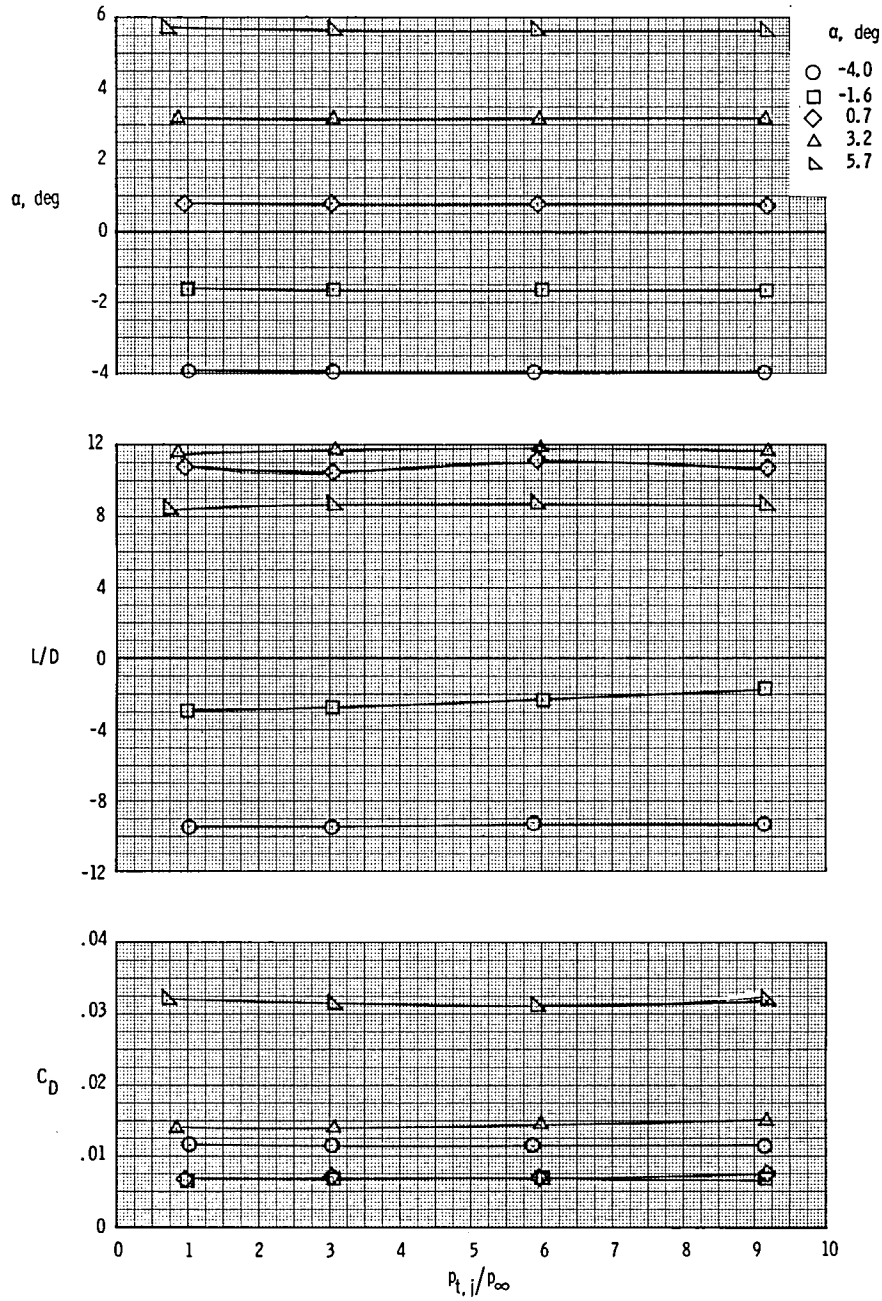

(d) M = 0.95.

Figure 19.- Continued.

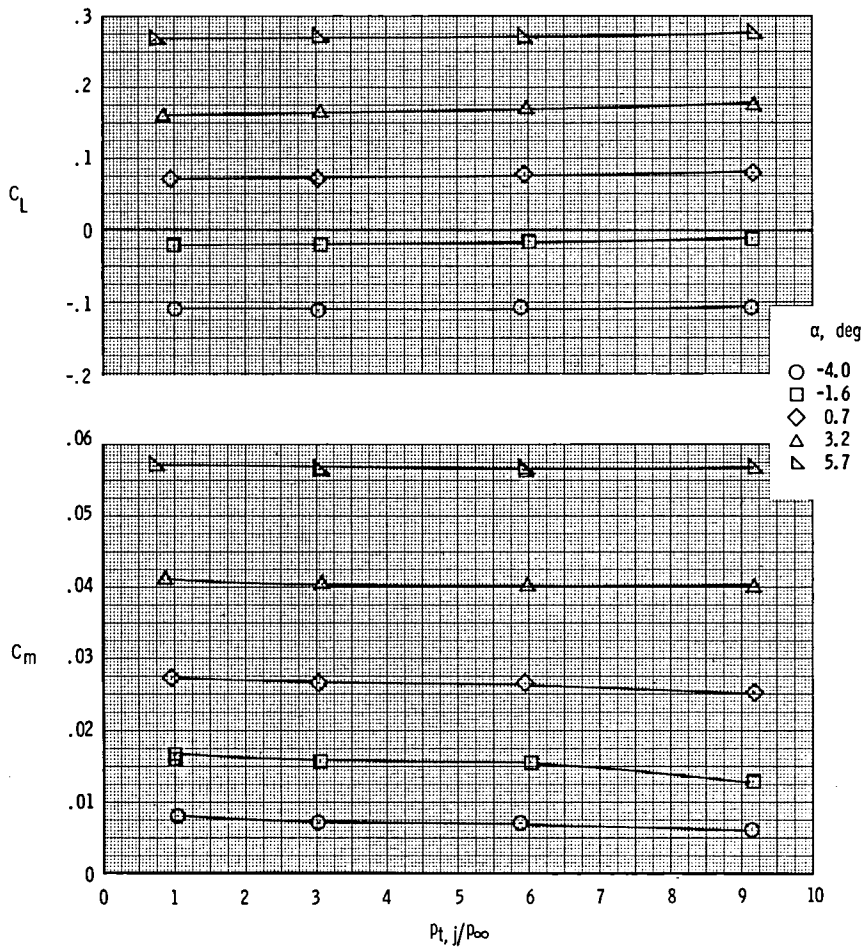

(d) Concluded.

Figure 19.- Continued.

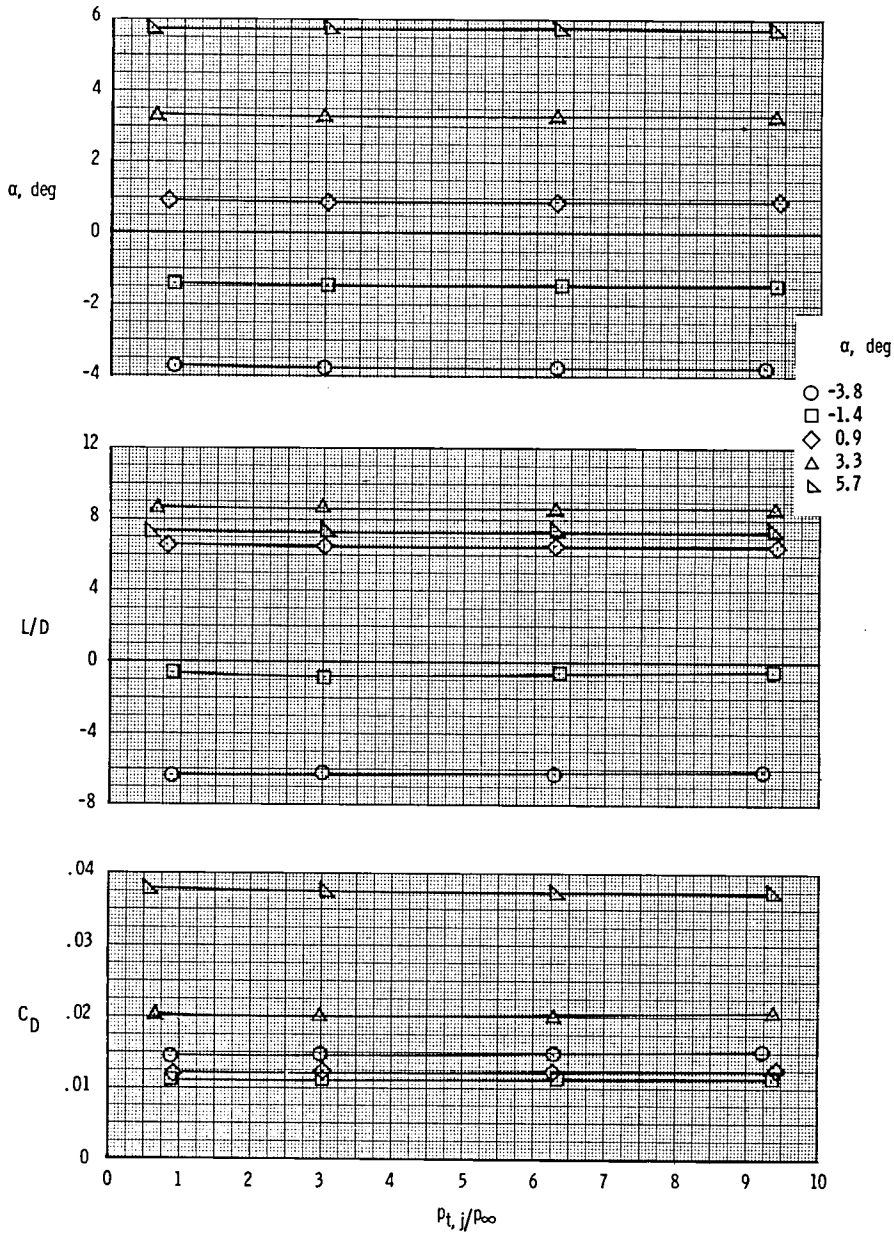

(e) M = 1.20.

Figure 19.- Continued.

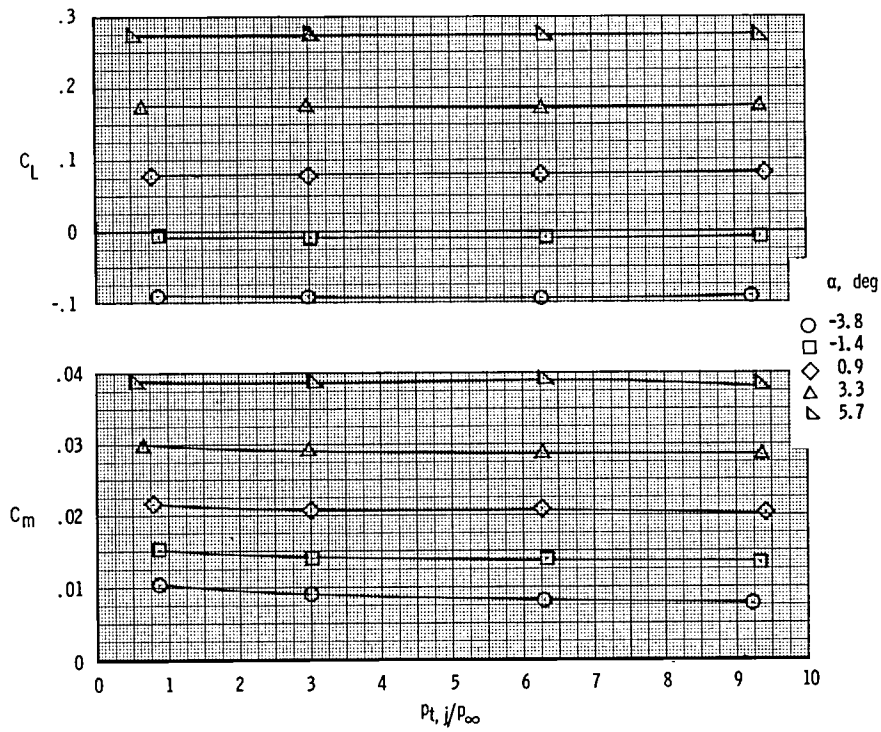

(e) Concluded.

Figure 19.- Concluded.

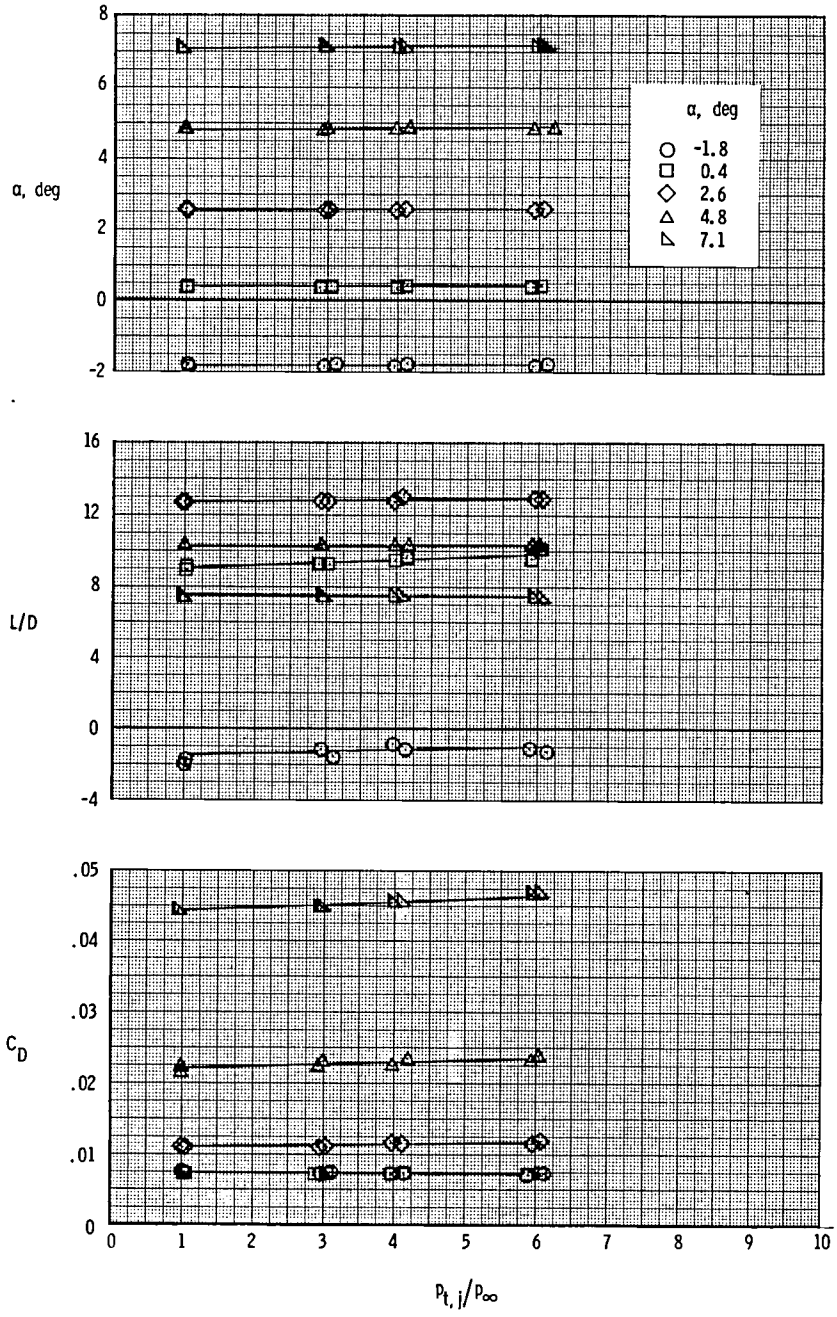

(a) M = 0.60.

Figure 20.- Variation of longitudinal aerodynamic characteristics with jet total-pressure ratio at $x_e/c = -0.17$, $y/(b/2) = 0.46$, $z_w/d_N = 1.50$, and non-A/B. $\delta_f = -10^o$.

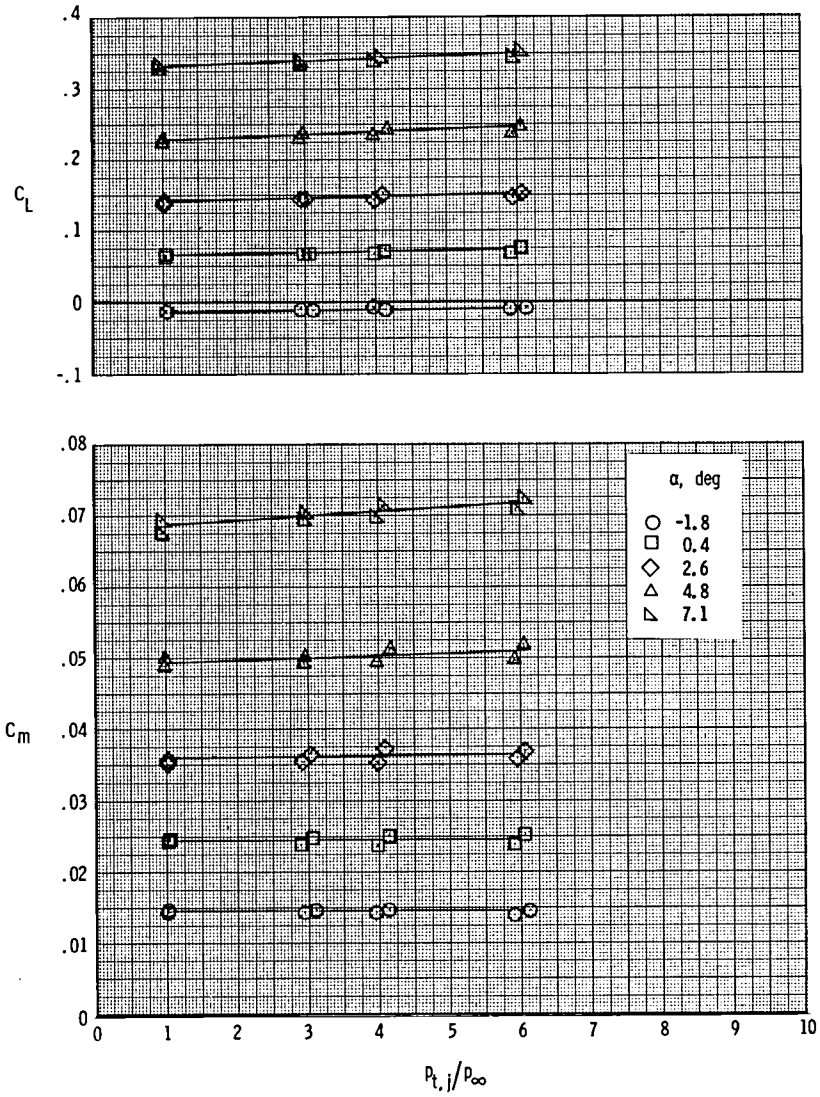

(a) Concluded.

Figure 20.- Continued.

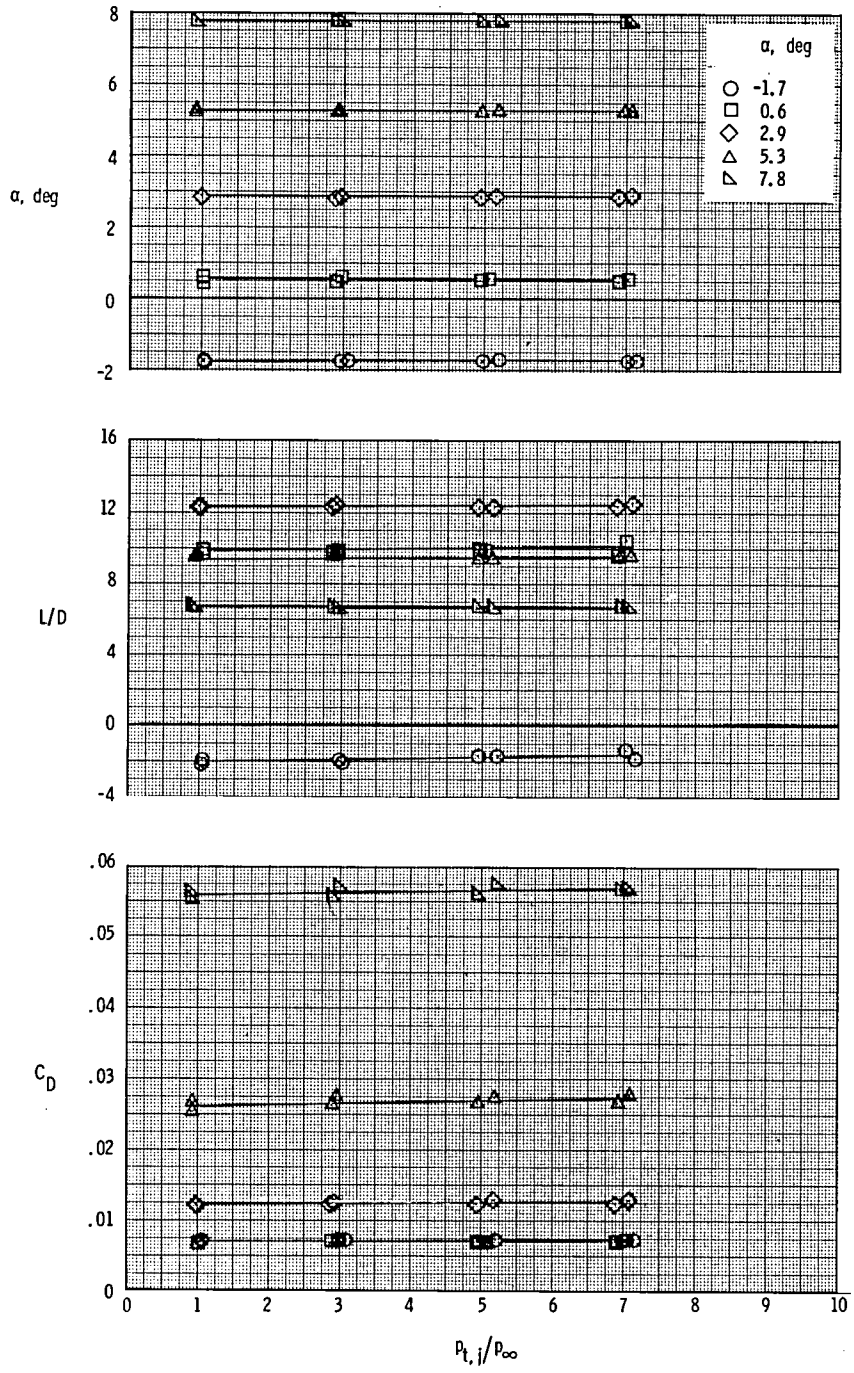

(b) M = 0.80.

Figure 20.- Continued.

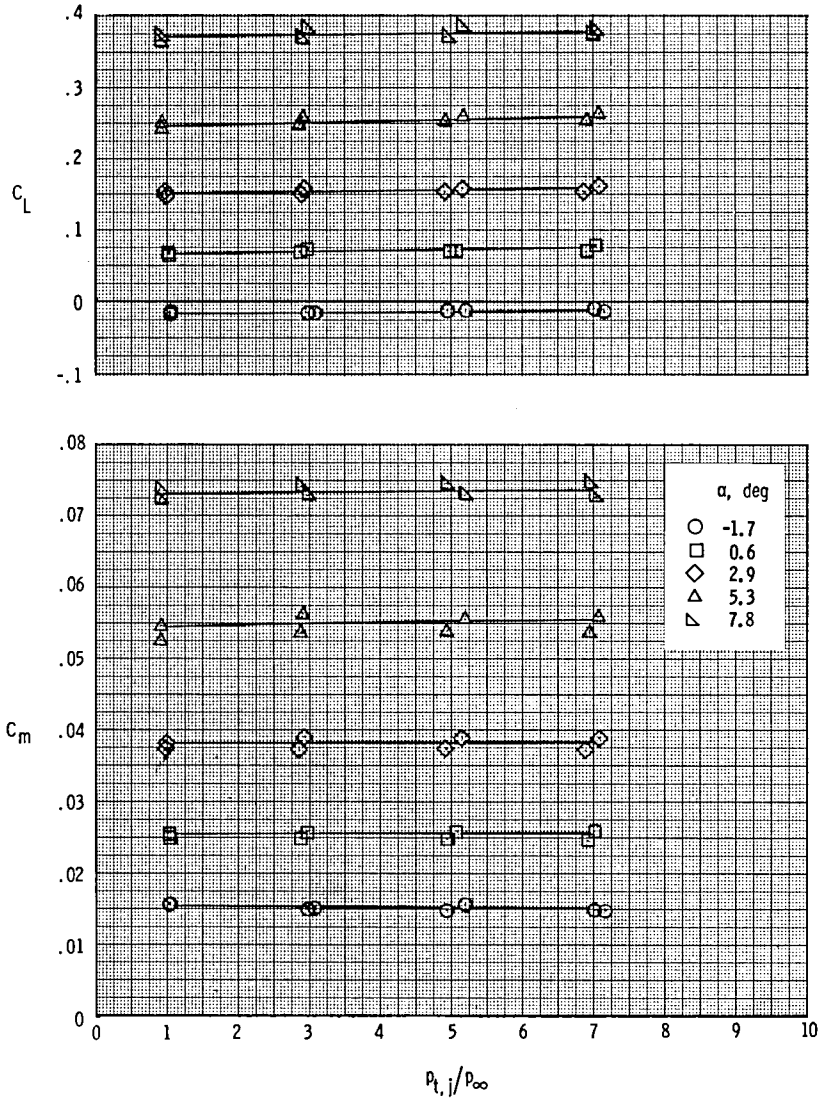

(b) Concluded.

Figure 20.- Continued.

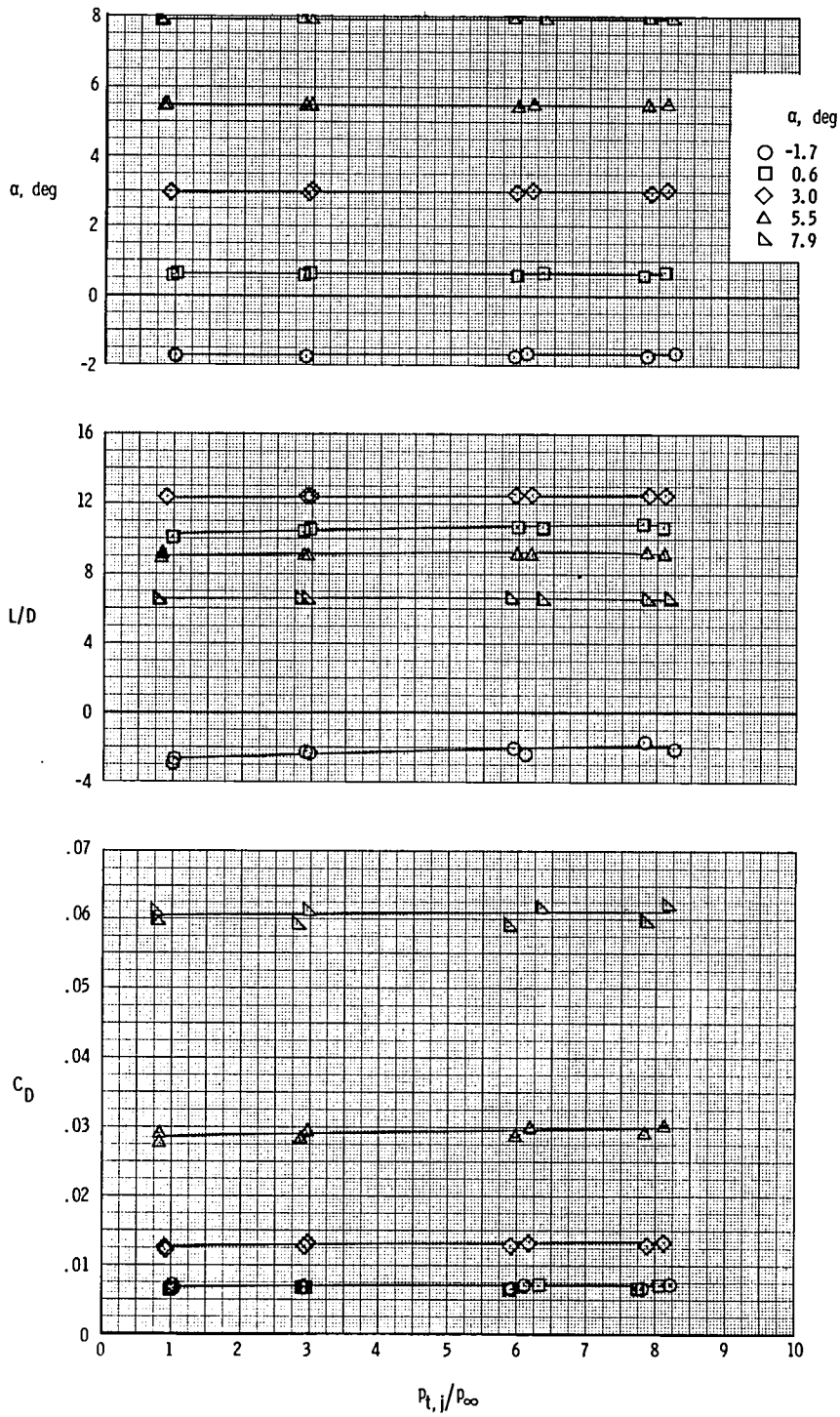

(c) M = 0.90.

Figure 20.- Continued.

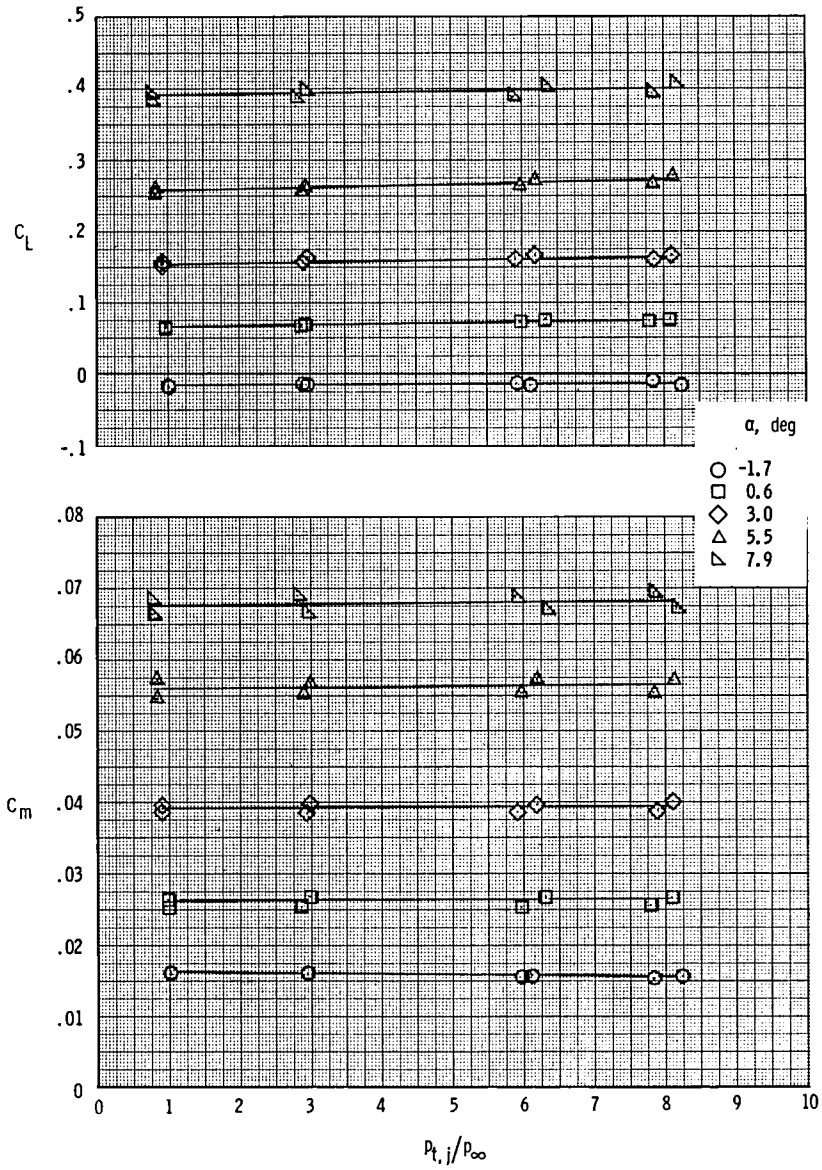

(c) Concluded.

Figure 20.- Continued.

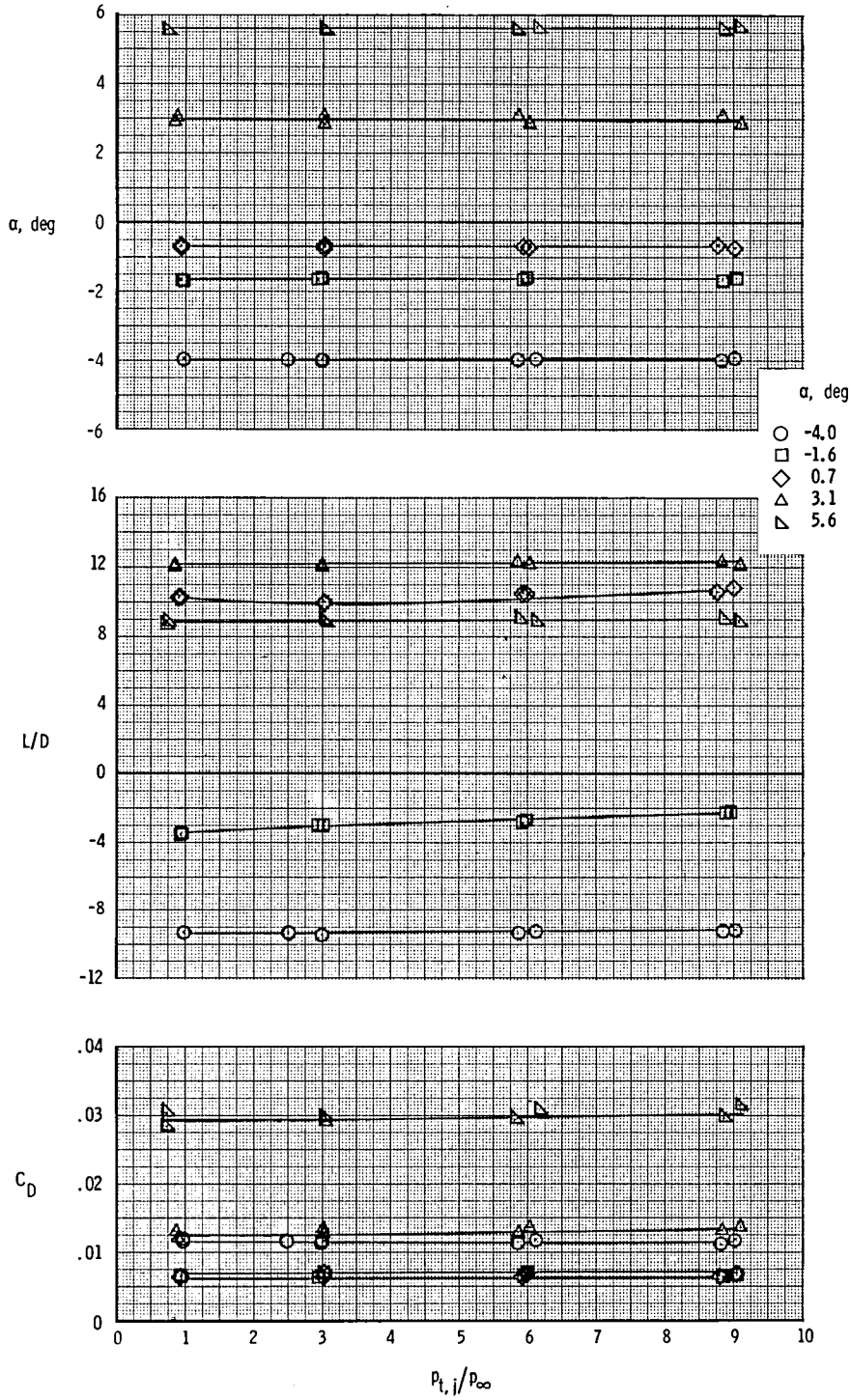

(d) M = 0.95.

Figure 20.- Continued.

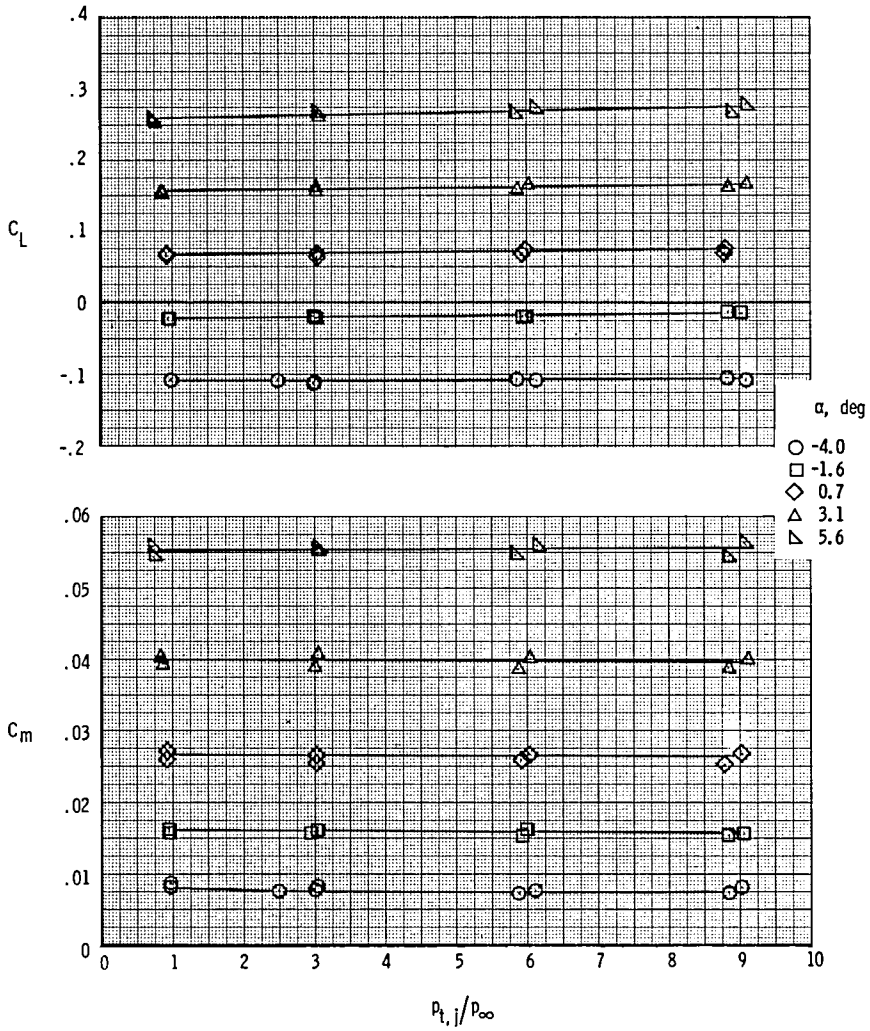

(d) Concluded.

Figure 20.- Continued.

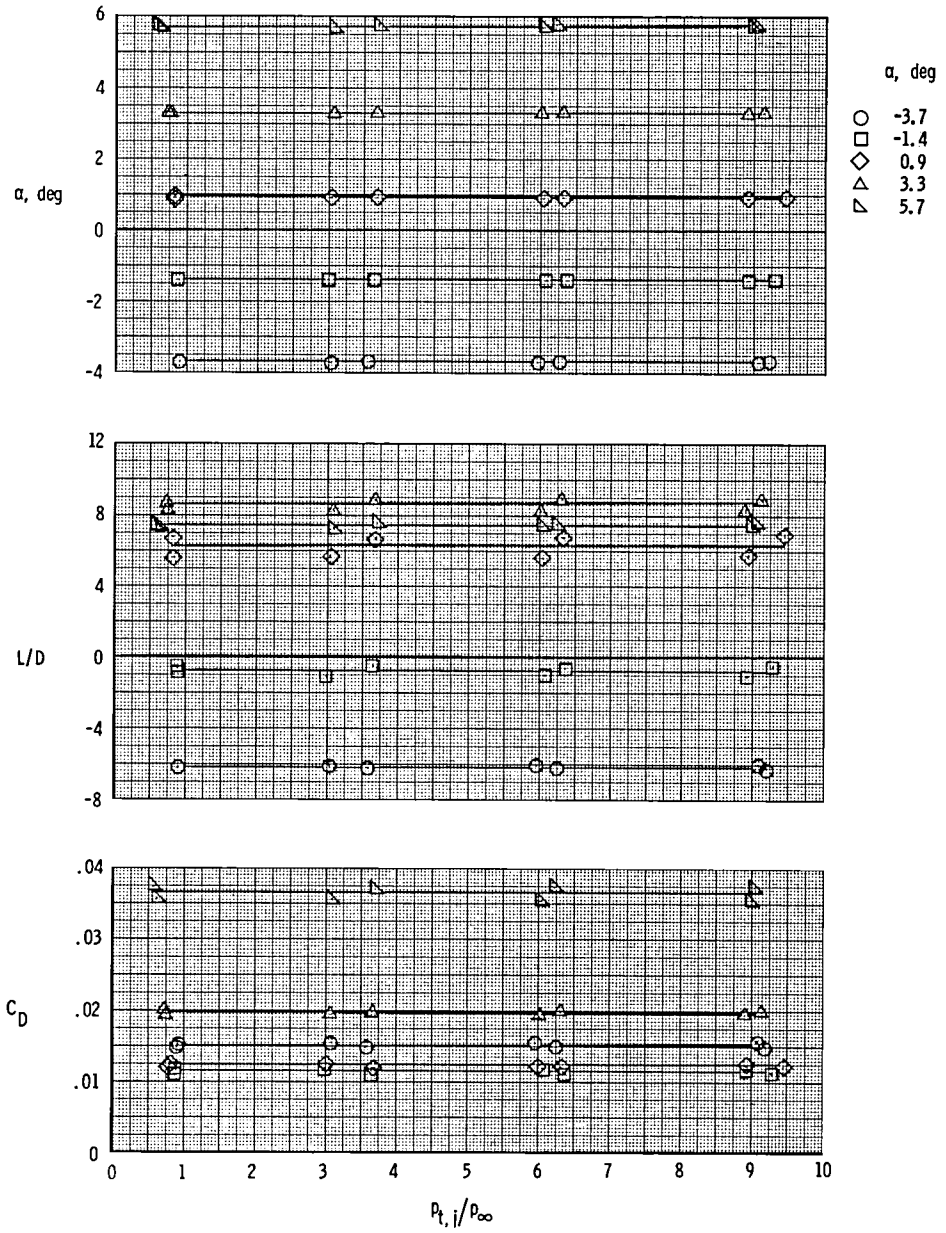

(e) M = 1.20.

Figure 20.- Continued.

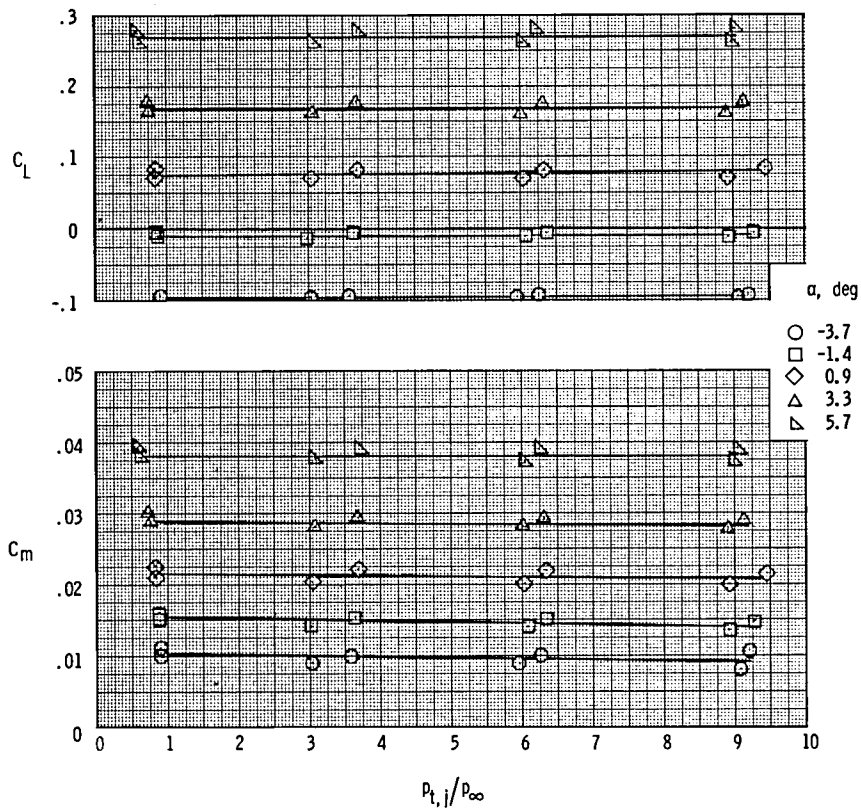

(e) Concluded.

Figure 20.- Concluded.

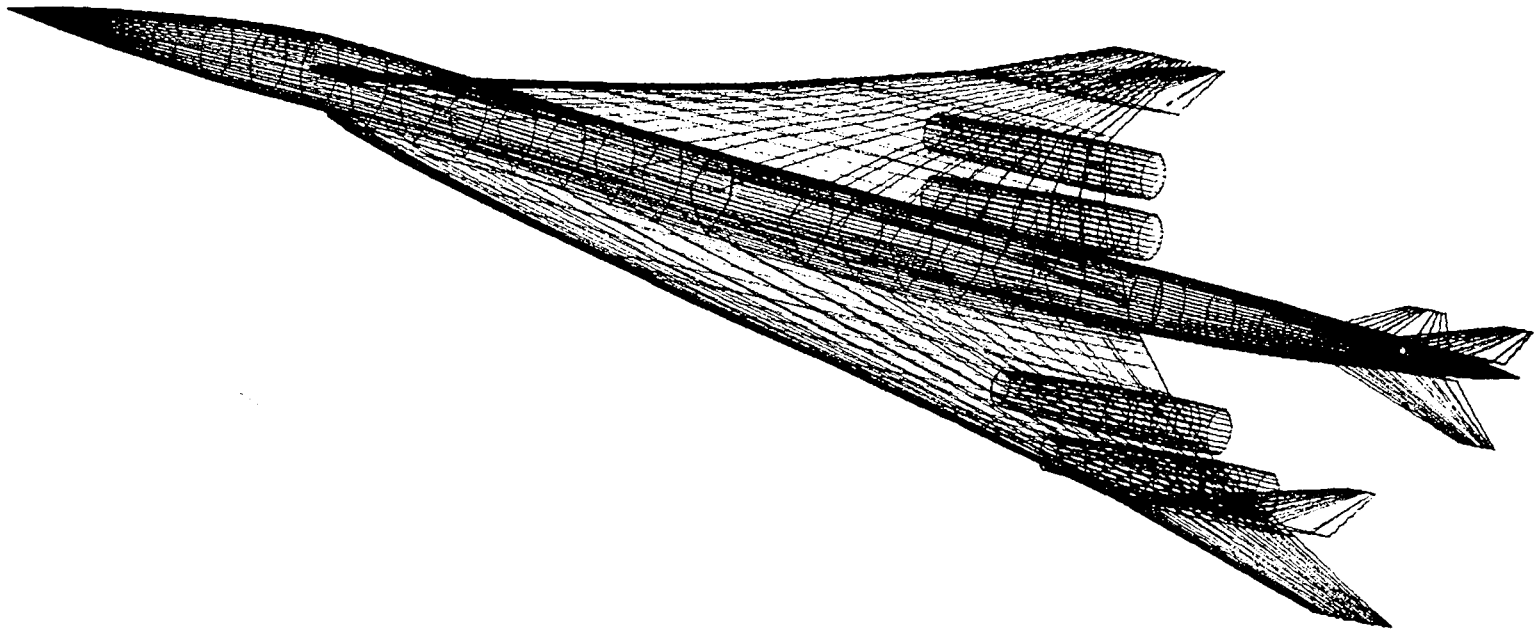

(a) Four engines under wing.

Figure 21.- Computer drawings of supersonic transport aircraft.

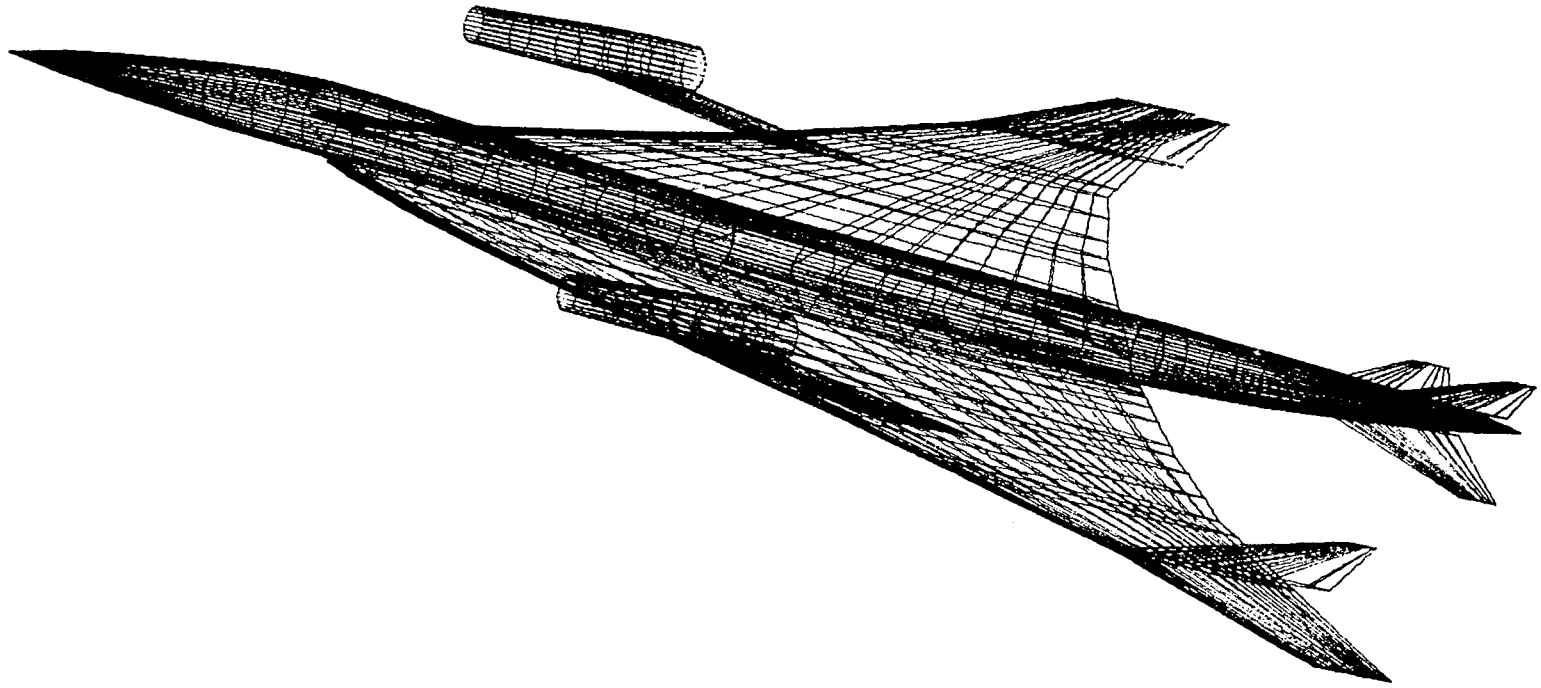

(b) Twin engines over wing.

Figure 21.- Continued.

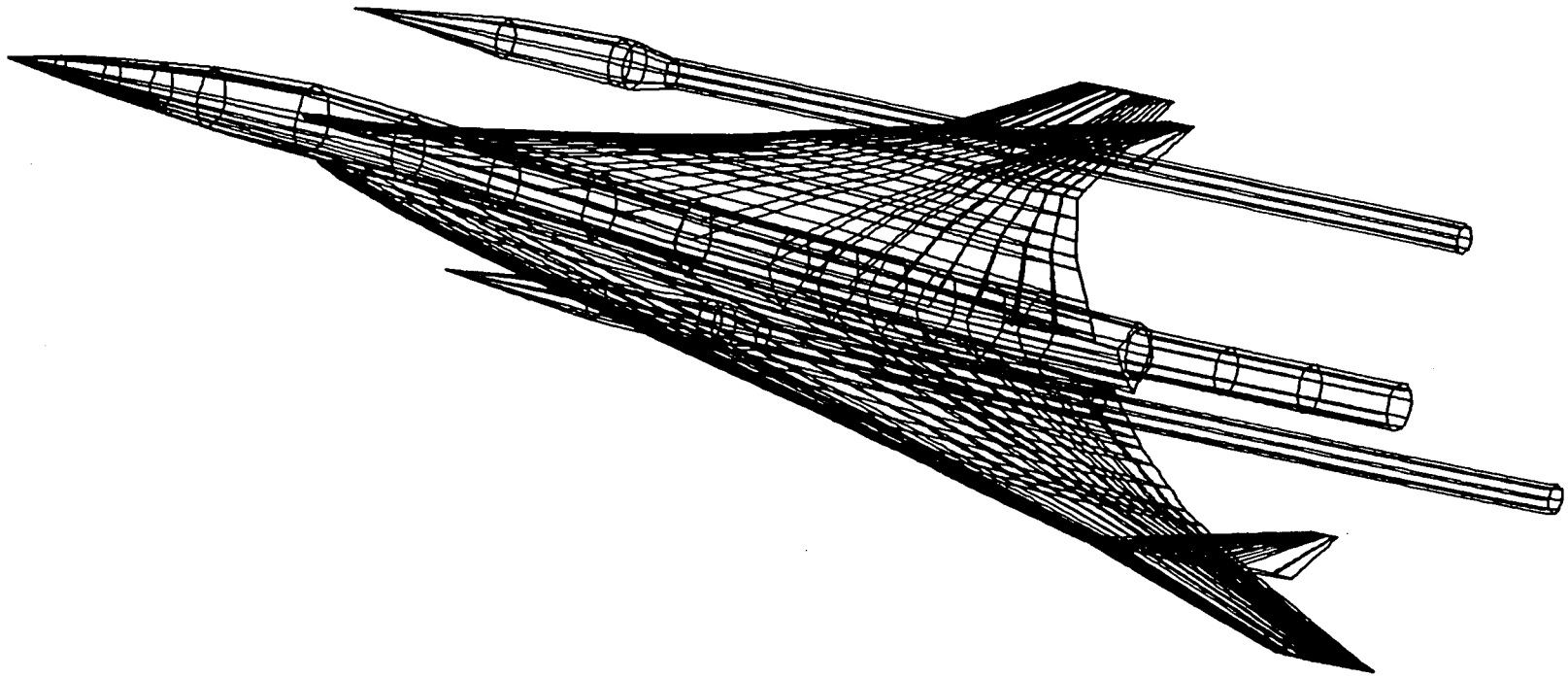

(c) Model used in this investigation for predicted results.

Figure 21.- Concluded.

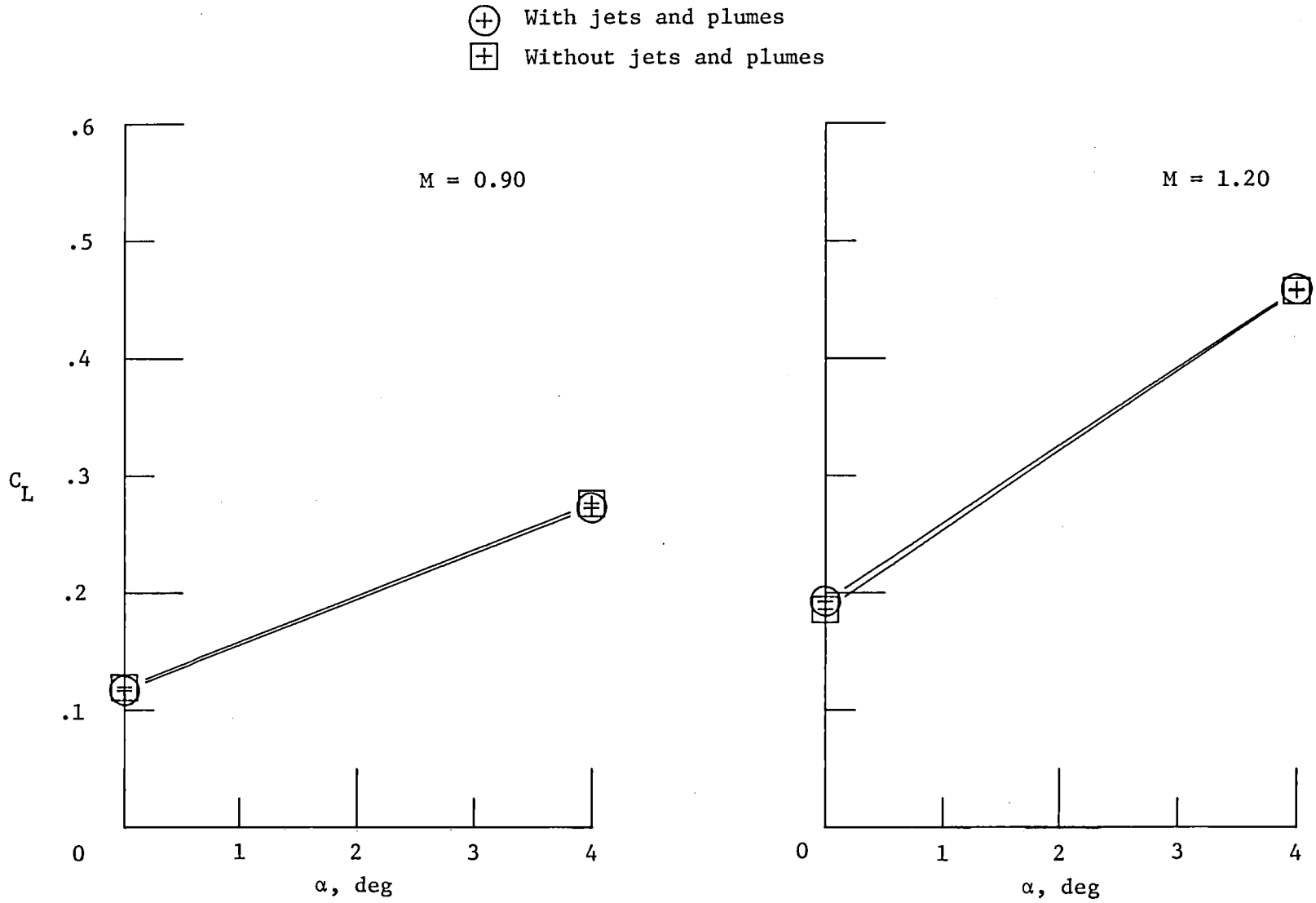

Figure 22.- Predicted lift coefficients at various angles of attack.

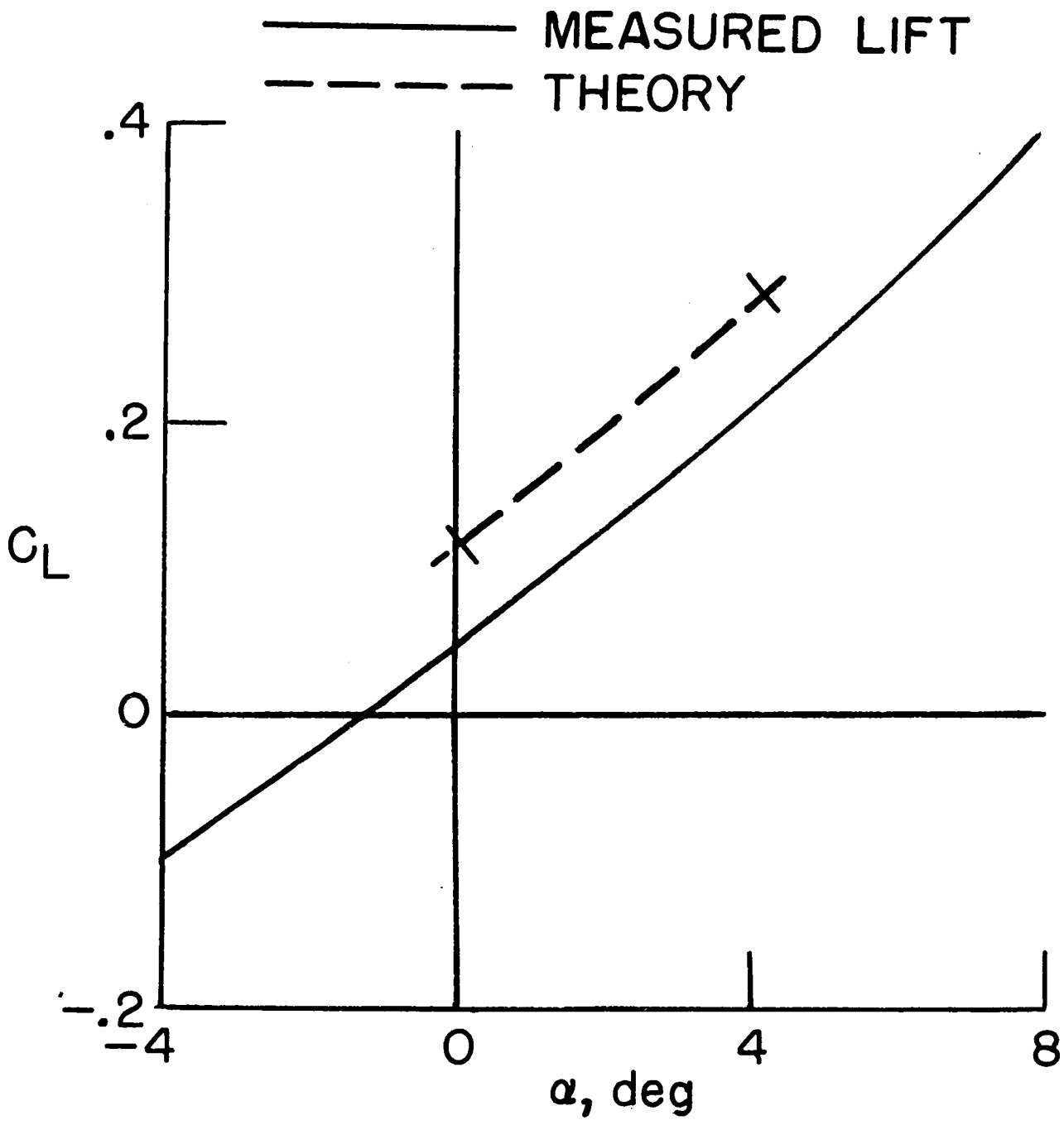

Figure 23.- Measured and predicted wing-body lift coefficients at M = 0.90, $x_e/c = -0.17$, $y/(b/2) = 0.46$, and $z_w/d_N = 1.50$.

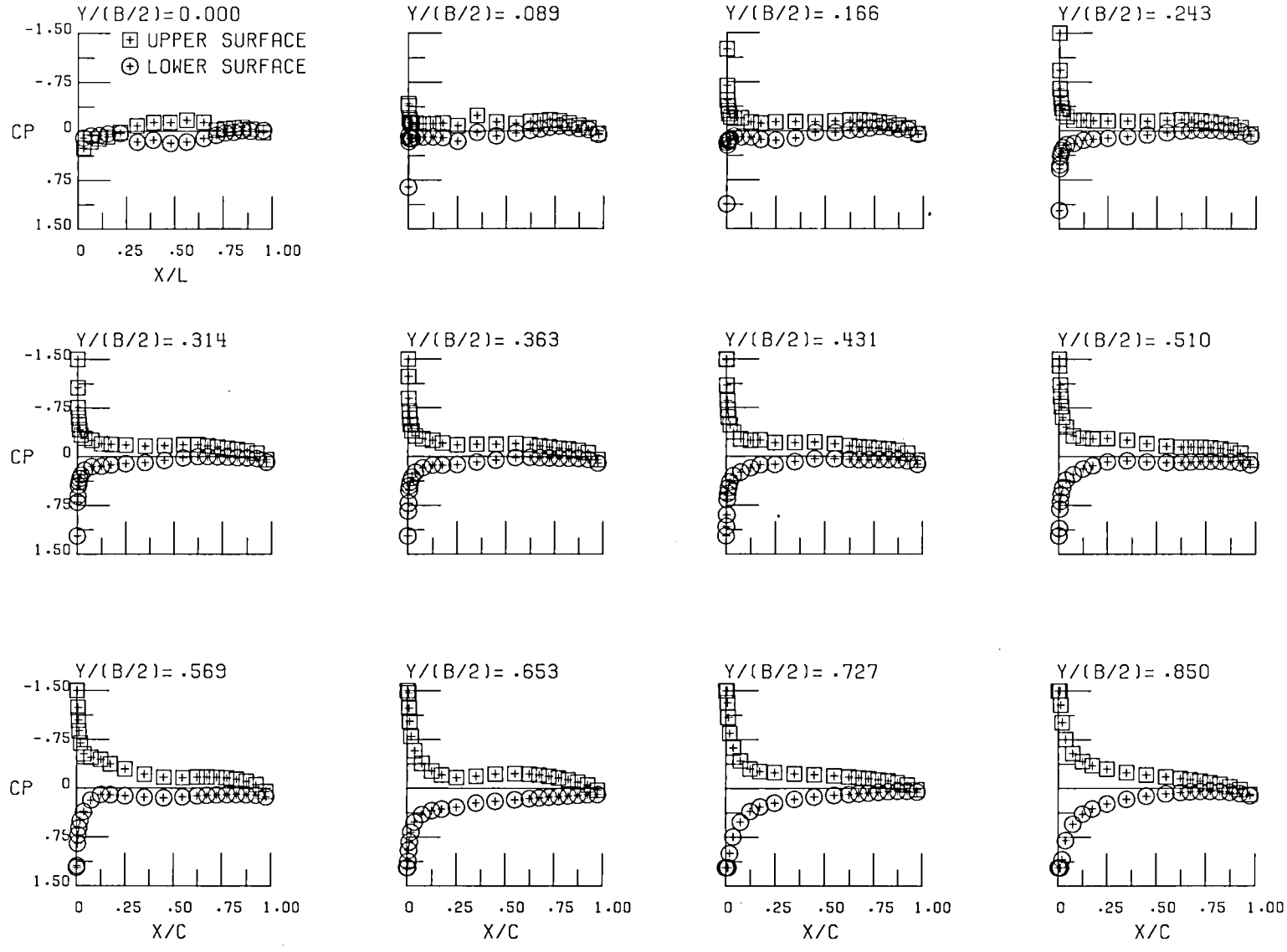

(a) M = 0.90, $\alpha = 4^{o}$, without jet nacelles.

Figure 24.- Predicted longitudinal pressure distributions.

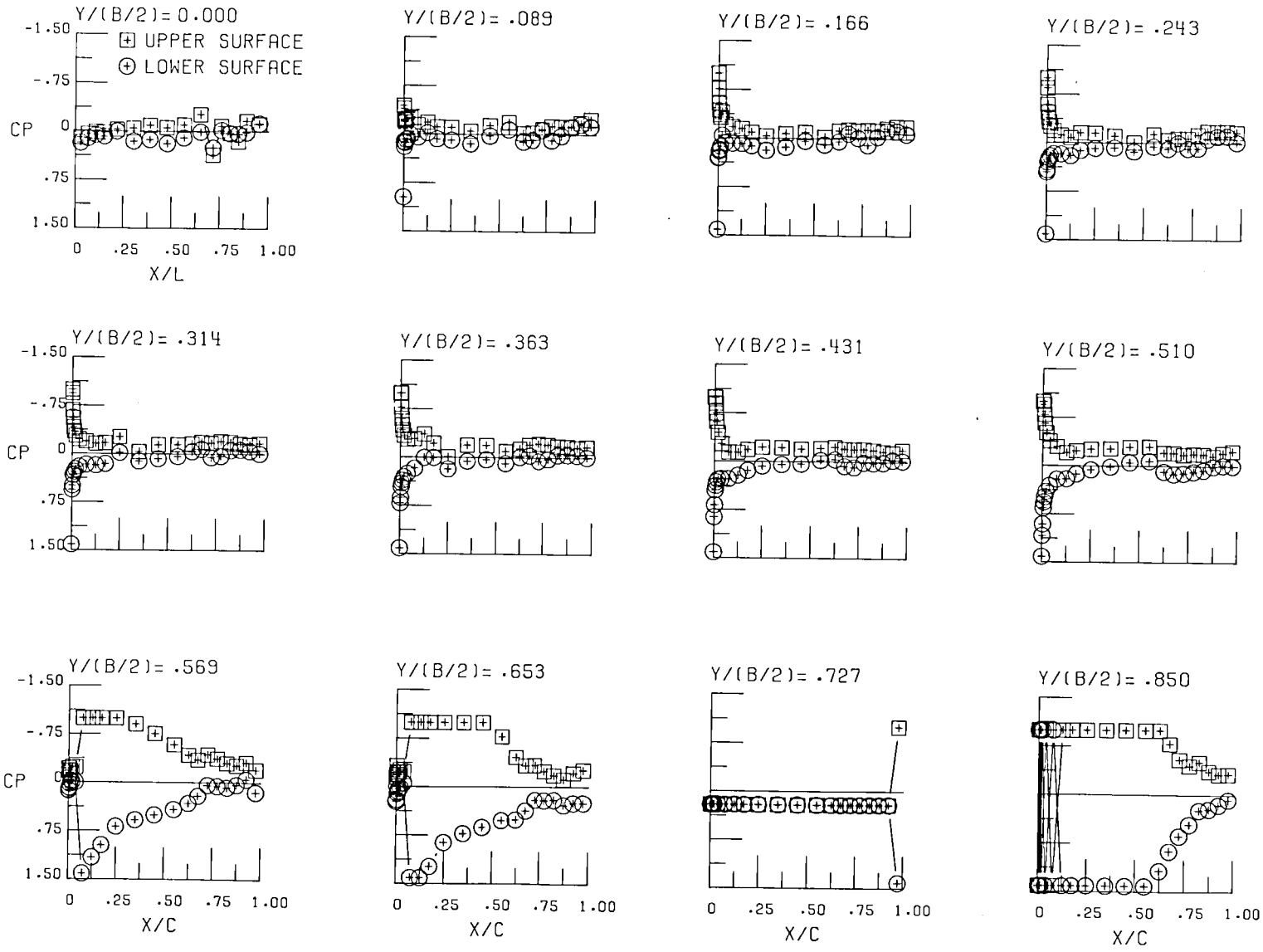

(b) M = 1.20, $\alpha = 4^{o}$, without jet nacelles.

Figure 24.- Continued.

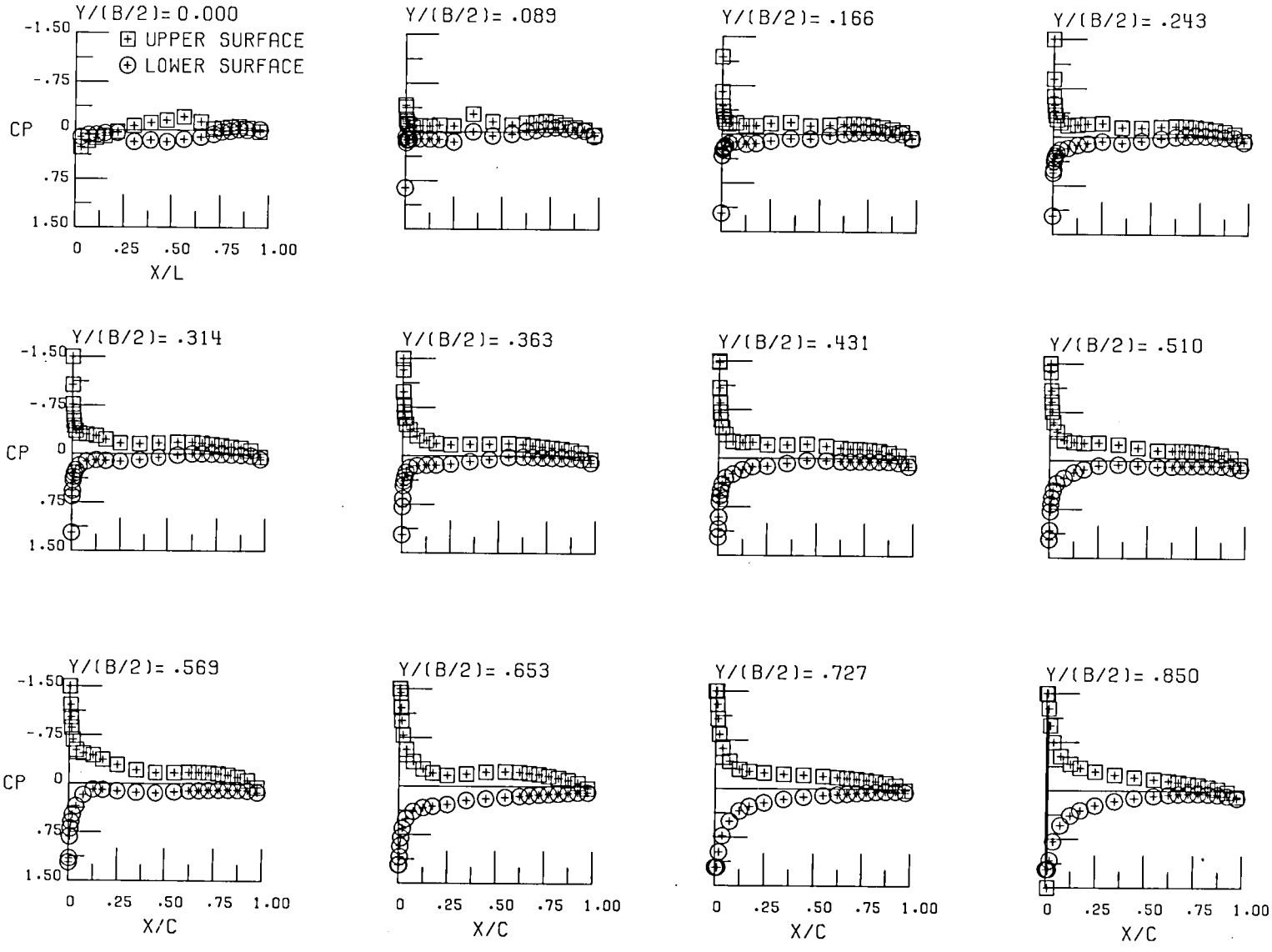

(c) M = 0.90, $\alpha = 4^{o}$, with jet nacelles.

Figure 24.- Continued.

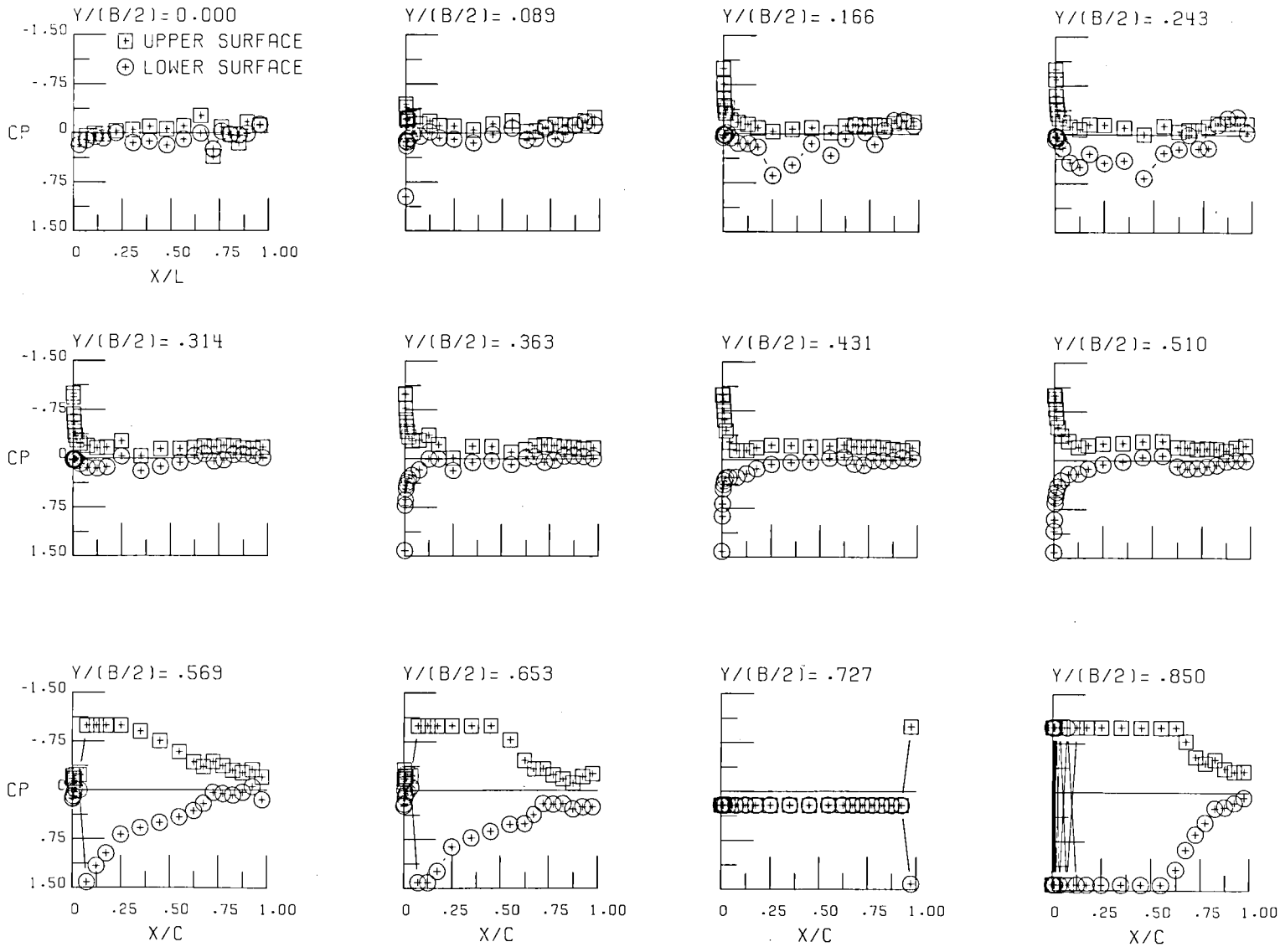

(d) M = 1.20, $\alpha = 4^{o}$, with jet nacelles.

Figure 24.- Concluded.

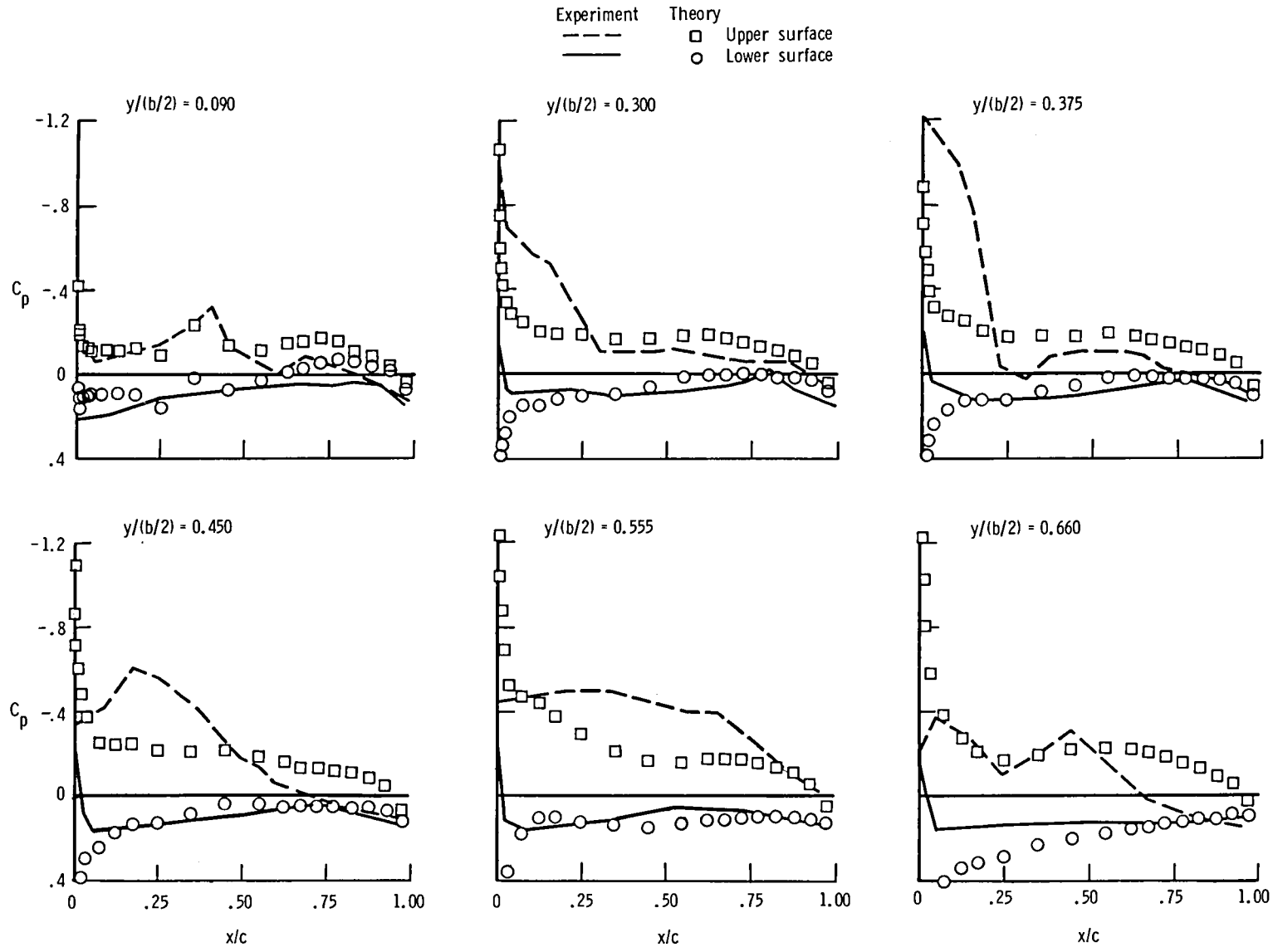

Figure 25.- Comparison between experimental and theoretical pressure coefficients at M = 0.90, $\alpha = 4^{o}$, jet off, $x_e/c = -0.17$, $y/(b/2) = 0.46$, and $z_w/d_N = 1.50$.

1. Report No.	2. Government Accession No.	3. Recipient's Catalog No.
NASA TM-80145		

4. Title and Subtitle	5. Report Date
TRANSONIC AERODYNAMIC CHARACTERISTICS OF A SUPERSONIC CRUISE AIRCRAFT RESEARCH MODEL WITH THE ENGINES SUSPENDED ABOVE THE WING	December 1979
	6. Performing Organization Code

7. Author(s)	8. Performing Organization Report No.
Charles E. Mercer and George T. Carson, Jr.	L-12811
	10. Work Unit No.
9. Performing Organization Name and Address	505-04-13-02
NASA Langley Research Center Hampton, VA 23665	11. Contract or Grant No.
	13. Type of Report and Period Covered
12. Sponsoring Agency Name and Address	Technical Memorandum
National Aeronautics and Space Administration Washington, DC 20546	14. Sponsoring Agency Code

15. Supplementary Notes

16. Abstract

An investigation was conducted in the Langley 16-foot transonic tunnel to determine the influence of upper-surface nacelle exhaust flow on the aerodynamic characteristics of a supersonic cruise aircraft research configuration over a range of Mach numbers from 0.60 to 1.20. The arrow-wing transport configuration with engines suspended over the wing was tested at angles of attack from -4° to 6° and jet total-pressure ratios from 1 to approximately 13. Wing-tip leading-edge flap deflections of -10° to 10° were tested with the wing-body configuration. Various nacelle locations (chordwise, spanwise, and vertical) were tested over the ranges of Mach numbers, angles of attack, and jet total-pressure ratios.

17. Key Words (Suggested by Author(s))	18. Distribution Statement
Aerodynamics Propulsion Jet effects Transport	Unclassified - Unlimited Subject Category 02

19. Security Classif. (of this report)	20. Security Classif. (of this page)	21. No. of Pages	22. Price*
Unclassified	Unclassified	195	$9.00

* For sale by the National Technical Information Service, Springfield, Virginia 22161

NASA-Langley, 1979

National Aeronautics and
Space Administration

Washington, D.C.
20546

Official Business
Penalty for Private Use, $300

SPECIAL FOURTH CLASS MAIL
BOOK

Postage and Fees Paid
National Aeronautics and
Space Administration
NASA-451

NASA

POSTMASTER: If Undeliverable (Section 158 Postal Manual) Do Not Return